

# **Characterization of the autophagy-modulating natural compound prodigiosin for the elimination of therapy-resistant tumor cells**

Inaugural-Dissertation

zur Erlangung des Doktorgrades  
der Mathematisch-Naturwissenschaftlichen Fakultät  
der Heinrich-Heine-Universität Düsseldorf

vorgelegt von

**Lena Berning**

aus Rheine

Düsseldorf, August 2023

aus dem Institut für Molekulare Medizin I  
der Heinrich-Heine-Universität Düsseldorf

Gedruckt mit der Genehmigung der  
Mathematisch-Naturwissenschaftlichen Fakultät der  
Heinrich-Heine-Universität Düsseldorf

Berichterstatter:

1. Univ.-Prof. Dr. Björn Stork
2. Univ.-Prof. Dr. Jörg Pietruszka

Tag der mündlichen Prüfung: 04. Dezember 2023

## Eidesstattliche Erklärung

Ich versichere an Eides statt, dass die Dissertation von mir selbständig und ohne unzulässige fremde Hilfe unter Beachtung der „Grundsätze zur Sicherung guter wissenschaftlicher Praxis an der Heinrich-Heine-Universität Düsseldorf“ erstellt worden ist. Die vorliegende Arbeit wurde von mir selbständig verfasst und keine anderen als die angegebenen Hilfsmittel verwendet. Alle wörtlich oder inhaltlich übernommenen Stellen habe ich als solche gekennzeichnet. Zudem versichere ich, dass ich die vorliegende Dissertation nur in diesem und keinem anderen Promotionsverfahren eingereicht habe und diesem kein früheres Promotionsverfahren vorausgegangen ist.

*Düsseldorf, 04.01.2024*

---

Ort, Datum

*L. Berning*

---

Lena Berning

## Acknowledgement

Zuerst möchte ich mich bei meinem Doktorvater Prof. Björn Stork für die hervorragende wissenschaftliche Betreuung, zielführende Diskussionen und zahlreiche konstruktive Ideen bedanken. Ich danke dir für deine uneingeschränkte Unterstützung, deinen steten Optimismus und die Fähigkeit, jede Situation mit Humor zu nehmen.

Ebenso gilt mein Dank Herrn Prof. Jörg Pietruszka für die Begutachtung dieser Dissertation als Zweitgutachter, sein großes Fachwissen über die Substanzklasse der Prodiginine und seine ansteckende Begeisterung über neue wissenschaftliche Erkenntnisse.

Bei Herrn Prof. Sebastian Wesselborg möchte ich mich für die Möglichkeit, diese Arbeit in seinem Institut für Molekulare Medizin I durchzuführen, bedanken.

Diese Arbeit wurde im Rahmen des interdisziplinären Graduiertenkollegs (GRK) 2158 durchgeführt und durch dieses gefördert. Ich möchte mich bei allen Mitgliedern des GRK2158 und auch bei der Düsseldorf School of Oncology (DSO) für die finanzielle und fachliche Förderung und die zahlreichen Möglichkeiten zum wissenschaftlichen Austausch bedanken.

Bedanken möchte ich mich auch bei allen Co-Autoren und Kollaborationspartnern, die wesentlich zu dieser Arbeit beigetragen haben. Erwähnen möchte ich hierbei vor allem Thomas Lenz und Dr. Gereon Poschmann (Molecular Proteomics Laboratory) für ihre großartige Expertise im Bereich der Proteomics und Tim Moritz Weber und Moritz Klischan (Institut für Bioorganische Chemie) für einen nie endenden Strom an neuen Compounds.

Weiterhin möchte ich mich bei den aktuellen und ehemaligen Mitgliedern der Molekularen Medizin I bedanken. Mein Dank geht vor allem an Annabelle und David, nicht nur für die hervorragende musikalische Untermalung innerhalb und außerhalb des Labors, sondern auch für eure Unterstützung und aufbauende Worte, wenn sie nötig waren.

Ich danke auch den Toxis und meiner Handballmannschaft. Durch euch ist Düsseldorf zu meiner Wahlheimat geworden und ihr habt es in stressigen Zeiten immer geschafft, den nötigen Ausgleich zu schaffen.

Meinen Eltern und meiner Schwester möchte ich für den uneingeschränkten Rückhalt danken. Mein Studium und diese Arbeit wären ohne euch nicht möglich gewesen. Danken möchte ich auch meinen Großeltern, die immer an mich geglaubt haben. Ich vermisse euch.

Zum Schluss möchte ich mich bei Marco bedanken. Ich hoffe, wir werden zusammen noch viele kleine und große Abenteuer erleben. Wie schön, dass es dich gibt und dass du immer für mich da bist.

## Abbreviations

3-MA	3-methyladenine
ADCD	autophagy-dependent cell death
ADME	absorption, distribution, metabolism and excretion
AMP	adenosine monophosphate
AMPK	AMP-activated protein kinase
AR	Ankyrin repeat
ATG	autophagy-related
ATP	adenosine triphosphate
BAK	Bcl-2 antagonist/killer
BAX	Bcl-2 associated X protein
Bcl-2	B-cell lymphoma 2
BH3	Bcl-2 homology 3
CAF	cancer-associated fibroblast
CALCOCO1	calcium-binding and coiled coil domain-containing protein 1
CETSA	cellular thermal shift assay
COX2	cyclooxygenase-2
CQ	chloroquine
DFCP	double FYVE domain containing protein
DISC	death-inducing signaling complex
DNA	deoxyribonucleic acid
EC <sub>50</sub>	half maximal effective concentration
ER	endoplasmic reticulum
FDA	U.S. Food and Drug Administration
FIP200	focal adhesion kinase-interacting protein of 200 kDa
GABARAP	GABA type A receptor-associated protein
GRASP55	Golgi reassembly stacking protein of 55 kDa
GRASP65	Golgi reassembly stacking protein of 65 kDa
GTP	guanosine triphosphate
HCQ	hydroxychloroquine
HER-2	human epidermal growth factor receptor 2

HSP70	heat shock-cognate protein of 70 kDa
HTS	high throughput screening
IC <sub>50</sub>	half maximal inhibitory concentration
KO	knockout
LAMP2A	lysosome-associated membrane protein 2A
LC3	(microtubule associated protein 1) light chain 3
LIR	LC3-interacting region
MBC	4-methoxy-2,2'-bipyrrole-5-carbaldehyde
MEK	mitogen-activated protein kinase kinase
MS	mass spectrometry
mTOR	mechanistic target of rapamycin
mTORC1	mTOR complex 1
NAC	<i>N</i> -acetyl-L-cysteine
NRBF2	nuclear receptor-binding factor 2
NRPS	non-ribosomal peptide synthetases
PAINS	pan-assay interference compounds
PARP-1	Poly (ADP-ribose) polymerase 1
PAT	palmitoyltransferase
PE	phosphatidylethanolamine
PI	phosphatidylinositol
PI3P	phosphatidylinositol 3-phosphate
PI4P	phosphatidylinositol 4-phosphate
PI4KIIIβ	phosphatidylinositol 4-kinase IIIβ
PtdIns3K	phosphatidylinositol 3-kinase
Raptor	regulatory-associated protein of mTOR
RNA	ribonucleic acid
ROS	reactive oxygen species
RTSA	ratio-based thermal shift assay analysis
S6K	p70S6 kinase
SAR	structure-activity relationship
SNAP	synaptosomal-associated protein

## Abbreviations

---

SNARE	soluble <i>N</i> -ethylmaleimide-sensitive-factor attachment receptor
SQSTM1	sequestosome 1 (also known as p62)
TBK1	TANK-binding kinase 1
TGN	<i>trans</i> -Golgi network
TPP	thermal proteome profiling
TPP-CCR	thermal proteome profiling compound concentration range
TPP-TR	thermal proteome profiling temperature range
UCC	urothelial carcinoma cell
UDS	ubiquitin-interacting motif docking site
UIR	UDS-interacting region
ULK1	UNC-51-like kinase 1
UVRAG	UV radiation resistance-associated gene protein
V-ATPase	vacuolar-type H <sup>+</sup> -translocating ATPase
VPS34	vacuolar protein sorting 34
WIPI	WD repeat domain phosphoinositide-interacting protein
$\alpha$ SNAP	soluble <i>N</i> -ethylmaleimide sensitive factor attachment protein $\alpha$

## Amino acids

Alanine	A	Ala
Cysteine	C	Cys
Aspartic acid	D	Asp
Glutamic acid	E	Glu
Phenylalanine	F	Phe
Glycine	G	Gly
Histidine	H	His
Isoleucine	I	Ile
Lysine	K	Lys
Leucine	L	Leu
Methionine	M	Met
Asparagine	N	Asn
Proline	P	Pro
Glutamine	Q	Gln
Arginine	R	Arg
Serine	S	Ser
Threonine	T	Thr
Valine	V	Val
Tryptophan	W	Trp
Tyrosine	Y	Tyr

# Table of Contents

Acknowledgement.....	I
Abbreviations .....	II
Amino acids.....	V
Summary .....	1
Zusammenfassung .....	2
1 Introduction .....	3
1.1 (Macro)autophagy .....	3
1.1.1 Crosstalk of autophagy and apoptosis .....	6
1.1.2 The role of the Golgi apparatus in autophagy .....	8
1.1.3 Role of autophagy in cancer and chemoresistance .....	11
1.2 The process of drug discovery.....	13
1.2.1 Natural products in drug discovery .....	14
1.2.2 Natural products as autophagy modulators for cancer therapy .....	15
1.2.3 A brief history of the natural compound prodigiosin .....	17
2 Aims of this work.....	19
3 Summary of publications.....	20
3.1 Publications within the scope of this dissertation.....	20
3.1.1 Publication 1 .....	20
3.1.2 Publication 2.....	21
3.1.3 Publication 3 .....	22
3.2 Publications beyond the scope of this dissertation .....	23
3.2.1 Publication 4.....	23
3.2.2 Publication 5.....	23
3.2.3 Publication 6.....	24
3.2.4 Publication 7.....	24
4 Discussion .....	25
4.1 Elimination of therapy-resistant cancer.....	25
4.2 Prodigiosin as a lead structure.....	27

## Table of Contents

---

4.3	Elucidation of the molecular mechanism .....	29
5	References .....	33
	Licensing & Copyright.....	49
	Appendix .....	50

## Summary

Autophagy is an evolutionary conserved intracellular recycling system for the degradation of unneeded or harmful cargo like long-lived or damaged proteins and organelles, pathogens and xenobiotics. During autophagy, the cargo is engulfed by double-membraned autophagosomes and transported to the lysosomes for degradation into new energy sources and building blocks. Alterations of the autophagic process are associated with the development and promotion of various diseases such as cancer. Upregulated autophagy has been linked to chemotherapy resistance, cancer cell survival in nutrient-deficient environments and tumor metastasis and thus represents a promising target for cancer therapy. Nature provides researchers with an almost inexhaustible pool of highly bioactive small molecules. Therefore, we aimed to find and characterize natural compounds as potent lead structures for anti-cancer drug discovery to overcome chemotherapy resistance. Our main focus hereby lay on the characterization of the bacterial secondary metabolite prodigiosin.

A major challenge in the treatment of bladder cancer is the development of cisplatin resistance, which has been associated with upregulated autophagy. We observed that prodigiosin acts as a potent inhibitor of autophagy and can overcome chemotherapy resistance by resensitizing bladder cancer cells to apoptotic cell death. Prodigiosin sensitized both cisplatin-sensitive and -resistant urothelial carcinoma cell lines to cisplatin treatment with synergistic effects. Therefore, we propose prodigiosin as a potent lead structure for the therapy of cisplatin-sensitive and -resistant urothelial carcinomas, either as a single agent or in combinatory therapeutic approaches.

During the drug discovery phase lead compounds are chemically derivatized to perform structure-activity relationship studies to optimize their potency, selectivity and pharmacokinetic properties. By utilizing a systematic cell viability screening, we have provided evidence that A-ring substituted prodiginines with electron-donating methyl substituents are superior in their cytotoxicity against cisplatin-resistant urothelial carcinoma cells compared to the parental compound prodigiosin.

Understanding the mode of action by unveiling preferably all molecular targets of a drug candidate is crucial for structure optimization and for the assessment and prevention of potential side effects. We have provided evidence that the Golgi protein GRASP55 is a molecular target of prodigiosin by using mass spectrometry-based thermal proteome profiling. We observed that prodigiosin treatment severely affects Golgi apparatus morphology and functionality and that autophagosomes accumulate at GRASP55-positive structures, pointing towards the involvement of an altered Golgi function in the autophagy-inhibitory effect of this natural compound. Therefore, we propose that prodigiosin affects autophagy and Golgi apparatus integrity in an interlinked mode of action involving the regulation of organelle alkalization and the Golgi stacking protein GRASP55.

## Zusammenfassung

Autophagie ist ein evolutionär konservierter intrazellulärer Recyclingprozess für den Abbau von langlebigen oder beschädigten Proteinen und Organellen, Krankheitserregern und Xenobiotika. Während der Autophagie werden die abzubauenen Zellbestandteile von Autophagosomen isoliert und zum Lysosom transportiert, wo sie zu neuen Makronährstoffen abgebaut werden. Veränderungen in der Autophagie werden mit der Entstehung verschiedener Krankheiten, wie z. B. Krebs, in Verbindung gebracht. Die Induktion von autophagischen Prozessen wurde mit Chemotherapieresistenz, dem Überleben von Krebszellen in nährstoffarmen Umgebungen und der Metastasierung von Tumoren assoziiert und stellt somit ein vielversprechendes Ziel für die Krebstherapie dar. Die Natur bietet Forschern ein nahezu unerschöpfliches Angebot an hoch bioaktiven Verbindungen. Daher haben wir uns zum Ziel gesetzt, Naturstoffe als potente Leitstrukturen für die Entwicklung von Krebsmedikamenten zur Überwindung von Chemotherapieresistenz zu finden und zu charakterisieren. Dabei lag unser Fokus auf der Charakterisierung des bakteriellen Sekundärmetaboliten Prodigiosin.

Eine Herausforderung bei der Behandlung von Blasenkrebs ist die Entwicklung von Cisplatinresistenzen, welche unter anderem mit einer hochregulierten Autophagie in Verbindung gebracht werden. Wir konnten beobachten, dass Prodigiosin als potenter Inhibitor der Autophagie Urothelkarzinomzellen für den Cisplatin-induzierten apoptotischen Zelltod resensibilisieren kann. Dabei zeigte Prodigiosin sowohl in Cisplatin-sensitiven als auch in Cisplatin-resistenten Zellen synergistische Effekte mit Cisplatin. Aus diesem Grund schlagen wir Prodigiosin als vielversprechende Leitstruktur für die Mono- oder Kombinationstherapie von Cisplatin-sensitiven und -resistenten Urothelkarzinomen vor.

Im Zuge der Arzneimittelforschung werden Leitstrukturen derivatisiert, um so mit ihnen Studien zur Struktur-Aktivitäts-Beziehung durchzuführen und ihre Potenz, Selektivität und pharmakokinetischen Eigenschaften zu optimieren. Mit Hilfe eines systematischen Zellviabilitätsscreenings konnten wir nachweisen, dass A-Ring-substituierte Prodiginine mit Methylsubstituenten im Vergleich zu Prodigiosin eine höhere Zytotoxizität gegen Cisplatin-resistente Urothelkarzinomzellen aufweisen.

Für die Strukturoptimierung eines Arzneimittelkandidaten ist es entscheidend, seinen molekularen Wirkmechanismus aufzuklären. Durch ein Massenspektrometrie-basiertes Verfahren konnten wir zeigen, dass Prodigiosin an das Golgi-Protein GRASP55 bindet. Wir haben beobachtet, dass die Behandlung mit Prodigiosin die Morphologie und Funktionalität des Golgi-Apparates stark beeinträchtigt und dass sich Autophagosomen an GRASP55-positiven Strukturen ansammeln, was auf eine veränderte Golgi-Funktion als Teil der Autophagie-hemmenden Wirkung dieses Naturstoffs hindeutet. Daher gehen wir davon aus, dass Prodigiosin die Autophagie und die Integrität des Golgi-Apparats in einem miteinander verknüpften Wirkmechanismus beeinflusst, der die pH-Veränderung saurer zellulärer Organellen und die Bindung an das Golgi-Strukturprotein GRASP55 beinhaltet.

# 1 Introduction

Autophagy is an intracellular waste management system that is evolutionary conserved between many organisms from yeast to mammalian cells and is crucial to maintain the cellular homeostasis through the degradation of unneeded or harmful cargo like long-lived or damaged proteins and organelles into new energy sources and building blocks. The term "autophagy" was introduced by Christian de Duve at a conference on lysosomes in 1963 and is derived from the Greek words “αυτός” meaning “self” and “φαγεῖν” meaning “to eat”. The Nobel Prize, awarded to Yoshinori Ōsumi in 2016 "for his discoveries of mechanisms for autophagy", underlines the scientific and clinical relevance of the autophagic process.

Dysregulated autophagy plays a role in numerous diseases. In cancer, autophagy is often referred to as a "double-edged sword". While the accumulation of harmful extracellular noxes and damaged proteins due to impaired autophagy can stimulate cancer induction or progression, upregulated autophagy can play a role in chemotherapy resistance, cancer cell survival in nutrient-deficient environments and tumor metastasis. Therefore, the autophagic machinery represents a promising target for cancer therapy. Our research idea is to find and characterize new natural compounds as modulators of autophagy to provide potent lead structures for the drug development process. Nature therefor provides chemists and biologists with an almost inexhaustible pool of highly bioactive, selective and structurally complex small molecules. With the identification of new autophagy inhibitors, our aim is to target cancer cells and overcome chemotherapy resistance.

## 1.1 (Macro)autophagy

The hypernym autophagy can be subdivided into three main classes, depending on the autophagic cargo and its delivery mechanism to the lysosome. Chaperone-mediated autophagy describes a process in which soluble cytosolic cargo proteins, containing the pentapeptide KFERQ as a specific targeting motif in their amino acid sequence, bind to the chaperone heat shock-cognate protein of 70 kDa (HSP70) and are then targeted to lysosomes. After transport to the lysosomal surface, cargo-HSP70 complexes are internalized by the lysosome-associated membrane protein 2A (LAMP2A) and are rapidly degraded (Kaushik and Cuervo 2018). During microautophagy, small cytosolic portions are directly incorporated into lysosomes (Wang, Klionsky, and Shen 2022). The most studied subform is macroautophagy, which is characterized by the transport of the autophagic cargo to the lysosome in double-membraned vesicles called autophagosomes and their fusion with lysosomes to autolysosomes for degradation and recycling (Yin, Pascual, and Klionsky 2016). In contrast to the other sub forms, the cargo of macroautophagy is not limited to cytosolic proteins, but rather diverse including, but not limited to, components of the nucleus, xenobiotics, pathogens and even whole cellular organelles.

Macroautophagy, hereafter referred to as autophagy, occurs at a basal level in all cells to prevent the accumulation of damaged macromolecules by recycling them into new energy sources and building blocks such as amino acids and lipids, thus playing a pivotal role in cellular quality control and homeostasis (Ariosa et al. 2021). Autophagy can be divided into the following chronological steps: initiation of autophagy, elongation of the isolation membrane, maturation of the autophagosome, fusion of autophagosome and lysosome, and finally, the degradation of autophagic cargo within the autolysosome (Yin, Pascual, and Klionsky 2016). In each of these steps, one or several of the following six distinct functional complexes consisting of autophagy-related (ATG) proteins are involved: the initiating UNC-51-like kinase 1 (ULK1) protein kinase complex, the class III phosphatidylinositol 3-kinase (PtdIns3K) complex, the transmembrane protein ATG9, the WD repeat domain phosphoinositide-interacting protein (WIPI) complex, the ATG5-ATG12-ATG16L conjugation system and the LC3/GABARAP-PE conjugation system (Suzuki et al. 2017).

Autophagy functions as a cellular survival mechanism that can be rapidly upregulated under certain stress conditions, such as starvation, absence of growth factors, hypoxia, endoplasmic reticulum (ER) stress, DNA damage and infections (Ariosa et al. 2021; Levine and Kroemer 2008). The central complex for the initiation of autophagy upon stress conditions is the ULK1 protein kinase complex, which consists of the Ser/Thr kinase ULK1, the adaptor proteins ATG13 and ATG101 and the focal adhesion kinase-interacting protein of 200 kDa (FIP200). The ULK1 complex integrates nutrient and energy stress signals from the mechanistic target of rapamycin (mTOR) (Hosokawa et al. 2009) and AMP-activated protein kinase (AMPK) (Ariosa et al. 2021; Mack et al. 2012). Under stress conditions like nutrient withdrawal, the mTOR complex 1 (mTORC1) dissociates from the ULK1 complex, leading to an autophagy-initiating autophosphorylation of ULK1 and ULK1-dependent phosphorylation of ATG13 and FIP200 (Ganley et al. 2009; Hosokawa et al. 2009; Jung et al. 2009; Kamada et al. 2010). The energy sensor AMPK, in turn, is activated by a low ATP:AMP ratio and has a dual mechanism for initiating autophagy. It activates the ULK1 complex directly through phosphorylation of ULK1 (Mack et al. 2012) and indirectly by phosphorylating the regulatory-associated protein of mTOR (Raptor) which inactivates mTORC1 (Gwinn et al. 2008).

To initiate the autophagic process, the ULK1 complex and the class III PtdIns3K complex I translocate to the autophagosome formation site (Itakura and Mizushima 2010; Matsunaga et al. 2010). At the autophagosome formation site, the class III PtdIns3K lipid kinase complex I, consisting of the catalytic subunit vacuolar protein sorting 34 (VPS34), Beclin-1, VPS15, ATG14 and the nuclear receptor-binding factor 2 (NRBF2), is activated through ULK1-dependent phosphorylation of Beclin-1 and ATG14 (Park et al. 2016; Russell et al. 2013). Once activated, VPS34 catalyzes the phosphorylation of phosphoinositide to phosphatidylinositol 3-phosphate (PI3P). Accumulation of PI3P on the isolation membrane is required for the recruitment of downstream effectors like double FYVE domain containing protein (DFCP) or WIPI1/2 (Axe et al. 2008; Matsunaga et al. 2010; Proikas-Cezanne et al. 2015) to pursue the autophagic process.

The PI3P binding protein WIPI2 is essential for the biogenesis of autophagosomes (Polson et al. 2010; Proikas-Cezanne et al. 2015) by binding to ATG16L and thereby recruiting the ATG12-ATG5-ATG16L complex to the isolation membrane (Dooley et al. 2014). For the assembly of this complex, ATG7 first binds ATP-dependently to ATG12 (Mizushima, Noda, et al. 1998) and then transfers it to ATG10 (Kaiser et al. 2012). Afterwards, ATG12 is conjugated to ATG5 (Mizushima, Sugita, et al. 1998), followed by the binding of the ATG12-ATG5 complex to dimerized ATG16L (Fujioka et al. 2010; Mizushima et al. 2003). The ATG12-ATG5-ATG16L complex is responsible for the lipidation of ATG8 family members (Otomo et al. 2013). The ATG8 family is a group of ubiquitin-like proteins consisting of the subfamilies microtubule associated protein 1 light chain 3 (LC3) and gamma-aminobutyric acid receptor-associated proteins (GABARAPs). To initialize the lipidation process, the C-terminus of LC3 is cleaved by ATG4 to expose a glycine residue, thereby producing LC3-I (Kabeya et al. 2000; Kirisako et al. 2000), which is activated by ATG7 (Noda et al. 2011) and subsequently transferred to ATG3. The ATG12-ATG5-ATG16L complex then binds to ATG3 and facilitates the conjugation to the lipid molecule phosphatidylethanolamine (PE) (Metlagel et al. 2013). The lipid source for autophagosome expansion is still controversial, but recent results indicate ER, Golgi, mitochondria and endosomes as candidates (Walker and Ktistakis 2020). Lipidated LC3 is termed LC3-II (Taherbhoy et al. 2011; Tanida, Ueno, and Kominami 2004; Kabeya et al. 2004) and is anchored to the inner and outer membrane of the building autophagosome by its lipid tail (Dooley et al. 2014), facilitating autophagosome expansion and closure (Nakatogawa, Ichimura, and Ohsumi 2007; Xie, Nair, and Klionsky 2008). To underline how crucial this lipidation step is for autophagy, previous experiments have shown that knockout of proteins like ATG3 or ATG5 leads to a complete blockage of autophagy (Fujita et al. 2008; Kuma et al. 2004). ATG8 family proteins like LC3 can act as a binding platform on the autophagosomal membrane. Therefore, an LC3-interacting region (LIR) motif can be found on many proteins of the autophagic machinery (Kraft et al. 2012; Lee and Lee 2016), as well as on selective autophagy receptors that target the autophagic cargo to the autophagosome (Birgisdottir, Lamark, and Johansen 2013; Kirkin and Rogov 2019). During autophagosome maturation, the ATG proteins are released from the outer autophagosomal membrane by ATG4-dependent cleavage of the lipidated LC3 (Nakatogawa et al. 2012) and ULK1-dependent phosphorylation of ATG4 acts as a switch for incorporation and release of LC3 into autophagosomal membranes (Pengo et al. 2017; Sanchez-Wandelmer et al. 2017).

The mature autophagosomes and lysosomes are transported to each other via microtubular structures (Lorincz and Juhasz 2020; Jahreiss, Menzies, and Rubinsztein 2008; Nakamura and Yoshimori 2017) for the fusion to autolysosomes. This autophagosome-lysosome fusion is facilitated by synaptosomal-associated proteins (SNAPs), soluble *N*-ethylmaleimide-sensitive-factor attachment receptors (SNAREs) (Lorincz and Juhasz 2020; Wang et al. 2016) and multiple small GTPases (Lorincz and Juhasz 2020; Stenmark 2009). Furthermore, many additional tethers like the Golgi protein GRASP55 have been described to promote autophagosome-lysosome fusion (Zhang et al. 2019; Zhang et al. 2018; Lorincz and Juhasz 2020). As a last step of autophagy, the lysosomal enzymes degrade the autophagic

cargo inside the autolysosome together with LC3 and selective autophagy receptors of the inner autophagosomal membrane to new energy sources and building blocks (Yim and Mizushima 2020). For an optimal proteolytic activity of the lysosomal hydrolases, a steady acidic environment has to be maintained inside the lysosome via proton pumping vacuolar-type  $H^+$ -translocating ATPases (V-ATPases) and chloride ion channels (Ishida et al. 2013; Mindell 2012).

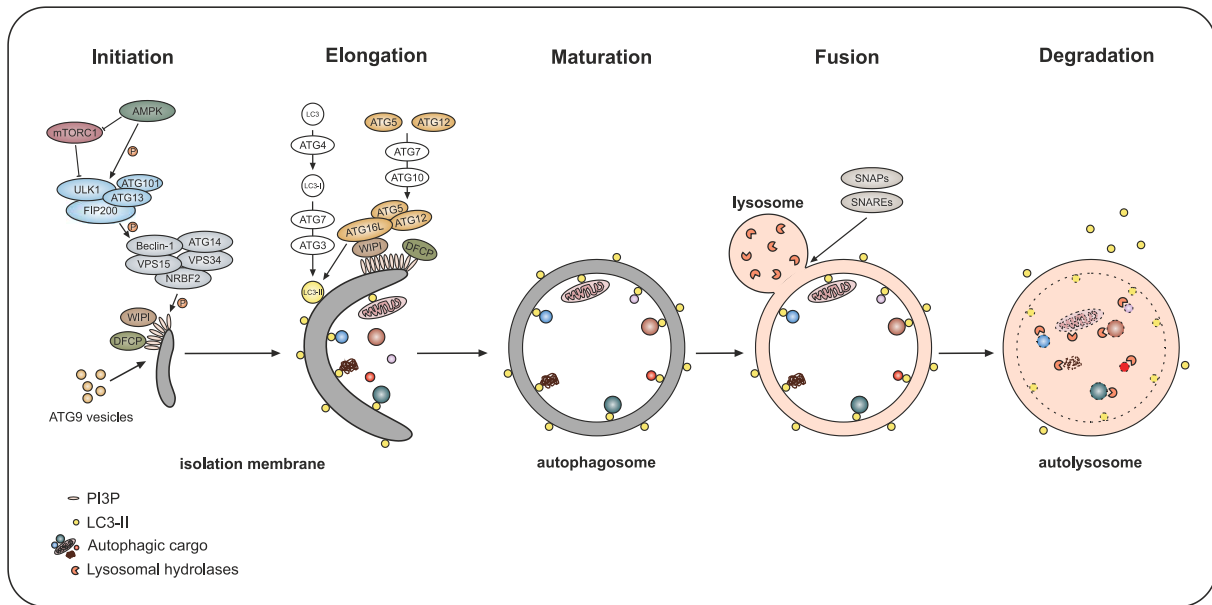


**Figure 1: The process of (Macro-)autophagy.** Upon cellular stress, AMPK and mTORC1 can activate the ULK1 complex, consisting of ULK1, FIP200, ATG13 and ATG101. The ULK1 complex, in turn, activates the class III PtdIns3K complex 1, consisting of Beclin-1, ATG14, VPS34, VPS15 and NRBF2. Both complexes translocate to the initiation membrane for the induction of autophagy. The class III PtdIns3K complex 1 generates PI3P that accumulates at the initiation membrane and recruits DFCP and WIPI. WIPI recruits the ATG12-ATG5-ATG16L complex, which, together with ATG7 and ATG3, is responsible for the lipidation of LC3. Lipidated LC3-II decorates the inner and outer membrane of the building phagophore and can bind the autophagic cargo like mitochondria, dysfunctional and aggregated proteins via selective autophagy receptors. After closure of the isolation membrane the fusion of the mature autophagosome with a lysosome to an autolysosome is facilitated by different tethering factors like SNAPs and SNAREs. Inside the autolysosome, lysosomal hydrolases degrade the cargo and LC3 of the inner autophagosomal membrane to new energy sources and building blocks, whereas LC3 attached to the outer autophagosomal membrane is recycled.

### 1.1.1 Crosstalk of autophagy and apoptosis

Almost every step of autophagy can be modulated by various proteins which are not classically involved in the above-described core autophagic machinery. Conversely, several ATG proteins do not only play a role in autophagy but emerging evidence suggests that most, if not all, components of the autophagic process have autophagy-independent functions. With these, the ATG proteins connect autophagy with diverse other signaling pathways, such as apoptosis (Galluzzi and Green 2019; Thorburn 2008).

Apoptosis describes a highly regulated and strictly controlled cell death mechanism of eukaryotic cells. It is crucial for various processes like embryonic development, the proper functioning of the immune system and generally as a homeostatic mechanism to maintain cell populations in tissues (Elmore 2007). Apoptosis can be divided into the extrinsic or death receptor pathway and the intrinsic or mitochondrial

pathway. The extrinsic pathway is activated by external death signals that activate death receptors on the cell surface, leading to the formation of the death-inducing signaling complex (DISC) and ultimately to the activation of the initiator caspase 8 (Kischkel et al. 1995). The intrinsic pathway can be activated by a multitude of internal stimuli, like DNA damage, hypoxia, viral infections and toxins. All of these stimuli lead to permeabilization of the outer mitochondrial membrane and subsequent release of cytochrome c, which binds and activates Apaf-1 and the initiator caspase 9, and thereby forms the apoptosome (Hill et al. 2004). Both pathways ultimately activate effector caspases, which are, like all caspases, cysteine proteases that can cleave their target proteins following aspartic acid residues (Alnemri et al. 1996). Activation of effector caspases also leads to the degradation of chromosomal DNA and induces cytoskeletal reorganization and disintegration of the cell into apoptotic bodies that are recycled by phagocytotic uptake to prevent inflammation (Fadok et al. 2001; Peter et al. 2010). The apoptotic and autophagic pathways can regulate each other and are both additionally influenced by several upstream signaling pathways (Bata and Cosford 2021). With autophagy promoting survival and apoptosis inducing cell death (Mukhopadhyay et al. 2014), both pathways and their crosstalk have an integral role in diverse pathological processes, including cancer, homeostasis and ageing.

A major switch for the interplay of autophagy and apoptosis are reactive oxygen species (ROS), which can be produced by xenobiotics like chemotherapeutics. Autophagy initiation can be mediated by superoxide which is increasingly produced during starvation (Chen, Azad, and Gibson 2009). Additionally, the excessive presence of ROS can lead to mitochondrial damage, leading to the induction of mitophagy and, in more severe cases, to the induction of the intrinsic apoptotic pathway. Another mediator is the tumor suppressor protein p53, which regulates the genomic stability, the decision between cell death and proliferation and the metabolism of the cell. Activated p53 can induce apoptosis by activating proapoptotic genes (Marino et al. 2014). The regulation of autophagy by p53 remains to be fully elucidated (Maiuri et al. 2010). Nevertheless, cytoplasmatic p53 has been shown to inhibit the formation of the ULK1 complex and thereby prevent autophagosome formation by coaggregating with FIP200 (Morselli et al. 2011). However, p53 can also activate autophagy by regulating the gene expression of the AMPK/mTOR pathway (Feng et al. 2007), while autophagy, in turn, has been shown to suppress p53 in some cancers and thereby promote cell survival and inhibit apoptotic cell death (Huo et al. 2013; Yang et al. 2020).

As another central part of this interplay, the B-cell lymphoma 2 (Bcl-2) family closely regulates the balance between cell survival and cell death (Adams and Cory 2018). It consists of pro-survival, pro-death and Bcl-2 homology 3 (BH3)-only proteins. The pro-survival Bcl-2 proteins can bind and inhibit the pro-death family members Bcl-2-associated X-protein (BAX) and Bcl-2 homologous antagonist/killer (BAK). For the induction of intrinsic apoptosis via cytochrome c release, BH3-only proteins bind the pro-survival Bcl-2 proteins and thereby release and activate BAX and BAK, which oligomerize and build pores in the outer mitochondrial membrane (Garrido et al. 2006). The regulatory mechanisms of Bcl-2 family proteins in autophagy are multifaceted, but their primary interaction partner

is Beclin-1 (Kang et al. 2011; Pattingre et al. 2005). At high nutrient levels, Beclin-1 forms a complex with Bcl-2 through its BH3 domain and is thereby retracted from interacting with VPS34, leading to a downregulation of autophagy (Pattingre et al. 2005). However, Beclin-1 has a weaker binding affinity to Bcl-2 than other BH3-containing proteins and is released from Bcl-2 under mild stress conditions to induce autophagy as a pro-survival mechanism while Bcl-2 still binds and inhibits the pro-apoptotic members of the Bcl-2 family. Under ongoing severe cellular stress, Bcl-2 is also released from the Bcl-2-BAX complex for the induction of apoptosis (Mukhopadhyay et al. 2014). After the cellular switch from pro-survival autophagy to apoptosis, autophagy is downregulated through the caspase-mediated cleavage of Beclin-1 (Luo and Rubinsztein 2010) and various other ATG proteins (Tsapras and Nezis 2017; Norman, Cohen, and Bampton 2010; Li et al. 2011; Oral et al. 2012). Conversely, autophagy can also downregulate apoptosis by degrading caspases (Tsapras and Nezis 2017; Hou et al. 2010) and damaged mitochondria to prevent the release of cytochrome c (Ma, Chen, et al. 2020). Normally, autophagy is a cytoprotective process as a response to cellular stress, but under certain conditions, excessively enhanced autophagic flux can lead to autophagy-dependent cell death (ADCD). ADCD defines a form of regulated cell death that strictly depends on the components of the autophagic machinery, rather than a change in autophagic flux that accommodates other forms of cell death (Bata and Cosford 2021; Galluzzi et al. 2018; Kriel and Loos 2019).

### **1.1.2 The role of the Golgi apparatus in autophagy**

The Golgi apparatus is located in the perinuclear region of mammalian cells (Ladinsky et al. 1999). It receives the majority of the endoplasmic reticulum output and acts as a processing and dispatching station for the sorting of newly synthesized soluble and transmembrane proteins and lipids (Viotti 2016; Rohn et al. 2000). After sorting and post-translational modifications, the proteins and lipids are transported to their final destinations, which can be the cell surface, secretory granules, lysosomes or the endosomal system (Bravo et al. 1994).

To fulfil these functions, the Golgi apparatus is organized in stacks of multiple flattened cisternae that are laterally linked into a ribbon-like structure that is established by the Golgi reassembly stacking proteins of 55 kDa (GRASP55) and of 65 kDa (GRASP65) (Klumperman 2011), which are located at the *trans* and *cis* cisternae, respectively (Barr et al. 1997; Shorter et al. 1999). These GRASP proteins possess a conserved GRASP domain at the N-terminus that contains a membrane anchor and form dimers and trans-oligomers to link the adjacent cisternae into stacks (Wang et al. 2003; Xiang and Wang 2010; Puthenveedu et al. 2006). Cargo from the ER enters a Golgi stack at the *cis*-side and is then transported through the medial and *trans*-Golgi network (TGN), where it is eventually sorted into transport carriers and secretory vesicles to be delivered to the final destinations (Glick and Nakano 2009; Tie et al. 2017). This strictly organized stacked structure is essential for the correct functioning of the

Golgi apparatus, since unstacking of the Golgi cisternae due to GRASP depletion or malfunction leads to accelerated protein trafficking and impairment of protein glycosylation (Wang and Seemann 2011; Wang et al. 2008).

In addition to being the central hub for post-translational modifications and sorting of proteins and lipids, the Golgi apparatus is involved in various cellular processes, including, but not limited to, mitosis, DNA repair, apoptosis, inflammation and autophagy (Deng et al. 2020; Kulkarni-Gosavi, Makhoul, and Gleeson 2019). The mutual influence of Golgi apparatus and autophagy becomes visible in multi-layered processes: (i) the Golgi apparatus plays a role in trafficking key proteins of the autophagic process, (ii) Golgi-related proteins are directly involved in the formation of autophagosomes and regulation of autophagy and (iii) Golgi fragmentation is accompanied by the selective autophagic degradation of the Golgi apparatus, named Golgiphagy.

In previous literature, the Golgi apparatus has been designated as an "assembly line" to the autophagosome (De Tito et al. 2020) and key regulators of the autophagic pathway traffic from the Golgi to the forming autophagosome. Those include the phosphatidylinositol 4-kinase III $\beta$  (PI4KIII $\beta$ ), which mediates PI4P production at the initiation membrane site and the lipid scramblase ATG9A (Judith et al. 2019; Deng et al. 2020). In mammalian cells, ATG9-containing vesicles localize at the TGN in nutrient-rich conditions, whereas during starvation-induced autophagy they can be found in both the perinuclear region and co-localized with endosomal compartments (Zhou et al. 2017; Imai et al. 2016; Mari et al. 2010). Thus, malfunctioning of the Golgi apparatus can influence ATG9 transportation from the Golgi to the building autophagosome and ultimately disrupt proper autophagosome formation.

Autophagy depends on the integrity and function of the Golgi apparatus, since the loss of Golgi-related proteins can interrupt the autophagic process. One major example for autophagy-relevant Golgi proteins is the soluble *N*-ethylmaleimide sensitive factor attachment protein  $\alpha$  ( $\alpha$ SNAP) which is a component of the vesicle trafficking machine that mediates the transport of vesicles from the ER to the *cis*-Golgi (Naydenov et al. 2014; Naydenov, Harris, Brown, et al. 2012). The loss of  $\alpha$ SNAP not only triggers Golgi fragmentation and impairs protein glycosylation (Naydenov et al. 2014), it also leads to the induction of autophagy (Naydenov, Harris, Morales, et al. 2012). Naydenov et al. described  $\alpha$ SNAP as a negative regulator of autophagy that acts by enhancing mTOR signalling and by regulating the integrity of the Golgi complex (Naydenov, Harris, Morales, et al. 2012). In addition, some Golgi apparatus related proteins play a direct role in the formation and regulation of autophagy (reviewed in (Deng et al. 2020)). One example is the Golgi stacking protein GRASP55, that has been previously described to act as a specific energy and nutrient sensor (Ahat, Li, and Wang 2019) and to be involved in unconventional secretion (Ahat et al. 2022; Nüchel et al. 2021) and autophagy (Lorincz and Juhasz 2020; Zhang et al. 2019; Zhang et al. 2018). GRASP55 can act as a bridging protein that facilitates autophagosome-lysosome fusion through a LIR motif and interaction with LAMP2 (Zhang et al. 2019; Zhang et al. 2018). Zhang et al. also described that GRASP55 interacts with Beclin-1 to facilitate the

assembly and membrane association of the PtdIns3K UV radiation resistance-associated gene protein (UVRAG) complex (Zhang et al. 2019). Furthermore, mTORC1—a major autophagy-regulating kinase—directly phosphorylates GRASP55 and thereby regulates its localization (Nüchel et al. 2021).

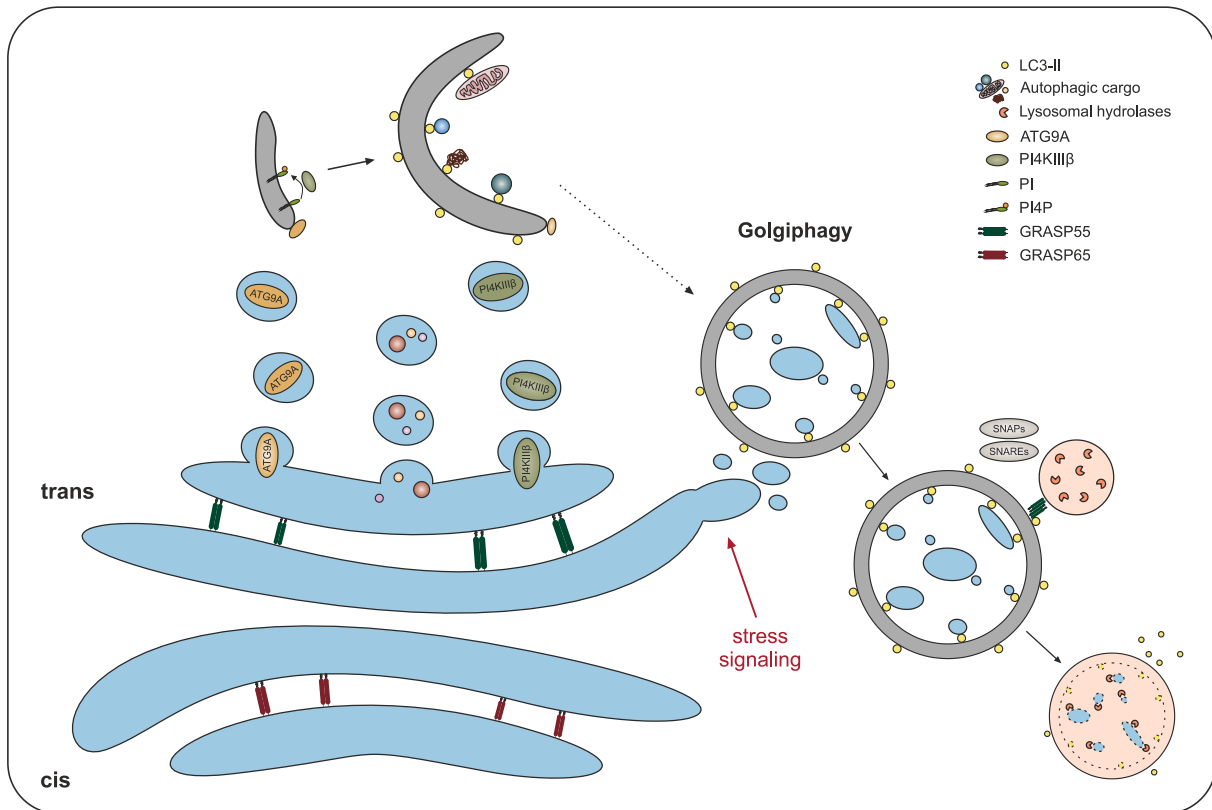


**Figure 2: The interplay of autophagy and the Golgi apparatus.** The stacked structure of the Golgi apparatus is established by the Golgi reassembly stacking proteins GRASP65 and GRASP55, which are located in the *cis* and *trans* cisternae, respectively. The Golgi apparatus acts as central hub for the sorting of proteins that are delivered to their final destinations in vesicles. Among those are key proteins for autophagy like the lipid scramblase ATG9A and PI4KIIIβ that mediates PI4P production at the initiation membrane. After autophagosome maturation, Golgi apparatus associated proteins like GRASP55, SNAPs and SNAREs are involved in autophagosome-lysosome fusion for the degradation of autophagic cargo. Cellular stress leads to Golgi fragmentation that is accompanied by the selective autophagic degradation of the Golgi apparatus, named Golgiphagy.

In contrast to other selective autophagic processes, Golgiphagy is rather unexplored. However, Nthiga et al. identified the soluble reticulophagy receptor calcium-binding and coiled coil domain-containing protein 1 (CALCOCO1) as a Golgiphagy receptor in response to nutrient deprivation (Nthiga, Kumar Shrestha, et al. 2021). CALCOCO1 can interact with Golgi membranes by binding to cytoplasmic Ankyrin repeat (AR) domains of specific Golgi resident palmitoyltransferases (PATs) to recruit ATG8-family proteins of the autophagy machinery via an atypical LIR-motif and a ubiquitin-interacting motif docking site (UDS)-interacting region (UIR) (Nthiga, Shrestha, et al. 2021). They observed that stress signals like nutrient starvation increase the amount of Golgi components leading to a disassembly of the Golgi apparatus into fragments. These fragments are then engulfed by autophagosomes and degraded to remove excess Golgi and to restore pre-stress status.

### **1.1.3 Role of autophagy in cancer and chemoresistance**

Whereas in the beginning of autophagy research the focus lay on identifying key proteins of the process, it progressively shifted towards more practical questions with the aim to understand what role autophagy plays in diverse disease settings and how the autophagic process can be regulated (Ariosa et al. 2021). Compared to other pathophysiologies in which autophagy plays a role like aging, metabolic and neurodegenerative diseases, the role of autophagy in cancer is quite complex (Levine and Kroemer 2008). Depending on the context and stage of tumor development, autophagy has a dual role either as a suppressive or a promotive force and is therefore frequently referred to as a "double-edged sword" (Kimmelman 2011; Rybstein et al. 2018; White 2015).

In the initial stages of tumor development, cytoprotective autophagy plays an anticancer role by maintaining cellular and genomic integrity (Nassour et al. 2019; Wen and Klionsky 2020). Dysfunctions in autophagy lead to a failure in protein and organelle quality control, toxic ROS production and ultimately to inflammation, tissue damage and genome instability, causing an increased susceptibility to malignant degeneration (Mizushima and Komatsu 2011; White 2012). The first study that linked autophagy and tumorigenesis was conducted by Beth Levine's group in 1999, who identified Beclin-1 as a haploinsufficient tumor suppressor in mice (Liang et al. 1999; Yue et al. 2003). The mice developed hepatocellular carcinoma after an allelic loss of Beclin-1 and subsequent studies have shown that a monoallelic deletion of Beclin-1 can be found in several cancer cell lines (Aita et al. 1999; Ariosa et al. 2021). Since then, mutations in several proteins directly or indirectly involved in the process of autophagy have been observed in various types of cancer, underlining the central role of autophagy in different stages of cancer development and progression. Those proteins include, but are not limited to ATG5, ATG7 (Takamura et al. 2011), UVRAG (Liang et al. 2006; Liang et al. 2007) and the V-ATPase (Whitton et al. 2018). These findings underline the important role of autophagy-associated proteins in the suppression of spontaneous tumorigenesis.

Being primarily a mechanism for stress tolerance and the promotion of cell survival under physiological conditions, autophagy can be misused by malignant cells for the support of disease progression and pathological proliferation (White 2012). During tumor development and expansion, autophagy is robustly activated in cancer cells of solid tumors due to multiple stressors, including starvation, hypoxia, damaging stimuli and growth factor deprivation (Degenhardt et al. 2006; White 2012). In this process, autophagy and secretory autophagy occurring in the circumjacent stroma cells like cancer-associated fibroblasts (CAFs) can provide nutrients to promote the initiation and malignant progression of cancer (Chaudhri et al. 2013; New et al. 2017; Salem et al. 2012). In addition to the promotion of the primary tumor, autophagy is also involved in metastasis, as shown by various studies that found enrichment of LC3 and other ATG proteins in metastatic cancer cells (Galavotti et al. 2013; Han et al. 2011; Lazova et al. 2012). The detachment from the main tumor usually leads to anoikis (a form of programmed cell death) of the malignant cells, but protective autophagy can be induced to promote cell survival (Fung et

al. 2008). Therefore, autophagy was included into the hallmarks of cancer as a sub item of the category "Resisting Cell Death" (Hanahan and Weinberg 2011).

The already enhanced autophagy in cancer cells can be further induced as a side effect of a multitude of commonly used anticancer therapies and contribute to chemotherapy resistance (Abedin et al. 2007; Carew et al. 2007; Chen and Karantza 2011). Conversely, inhibition of autophagy can be used to sensitize cancer cells to the lethal effects of cancer therapies, including chemotherapy, radiotherapy and targeted therapies (Amaravadi et al. 2007; Chen et al. 2010; Hu et al. 2012; Schlötermann et al. 2018). For this purpose, researchers are interested to unravel the molecular mechanisms of the highly complex process of autophagy induction in cancer cells to find potential therapeutic targets for drug development.

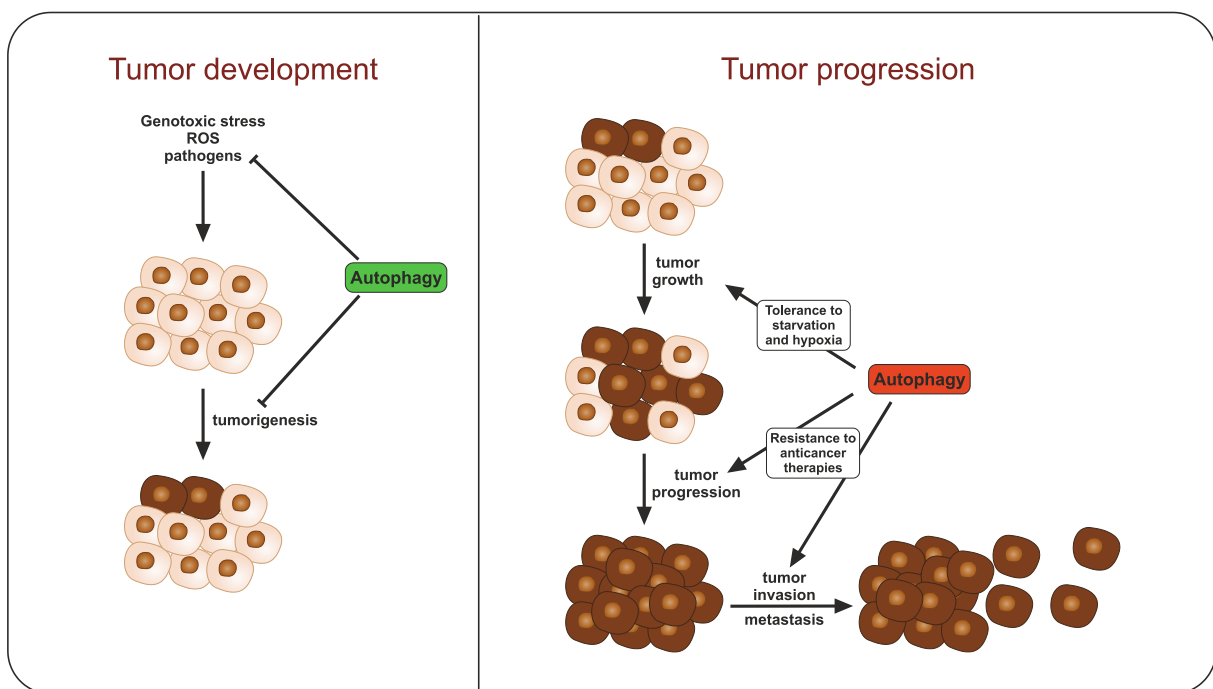


**Figure 3 The dual role of autophagy in cancer.** Under physiological conditions, autophagy plays a cytoprotective role by maintaining cellular and genomic integrity. Defects in autophagy make cells vulnerable to genotoxic stress, ROS and pathogens and favor tumorigenesis. In malignant cells, autophagy contributes to stress tolerance and energy supply and thereby promotes tumor growth. Enhanced autophagy can also lead to resistance to anticancer therapies and tumor invasion and metastasis.

For the inhibition of early stage autophagy, the catalytic subunits of the ULK1 complex and the class III PtdIns3K complex I, which play a crucial role in phagophore nucleation, are potential targets (Santana-Codina, Mancias, and Kimmelman 2017). Additionally, as a master regulator of autophagy, mTOR has become an appealing therapeutic target. For example, the mTOR inhibitor everolimus, a paralogue of rapamycin, has been approved by the FDA for the treatment of several cancers (Kim and Guan 2015). However, the effectiveness of mTOR inhibition seems to depend on cancer cell type, and with mTOR being a central signalling hub of cell metabolism, blocking mTOR activity can lead to severe side effects (Wen and Klionsky 2020). The clinical focus currently lays on the inhibition of late-stage autophagy by blocking the degradation of autophagic cargo utilizing chloroquine (CQ) and hydroxychloroquine (HCQ) which are already approved drugs for other clinical indications. Although clinical trials of CQ

and HCQ in combination with a variety of other therapeutic compounds have shown promising results, the downside of these compounds is their lack of specificity (Wen and Klionsky 2020). They can not only interfere with other biological processes, but also huge variations in the maximum tolerated dose and an inconsistent autophagy inhibition have been observed because their uptake is highly dependent on the pH, which can differ between different tumor microenvironments (Pellegrini et al. 2014). The balance between therapeutic potency and cytotoxicity of autophagy inhibitors must be considered due to the crucial role of autophagy in cell homeostasis to provide a sufficient therapeutic window. Moreover, patients with tumors prone to autophagy modulation due to a genetic predisposition should be identified to optimize the therapeutic outcome (Wen and Klionsky 2020; White 2012). As a conclusion, after more than 60 years of autophagy research, we have barely scratched the surface of the complexity of the autophagic process, its interaction partners and manipulation strategies that might become potent therapies.

## **1.2 The process of drug discovery**

Modern drug discovery can be distinguished into two different approaches. First, the target identification and structure optimization of a specific molecule with known biological activity. This strategy is mostly applied for off-target use of already approved drugs, traditional medicines and natural compounds of which it is known by experience that they have a biological activity. Second, the more classical approach, in which compound libraries are screened to find a modulator of a specified molecular target. The process can be distinguished into the drug discovery, the drug development and the clinical phase.

During drug discovery, the first step is to develop a hypothesis, which proteins and pathways are key players in a disease setting that has not been adequately addressed so far. After validation of the identified target, the next step is the development of biochemical and/or cell-based high throughput screening (HTS) assays with the capacity to screen large compound libraries to identify molecules of interest (Hughes et al. 2011). To allow a knowledge-based selection of hit molecules, HTS is often accompanied by virtual screens and molecular modelling (McInnes 2007). Compounds that are known to be frequent hitters, toxic or pan-assay interference compounds (PAINS) have to be ruled out (Baell and Holloway 2010).

With the identified lead structures, chemistry programmes are run to optimize the potency, selectivity and pharmacokinetic properties of the compounds by synthesising various structural analogues. In this process, the compounds are clustered based on their structure to identify a structure-activity relationship (SAR). The lead compounds should be modified to obey more drug-like chemical parameters as defined by Lipinski's Rule of Five (Lipinski 2004; Lipinski et al. 2001). Those rules include that the drug candidate should contain no more than 5 hydrogen bond donors and 10 hydrogen bond acceptors, a

molecular mass less than 500 daltons and a calculated octanol-water coefficient that does not exceed 5. The analogue libraries are then screened in various *in vitro* assays designed to provide important information regarding their physicochemical properties, their activity and their absorption, distribution, metabolism and excretion (ADME). Simultaneously, a synthesis or extraction procedure for the production of large amounts of the active ingredient and a suitable administration form have to be developed. This lead optimization phase should result in only a handful of candidates for preclinical testing, which are then examined in genotoxicity models such as the Ames test (Ames et al. 1973) and in animal models for the determination of their pharmacodynamic and pharmacokinetic properties and for toxicity and efficacy testing (Ciociola et al. 2014).

After the drug candidate is regarded as biologically active and safe in preclinical testing, clinical trials are performed to ensure the drug's safety and efficacy in humans and that the benefits for the patient outweigh the side effects and risks. Clinical investigations of a study drug are organized in four phases. Phase 1 studies are mostly conducted in a small number of healthy volunteers to investigate the metabolic and pharmacologic drug profiles and to identify possible side effects. Phase 2 and 3 trials are carried out with a control group in first a small and then a larger group of patients to evaluate the effectiveness of the drug in a specific disease and to determine an effective dose. Phase 4 studies are observational studies that are carried out after the drug is approved for marketing.

Of often millions of compounds that are initially screened, only a small fraction will be considered as suitable for further *in vitro* testing and even less compounds pass the preclinical phase. Since only one in ten compounds that enter the clinical phase reaches the market and the financial consequences of failure at this stage are much higher, "failing fast and cheap" is very important in drug discovery (Hughes et al. 2011). Therefore, the development of suitable and robust test systems that are optimized for the targeted disease setting and understanding the mechanism of action early in the drug discovery process are crucial. Taken together, developing a new drug from initial idea to market approval requires on average over 10 years and an investment exceeding \$ 1 billion (Ciociola et al. 2014; DiMasi, Grabowski, and Hansen 2016; Hughes et al. 2011).

### **1.2.1 Natural products in drug discovery**

As long as we can remember, plants have been used as traditional medicine. The "Ebers papyrus" from 1500 BCE already documented more than 700 medically used plants and spices and can therefore be seen as one of the first review papers in the history of medical research (Borchardt 2002; Hartmann 2016). Not only in the distant past, but even as late as in the year 1985, the World Health Organization estimated that 80% of the world population predominantly relied on plant-derived traditional medicines for their health care (Farnsworth et al. 1985). Moreover, the use of compounds derived from nature is not limited to traditional medicine, but has also become a valuable source for modern pharmaceutical

research. Statistically, more than 50% of drugs approved by the FDA from 1939 to 2016 were natural products, their derivatives or inspired by structural motifs of natural compounds (Chen et al. 2020).

Nevertheless, in recent years, pharmaceutical companies have relied more and more on new chemical techniques like combinatorial chemistry to generate extensive molecular libraries for HTS. Due to the enormous amount of time needed for their extraction and often incomplete purification, it was assumed that natural products would become progressively irrelevant for modern pharmaceutical research (Cragg and Newman 2013). However, since the output of the pharmaceutical industry declines and solutions like total or partial synthesis of natural compounds emerge, it is clear that nature will continue to play a pivotal role in the process of drug discovery (Cragg and Newman 2013). Moreover, it is presumed that only 6% of higher plant species have been systemically investigated for their pharmacological potential (Fabricant and Farnsworth 2001) and that the marine environment and other extreme environments like (ant)arctic bio organisms remain almost unexplored (Newman and Cragg 2004; Newman and Hill 2006). Similarly, only a miniscule amount of microorganisms have been successfully cultivated and investigated regarding their secondary metabolites (Cragg and Newman 2013). In recent years, genome mining and the investigation of gene clusters encoding enzymes that are involved in the biosynthesis of microbial secondary metabolites have proven to be a valuable tool for the targeted discovery of novel bioactive compounds.

In conclusion, it can be stated that, although the implementation of natural product-based new medicine is a lengthy and costly process, in part due to the difficulties associated with comprehensively understanding their mechanism of action as well as their side effects (Chen et al. 2020), natural sources remain a precious source for highly bioactive new drug candidates. Compared to chemically synthesized drugs, natural products possess remarkable advantages in terms of structural novelty, biocompatibility and functional diversity, stemming from long-term natural selection-based optimizations in their evolution (Carlson 2010).

### **1.2.2 Natural products as autophagy modulators for cancer therapy**

Despite frequent advances in research, cancer remains a leading cause of death (Siegel et al. 2023) that should be addressed by the discovery of potent new anticancer drugs. For this, natural products have proven to be a valuable source for an almost inexhaustible diversity of bioactive compounds with a complexity in structure that is often superior to compounds derived from synthetic approaches. Currently, natural compounds and their derivatives make up nearly 50% of small molecules that have been approved by the FDA for cancer treatment since the 1940s (Newman and Cragg 2012). Some natural products, like mitotic agents or the ROS scavenger *N*-acetyl-L-cysteine (NAC), modulate autophagy as a subsidiary effect, but possess a different main mechanism of action. We, however, aim

to find targeted modulators of autophagy to minimize side effects and to gain a deeper understanding of the autophagic mechanisms involved in resistance development in cancer therapy.

One of the first clinically characterized autophagy inducers was the mTOR inhibitor rapamycin that was isolated from the bacterium *Streptomyces hygroscopicus* found on the eponymous Easter Island (Rapa Nui) (Vezina, Kudelski, and Sehgal 1975; Dumont and Su 1996). Rapamycin and its analogues were first approved as immunosuppressants during transplantations and later against various types of cancer (Bhaoighill and Dunlop 2019; Saran, Foti, and Dufour 2015). However, mTOR acts as a central signalling hub of cell metabolism and its inhibition can lead to severe side effects like hyperlipidaemia and hyperglycaemia (Deng et al. 2020; Wen and Klionsky 2020). CQ and HCQ, the chemical derivatives of quinine isolated from *Cinchona officinalis*, were initially developed as antimalarial drugs (Mohammadi et al. 2020). After the discovery of autophagy inhibiting properties via the alkalization of lysosomes, CQ and HCQ were tested as potential anti-cancer drugs both as monotherapy and in combination with classical chemotherapeutics in several clinical trials (Eldredge et al. 2013; Burikhanov et al. 2017; Molenaar et al. 2017; Arnaout et al. 2019; Khurshed et al. 2021). However, as already described (chapter 1.1.3), major pitfalls of these compounds are their lack of specificity and that the molecular mechanism of these compounds has not been fully elucidated so far, hindering targeted structural optimization. CQ, HCQ and rapalogues are a good example for the development of new anticancer drugs by repurposing drugs that were already approved for other diseases. A major advantage of this approach is the availability of a huge amount of preclinical and clinical safety data and insights regarding the molecular mechanism of action. However, none of these compounds displays a targeted and exclusive approach for autophagy modulation in cancer therapy.

Examples for autophagy inhibitors that target early steps of the autophagic process are the fungal metabolite wortmannin and its concurrent synthetic derivatives 3-methyladenine (3-MA), KU55993 and LY294002 (Farkas, Daugaard, and Jäättelä 2011). While wortmannin is a pan inhibitor of the PI3K superfamily, 3-MA was initially described as more specific for VPS34, which is the only known class III PI3K that is involved in autophagy by mediating the production of PI3P that is required for autophagosome formation (Blommaert et al. 1997; Petiot et al. 2000). An article by Wu et al. however, described differential temporal effects of 3-MA on class I and class III PI3K kinases (Wu et al. 2010a). Although these compounds eventually sensitize tumor cells to death, as non-specific PI3K inhibitors, they affect several processes and are toxic after long-term exposure (Wu et al. 2010b; Al-Bari et al. 2021), hindering their clinical application. The synthetic compound PX-866, another derivative of wortmannin, also acts as a pan-isoform inhibitor of PI3K. Harder et al. have shown that PX-866 can block temozolomide-induced autophagy and promotes apoptosis in glioblastoma cells (Harder et al. 2019). Interestingly, PX-866 is relatively well tolerated without any evidence of cumulative toxicity and has been investigated in several clinical trials for the treatment of patients with recurrent or metastatic cancer (Hotte et al. 2019; Yam et al. 2018; Pitz et al. 2015). The path of development from the fungal

metabolite wortmannin to the clinical candidate PX-866 sets an example that natural compounds, which initially might display non-favorable pharmacokinetic properties or possess toxic characteristics, can serve as lead structures for optimized and very potent semi-synthetic or synthetic structures that can modulate autophagy for anti-cancer therapy.

### **1.2.3 A brief history of the natural compound prodigiosin**

Although prodigiosin was first extracted from *Serratia marcescens* in 1929 (Wrede and Hettche 1929), historical literature is full of reports about "bleeding bread" (Gerber 1975; Bennett and Bentley 2000; Gaughran 1969). This phenomenon was most likely caused by red pigment producing bacteria of the *Serratia* and *Streptomyces* genera, which grow on many starch-rich culture media. When those colonies reach maturity, they can become liquid and then be mistaken for blood droplets (Fürstner 2003). In the European middle ages "bleeding" communion wafers were seen as miracles (Garlaschelli 1999) and one of the most famous examples of this phenomenon happened in 1263 in Bolsena. A priest noticed "blood droplets" dripping from the host during a pilgrimage to Rome and this apparent miracle was approved by the then pope Urban IV. It is assumed that this event led him to the implementation of the festival of Corpus Christi, which is still celebrated as a public holiday in many countries and to the construction of the cathedral in Orvieto, where the relics of this "miracle" are kept for pilgrims (Fürstner 2003). However, this phenomenon not only led to mostly harmless religious misbelief, but was also over centuries used as a pretense for bloodthirsty persecutions and pogroms of Jews who were accused of having stabbed and thereby desecrated hosts (Bennett and Bentley 2000; Gaughran 1969). Most of these events may be attributed to metabolites produced by *Serratia marcescens* and its relatives, since their colonies are closest to look like droplets of fresh blood (Fürstner 2003).

This went on until 1819, when "bleeding" food repeatedly appeared in a village in northern Italy. While the general population traced this back to witchcraft, three scientists (a botanist, a pharmacist and a physician) independently suggested fermentation as reason for the "bleeding" (Bennett and Bentley 2000; Gaughran 1969). Although they mistakenly thought that fungi were the creators of the red pigments, their studies possibly represent the first scientific investigations of prodigiosin producing microorganisms. The pharmacist Bartolomeo Bizio also suggested the name *Micrococcus prodigiosus* for this colorful microorganism, referring to the historical and "prodigious" events it was involved in. Albeit this name was not established for the microorganisms in the scientific community, it became eponymous for the colorful substance class produced by them (Fürstner 2003). Later on, the *Serratia* strains became a seemingly harmless microbial study object until their recognition as potentially toxic a few decades ago (Aucken and Pitt 1998; Hejazi and Falkiner 1997).

After discovering that the red pigments are produced by microorganisms in the early 19<sup>th</sup> century, it took more than a century until prodigiosin was first extracted from *Serratia marcescens* by Wrede and

Hettche (Wrede and Hettche 1929) and only in the 1960s the chemical structure was fully elucidated with the help of total synthesis (Rapoport and Holden 2002; Wasserman, Mc, and Santer 1960). Due to rapid advances in spectroscopic techniques, it was discovered that prodigiosin belongs to a compound class with several structural relatives that share a congeneric conjugated scaffold of A-, B- and C-ring pyrroles with differing alkyl substituents (reviewed in (Fürstner 2003; Hu et al. 2016)) and over the last 70 years, there has been a rising number of achiral and chiral prodiginines of natural, semisynthetic and synthetic origin (Clift and Thomson 2009; Haynes et al. 2011; Boger and Patel 2002; Rapoport and Willson 2002; Fürstner, Grabowski, and Lehmann 1999).

It has been reported, that prodiginines exhibit biological activities in a broad spectrum of organisms including, but not limited to, microorganisms (Herraez et al. 2019; Lapenda et al. 2015), the malaria parasite *Plasmodium falciparum* (Isaka et al. 2002; Kim et al. 1999; Lapenda et al. 2015), cancerous cells (Montaner and Perez-Tomas 2001; Montaner et al. 2000; Yamamoto et al. 2000; Yamamoto et al. 1999), plants, nematodes and fungi (Habash et al. 2020). However, the mechanism of action of prodigiosin in malignant mammalian cells is discussed controversially in literature. The effects described for this class of natural compounds include the induction of apoptotic cell death (Ji et al. 2019; Li et al. 2018; Lin et al. 2019; Sam and Ghoreishi 2018; Yenkeje, Sam, and Esmaeillou 2017), immunosuppressive properties (Magae et al. 1996; Kawauchi et al. 1997), the modulation of autophagy (Klein et al. 2018; Klein et al. 2017; Zhao et al. 2020) and the activity as an H<sup>+</sup>/Cl<sup>-</sup> symporter that can uncouple proton gradients (Seganish and Davis 2005; Sato et al. 1998). The discrepant observations between groups might be explained by a cell type dependent and multilayered mechanism of action.

Chemical derivatization and SAR studies led to the synthesis and characterization of several prodigiosin derivatives (Habash et al. 2020; Hu et al. 2016; Klein et al. 2017) and the development of the synthetic prodiginine analogue obatoclax mesylate (GX15-070), which has been evaluated in several phase II clinical trials for the treatment of leukemia (Schimmer et al. 2014), lymphomas (Oki et al. 2012) and small-cell lung cancer (Paik et al. 2011). However, obatoclax mesylate has not been approved for clinical application so far. While the example of Obatoclax demonstrates the great potential and efficacy of prodiginines against cancer cells, the fact that this compound has not been approved for the market shows that further research and development is required.

## 2 Aims of this work

The aims of this dissertation were the characterization of autophagy-modulating natural compounds through the investigation of these compounds in terms of overcoming chemotherapy resistance in cancer cells and the identification of their target proteins and pathways to improve the understanding of the mechanism of action and to optimize these lead structures into drug candidates. The main focus hereby lay on the characterization of the bacterial secondary metabolite prodigiosin. These aims have been addressed in several (collaboration) projects that have been published or are being revised for publication.

In the first project, the natural compound prodigiosin was investigated in cisplatin-sensitive and -resistant bladder cancer cells. Prodigiosin was used in mono- and combination therapy together with cisplatin to overcome cisplatin resistance and the effects of prodigiosin on autophagy and apoptosis were characterized.

In the second project, chemically synthesized prodigiosin derivatives were subjected to a systematic cell viability screening in cisplatin-sensitive and -resistant bladder cancer cells. The results of this screening give insights into the structure-activity relationship of prodiginines.

In the third project, the molecular mechanism of prodigiosin in cancer cells was investigated. Utilizing a proteomics approach, a protein target was identified and validated for this natural compound. The insights into the molecular mechanisms of prodigiosin can support the optimization of the compound as a drug candidate.

## 3 Summary of publications

### 3.1 Publications within the scope of this dissertation

The full original texts of these manuscripts can be found in the appendix of this dissertation.

#### 3.1.1 Publication 1

##### **Prodigiosin Sensitizes Sensitive and Resistant Urothelial Carcinoma Cells to Cisplatin Treatment**

Lena Berning, David Schlütermann, Annabelle Friedrich, Niklas Berleth, Yadong Sun, Wenxian Wu, María José Mendiburo, Jana Deitersen, Hannah U. C. Brass, Margaretha A. Skowron, Michèle J. Hoffmann, Günter Niegisch, Jörg Pietruszka, Björn Stork

*Molecules*, Volume 26, Issue 5, 1294, February 2021

DOI: 10.3390/molecules26051294

Complex resistance mechanisms, that include alterations in autophagy and apoptosis signalling, limit the success of cisplatin-based treatment of urothelial carcinomas. The secondary bacterial metabolite prodigiosin was shown to affect both autophagy and apoptosis. By analyzing the activity of prodigiosin alone or in combination with cisplatin, we found that prodigiosin sensitized both cisplatin-sensitive and -resistant urothelial carcinoma cells (UCCs) to cisplatin treatment with synergistic effects in most tested cell lines. Treatment with prodigiosin blocked autophagy in UCCs and resensitized cisplatin-resistant cells to apoptotic cell death. These effects of prodigiosin are at least partially mediated by an altered lysosomal function, since we detected reduced activities of cathepsin B and L. Prodigiosin appears to be a promising candidate for the therapy of cisplatin-resistant urothelial carcinomas, either as a single agent or in combinatory therapeutic approaches.

##### **Author contribution:**

The author of this dissertation designed the experiments and performed viability assays, immunoblot analyses, fluorescence microscopy and cathepsin activity assays. In addition, the author analyzed and interpreted the data and wrote the manuscript.

Relative contribution: about 85%.

### 3.1.2 Publication 2

#### **Prodiginine ligating enzymes exhibit an extended substrate acceptance for A-ring-associated alkyl-substitutions**

Tim Moritz Weber, Alexandra Leyens, Lena Berning, Björn Stork, Jörg Pietruszka

*Catalysis Science & Technology*, Volume 13, 6165, September 2023

DOI: 10.1039/d3cy00913k

Prodigiosin belongs to the prodiginine family, which is a class of secondary metabolite alkaloids of bacterial origin that is known for multifarious biological activities. Prodiginine biosynthesis is based on a converging route with a final ATP- and enzyme-dependent condensation reaction between the bipyrrole precursor MBC and miscellaneously substituted monopyrroles. We synthesized six 5'-n-alkyl derivatives of MBC, validated their suitability for condensation with monopyrroles by different known ligating enzymes, and found an overall broad acceptance of short- and medium-chain alkylated MBC derivatives. In addition, a systematic cell viability screening of chemically synthesized prodiginines with 5-n-alkylation on the A-ring in cisplatin-sensitive and -resistant UCCs revealed that methyl substituents increased the cytotoxicity of the derivatives compared to prodigiosin and the former clinical candidate obatoclax mesylate.

#### **Author contribution:**

The author of this dissertation performed viability assays, analyzed and interpreted the data, contributed ideas and suggestions to the project, discussed the results and commented on the manuscript.

Relative contribution: about 10%.

### 3.1.3 Publication 3

#### **The Golgi stacking protein GRASP55 is targeted by the natural compound prodigiosin**

Lena Berning, Thomas Lenz, Ann Kathrin Bergmann, Gereon Poschmann, Hannah U. C. Brass, David Schlütermann, Annabelle Friedrich, María José Mendiburo, Céline David, Seda Akgün, Jörg Pietruszka, Kai Stühler, Björn Stork

*Cell Communication and Signaling, Volume 21, Issue 1, 275, October 2023*

DOI: 10.1186/s12964-023-01275-1

Prodigiosin has been reported to affect cancer cells but not non-malignant cells, rendering prodigiosin a promising lead compound for anticancer drug discovery. However, a direct protein target has not yet been experimentally identified. Utilizing mass spectrometry-based thermal proteome profiling, we identified the Golgi stacking protein GRASP55 as a potential target of prodigiosin. Treatment with prodigiosin severely affects Golgi morphology and functionality and prodigiosin-dependent cytotoxicity can be partially reduced in GRASP55 knockout cells. By analyzing autophagy-related protein abundance and cathepsin activity, we found that prodigiosin treatment blocks autophagic flux. We observed that autophagosomes accumulate at GRASP55-positive structures, pointing towards an involvement of an altered Golgi function in the autophagy-inhibitory effect of this natural compound. These results suggest that prodigiosin affects autophagy and Golgi apparatus integrity in an interlinked mode of action involving the regulation of organelle alkalization and the Golgi stacking protein GRASP55.

#### **Author contribution:**

The author of this dissertation designed the experiments and performed viability assays, immunoblot analyses, cathepsin activity assays, fluorescence microscopy, generation of a GRASP55 KO cell line and sample preparation for TPP and electron microscopy. In addition, the author analyzed and interpreted the data and wrote the manuscript.

Relative contribution: about 75%.

## 3.2 Publications beyond the scope of this dissertation

The author of this dissertation has contributed to several additional publications. However, these are not discussed here or attached to this work, as they would go beyond the scope of this dissertation.

### 3.2.1 Publication 4

#### **High-throughput screening for natural compound-based autophagy modulators reveals novel chemotherapeutic mode of action for Arzanol**

Jana Deitersen, Lena Berning, Fabian Stuhldreier, Sara Ceccacci, David Schlütermann, Annabelle Friedrich, Wenxian Wu, Yadong Sun, Philip Böhler, Niklas Berleth, María José Mendiburo, Sabine Seggewiß, Ruchika Anand, Andreas S Reichert, Maria Chiara Monti, Peter Proksch, Björn Stork

*Cell Death & Disease, Volume 12, Issue 6, 560, May 2021*

DOI: 10.1038/s41419-021-03830-5

#### **Author contribution:**

The author of this dissertation performed cell viability assays, microscopy and cellular metabolism analyses and contributed ideas and suggestions to the project, gave technical support, discussed the results and commented on the manuscript.

Relative contribution: about 25%.

### 3.2.2 Publication 5

#### **FIP200 controls the TBK1 activation threshold at SQSTM1/p62-positive condensates**

David Schlütermann, Niklas Berleth, Jana Deitersen, Nora Wallot-Hieke, Olena Friesen, Wenxian Wu, Fabian Stuhldreier, Yadong Sun, Lena Berning, Annabelle Friedrich, María José Mendiburo, Christoph Peter, Constanze Wiek, Helmut Hanenberg, Anja Stefanski, Kai Stühler, Björn Stork

*Scientific Reports, Volume 11, Issue 1, 13863, July 2021*

DOI: 10.1038/s41598-021-92408-4

#### **Author contribution:**

The author of this dissertation gave technical support, discussed the results and commented on the manuscript

Relative contribution: about 2%.

### 3.2.3 Publication 6

**Fin56-induced ferroptosis is supported by autophagy-mediated GPX4 degradation and functions synergistically with mTOR inhibition to kill bladder cancer cells**

Yadong Sun, Niklas Berleth, Wenxian Wu, David Schlütermann, Jana Deitersen, Fabian Stuhldreier, Lena Berning, Annabelle Friedrich, Seda Akgün, María José Mendiburo, Sebastian Wesselborg, Marcus Conrad, Carsten Berndt, Björn Stork

*Cell Death & Disease, Volume 12, Issue 11, 1028, October 2021*

DOI: 10.1038/s41419-021-04306-2

**Author contribution:**

The author of this dissertation gave technical support, discussed the results and commented on the manuscript

Relative contribution: about 2%.

### 3.2.4 Publication 7

**Modular Approach for the Synthesis and Bioactivity Profiling of 8,8'-Biflavones**

Moritz K. T. Klischan, Flaminia Mazzone, Lena Berning, Julian Greb, Max Schlamkow, Mona Haase, Wolfgang Frey, Björn Stork, Klaus Pfeffer, Jörg Pietruszka

*ACS Omega, Volume 8, Issue 44, 41816, October 2023*

DOI: 10.1021/acsomega.3c06503

**Author contribution:**

The author of this dissertation performed viability assays, analyzed and interpreted the data, contributed ideas and suggestions to the project, discussed the results and commented on the manuscript.

Relative contribution: about 10%.

## 4 Discussion

As the number of new cancer cases continuously rises with simultaneously only minor declines in cancer death rates, the need for novel anti-tumor drug candidates is high. Therefore nature displays an almost inexhaustible source for new pharmacologically active molecules. The unveiling of the mode of action of these new drug candidates is crucial for the assessment of potential side effects and for the understanding of structure-activity relationships. The projects presented in this dissertation can be seen as part of the early drug discovery phase and contributed to a better understanding of the molecular mechanism and characterization of the anti-cancer properties of the natural compound prodigiosin. Within the work of this dissertation, we characterized prodigiosin as a potent inhibitor of autophagy that can overcome chemotherapy-resistance by resensitizing bladder cancer cells to cisplatin-induced apoptosis. In addition, we subjected several prodigiosin derivatives to a systematic cell viability screening to gain insights into the structure-activity relationship of prodiginines. Finally, we were able to unveil the Golgi protein GRASP55 as an effector protein of prodigiosin and thereby we contributed to elucidating the mechanism of action of this natural compound.

### 4.1 Elimination of therapy-resistant cancer

Bladder cancer is one of the 10 most common cancers worldwide, with a poor prognosis for patients diagnosed with muscle-invasive and metastatic carcinomas (Nadal and Bellmunt 2019). A major cause for the high mortality rate is the development of resistance to platin-based chemotherapy, which is the standard of care for these patients (Leitlinienprogramm Onkologie Deutsche Krebsgesellschaft 2020; Alfred Witjes et al. 2017). Autophagy has been described as one mechanism of cisplatin resistance (Ma, Li, et al. 2020; Yu et al. 2014; Xiao et al. 2016; Mani et al. 2015; Galluzzi et al. 2012) and previous work of our group has shown an increased expression of various ATG proteins in cisplatin-resistant bladder cancer cell lines and that targeting cytoprotective autophagy with autophagy inhibitors increased cisplatin efficacy in resistant tumor cells (Schlütermann et al. 2018).

Prodigiosin has previously been described as a potent modulator of autophagy that exerts strong anti-cancer activity (Cheng et al. 2018; Ji et al. 2019; Klein et al. 2017; Lin and Weng 2018; Zhao et al. 2020). In our study about the efficacy of prodigiosin in bladder carcinomas we found that prodigiosin was cytotoxic in bladder cancer cells with  $IC_{50}$  values in the nanomolar range for all tested cell lines (chapter 3.2.1). Compared to an average  $IC_{50}$  value of 2.1  $\mu M$  in a screening of around 60 cancer cell lines implemented by the National Cancer Institute (Perez-Tomas and Vinas 2010), prodigiosin actually seems to be particularly effective against bladder carcinoma cells. The effects of prodigiosin on autophagy have been discussed controversially in literature. While some groups describe an inhibition of the autophagic process (Ji et al. 2019; Klein et al. 2017; Zhao et al. 2020), others described the

induction of autophagic cell death (Cheng et al. 2018; Lin and Weng 2018). As shown by autophagic flux assays using bafilomycin A<sub>1</sub> and cathepsin activity assays, in our hands prodigiosin rather acts as a strong inhibitor of autophagy.

Noteworthy, IC<sub>50</sub> values of prodigiosin-mediated cytotoxicity were lower in cisplatin resistant cells than in their sensitive precursors. This might be explained by the fact that the effect of autophagy modulation strongly depends on cancer type and progression. While some groups observed upregulated autophagy in different cancer types which developed a cisplatin resistance and successfully inhibited autophagy to resensitize the cancer cells to cisplatin treatment (Hu et al. 2020; Su et al. 2016; Bao et al. 2015; Wang and Wu 2014; Huang et al. 2013; Garcia-Cano et al. 2015), there are other studies describing that autophagic flux is not enhanced but reduced in cisplatin resistant cancer and that induction of autophagy showed beneficial effects for cisplatin efficacy (Gu, Fei, and Zhu 2020; Garcia-Cano et al. 2015; Sirichanchuen, Pengsuparp, and Chanvorachote 2012). Recently, Gasiorkiewicz et al. reviewed autophagy-modulating compounds that chemosensitize for cisplatin in cancer therapy (Gasiorkiewicz et al. 2021). Among these compounds are classical autophagy inhibitors, compounds with specific autophagy-related targets, and natural compounds. It appears that both the inhibition of the cytoprotective functions and the induction of death-promoting functions of autophagy can be therapeutically relevant.

In our study, prodigiosin not only decreased the viability of different cisplatin-sensitive and -resistant urothelial carcinoma cell lines, but also sensitized them to cisplatin treatment by overcoming cisplatin-induced apoptosis resistance. The complex interplay between autophagy and apoptosis has been described in chapter 1.1.1. A major hub for this interplay is the interaction of the antiapoptotic members of the Bcl-2 family of proteins and Beclin-1 of the class III PtdIns3K complex I through their BH3-domains (Kang et al. 2011; Luo and Rubinsztein 2010; Mukhopadhyay et al. 2014; Pattingre et al. 2005). Inspired by the structure of prodigiosin, the synthetic prodiginine analogue obatoclax mesylate (GX15-070) was developed and has been evaluated in several phase II clinical trials for the treatment of leukemia (Schimmer et al. 2014), lymphomas (Oki et al. 2012) and small-cell lung cancer (Paik et al. 2011). The BH3-mimetic obatoclax has been reported to induce apoptotic cell death by antagonizing all antiapoptotic Bcl-2 family proteins (Zhai et al. 2006). The impact on autophagy however seems to be multifarious. Against expectations, the obatoclax-mediated induction of autophagy appears to be independent of Beclin-1 (Bata and Cosford 2021; Heidari, Hicks, and Harada 2010; McCoy et al. 2010). In addition, the role of autophagy in obatoclax-induced cell death has been controversially discussed in literature. While Yu and Liu reported that blockage of autophagy inhibited cell death (Yu and Liu 2013), Pan et al. found that inhibition of autophagy enhanced obatoclax induced cytotoxicity, suggesting a pro-survival function of autophagy (Pan et al. 2010). However, the complex and not fully elucidated mechanism of action of the prodigiosin analogue obatoclax shows the importance of characterizing the effects of prodigiosin and its analogues in malignant cells in order to optimize the structure to exploit the full pharmacological potential of these compounds.

## 4.2 Prodigiosin as a lead structure

After the proof of effectiveness against chemotherapy-resistant tumor cells, prodigiosin presents itself as an interesting drug candidate. During the drug discovery phase the next step for lead compounds is the synthesis of structural analogues to identify SARs and to optimize the potency, selectivity and pharmacokinetic properties. Prodigiosin already meets Lipinski's Rule of Five (Lipinski 2004; Lipinski et al. 2001) and ADME predictions showed that based on drug-likeness, physicochemical and pharmacokinetic parameters it already has desirable drug-like properties such as a good oral availability and intestinal absorption (Anwar et al. 2020; Sundararajan et al. 2023). A potential challenge is the limited aqueous solubility that could be enhanced by structural modifications like the integration of hydrophilic residues or by employing nanoscale drug formulations (Guryanov et al. 2020). By applying the Ames and micronucleus test, Guryanov et al. showed that prodigiosin does not exhibit a significant genotoxic potential (Guryanov et al. 2013).

An additional beneficial characteristic of prodigiosin is the reported sensitivity of cancer cells towards this compound and the concomitant absence of effects on non-malignant cells that has been previously reported. For instance, prodigiosin showed higher cytotoxicity in lung carcinoma (Davient et al. 2018) and breast cancer (Yamamoto et al. 2000) cells than in associated epithelial cell lines and fibroblasts. In addition, Montaner et al. showed prodigiosin-mediated cell death in colon cancer cells and hematopoietic cancer cell lines but observed no cytotoxic effects in non-malignant cells (Montaner and Perez-Tomas 2001; Montaner et al. 2000). Hong et al. reported that prodigiosin induced cell-cycle arrest and apoptosis through restoration of p53 signaling in p53-deficient human colon cancer cells with little to no cytotoxicity in normal human fibroblasts and no display of genotoxicity (Hong et al. 2014). In addition to promising *in silico* and *in vitro* results, prodigiosin showed no side effects in first *in vivo* studies. It significantly inhibited tumor growth of hepatocellular carcinoma xenografts without pathological changes in any organs (Yamamoto et al. 1999) and showed no additional adverse effects in a combination study with 5-fluorouracil in colorectal cancer in mice (Zhao et al. 2020). Taken together, prodigiosin as a lead structure already possesses desirable clinical properties, but further studies concerning ADME *in vitro* and *in vivo* are required and side effects of prodigiosin on healthy tissues need to be carefully assessed.

All prodiginines share a congeneric conjugated scaffold of A-, B- and C-ring pyrroles with decorations on the ring systems. Over the last 70 years, there has been a rising number of achiral and chiral prodiginines of natural, semisynthetic and synthetic origin (Clift and Thomson 2009; Haynes et al. 2011; Boger and Patel 2002; Rapoport and Willson 2002; Fürstner, Grabowski, and Lehmann 1999). With increasing serendipities of naturally occurring prodiginines and prodiginine-producing bacterial strains the quantity of known bacterial gene clusters involved in the biosynthesis of this compound class is constantly rising. Numerous clusters among diverse bacterial species have been identified by genome mining and analyses of mutant strains (Xie et al. 2012; Williamson et al. 2005; Grenade et al. 2023;

Wang et al. 2021; Salem et al. 2014). All of these gene clusters encode for non-ribosomal peptide synthetases (NRPS) of type II (Jaremko et al. 2020; Cerdeno, Bibb, and Challis 2001) that assemble the two key precursors: the bipyrrole and the monopyrrole part (Hu et al. 2016; Chawrai et al. 2008; Wasserman et al. 1973; Harris et al. 2004). This, combined with synthetic methods, enables the design of multiple prodigiosin derivatives for structural studies to elucidate the SAR of prodiginines.

The biosynthesis of prodiginines exclusively relies on utilization of 4-methoxy-2,2'-bipyrrole-5-carbaldehyde (MBC) that is built from the amino acid L-proline as bipyrrole condensation partner and with few exceptions no naturally occurring A-ring substituted prodiginines have been found to date (Feher et al. 2008). Hence, from today's view a broad accessibility of A-ring substituted prodiginines by biosynthetic methods seems not feasible, but those derivatives can be assessed by total synthesis. Although some studies addressed the synthesis of A-ring substituted prodiginines, either they did not investigate the biological effects of these derivatives (Chawrai et al. 2008) or their main focus lay on other components of the structure (D'Alessio et al. 2000; Melvin et al. 2000). But since both D'Alessio et al. and Melvin et al. observed positive effects after adding electron-donating alkyl substitutions in 5-position of the A-ring (D'Alessio et al. 2000; Melvin et al. 2000), our aim was to investigate these modifications of prodigiosin systematically for their impact on prodigiosin-mediated cell death.

For this purpose, a compound library of A-ring alkylated prodiginines was synthesized and screened for their cytotoxicity in cisplatin-sensitive and -resistant bladder carcinoma cells with the parent compound prodigiosin and the former clinical candidate obatoclax-mesylate as references (chapter 3.2.2). We observed that the addition of an electron-donating methyl group in 5-position of the A-ring resulted in an increase of cytotoxicity, whereas further chain elongation led to a constant loss of biological activity with each step of elongation. Subsequently, we chose the most potent methyl-substituted derivative and tested alkyl chain length variations in 4-position of the C-ring. All tested methylated derivatives showed similar  $IC_{50}$  values which were up to 2.6-fold lower than for prodigiosin in cisplatin-resistant bladder carcinoma cells. Interestingly, both C-ring variations led to significantly faster cytotoxic effects, suggesting substantial improvements compared to the only A-ring methylated derivative, prodigiosin and obatoclax mesylate.

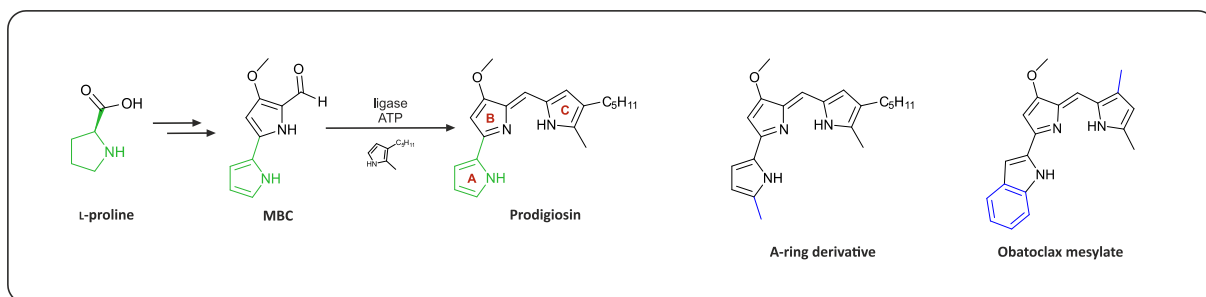


**Figure 4: Biosynthesis of Prodigiosin and structures of prodigiosin derivatives.**

We hypothesize that the electron-donating alkyl substituent on the A-ring tightens the bond between the B-ring nitrogen and the proton from the chloride counter ion, thereby increasing the  $pK_a$  value and

facilitating the trespass of the charged complex through the membrane. Fürstner described that the complex of the protonated prodigiosin and the chloride is lipophilic and tight enough to penetrate biological membranes (Fürstner 2003). Longer A-ring alkyl chains could possibly function as membrane anchors, preventing the cellular or organelle entry of these derivatives and thereby reduce their biological activity. This phenomenon already became apparent in earlier studies, where longer alkyl chains on the C-ring drastically decreased autophagy modulation of prodigiosin derivatives (Klein et al. 2017). However, these are speculations and the mechanism of action of prodigiosin has to be further elucidated in order to fully understand the SAR and to optimize the promising lead compound prodigiosin for possible future clinical applications.

### 4.3 Elucidation of the molecular mechanism

Prodigiosin and its derivatives exhibit biological activities in a broad spectrum of organisms including, but not limited to, microorganisms (Herraez et al. 2019; Lapenda et al. 2015), the malaria parasite *Plasmodium falciparum* (Isaka et al. 2002; Kim et al. 1999; Lapenda et al. 2015), cancerous cells (Montaner and Perez-Tomas 2001; Montaner et al. 2000; Yamamoto et al. 2000; Yamamoto et al. 1999), plants, nematodes and fungi (Habash et al. 2020). When dealing with natural compounds that display a high bioactivity, one has to be aware that natural compounds often possess multiple targets in mammalian cells and other organisms and that these targets often have multifarious functions. The positive side of natural compounds affecting various molecular pathways at once in malignant cells is a lesser chance for the development of chemotherapy resistance. Nevertheless, understanding the mode of action by unveiling preferably all molecular targets of a drug candidate is crucial for structural optimization and for the assessment and prevention of potential side effects.

For prodigiosin, several potential protein targets have already been described. Krishna et al. published an *in silico* molecular docking analysis, where they identified prodigiosin and cycloprodigiosin as potential COX-2 inhibitors for anti-inflammatory use (Krishna et al. 2013). In a recent manuscript, Sundararajan et al. used molecular docking and molecular dynamics simulation studies to characterize prodigiosin as an inhibitor of PARP-1 (Sundararajan et al. 2023). In addition, Paul et al. utilized inverse virtual screening methods and reported several potential prodigiosin-interacting proteins including HER-2, MEK, and S6K (Paul et al. 2023). However, in these studies the target identification is solely based on computational methods and has not been validated experimentally so far, qualifying these studies rather as explorative.

Commonly used techniques for target identification often require the synthesis of a derivatized probe. Derivatization bears multiple disadvantages like being time- and cost-intensive, a possible affection of the active drug conformation and the risk of steric interference (Chang, Kim, and Kwon 2016; Fang 2014). In the last decades, the identification of protein targets was improved by the utilization of several

mass spectrometry (MS)-based screening methods (Feng et al. 2023). In our study, we used the thermal proteome profiling (TPP)/ratio-based thermal shift assay analysis (RTSA) approach as an unbiased and label-free target identification method which does not involve a chemical modification of prodigiosin or possible target proteins (Johnson et al. 2023). TPP combines the cellular thermal shift assay (CETSA) which is based on the principle of thermal stabilization of intracellular proteins when they are bound to a small molecule (Martinez Molina et al. 2013; Jafari et al. 2014) with multiplexed quantitative MS analysis (Savitski et al. 2014; Franken et al. 2015).

We identified several proteins that were stabilized against thermal denaturation after treatment with prodigiosin (chapter 3.1.3). Although we focused on the Golgi apparatus stacking protein GRASP55 for target validation and further evaluations, other identified target candidates may also be worth further investigation to fully elucidate the probably complex mechanism of action of prodigiosin. GRASP55 showed a high statistical significance of thermal stabilization in two independent TPP experiments, a low EC<sub>50</sub> value and could be confirmed by CETSA and therefore presents itself as a highly probable direct protein target of prodigiosin. With CETSA/TPP approaches, it can be difficult to distinguish between primary effects (direct binding) and secondary abundance effects due to affected upstream processes (Lenz and Stühler 2022), but neither in the TPP-TR/RTSA nor in the TPP-CCR analysis, GRASP55 showed differential intensities at 37 °C, excluding an abundance effect. After target identification, further experiments are required for multidimensional target validation (Feng et al. 2023) to determine how prodigiosin interacts with the target proteins (backward validation) and which cellular pathways and downstream effects are affected (forward validation) (Tu et al. 2023). For backward validation, molecular modelling of the small molecule-to-protein binding, co-crystallization studies or enzyme kinetics with purified proteins are often the methods of choice. In the case of GRASP55, those methods are not feasible because only the N-terminal GRASP domain of GRASP55 (residues 1-207) has been successfully crystallized so far (Truschel et al. 2011; Li, Feng, and Liu 2013), impeding reliable computational modelling and co-crystallization studies. For forward validation, knockout and knockdown studies are widely used. In our hands, KO of GRASP55 significantly reduced prodigiosin cytotoxicity, indirectly confirming GRASP55 as a target although prodigiosin is still clearly cytotoxic in GRASP55 KO cells, demonstrating that additional target candidates and mechanisms are involved in prodigiosin-mediated reduction of cancer cell viability.

Additionally, morphological examination confirmed the Golgi apparatus as a target of prodigiosin. Prodigiosin treatment leads to a severely dilated and disorganized Golgi apparatus in a concentration-dependent manner. It should be noted, however, that the severe effects after treatment with high prodigiosin concentrations occur rather due to the H<sup>+</sup>/Cl<sup>-</sup> symporter activity of prodigiosin that leads to uncoupling of the proton gradient, which is maintained across the Golgi membrane (Sato et al. 1998; Konno et al. 1998; Ohkuma et al. 1998) and to similar phenotypical effects as the known ionophore monensin (Dinter and Berger 1998; Mollenhauer, Morre, and Rowe 1990; Vanneste et al. 2019). The ion carrier properties of prodigiosin provide a good example for a small molecule being bioactive

through mechanisms that do not involve the direct binding of proteins, which will therefore not be revealed by classical target finding assays. To characterize the effects of prodigiosin binding to GRASP55 on Golgi apparatus morphology and function, the assessment of prodigiosin derivatives that lack the ion symporter properties would be favourable.

The complex interplay between Golgi apparatus and autophagic machinery and the inhibitory effects of prodigiosin on autophagy were described in chapters 1.1.2 and 4.1, respectively. We propose a multi-layered effect of prodigiosin on the autophagic pathway via its effects on Golgi structure in general and/or on GRASP55 in particular. We presume: (i) an impaired trafficking of key autophagic proteins due to a severely disturbed Golgi apparatus structure, manifesting in smaller autophagosomes and lysosomes, (ii) prodigiosin-mediated alkalization of lysosomes resulting in a complete blockade of autophagic flux, (iii) interference of prodigiosin in the GRASP55-mediated fusion of autophagosome and lysosome and (iv) the induction of Golgiphagy, as shown by the massive accumulation of autophagosomal membranes in the perinuclear area. Structural derivatives that lack either GRASP55 binding or ion symporter qualities could help to investigate the individual contributions of the different aspects of prodigiosin effects on Golgi apparatus and autophagy.

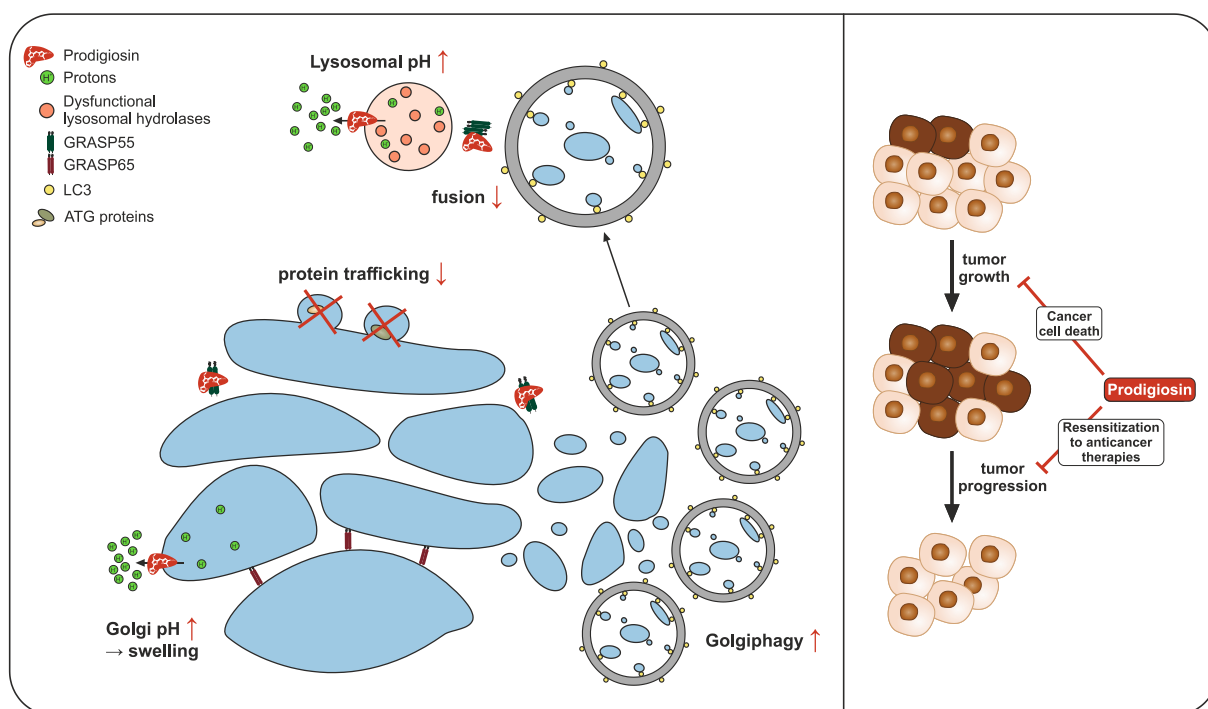


**Figure 5: The multifarious mechanism of action of prodigiosin in tumor cells.** Treatment with prodigiosin leads to shorter, less and dilated Golgi cisternae through its interaction with GRASP55. Additionally, prodigiosin leads to a swelling of the Golgi cisternae via its  $H^+/Cl^-$  symporter activity that leads to uncoupling of the proton gradient, which is maintained across the Golgi membrane. Because of the severely disturbed Golgi apparatus structure, the trafficking of key autophagic proteins to the isolation membrane is impaired. Prodigiosin has a dual mechanism of blocking late steps of autophagy through the alkalization of lysosomes and the interference in the GRASP55-mediated fusion of autophagosome and lysosome. In addition, prodigiosin treatment leads to the induction of Golgiphagy and a massive accumulation of autophagosomes at the Golgi apparatus. As a consequence of these effects, prodigiosin leads to an induction of cancer cell death and resensitizes malignant cells to chemotherapy to inhibit tumor progression.

---

In summary, we characterized the natural compound prodigiosin as a potent lead structure for anti-cancer drug discovery. We propose prodigiosin as a promising drug candidate that resensitizes cisplatin-resistant malignancies to chemotherapy and recommend A-ring alkylations as an auspicious approach to optimize the biological activity of this natural compound. In addition, we identified GRASP55 as a molecular target of prodigiosin and propose further investigation of the impact of this interaction. This work provides an example how precious natural compound research in combination with synthetic and semi-synthetic approaches is not only to find new lead structures for pharmaceutical research, but also to elucidate the complex interplay of different molecular pathways of the cellular machinery. Overall, this dissertation contributed to decipher the molecular mode of action of the potent anti-cancer effects of the highly interesting natural compound prodigiosin.

## 5 References

- Abedin, M. J., D. Wang, M. A. McDonnell, U. Lehmann, and A. Kelekar. 2007. 'Autophagy delays apoptotic death in breast cancer cells following DNA damage', *Cell Death Differ*, 14: 500-10.
- Adams, J. M., and S. Cory. 2018. 'The BCL-2 arbiters of apoptosis and their growing role as cancer targets', *Cell Death Differ*, 25: 27-36.
- Ahat, E., S. Bui, J. Zhang, F. da Veiga Leprevost, L. Sharkey, W. Reid, A. I. Nesvizhskii, H. L. Paulson, and Y. Wang. 2022. 'GRASP55 regulates the unconventional secretion and aggregation of mutant huntingtin', *J Biol Chem*, 298: 102219.
- Ahat, E., J. Li, and Y. Wang. 2019. 'New Insights Into the Golgi Stacking Proteins', *Front Cell Dev Biol*, 7: 131.
- Aita, V. M., X. H. Liang, V. V. Murty, D. L. Pincus, W. Yu, E. Cayanis, S. Kalachikov, T. C. Gilliam, and B. Levine. 1999. 'Cloning and genomic organization of beclin 1, a candidate tumor suppressor gene on chromosome 17q21', *Genomics*, 59: 59-65.
- Al-Bari, Md Abdul Alim, Yuko Ito, Samrein Ahmed, Nada Radwan, Hend S. Ahmed, and Nabil Eid. 2021. 'Targeting Autophagy with Natural Products as a Potential Therapeutic Approach for Cancer', *International Journal of Molecular Sciences*, 22: 9807.
- Alfred Witjes, J., T. Lebre, E. M. Comperat, N. C. Cowan, M. De Santis, H. M. Bruins, V. Hernandez, E. L. Espinos, J. Dunn, M. Rouanne, Y. Neuzillet, E. Veskimäe, A. G. van der Heijden, G. Gakis, and M. J. Ribal. 2017. 'Updated 2016 EAU Guidelines on Muscle-invasive and Metastatic Bladder Cancer', *Eur Urol*, 71: 462-75.
- Alnemri, E. S., D. J. Livingston, D. W. Nicholson, G. Salvesen, N. A. Thornberry, W. W. Wong, and J. Yuan. 1996. 'Human ICE/CED-3 protease nomenclature', *Cell*, 87: 171.
- Amaravadi, R. K., D. Yu, J. J. Lum, T. Bui, M. A. Christophorou, G. I. Evan, A. Thomas-Tikhonenko, and C. B. Thompson. 2007. 'Autophagy inhibition enhances therapy-induced apoptosis in a Myc-induced model of lymphoma', *J Clin Invest*, 117: 326-36.
- Ames, B. N., W. E. Durston, E. Yamasaki, and F. D. Lee. 1973. 'Carcinogens are mutagens: a simple test system combining liver homogenates for activation and bacteria for detection', *Proc Natl Acad Sci U S A*, 70: 2281-5.
- Anwar, M. M., M. Shalaby, A. M. Embaby, H. Saeed, M. M. Agwa, and A. Hussein. 2020. 'Prodigiosin/PU-H71 as a novel potential combined therapy for triple negative breast cancer (TNBC): preclinical insights', *Sci Rep*, 10: 14706.
- Ariosa, A. R., V. Lahiri, Y. Lei, Y. Yang, Z. Yin, Z. Zhang, and D. J. Klionsky. 2021. 'A perspective on the role of autophagy in cancer', *Biochim Biophys Acta Mol Basis Dis*, 1867: 166262.
- Arnaout, A., S. J. Robertson, G. R. Pond, H. Lee, A. Jeong, L. Ianni, L. Kroeger, J. Hilton, S. Coupland, C. Gottlieb, B. Hurley, A. McCarthy, and M. Clemons. 2019. 'A randomized, double-blind, window of opportunity trial evaluating the effects of chloroquine in breast cancer patients', *Breast Cancer Res Treat*, 178: 327-35.
- Aucken, H. M., and T. L. Pitt. 1998. 'Antibiotic resistance and putative virulence factors of *Serratia marcescens* with respect to O and K serotypes', *J Med Microbiol*, 47: 1105-13.
- Axe, Elizabeth L., Simon A. Walker, Maria Manifava, Priya Chandra, H. Llewelyn Roderick, Anja Habermann, Gareth Griffiths, and Nicholas T. Ktistakis. 2008. 'Autophagosome formation from membrane compartments enriched in phosphatidylinositol 3-phosphate and dynamically connected to the endoplasmic reticulum', *Journal of Cell Biology*, 182: 685-701.
- Baell, J. B., and G. A. Holloway. 2010. 'New substructure filters for removal of pan assay interference compounds (PAINS) from screening libraries and for their exclusion in bioassays', *J Med Chem*, 53: 2719-40.
- Bao, Lingjie, Melba C. Jaramillo, Zhenbo Zhang, Yunxi Zheng, Ming Yao, Donna D. Zhang, and Xiaofang Yi. 2015. 'Induction of autophagy contributes to cisplatin resistance in human ovarian cancer cells', *Molecular Medicine Reports*, 11: 91-98.
- Barr, F. A., M. Puype, J. Vandekerckhove, and G. Warren. 1997. 'GRASP65, a protein involved in the stacking of Golgi cisternae', *Cell*, 91: 253-62.

- Bata, N., and N. D. P. Cosford. 2021. 'Cell Survival and Cell Death at the Intersection of Autophagy and Apoptosis: Implications for Current and Future Cancer Therapeutics', *ACS Pharmacol Transl Sci*, 4: 1728-46.
- Bennett, J. W., and R. Bentley. 2000. 'Seeing red: the story of prodigiosin', *Adv Appl Microbiol*, 47: 1-32.
- Bhaoighill, M. N., and E. A. Dunlop. 2019. 'Mechanistic target of rapamycin inhibitors: successes and challenges as cancer therapeutics', *Cancer Drug Resist*, 2: 1069-85.
- Birgisdottir, A. B., T. Lamark, and T. Johansen. 2013. 'The LIR motif - crucial for selective autophagy', *J Cell Sci*, 126: 3237-47.
- Blommaert, E. F., U. Krause, J. P. Schellens, H. Vreeling-Sindelarova, and A. J. Meijer. 1997. 'The phosphatidylinositol 3-kinase inhibitors wortmannin and LY294002 inhibit autophagy in isolated rat hepatocytes', *Eur J Biochem*, 243: 240-6.
- Boger, Dale L., and Mona Patel. 2002. 'Total synthesis of prodigiosin, prodigiosene, and desmethoxyprodigiosin: Diels-Alder reactions of heterocyclic azadienes and development of an effective palladium(II)-promoted 2,2'-bipyrrole coupling procedure', *The Journal of Organic Chemistry*, 53: 1405-15.
- Borchardt, J. K. 2002. 'The Beginnings of Drug Therapy: Ancient Mesopotamian Medicine', *Drug News Perspect*, 15: 187-92.
- Bravo, D. A., J. B. Gleason, R. I. Sanchez, R. A. Roth, and R. S. Fuller. 1994. 'Accurate and efficient cleavage of the human insulin proreceptor by the human proprotein-processing protease furin. Characterization and kinetic parameters using the purified, secreted soluble protease expressed by a recombinant baculovirus', *Journal of Biological Chemistry*, 269: 25830-37.
- Burikhanov, R., N. Hebbbar, S. K. Noothi, N. Shukla, J. Sledziona, N. Araujo, M. Kudrimoti, Q. J. Wang, D. S. Watt, D. R. Welch, J. Maranchie, A. Harada, and V. M. Rangnekar. 2017. 'Chloroquine-Inducible Par-4 Secretion Is Essential for Tumor Cell Apoptosis and Inhibition of Metastasis', *Cell Rep*, 18: 508-19.
- Carew, J. S., S. T. Nawrocki, C. N. Kahue, H. Zhang, C. Yang, L. Chung, J. A. Houghton, P. Huang, F. J. Giles, and J. L. Cleveland. 2007. 'Targeting autophagy augments the anticancer activity of the histone deacetylase inhibitor SAHA to overcome Bcr-Abl-mediated drug resistance', *Blood*, 110: 313-22.
- Carlson, E. E. 2010. 'Natural products as chemical probes', *ACS Chem Biol*, 5: 639-53.
- Cerdeno, A. M., M. J. Bibb, and G. L. Challis. 2001. 'Analysis of the prodiginine biosynthesis gene cluster of *Streptomyces coelicolor* A3(2): new mechanisms for chain initiation and termination in modular multienzymes', *Chem Biol*, 8: 817-29.
- Chang, J., Y. Kim, and H. J. Kwon. 2016. 'Advances in identification and validation of protein targets of natural products without chemical modification', *Nat Prod Rep*, 33: 719-30.
- Chaudhri, V. K., G. G. Salzler, S. A. Dick, M. S. Buckman, R. Sordella, E. D. Karoly, R. Mohney, B. M. Stiles, O. Elemento, N. K. Altorki, and T. E. McGraw. 2013. 'Metabolic alterations in lung cancer-associated fibroblasts correlated with increased glycolytic metabolism of the tumor', *Mol Cancer Res*, 11: 579-92.
- Chawrai, S. R., N. R. Williamson, G. P. Salmond, and F. J. Leeper. 2008. 'Chemoenzymatic synthesis of prodigiosin analogues--exploring the substrate specificity of PigC', *Chem Commun (Camb)*: 1862-4.
- Chen, N., and V. Karantza. 2011. 'Autophagy as a therapeutic target in cancer', *Cancer Biol Ther*, 11: 157-68.
- Chen, S., S. K. Rehman, W. Zhang, A. Wen, L. Yao, and J. Zhang. 2010. 'Autophagy is a therapeutic target in anticancer drug resistance', *Biochim Biophys Acta*, 1806: 220-9.
- Chen, X., Y. Wang, N. Ma, J. Tian, Y. Shao, B. Zhu, Y. K. Wong, Z. Liang, C. Zou, and J. Wang. 2020. 'Target identification of natural medicine with chemical proteomics approach: probe synthesis, target fishing and protein identification', *Signal Transduct Target Ther*, 5: 72.
- Chen, Y., M. B. Azad, and S. B. Gibson. 2009. 'Superoxide is the major reactive oxygen species regulating autophagy', *Cell Death Differ*, 16: 1040-52.

- Cheng, S. Y., N. F. Chen, H. M. Kuo, S. N. Yang, C. S. Sung, P. J. Sung, Z. H. Wen, and W. F. Chen. 2018. 'Prodigiosin stimulates endoplasmic reticulum stress and induces autophagic cell death in glioblastoma cells', *Apoptosis*, 23: 314-28.
- Ciociola, A. A., L. B. Cohen, P. Kulkarni, and F. DA-Related Matters Committee of the American College of Gastroenterology. 2014. 'How drugs are developed and approved by the FDA: current process and future directions', *Am J Gastroenterol*, 109: 620-3.
- Clift, M. D., and R. J. Thomson. 2009. 'Development of a merged conjugate addition/oxidative coupling sequence. Application to the enantioselective total synthesis of metacycloprodigiosin and prodigiosin R1', *J Am Chem Soc*, 131: 14579-83.
- Cragg, G. M., and D. J. Newman. 2013. 'Natural products: a continuing source of novel drug leads', *Biochim Biophys Acta*, 1830: 3670-95.
- D'Alessio, R., A. Bargiotti, O. Carlini, F. Colotta, M. Ferrari, P. Gnocchi, A. Isetta, N. Mongelli, P. Motta, A. Rossi, M. Rossi, M. Tibolla, and E. Vanotti. 2000. 'Synthesis and immunosuppressive activity of novel prodigiosin derivatives', *J Med Chem*, 43: 2557-65.
- Davient, B., J. P. Z. Ng, Q. Xiao, L. Li, and L. Yang. 2018. 'Comparative Transcriptomics Unravels Prodigiosin's Potential Cancer-Specific Activity Between Human Small Airway Epithelial Cells and Lung Adenocarcinoma Cells', *Front Oncol*, 8: 573.
- De Tito, S., J. H. Hervas, A. R. van Vliet, and S. A. Tooze. 2020. 'The Golgi as an Assembly Line to the Autophagosome', *Trends Biochem Sci*, 45: 484-96.
- Degenhardt, K., R. Mathew, B. Beaudoin, K. Bray, D. Anderson, G. Chen, C. Mukherjee, Y. Shi, C. Gelinas, Y. Fan, D. A. Nelson, S. Jin, and E. White. 2006. 'Autophagy promotes tumor cell survival and restricts necrosis, inflammation, and tumorigenesis', *Cancer Cell*, 10: 51-64.
- Deng, S., J. Liu, X. Wu, and W. Lu. 2020. 'Golgi Apparatus: A Potential Therapeutic Target for Autophagy-Associated Neurological Diseases', *Front Cell Dev Biol*, 8: 564975.
- DiMasi, J. A., H. G. Grabowski, and R. W. Hansen. 2016. 'Innovation in the pharmaceutical industry: New estimates of R&D costs', *J Health Econ*, 47: 20-33.
- Dinter, A., and E. G. Berger. 1998. 'Golgi-disturbing agents', *Histochem Cell Biol*, 109: 571-90.
- Dooley, H. C., M. Razi, H. E. Polson, S. E. Girardin, M. I. Wilson, and S. A. Tooze. 2014. 'WIPI2 links LC3 conjugation with PI3P, autophagosome formation, and pathogen clearance by recruiting Atg12-5-16L1', *Mol Cell*, 55: 238-52.
- Dumont, F. J., and Q. Su. 1996. 'Mechanism of action of the immunosuppressant rapamycin', *Life Sci*, 58: 373-95.
- Eldredge, H. B., A. Denittis, J. B. Duhadaway, M. Chernick, R. Metz, and G. C. Prendergast. 2013. 'Concurrent Whole Brain Radiotherapy and Short-Course Chloroquine in Patients with Brain Metastases: A Pilot Trial', *J Radiat Oncol*, 2: 315-321.
- Elmore, S. 2007. 'Apoptosis: a review of programmed cell death', *Toxicol Pathol*, 35: 495-516.
- Fabricant, D. S., and N. R. Farnsworth. 2001. 'The value of plants used in traditional medicine for drug discovery', *Environ Health Perspect*, 109 Suppl 1: 69-75.
- Fadok, V. A., A. de Cathelineau, D. L. Daleke, P. M. Henson, and D. L. Bratton. 2001. 'Loss of phospholipid asymmetry and surface exposure of phosphatidylserine is required for phagocytosis of apoptotic cells by macrophages and fibroblasts', *J Biol Chem*, 276: 1071-7.
- Fang, Y. 2014. 'Label-free drug discovery', *Front Pharmacol*, 5: 52.
- Farkas, Thomas, Mads Daugaard, and Marja Jäättelä. 2011. 'Identification of Small Molecule Inhibitors of Phosphatidylinositol 3-Kinase and Autophagy', *Journal of Biological Chemistry*, 286: 38904-12.
- Farnsworth, Norman R., Akerle Olayiwola, Audrey S. Bingel, Djaja D. Soejarto, and Zhengang Guo. 1985. 'Medical plants in therapy', *Bull World Health Organ*, 63: 965-81.
- Feher, D., R. S. Barlow, P. S. Lorenzo, and T. K. Hemscheidt. 2008. 'A 2-substituted prodiginine, 2-(p-hydroxybenzyl)prodigiosin, from *Pseudoalteromonas rubra*', *J Nat Prod*, 71: 1970-2.
- Feng, F., W. Zhang, Y. Chai, D. Guo, and X. Chen. 2023. 'Label-free target protein characterization for small molecule drugs: recent advances in methods and applications', *J Pharm Biomed Anal*, 223: 115107.

- Feng, Z., W. Hu, E. de Stanchina, A. K. Teresky, S. Jin, S. Lowe, and A. J. Levine. 2007. 'The regulation of AMPK beta1, TSC2, and PTEN expression by p53: stress, cell and tissue specificity, and the role of these gene products in modulating the IGF-1-AKT-mTOR pathways', *Cancer Res*, 67: 3043-53.
- Franken, H., T. Mathieson, D. Childs, G. M. Sweetman, T. Werner, I. Togel, C. Doce, S. Gade, M. Bantscheff, G. Drewes, F. B. Reinhard, W. Huber, and M. M. Savitski. 2015. 'Thermal proteome profiling for unbiased identification of direct and indirect drug targets using multiplexed quantitative mass spectrometry', *Nat Protoc*, 10: 1567-93.
- Fujioka, Y., N. N. Noda, H. Nakatogawa, Y. Ohsumi, and F. Inagaki. 2010. 'Dimeric coiled-coil structure of *Saccharomyces cerevisiae* Atg16 and its functional significance in autophagy', *J Biol Chem*, 285: 1508-15.
- Fujita, N., M. Hayashi-Nishino, H. Fukumoto, H. Omori, A. Yamamoto, T. Noda, and T. Yoshimori. 2008. 'An Atg4B mutant hampers the lipidation of LC3 paralogues and causes defects in autophagosome closure', *Mol Biol Cell*, 19: 4651-9.
- Fung, C., R. Lock, S. Gao, E. Salas, and J. Debnath. 2008. 'Induction of autophagy during extracellular matrix detachment promotes cell survival', *Mol Biol Cell*, 19: 797-806.
- Fürstner, A. 2003. 'Chemistry and biology of roseophilin and the prodigiosin alkaloids: a survey of the last 2500 years', *Angew Chem Int Ed Engl*, 42: 3582-603.
- Fürstner, A., J. Grabowski, and C. W. Lehmann. 1999. 'Total Synthesis and Structural Refinement of the Cyclic Tripyrrole Pigment Nonylprodigiosin', *J Org Chem*, 64: 8275-80.
- Fürstner, Alois. 2003. 'Chemie und Biologie des Roseophilins und der Prodigiosin-Alkaloide: 2500 Jahre im Überblick', *Angewandte Chemie*, 115: 3706-28.
- Galavotti, S., S. Bartesaghi, D. Faccenda, M. Shaked-Rabi, S. Sanzone, A. McEvoy, D. Dinsdale, F. Condorelli, S. Brandner, M. Campanella, R. Grose, C. Jones, and P. Salomoni. 2013. 'The autophagy-associated factors DRAM1 and p62 regulate cell migration and invasion in glioblastoma stem cells', *Oncogene*, 32: 699-712.
- Galluzzi, L., and D. R. Green. 2019. 'Autophagy-Independent Functions of the Autophagy Machinery', *Cell*, 177: 1682-99.
- Galluzzi, L., L. Senovilla, I. Vitale, J. Michels, I. Martins, O. Kepp, M. Castedo, and G. Kroemer. 2012. 'Molecular mechanisms of cisplatin resistance', *Oncogene*, 31: 1869-83.
- Galluzzi, L., I. Vitale, S. A. Aaronson, J. M. Abrams, D. Adam, P. Agostinis, E. S. Alnemri, L. Altucci, I. Amelio, D. W. Andrews, M. Annicchiarico-Petruzzelli, A. V. Antonov, E. Arama, E. H. Baehrecke, N. A. Barlev, N. G. Bazan, F. Bernassola, M. J. M. Bertrand, K. Bianchi, M. V. Blagosklonny, K. Blomgren, C. Borner, P. Boya, C. Brenner, M. Campanella, E. Candi, D. Carmona-Gutierrez, F. Cecconi, F. K. Chan, N. S. Chandel, E. H. Cheng, J. E. Chipuk, J. A. Cidlowski, A. Ciechanover, G. M. Cohen, M. Conrad, J. R. Cubillos-Ruiz, P. E. Czabotar, V. D'Angiolella, T. M. Dawson, V. L. Dawson, V. De Laurenzi, R. De Maria, K. M. Debatin, R. J. DeBerardinis, M. Deshmukh, N. Di Daniele, F. Di Virgilio, V. M. Dixit, S. J. Dixon, C. S. Duckett, B. D. Dynlacht, W. S. El-Deiry, J. W. Elrod, G. M. Fimia, S. Fulda, A. J. Garcia-Saez, A. D. Garg, C. Garrido, E. Gavathiotis, P. Golstein, E. Gottlieb, D. R. Green, L. A. Greene, H. Gronemeyer, A. Gross, G. Hajnoczky, J. M. Hardwick, I. S. Harris, M. O. Hengartner, C. Hetz, H. Ichijo, M. Jaattela, B. Joseph, P. J. Jost, P. P. Juin, W. J. Kaiser, M. Karin, T. Kaufmann, O. Kepp, A. Kimchi, R. N. Kitsis, D. J. Klionsky, R. A. Knight, S. Kumar, S. W. Lee, J. J. Lemasters, B. Levine, A. Linkermann, S. A. Lipton, R. A. Lockshin, C. Lopez-Otin, S. W. Lowe, T. Luedde, E. Lugli, M. MacFarlane, F. Madeo, M. Malewicz, W. Malorni, G. Manic, J. C. Marine, S. J. Martin, J. C. Martinou, J. P. Medema, P. Mehlen, P. Meier, S. Melino, E. A. Miao, J. D. Molkentin, U. M. Moll, C. Munoz-Pinedo, S. Nagata, G. Nunez, A. Oberst, M. Oren, M. Overholtzer, M. Pagano, T. Panaretakis, M. Pasparakis, J. M. Penninger, D. M. Pereira, S. Pervaiz, M. E. Peter, M. Piacentini, P. Pinton, J. H. M. Prehn, H. Puthalakath, G. A. Rabinovich, M. Rehm, R. Rizzuto, C. M. P. Rodrigues, D. C. Rubinsztein, T. Rudel, K. M. Ryan, E. Sayan, L. Scorrano, F. Shao, Y. Shi, J. Silke, H. U. Simon, A. Sistigu, B. R. Stockwell, A. Strasser, G. Szabadkai, S. W. G. Tait, D. Tang, N. Tavernarakis, A. Thorburn, Y. Tsujimoto, B. Turk, T. Vanden Berghe, P. Vandenabeele, M. G. Vander Heiden, A. Villunger, H. W. Virgin, K. H. Vousden, D.

- Vucic, E. F. Wagner, H. Walczak, D. Wallach, Y. Wang, J. A. Wells, W. Wood, J. Yuan, Z. Zakeri, B. Zhivotovsky, L. Zitvogel, G. Melino, and G. Kroemer. 2018. 'Molecular mechanisms of cell death: recommendations of the Nomenclature Committee on Cell Death 2018', *Cell Death Differ*, 25: 486-541.
- Ganley, I. G., H. Lam du, J. Wang, X. Ding, S. Chen, and X. Jiang. 2009. 'ULK1.ATG13.FIP200 complex mediates mTOR signaling and is essential for autophagy', *J Biol Chem*, 284: 12297-305.
- Garcia-Cano, J., G. Ambroise, R. Pascual-Serra, M. C. Carrion, L. Serrano-Oviedo, M. Ortega-Muelas, F. J. Cimas, S. Sabater, M. J. Ruiz-Hidalgo, I. Sanchez Perez, A. Mas, F. A. Jalon, A. Vazquez, and R. Sanchez-Prieto. 2015. 'Exploiting the potential of autophagy in cisplatin therapy: A new strategy to overcome resistance', *Oncotarget*, 6: 15551-65.
- Garlaschelli, Luigi. 1999. 'Chemie der Wunder', *Chemie in unserer Zeit*, 33: 152-57.
- Garrido, C., L. Galluzzi, M. Brunet, P. E. Puig, C. Didelot, and G. Kroemer. 2006. 'Mechanisms of cytochrome c release from mitochondria', *Cell Death Differ*, 13: 1423-33.
- Gasiorkiewicz, B. M., P. Koczurkiewicz-Adamczyk, K. Piska, and E. Pekala. 2021. 'Autophagy modulating agents as chemosensitizers for cisplatin therapy in cancer', *Invest New Drugs*, 39: 538-63.
- Gaughran, E. R. 1969. 'From superstition to science: the history of a bacterium', *Trans N Y Acad Sci*, 31: 3-24.
- Gerber, N. N. 1975. 'Prodigiosin-like pigments', *CRC Crit Rev Microbiol*, 3: 469-85.
- Glick, B. S., and A. Nakano. 2009. 'Membrane traffic within the Golgi apparatus', *Annu Rev Cell Dev Biol*, 25: 113-32.
- Grenade, N. L., D. S. Chiriac, A. R. O. Pasternak, J. L. Babulic, B. E. Rowland, G. W. Howe, and A. C. Ross. 2023. 'Discovery of a Tambjamine Gene Cluster in Streptomyces Suggests Convergent Evolution in Bipyrrrole Natural Product Biosynthesis', *ACS Chem Biol*, 18: 223-29.
- Gu, Y., Z. Fei, and R. Zhu. 2020. 'miR-21 modulates cisplatin resistance of gastric cancer cells by inhibiting autophagy via the PI3K/Akt/mTOR pathway', *Anticancer Drugs*, 31: 385-93.
- Guryanov, I. D., N. S. Karamova, D. V. Yusupova, O. I. Gnezdilov, and L. A. Koshkarova. 2013. 'Bacterial pigment prodigiosin and its genotoxic effect', *Russian Journal of Bioorganic Chemistry*, 39: 106-11.
- Guryanov, I., E. Naumenko, F. Akhatova, G. Lazzara, G. Cavallaro, L. Nigamatzyanova, and R. Fakhrullin. 2020. 'Selective Cytotoxic Activity of Prodigiosin@halloysite Nanoformulation', *Front Bioeng Biotechnol*, 8: 424.
- Gwinn, D. M., D. B. Shackelford, D. F. Egan, M. M. Mihaylova, A. Mery, D. S. Vasquez, B. E. Turk, and R. J. Shaw. 2008. 'AMPK phosphorylation of raptor mediates a metabolic checkpoint', *Mol Cell*, 30: 214-26.
- Habash, S. S., H. U. C. Brass, A. S. Klein, D. P. Klebl, T. M. Weber, T. Classen, J. Pietruszka, F. M. W. Grundler, and A. S. S. Schleker. 2020. 'Novel Prodiginine Derivatives Demonstrate Bioactivities on Plants, Nematodes, and Fungi', *Front Plant Sci*, 11: 579807.
- Han, C., B. Sun, W. Wang, W. Cai, D. Lou, Y. Sun, and X. Zhao. 2011. 'Overexpression of microtubule-associated protein-1 light chain 3 is associated with melanoma metastasis and vasculogenic mimicry', *Tohoku J Exp Med*, 223: 243-51.
- Hanahan, D., and R. A. Weinberg. 2011. 'Hallmarks of cancer: the next generation', *Cell*, 144: 646-74.
- Harder, B. G., S. Peng, C. P. Sereduk, A. M. Sodoma, G. J. Kitange, J. C. Loftus, J. N. Sarkaria, and N. L. Tran. 2019. 'Inhibition of phosphatidylinositol 3-kinase by PX-866 suppresses temozolomide-induced autophagy and promotes apoptosis in glioblastoma cells', *Mol Med*, 25: 49.
- Harris, A. K. P., N. R. Williamson, H. Slater, A. Cox, S. Abbasi, I. Foulds, H. T. Simonsen, F. J. Leeper, and G. P. C. Salmond. 2004. 'The Serratia gene cluster encoding biosynthesis of the red antibiotic, prodigiosin, shows species- and strain-dependent genome context variation', *Microbiology (Reading)*, 150: 3547-60.

- Hartmann, A. 2016. 'Back to the roots - dermatology in ancient Egyptian medicine', *J Dtsch Dermatol Ges*, 14: 389-96.
- Haynes, S. W., P. K. Sydor, C. Corre, L. Song, and G. L. Challis. 2011. 'Stereochemical elucidation of streptorubin B', *J Am Chem Soc*, 133: 1793-8.
- Heidari, N., M. A. Hicks, and H. Harada. 2010. 'GX15-070 (obatoclax) overcomes glucocorticoid resistance in acute lymphoblastic leukemia through induction of apoptosis and autophagy', *Cell Death Dis*, 1: e76.
- Hejazi, A., and F. R. Falkner. 1997. 'Serratia marcescens', *J Med Microbiol*, 46: 903-12.
- Herraez, R., A. Mur, A. Merlos, M. Vinas, and T. Vinuesa. 2019. 'Using prodigiosin against some gram-positive and gram-negative bacteria and Trypanosoma cruzi', *J Venom Anim Toxins Incl Trop Dis*, 25: e20190001.
- Hill, M. M., C. Adrain, P. J. Duriez, E. M. Creagh, and S. J. Martin. 2004. 'Analysis of the composition, assembly kinetics and activity of native Apaf-1 apoptosomes', *EMBO J*, 23: 2134-45.
- Hong, B., V. V. Prabhu, S. Zhang, A. P. van den Heuvel, D. T. Dicker, L. Kopelovich, and W. S. El-Deiry. 2014. 'Prodigiosin rescues deficient p53 signaling and antitumor effects via upregulating p73 and disrupting its interaction with mutant p53', *Cancer Res*, 74: 1153-65.
- Hosokawa, N., T. Hara, T. Kaizuka, C. Kishi, A. Takamura, Y. Miura, S. Iemura, T. Natsume, K. Takehana, N. Yamada, J. L. Guan, N. Oshiro, and N. Mizushima. 2009. 'Nutrient-dependent mTORC1 association with the ULK1-Atg13-FIP200 complex required for autophagy', *Mol Biol Cell*, 20: 1981-91.
- Hotte, S. J., K. N. Chi, A. M. Joshua, D. Tu, R. J. Macfarlane, R. W. Gregg, J. D. Ruether, N. S. Basappa, D. Finch, M. Salim, E. W. Winkquist, V. Torri, S. North, C. Kollmannsberger, S. L. Ellard, B. J. Eigl, A. Tinker, A. L. Allan, K. Beja, M. Annala, J. Powers, A. W. Wyatt, L. Seymour, and Group Canadian Cancer Trials. 2019. 'A Phase II Study of PX-866 in Patients With Recurrent or Metastatic Castration-resistant Prostate Cancer: Canadian Cancer Trials Group Study IND205', *Clin Genitourin Cancer*, 17: 201-08 e1.
- Hou, W., J. Han, C. Lu, L. A. Goldstein, and H. Rabinowich. 2010. 'Autophagic degradation of active caspase-8: a crosstalk mechanism between autophagy and apoptosis', *Autophagy*, 6: 891-900.
- Hu, D. X., D. M. Withall, G. L. Challis, and R. J. Thomson. 2016. 'Structure, Chemical Synthesis, and Biosynthesis of Prodigiosin Natural Products', *Chem Rev*, 116: 7818-53.
- Hu, Y. L., A. Jahangiri, M. Delay, and M. K. Aghi. 2012. 'Tumor cell autophagy as an adaptive response mediating resistance to treatments such as antiangiogenic therapy', *Cancer Res*, 72: 4294-9.
- Hu, Z., M. Cai, Y. Zhang, L. Tao, and R. Guo. 2020. 'miR-29c-3p inhibits autophagy and cisplatin resistance in ovarian cancer by regulating FOXO1/ATG14 pathway', *Cell Cycle*, 19: 193-206.
- Huang, Y., Q. Xi, Y. Chen, J. Wang, P. Peng, S. Xia, and S. Yu. 2013. 'A dual mTORC1 and mTORC2 inhibitor shows antitumor activity in esophageal squamous cell carcinoma cells and sensitizes them to cisplatin', *Anticancer Drugs*, 24: 889-98.
- Hughes, J. P., S. Rees, S. B. Kalindjian, and K. L. Philpott. 2011. 'Principles of early drug discovery', *Br J Pharmacol*, 162: 1239-49.
- Huo, Y., H. Cai, I. Teplova, C. Bowman-Colin, G. Chen, S. Price, N. Barnard, S. Ganesan, V. Karantza, E. White, and B. Xia. 2013. 'Autophagy opposes p53-mediated tumor barrier to facilitate tumorigenesis in a model of PALB2-associated hereditary breast cancer', *Cancer Discov*, 3: 894-907.
- Imai, K., F. Hao, N. Fujita, Y. Tsuji, Y. Oe, Y. Araki, M. Hamasaki, T. Noda, and T. Yoshimori. 2016. 'Atg9A trafficking through the recycling endosomes is required for autophagosome formation', *J Cell Sci*, 129: 3781-91.
- Isaka, M., A. Jaturapat, J. Kramyu, M. Tanticharoen, and Y. Thebtaranonth. 2002. 'Potent in vitro antimalarial activity of metacycloprodigiosin isolated from Streptomyces spectabilis BCC 4785', *Antimicrob Agents Chemother*, 46: 1112-3.

- Ishida, Y., S. Nayak, J. A. Mindell, and M. Grabe. 2013. 'A model of lysosomal pH regulation', *J Gen Physiol*, 141: 705-20.
- Itakura, E., and N. Mizushima. 2010. 'Characterization of autophagosome formation site by a hierarchical analysis of mammalian Atg proteins', *Autophagy*, 6: 764-76.
- Jafari, R., H. Almqvist, H. Axelsson, M. Ignatushchenko, T. Lundback, P. Nordlund, and D. Martinez Molina. 2014. 'The cellular thermal shift assay for evaluating drug target interactions in cells', *Nat Protoc*, 9: 2100-22.
- Jahreiss, L., F. M. Menzies, and D. C. Rubinsztein. 2008. 'The itinerary of autophagosomes: from peripheral formation to kiss-and-run fusion with lysosomes', *Traffic*, 9: 574-87.
- Jaremko, M. J., T. D. Davis, J. C. Corpuz, and M. D. Burkart. 2020. 'Type II non-ribosomal peptide synthetase proteins: structure, mechanism, and protein-protein interactions', *Nat Prod Rep*, 37: 355-79.
- Ji, S., R. Sun, K. Xu, Z. Man, J. Ji, Y. Pu, L. Yin, J. Zhang, and Y. Pu. 2019. 'Prodigiosin induces apoptosis and inhibits autophagy via the extracellular signal-regulated kinase pathway in K562 cells', *Toxicol In Vitro*, 60: 107-15.
- Johnson, F. D., C. S. Hughes, A. Liu, W. W. Lockwood, and G. B. Morin. 2023. 'Tandem mass tag-based thermal proteome profiling for the discovery of drug-protein interactions in cancer cells', *STAR Protoc*, 4: 102012.
- Judith, D., H. B. J. Jefferies, S. Boeing, D. Frith, A. P. Snijders, and S. A. Tooze. 2019. 'ATG9A shapes the forming autophagosome through Arfaptin 2 and phosphatidylinositol 4-kinase IIIbeta', *J Cell Biol*, 218: 1634-52.
- Jung, C. H., C. B. Jun, S. H. Ro, Y. M. Kim, N. M. Otto, J. Cao, M. Kundu, and D. H. Kim. 2009. 'ULK-Atg13-FIP200 complexes mediate mTOR signaling to the autophagy machinery', *Mol Biol Cell*, 20: 1992-2003.
- Kabeya, Y., N. Mizushima, T. Ueno, A. Yamamoto, T. Kirisako, T. Noda, E. Kominami, Y. Ohsumi, and T. Yoshimori. 2000. 'LC3, a mammalian homologue of yeast Apg8p, is localized in autophagosome membranes after processing', *EMBO J*, 19: 5720-8.
- Kabeya, Y., N. Mizushima, A. Yamamoto, S. Oshitani-Okamoto, Y. Ohsumi, and T. Yoshimori. 2004. 'LC3, GABARAP and GATE16 localize to autophagosomal membrane depending on form-II formation', *J Cell Sci*, 117: 2805-12.
- Kaiser, S. E., K. Mao, A. M. Taherbhoy, S. Yu, J. L. Olszewski, D. M. Duda, I. Kurinov, A. Deng, T. D. Fenn, D. J. Klionsky, and B. A. Schulman. 2012. 'Noncanonical E2 recruitment by the autophagy E1 revealed by Atg7-Atg3 and Atg7-Atg10 structures', *Nat Struct Mol Biol*, 19: 1242-9.
- Kamada, Y., K. Yoshino, C. Kondo, T. Kawamata, N. Oshiro, K. Yonezawa, and Y. Ohsumi. 2010. 'Tor directly controls the Atg1 kinase complex to regulate autophagy', *Mol Cell Biol*, 30: 1049-58.
- Kang, R., H. J. Zeh, M. T. Lotze, and D. Tang. 2011. 'The Beclin 1 network regulates autophagy and apoptosis', *Cell Death Differ*, 18: 571-80.
- Kaushik, S., and A. M. Cuervo. 2018. 'The coming of age of chaperone-mediated autophagy', *Nat Rev Mol Cell Biol*, 19: 365-81.
- Kawauchi, K., K. Shibutani, H. Yagisawa, H. Kamata, S. Nakatsuji, H. Anzai, Y. Yokoyama, Y. Ikegami, Y. Moriyama, and H. Hirata. 1997. 'A possible immunosuppressant, cycloprodigiosin hydrochloride, obtained from *Pseudoalteromonas denitrificans*', *Biochem Biophys Res Commun*, 237: 543-7.
- Khurshed, M., R. J. Molenaar, M. E. van Linde, R. A. Mathot, E. A. Struys, T. van Wezel, C. J. F. van Noorden, H. J. Klumpen, Jvmg Bovee, and J. W. Wilmink. 2021. 'A Phase Ib Clinical Trial of Metformin and Chloroquine in Patients with IDH1-Mutated Solid Tumors', *Cancers (Basel)*, 13: 2474.
- Kim, H. S., M. Hayashi, Y. Shibata, Y. Wataya, T. Mitamura, T. Horii, K. Kawauchi, H. Hirata, S. Tsuboi, and Y. Moriyama. 1999. 'Cycloprodigiosin hydrochloride obtained from *Pseudoalteromonas denitrificans* is a potent antimalarial agent', *Biol Pharm Bull*, 22: 532-4.
- Kim, Y. C., and K. L. Guan. 2015. 'mTOR: a pharmacologic target for autophagy regulation', *J Clin Invest*, 125: 25-32.

- Kimmelman, A. C. 2011. 'The dynamic nature of autophagy in cancer', *Genes Dev*, 25: 1999-2010.
- Kirisako, T., Y. Ichimura, H. Okada, Y. Kabeya, N. Mizushima, T. Yoshimori, M. Ohsumi, T. Takao, T. Noda, and Y. Ohsumi. 2000. 'The reversible modification regulates the membrane-binding state of Apg8/Aut7 essential for autophagy and the cytoplasm to vacuole targeting pathway', *J Cell Biol*, 151: 263-76.
- Kirkin, V., and V. V. Rogov. 2019. 'A Diversity of Selective Autophagy Receptors Determines the Specificity of the Autophagy Pathway', *Mol Cell*, 76: 268-85.
- Kischkel, F. C., S. Hellbardt, I. Behrmann, M. Germer, M. Pawlita, P. H. Krammer, and M. E. Peter. 1995. 'Cytotoxicity-dependent APO-1 (Fas/CD95)-associated proteins form a death-inducing signaling complex (DISC) with the receptor', *EMBO J*, 14: 5579-88.
- Klein, A. S., H. U. C. Brass, D. P. Klebl, T. Classen, A. Loeschcke, T. Drepper, S. Sievers, K. E. Jaeger, and J. Pietruszka. 2018. 'Preparation of Cyclic Prodiginines by Mutasynthesis in *Pseudomonas putida* KT2440', *Chembiochem*, 19: 1545-52.
- Klein, A. S., A. Domrose, P. Bongen, H. U. C. Brass, T. Classen, A. Loeschcke, T. Drepper, L. Laraia, S. Sievers, K. E. Jaeger, and J. Pietruszka. 2017. 'New Prodigiosin Derivatives Obtained by Mutasynthesis in *Pseudomonas putida*', *ACS Synth Biol*, 6: 1757-65.
- Klumperman, J. 2011. 'Architecture of the mammalian Golgi', *Cold Spring Harb Perspect Biol*, 3: a005181.
- Konno, H., H. Matsuya, M. Okamoto, T. Sato, Y. Tanaka, K. Yokoyama, T. Kataoka, K. Nagai, H. H. Wasserman, and S. Ohkuma. 1998. 'Prodigiosins uncouple mitochondrial and bacterial F-ATPases: evidence for their H<sup>+</sup>/Cl<sup>-</sup> symport activity', *J Biochem*, 124: 547-56.
- Kraft, C., M. Kijanska, E. Kalie, E. Siergiejuk, S. S. Lee, G. Semplicio, I. Stoffel, A. Brezovich, M. Verma, I. Hansmann, G. Ammerer, K. Hofmann, S. Tooze, and M. Peter. 2012. 'Binding of the Atg1/ULK1 kinase to the ubiquitin-like protein Atg8 regulates autophagy', *EMBO J*, 31: 3691-703.
- Kriel, J., and B. Loos. 2019. 'The good, the bad and the autophagosome: exploring unanswered questions of autophagy-dependent cell death', *Cell Death Differ*, 26: 640-52.
- Krishna, P. S., K. Vani, M. R. Prasad, B. Samatha, N. S. Bindu, M. A. Charya, and P. Reddy Shetty. 2013. 'In -silico molecular docking analysis of prodigiosin and cycloprodigiosin as COX-2 inhibitors', *Springerplus*, 2: 172.
- Kulkarni-Gosavi, P., C. Makhoul, and P. A. Gleeson. 2019. 'Form and function of the Golgi apparatus: scaffolds, cytoskeleton and signalling', *FEBS Lett*, 593: 2289-305.
- Kuma, A., M. Hatano, M. Matsui, A. Yamamoto, H. Nakaya, T. Yoshimori, Y. Ohsumi, T. Tokuhi, and N. Mizushima. 2004. 'The role of autophagy during the early neonatal starvation period', *Nature*, 432: 1032-6.
- Ladinsky, M. S., D. N. Mastronarde, J. R. McIntosh, K. E. Howell, and L. A. Staehelin. 1999. 'Golgi structure in three dimensions: functional insights from the normal rat kidney cell', *J Cell Biol*, 144: 1135-49.
- Lapenda, J. C., P. A. Silva, M. C. Vicalvi, K. X. Sena, and S. C. Nascimento. 2015. 'Antimicrobial activity of prodigiosin isolated from *Serratia marcescens* UFPEDA 398', *World J Microbiol Biotechnol*, 31: 399-406.
- Lazova, R., R. L. Camp, V. Klump, S. F. Siddiqui, R. K. Amaravadi, and J. M. Pawelek. 2012. 'Punctate LC3B expression is a common feature of solid tumors and associated with proliferation, metastasis, and poor outcome', *Clin Cancer Res*, 18: 370-9.
- Lee, Y. K., and J. A. Lee. 2016. 'Role of the mammalian ATG8/LC3 family in autophagy: differential and compensatory roles in the spatiotemporal regulation of autophagy', *BMB Rep*, 49: 424-30.
- Leitlinienprogramm Onkologie Deutsche Krebsgesellschaft, Deutsche Krebshilfe, AWMF. 2020. "S3-Leitlinie Früherkennung, Diagnose, Therapie und Nachsorge des Harnblasenkarzinoms, Langversion 2.0, 2020, AWMF-Registrierungsnummer 032/038OL (In German)." In.

- Lenz, T., and K. Stühler. 2022. 'Small Molecule Arranged Thermal Proximity Coaggregation (smarTPCA)-A Novel Approach to Characterize Protein-Protein Interactions in Living Cells by Similar Isothermal Dose-Responses', *Int J Mol Sci*, 23: 5605.
- Levine, B., and G. Kroemer. 2008. 'Autophagy in the pathogenesis of disease', *Cell*, 132: 27-42.
- Li, D., J. Liu, X. Wang, D. Kong, W. Du, H. Li, C. Y. Hse, T. Shupe, D. Zhou, and K. Zhao. 2018. 'Biological Potential and Mechanism of Prodigiosin from *Serratia marcescens* Subsp. *lawsoniana* in Human Choriocarcinoma and Prostate Cancer Cell Lines', *Int J Mol Sci*, 19: 3465.
- Li, H., P. Wang, Q. Sun, W. X. Ding, X. M. Yin, R. W. Sobol, D. B. Stolz, J. Yu, and L. Zhang. 2011. 'Following cytochrome c release, autophagy is inhibited during chemotherapy-induced apoptosis by caspase 8-mediated cleavage of Beclin 1', *Cancer Res*, 71: 3625-34.
- Li, X., Y. Feng, and X. Liu. 2013. 'Crystallization and preliminary crystallographic studies of GRASP65 GRASP domain from *Rattus norvegicus*', *Acta Crystallogr Sect F Struct Biol Cryst Commun*, 69: 792-5.
- Liang, C., P. Feng, B. Ku, I. Dotan, D. Canaani, B. H. Oh, and J. U. Jung. 2006. 'Autophagic and tumour suppressor activity of a novel Beclin1-binding protein UVRAG', *Nat Cell Biol*, 8: 688-99.
- Liang, C., P. Feng, B. Ku, B. H. Oh, and J. U. Jung. 2007. 'UVRAG: a new player in autophagy and tumor cell growth', *Autophagy*, 3: 69-71.
- Liang, X. H., S. Jackson, M. Seaman, K. Brown, B. Kempkes, H. Hibshoosh, and B. Levine. 1999. 'Induction of autophagy and inhibition of tumorigenesis by beclin 1', *Nature*, 402: 672-6.
- Lin, P. B., J. Shen, P. Y. Ou, L. Y. Liu, Z. Y. Chen, F. J. Chu, J. Wang, and X. B. Jin. 2019. 'Prodigiosin isolated from *Serratia marcescens* in the *Periplaneta americana* gut and its apoptosis-inducing activity in HeLa cells', *Oncol Rep*, 41: 3377-85.
- Lin, S. R., and C. F. Weng. 2018. 'PG-Priming Enhances Doxorubicin Influx to Trigger Necrotic and Autophagic Cell Death in Oral Squamous Cell Carcinoma', *J Clin Med*, 7: 375.
- Lipinski, C. A. 2004. 'Lead- and drug-like compounds: the rule-of-five revolution', *Drug Discov Today Technol*, 1: 337-41.
- Lipinski, C. A., F. Lombardo, B. W. Dominy, and P. J. Feeney. 2001. 'Experimental and computational approaches to estimate solubility and permeability in drug discovery and development settings', *Adv Drug Deliv Rev*, 46: 3-26.
- Lorincz, P., and G. Juhasz. 2020. 'Autophagosome-Lysosome Fusion', *J Mol Biol*, 432: 2462-82.
- Luo, S., and D. C. Rubinsztein. 2010. 'Apoptosis blocks Beclin 1-dependent autophagosome synthesis: an effect rescued by Bcl-xL', *Cell Death Differ*, 17: 268-77.
- Ma, K., G. Chen, W. Li, O. Kepp, Y. Zhu, and Q. Chen. 2020. 'Mitophagy, Mitochondrial Homeostasis, and Cell Fate', *Front Cell Dev Biol*, 8: 467.
- Ma, K., S. Li, X. Huo, M. Guo, X. Du, C. Li, X. Liu, J. Lv, and Z. Chen. 2020. 'Exploring the mechanism of cisplatin resistance by transcriptome sequencing and reversing the chemoresistance by autophagy inhibition in small cell lung cancer', *Biochem Biophys Res Commun*, 533: 474-80.
- Mack, H. I., B. Zheng, J. M. Asara, and S. M. Thomas. 2012. 'AMPK-dependent phosphorylation of ULK1 regulates ATG9 localization', *Autophagy*, 8: 1197-214.
- Magae, J., M. W. Miller, K. Nagai, and G. M. Shearer. 1996. 'Effect of metacycloprodigiosin, an inhibitor of killer T cells on murine skin and heart transplants', *J Antibiot (Tokyo)*, 49: 86-90.
- Maiuri, M. C., L. Galluzzi, E. Morselli, O. Kepp, S. A. Malik, and G. Kroemer. 2010. 'Autophagy regulation by p53', *Curr Opin Cell Biol*, 22: 181-5.
- Mani, J., S. Vallo, S. Rakel, P. Antonietti, F. Gessler, R. Blaheta, G. Bartsch, M. Michaelis, J. Cinatl, A. Haferkamp, and D. Kogel. 2015. 'Chemoresistance is associated with increased cytoprotective autophagy and diminished apoptosis in bladder cancer cells treated with the BH3 mimetic (-)-Gossypol (AT-101)', *BMC Cancer*, 15: 224.

- Mari, M., J. Griffith, E. Rieter, L. Krishnappa, D. J. Klionsky, and F. Reggiori. 2010. 'An Atg9-containing compartment that functions in the early steps of autophagosome biogenesis', *J Cell Biol*, 190: 1005-22.
- Marino, G., M. Niso-Santano, E. H. Baehrecke, and G. Kroemer. 2014. 'Self-consumption: the interplay of autophagy and apoptosis', *Nat Rev Mol Cell Biol*, 15: 81-94.
- Martinez Molina, D., R. Jafari, M. Ignatushchenko, T. Seki, E. A. Larsson, C. Dan, L. Sreekumar, Y. Cao, and P. Nordlund. 2013. 'Monitoring drug target engagement in cells and tissues using the cellular thermal shift assay', *Science*, 341: 84-7.
- Matsunaga, K., E. Morita, T. Saitoh, S. Akira, N. T. Ktistakis, T. Izumi, T. Noda, and T. Yoshimori. 2010. 'Autophagy requires endoplasmic reticulum targeting of the PI3-kinase complex via Atg14L', *J Cell Biol*, 190: 511-21.
- McCoy, F., J. Hurwitz, N. McTavish, I. Paul, C. Barnes, B. O'Hagan, K. Odrzywol, J. Murray, D. Longley, G. McKerr, and D. A. Fennell. 2010. 'Obatoclox induces Atg7-dependent autophagy independent of beclin-1 and BAX/BAK', *Cell Death Dis*, 1: e108.
- McInnes, C. 2007. 'Virtual screening strategies in drug discovery', *Curr Opin Chem Biol*, 11: 494-502.
- Melvin, Matt S., John T. Tomlinson, Gilda R. Saluta, Gregory L. Kucera, Neils Lindquist, and Richard A. Manderville. 2000. 'Double-Strand DNA Cleavage by Copper-Prodigiosin', *Journal of the American Chemical Society*, 122: 6333-34.
- Metlagel, Z., C. Otomo, G. Takaesu, and T. Otomo. 2013. 'Structural basis of ATG3 recognition by the autophagic ubiquitin-like protein ATG12', *Proc Natl Acad Sci U S A*, 110: 18844-9.
- Mindell, J. A. 2012. 'Lysosomal acidification mechanisms', *Annu Rev Physiol*, 74: 69-86.
- Mizushima, N., and M. Komatsu. 2011. 'Autophagy: renovation of cells and tissues', *Cell*, 147: 728-41.
- Mizushima, N., A. Kuma, Y. Kobayashi, A. Yamamoto, M. Matsubae, T. Takao, T. Natsume, Y. Ohsumi, and T. Yoshimori. 2003. 'Mouse Apg16L, a novel WD-repeat protein, targets to the autophagic isolation membrane with the Apg12-Apg5 conjugate', *J Cell Sci*, 116: 1679-88.
- Mizushima, N., T. Noda, T. Yoshimori, Y. Tanaka, T. Ishii, M. D. George, D. J. Klionsky, M. Ohsumi, and Y. Ohsumi. 1998. 'A protein conjugation system essential for autophagy', *Nature*, 395: 395-8.
- Mizushima, N., H. Sugita, T. Yoshimori, and Y. Ohsumi. 1998. 'A new protein conjugation system in human. The counterpart of the yeast Apg12p conjugation system essential for autophagy', *J Biol Chem*, 273: 33889-92.
- Mohammadi, S., B. Jafari, P. Asgharian, M. Martorell, and J. Sharifi-Rad. 2020. 'Medicinal plants used in the treatment of Malaria: A key emphasis to Artemisia, Cinchona, Cryptolepis, and Tabebuia genera', *Phytother Res*, 34: 1556-69.
- Molenaar, R. J., R. J. S. Coelen, M. Khurshed, E. Roos, M. W. A. Caan, M. E. van Linde, M. Kouwenhoven, J. A. M. Bramer, Jvmg Bovee, R. A. Mathot, H. J. Klumpen, H. W. M. van Laarhoven, C. J. F. van Noorden, W. P. Vandertop, H. Gelderblom, T. M. van Gulik, and J. W. Wilmink. 2017. 'Study protocol of a phase IB/II clinical trial of metformin and chloroquine in patients with IDH1-mutated or IDH2-mutated solid tumours', *BMJ Open*, 7: e014961.
- Mollenhauer, H. H., D. J. Morre, and L. D. Rowe. 1990. 'Alteration of intracellular traffic by monensin; mechanism, specificity and relationship to toxicity', *Biochim Biophys Acta*, 1031: 225-46.
- Montaner, B., S. Navarro, M. Pique, M. Vilaseca, M. Martinell, E. Giralt, J. Gil, and R. Perez-Tomas. 2000. 'Prodigiosin from the supernatant of *Serratia marcescens* induces apoptosis in haematopoietic cancer cell lines', *Br J Pharmacol*, 131: 585-93.
- Montaner, B., and R. Perez-Tomas. 2001. 'Prodigiosin-induced apoptosis in human colon cancer cells', *Life Sci*, 68: 2025-36.
- Morselli, E., S. Shen, C. Ruckenstein, M. A. Bauer, G. Marino, L. Galluzzi, A. Criollo, M. Michaud, M. C. Maiuri, T. Chano, F. Madeo, and G. Kroemer. 2011. 'p53 inhibits autophagy by interacting with the human ortholog of yeast Atg17, RB1CC1/FIP200', *Cell Cycle*, 10: 2763-9.

- Mukhopadhyay, S., P. K. Panda, N. Sinha, D. N. Das, and S. K. Bhutia. 2014. 'Autophagy and apoptosis: where do they meet?', *Apoptosis*, 19: 555-66.
- Nadal, R., and J. Bellmunt. 2019. 'Management of metastatic bladder cancer', *Cancer Treat Rev*, 76: 10-21.
- Nakamura, S., and T. Yoshimori. 2017. 'New insights into autophagosome-lysosome fusion', *J Cell Sci*, 130: 1209-16.
- Nakatogawa, H., Y. Ichimura, and Y. Ohsumi. 2007. 'Atg8, a ubiquitin-like protein required for autophagosome formation, mediates membrane tethering and hemifusion', *Cell*, 130: 165-78.
- Nakatogawa, H., J. Ishii, E. Asai, and Y. Ohsumi. 2012. 'Atg4 recycles inappropriately lipidated Atg8 to promote autophagosome biogenesis', *Autophagy*, 8: 177-86.
- Nassour, J., R. Radford, A. Correia, J. M. Fuste, B. Schoell, A. Jauch, R. J. Shaw, and J. Karlseder. 2019. 'Autophagic cell death restricts chromosomal instability during replicative crisis', *Nature*, 565: 659-63.
- Naydenov, N. G., A. Feygin, L. Wang, and A. I. Ivanov. 2014. 'N-ethylmaleimide-sensitive factor attachment protein alpha (alphaSNAP) regulates matrix adhesion and integrin processing in human epithelial cells', *J Biol Chem*, 289: 2424-39.
- Naydenov, N. G., G. Harris, B. Brown, K. L. Schaefer, S. K. Das, P. B. Fisher, and A. I. Ivanov. 2012. 'Loss of soluble N-ethylmaleimide-sensitive factor attachment protein alpha (alphaSNAP) induces epithelial cell apoptosis via down-regulation of Bcl-2 expression and disruption of the Golgi', *J Biol Chem*, 287: 5928-41.
- Naydenov, N. G., G. Harris, V. Morales, and A. I. Ivanov. 2012. 'Loss of a membrane trafficking protein alphaSNAP induces non-canonical autophagy in human epithelia', *Cell Cycle*, 11: 4613-25.
- New, J., L. Arnold, M. Ananth, S. Alvi, M. Thornton, L. Werner, O. Tawfik, H. Dai, Y. Shnyder, K. Kakarala, T. T. Tsue, D. A. Girod, W. X. Ding, S. Anant, and S. M. Thomas. 2017. 'Secretory Autophagy in Cancer-Associated Fibroblasts Promotes Head and Neck Cancer Progression and Offers a Novel Therapeutic Target', *Cancer Res*, 77: 6679-91.
- Newman, D. J., and G. M. Cragg. 2004. 'Marine natural products and related compounds in clinical and advanced preclinical trials', *J Nat Prod*, 67: 1216-38.
- Newman, D. J., and G. M. Cragg. 2012. 'Natural products as sources of new drugs over the 30 years from 1981 to 2010', *J Nat Prod*, 75: 311-35.
- Newman, D. J., and R. T. Hill. 2006. 'New drugs from marine microbes: the tide is turning', *J Ind Microbiol Biotechnol*, 33: 539-44.
- Noda, N. N., K. Satoo, Y. Fujioka, H. Kumeta, K. Ogura, H. Nakatogawa, Y. Ohsumi, and F. Inagaki. 2011. 'Structural basis of Atg8 activation by a homodimeric E1, Atg7', *Mol Cell*, 44: 462-75.
- Norman, J. M., G. M. Cohen, and E. T. Bampton. 2010. 'The in vitro cleavage of the hAtg proteins by cell death proteases', *Autophagy*, 6: 1042-56.
- Nthiga, T. M., B. Kumar Shrestha, T. Lamark, and T. Johansen. 2021. 'The soluble reticulophagy receptor CALCOCO1 is also a Golgiphagy receptor', *Autophagy*, 17: 2051-52.
- Nthiga, T. M., B. K. Shrestha, J. A. Bruun, K. B. Larsen, T. Lamark, and T. Johansen. 2021. 'Regulation of Golgi turnover by CALCOCO1-mediated selective autophagy', *J Cell Biol*, 220: e202006128.
- Nüchel, J., M. Tauber, J. L. Nolte, M. Morgelin, C. Turk, B. Eckes, C. Demetriades, and M. Plomann. 2021. 'An mTORC1-GRASP55 signaling axis controls unconventional secretion to reshape the extracellular proteome upon stress', *Mol Cell*, 81: 3275-93 e12.
- Ohkuma, S., T. Sato, M. Okamoto, H. Matsuya, K. Arai, T. Kataoka, K. Nagai, and H. H. Wasserman. 1998. 'Prodigosins uncouple lysosomal vacuolar-type ATPase through promotion of H<sup>+</sup>/Cl<sup>-</sup> symport', *Biochem J*, 334 ( Pt 3): 731-41.
- Oki, Y., A. Copeland, F. Hagemester, L. E. Fayad, M. Fanale, J. Romaguera, and A. Younes. 2012. 'Experience with obatoclax mesylate (GX15-070), a small molecule pan-Bcl-2 family antagonist in patients with relapsed or refractory classical Hodgkin lymphoma', *Blood*, 119: 2171-2.

- Oral, O., D. Oz-Arslan, Z. Itah, A. Naghavi, R. Deveci, S. Karacali, and D. Gozuacik. 2012. 'Cleavage of Atg3 protein by caspase-8 regulates autophagy during receptor-activated cell death', *Apoptosis*, 17: 810-20.
- Otomo, C., Z. Metlagel, G. Takaesu, and T. Otomo. 2013. 'Structure of the human ATG12~ATG5 conjugate required for LC3 lipidation in autophagy', *Nat Struct Mol Biol*, 20: 59-66.
- Paik, P. K., C. M. Rudin, M. C. Pietanza, A. Brown, N. A. Rizvi, N. Takebe, W. Travis, L. James, M. S. Ginsberg, R. Juergens, S. Markus, L. Tyson, S. Subzwari, M. G. Kris, and L. M. Krug. 2011. 'A phase II study of obatoclox mesylate, a Bcl-2 antagonist, plus topotecan in relapsed small cell lung cancer', *Lung Cancer*, 74: 481-5.
- Pan, J., C. Cheng, S. Verstovsek, Q. Chen, Y. Jin, and Q. Cao. 2010. 'The BH3-mimetic GX15-070 induces autophagy, potentiates the cytotoxicity of carboplatin and 5-fluorouracil in esophageal carcinoma cells', *Cancer Lett*, 293: 167-74.
- Park, J. M., C. H. Jung, M. Seo, N. M. Otto, D. Grunwald, K. H. Kim, B. Moriarity, Y. M. Kim, C. Starker, R. S. Nho, D. Voytas, and D. H. Kim. 2016. 'The ULK1 complex mediates MTORC1 signaling to the autophagy initiation machinery via binding and phosphorylating ATG14', *Autophagy*, 12: 547-64.
- Pattingre, S., A. Tassa, X. Qu, R. Garuti, X. H. Liang, N. Mizushima, M. Packer, M. D. Schneider, and B. Levine. 2005. 'Bcl-2 antiapoptotic proteins inhibit Beclin 1-dependent autophagy', *Cell*, 122: 927-39.
- Paul, T., P. Bhardwaj, A. Mondal, T. K. Bandyopadhyay, N. Mahata, and B. Bhunia. 2023. 'Identification of Novel Protein Targets of Prodigiosin for Breast Cancer Using Inverse Virtual Screening Methods', *Appl Biochem Biotechnol*, preprint, 10.1007/s12010-023-04426-9.
- Pellegrini, P., A. Strambi, C. Zipoli, M. Hagg-Olofsson, M. Buoncervello, S. Linder, and A. De Milito. 2014. 'Acidic extracellular pH neutralizes the autophagy-inhibiting activity of chloroquine: implications for cancer therapies', *Autophagy*, 10: 562-71.
- Pengo, N., A. Agrotis, K. Prak, J. Jones, and R. Ketteler. 2017. 'A reversible phospho-switch mediated by ULK1 regulates the activity of autophagy protease ATG4B', *Nat Commun*, 8: 294.
- Perez-Tomas, R., and M. Vinas. 2010. 'New insights on the antitumoral properties of prodiginines', *Curr Med Chem*, 17: 2222-31.
- Peter, C., S. Wesselborg, M. Herrmann, and K. Lauber. 2010. 'Dangerous attraction: phagocyte recruitment and danger signals of apoptotic and necrotic cells', *Apoptosis*, 15: 1007-28.
- Petiot, A., E. Ogier-Denis, E. F. Blommaert, A. J. Meijer, and P. Codogno. 2000. 'Distinct classes of phosphatidylinositol 3'-kinases are involved in signaling pathways that control macroautophagy in HT-29 cells', *J Biol Chem*, 275: 992-8.
- Pitz, M. W., E. A. Eisenhauer, M. V. MacNeil, B. Thiessen, J. C. Easaw, D. R. Macdonald, D. D. Eisenstat, A. S. Kakumanu, M. Salim, H. Chalchal, J. Squire, M. S. Tsao, S. Kamel-Reid, S. Banerji, D. Tu, J. Powers, D. F. Hausman, and W. P. Mason. 2015. 'Phase II study of PX-866 in recurrent glioblastoma', *Neuro Oncol*, 17: 1270-4.
- Polson, H. E., J. de Lartigue, D. J. Rigden, M. Reedijk, S. Urbe, M. J. Clague, and S. A. Tooze. 2010. 'Mammalian Atg18 (WIPI2) localizes to omegasome-anchored phagophores and positively regulates LC3 lipidation', *Autophagy*, 6: 506-22.
- Proikas-Cezanne, T., Z. Takacs, P. Donnes, and O. Kohlbacher. 2015. 'WIPI proteins: essential PtdIns3P effectors at the nascent autophagosome', *J Cell Sci*, 128: 207-17.
- Puthenveedu, M. A., C. Bachert, S. Puri, F. Lanni, and A. D. Linstedt. 2006. 'GM130 and GRASP65-dependent lateral cisternal fusion allows uniform Golgi-enzyme distribution', *Nat Cell Biol*, 8: 238-48.
- Rapoport, Henry, and Kenneth G. Holden. 2002. 'The Synthesis of Prodigiosin', *Journal of the American Chemical Society*, 84: 635-42.
- Rapoport, Henry, and Clyde D. Willson. 2002. 'The Preparation and Properties of Some Methoxyppyroles', *Journal of the American Chemical Society*, 84: 630-35.

- Rohn, W. M., Y. Rouille, S. Waguri, and B. Hoflack. 2000. 'Bi-directional trafficking between the trans-Golgi network and the endosomal/lysosomal system', *J Cell Sci*, 113 ( Pt 12): 2093-101.
- Russell, R. C., Y. Tian, H. Yuan, H. W. Park, Y. Y. Chang, J. Kim, H. Kim, T. P. Neufeld, A. Dillin, and K. L. Guan. 2013. 'ULK1 induces autophagy by phosphorylating Beclin-1 and activating VPS34 lipid kinase', *Nat Cell Biol*, 15: 741-50.
- Rybstein, M. D., J. M. Bravo-San Pedro, G. Kroemer, and L. Galluzzi. 2018. 'The autophagic network and cancer', *Nat Cell Biol*, 20: 243-51.
- Salem, A. F., D. Whitaker-Menezes, Z. Lin, U. E. Martinez-Outschoorn, H. B. Tanowitz, M. S. Al-Zoubi, A. Howell, R. G. Pestell, F. Sotgia, and M. P. Lisanti. 2012. 'Two-compartment tumor metabolism: autophagy in the tumor microenvironment and oxidative mitochondrial metabolism (OXPHOS) in cancer cells', *Cell Cycle*, 11: 2545-56.
- Salem, S. M., P. Kancharla, G. Florova, S. Gupta, W. Lu, and K. A. Reynolds. 2014. 'Elucidation of final steps of the marineosins biosynthetic pathway through identification and characterization of the corresponding gene cluster', *J Am Chem Soc*, 136: 4565-74.
- Sam, M. R., and S. Ghoreishi. 2018. 'Prodigiosin produced by *Serratia marcescens* inhibits expression of MMP-9 and survivin and promotes caspase-3 activation with induction of apoptosis in acute lymphoblastic leukaemia cells', *J Appl Microbiol*, 125: 1017-29.
- Sanchez-Wandelmer, J., F. Kriegenburg, S. Rohringer, M. Schuschnig, R. Gomez-Sanchez, B. Zens, S. Abreu, R. Hardenberg, D. Hollenstein, J. Gao, C. Ungermann, S. Martens, C. Kraft, and F. Reggiori. 2017. 'Atg4 proteolytic activity can be inhibited by Atg1 phosphorylation', *Nat Commun*, 8: 295.
- Santana-Codina, N., J. D. Mancias, and A. C. Kimmelman. 2017. 'The Role of Autophagy in Cancer', *Annu Rev Cancer Biol*, 1: 19-39.
- Saran, U., M. Foti, and J. F. Dufour. 2015. 'Cellular and molecular effects of the mTOR inhibitor everolimus', *Clin Sci (Lond)*, 129: 895-914.
- Sato, T., H. Konno, Y. Tanaka, T. Kataoka, K. Nagai, H. H. Wasserman, and S. Ohkuma. 1998. 'Prodigiosins as a new group of H<sup>+</sup>/Cl<sup>-</sup> symporters that uncouple proton translocators', *J Biol Chem*, 273: 21455-62.
- Savitski, M. M., F. B. Reinhard, H. Franken, T. Werner, M. F. Savitski, D. Eberhard, D. Martinez Molina, R. Jafari, R. B. Dovega, S. Klaeger, B. Kuster, P. Nordlund, M. Bantscheff, and G. Drewes. 2014. 'Tracking cancer drugs in living cells by thermal profiling of the proteome', *Science*, 346: 1255784.
- Schimmer, A. D., A. Raza, T. H. Carter, D. Claxton, H. Erba, D. J. DeAngelo, M. S. Tallman, C. Goard, and G. Borthakur. 2014. 'A multicenter phase I/II study of obatoclox mesylate administered as a 3- or 24-hour infusion in older patients with previously untreated acute myeloid leukemia', *PLoS One*, 9: e108694.
- Schlütermann, D., M. A. Skowron, N. Berleth, P. Bohler, J. Deitersen, F. Stuhldreier, N. Wallot-Hieke, W. Wu, C. Peter, M. J. Hoffmann, G. Niegisch, and B. Stork. 2018. 'Targeting urothelial carcinoma cells by combining cisplatin with a specific inhibitor of the autophagy-inducing class III PtdIns3K complex', *Urol Oncol*, 36: 160 e1-60 e13.
- Seganish, J. L., and J. T. Davis. 2005. 'Prodigiosin is a chloride carrier that can function as an anion exchanger', *Chem Commun (Camb)*: 5781-3.
- Shorter, J., R. Watson, M. E. Giannakou, M. Clarke, G. Warren, and F. A. Barr. 1999. 'GRASP55, a second mammalian GRASP protein involved in the stacking of Golgi cisternae in a cell-free system', *EMBO J*, 18: 4949-60.
- Siegel, R. L., K. D. Miller, N. S. Wagle, and A. Jemal. 2023. 'Cancer statistics, 2023', *CA Cancer J Clin*, 73: 17-48.
- Sirichanchuen, B., T. Pengsuparp, and P. Chanvorachote. 2012. 'Long-term cisplatin exposure impairs autophagy and causes cisplatin resistance in human lung cancer cells', *Mol Cell Biochem*, 364: 11-8.
- Stenmark, H. 2009. 'Rab GTPases as coordinators of vesicle traffic', *Nat Rev Mol Cell Biol*, 10: 513-25.

- Su, Y. C., G. V. Davuluri, C. H. Chen, D. C. Shiau, C. C. Chen, C. L. Chen, Y. S. Lin, and C. P. Chang. 2016. 'Galectin-1-Induced Autophagy Facilitates Cisplatin Resistance of Hepatocellular Carcinoma', *PLoS One*, 11: e0148408.
- Sundararajan, P., D. Dharmaraj Rajaselvi, S. Vivekananthan, and S. Priya Ramasamy. 2023. 'In-silico method for elucidation of prodigiosin as PARP-1 inhibitor a prime target of Triple-negative breast cancer', *Bioorg Chem*, 138: 106618.
- Suzuki, H., T. Osawa, Y. Fujioka, and N. N. Noda. 2017. 'Structural biology of the core autophagy machinery', *Curr Opin Struct Biol*, 43: 10-17.
- Taherbhoy, A. M., S. W. Tait, S. E. Kaiser, A. H. Williams, A. Deng, A. Nourse, M. Hammel, I. Kurinov, C. O. Rock, D. R. Green, and B. A. Schulman. 2011. 'Atg8 transfer from Atg7 to Atg3: a distinctive E1-E2 architecture and mechanism in the autophagy pathway', *Mol Cell*, 44: 451-61.
- Takamura, A., M. Komatsu, T. Hara, A. Sakamoto, C. Kishi, S. Waguri, Y. Eishi, O. Hino, K. Tanaka, and N. Mizushima. 2011. 'Autophagy-deficient mice develop multiple liver tumors', *Genes Dev*, 25: 795-800.
- Tanida, I., T. Ueno, and E. Kominami. 2004. 'LC3 conjugation system in mammalian autophagy', *Int J Biochem Cell Biol*, 36: 2503-18.
- Thorburn, A. 2008. 'Apoptosis and autophagy: regulatory connections between two supposedly different processes', *Apoptosis*, 13: 1-9.
- Tie, H. C., B. Chen, X. Sun, L. Cheng, and L. Lu. 2017. 'Quantitative Localization of a Golgi Protein by Imaging Its Center of Fluorescence Mass', *J Vis Exp*, 4: 55996.
- Truschel, S. T., D. Sengupta, A. Foote, A. Heroux, M. R. Macbeth, and A. D. Linstedt. 2011. 'Structure of the membrane-tethering GRASP domain reveals a unique PDZ ligand interaction that mediates Golgi biogenesis', *J Biol Chem*, 286: 20125-9.
- Tsaprass, P., and I. P. Nezis. 2017. 'Caspase involvement in autophagy', *Cell Death Differ*, 24: 1369-79.
- Tu, Y., L. Tan, H. Tao, Y. Li, and H. Liu. 2023. 'CETSA and thermal proteome profiling strategies for target identification and drug discovery of natural products', *Phytomedicine*, 116: 154862.
- Vanneste, M., Q. Huang, M. Li, D. Moose, L. Zhao, M. A. Stamnes, M. Schultz, M. Wu, and M. D. Henry. 2019. 'High content screening identifies monensin as an EMT-selective cytotoxic compound', *Sci Rep*, 9: 1200.
- Vezina, C., A. Kudelski, and S. N. Sehgal. 1975. 'Rapamycin (AY-22,989), a new antifungal antibiotic. I. Taxonomy of the producing streptomycete and isolation of the active principle', *J Antibiot (Tokyo)*, 28: 721-6.
- Viotti, C. 2016. 'ER to Golgi-Dependent Protein Secretion: The Conventional Pathway', *Methods Mol Biol*, 1459: 3-29.
- Walker, S. A., and N. T. Ktistakis. 2020. 'Autophagosome Biogenesis Machinery', *J Mol Biol*, 432: 2449-61.
- Wang, J., and G. S. Wu. 2014. 'Role of autophagy in cisplatin resistance in ovarian cancer cells', *J Biol Chem*, 289: 17163-73.
- Wang, L., D. J. Klionsky, and H. M. Shen. 2023. 'The emerging mechanisms and functions of microautophagy', *Nat Rev Mol Cell Biol*, 24: 186-203.
- Wang, X., T. Isbrandt, E. O. Christensen, J. Melchiorsen, T. O. Larsen, S. D. Zhang, and L. Gram. 2021. 'Identification and Verification of the Prodigiosin Biosynthetic Gene Cluster (BGC) in *Pseudoalteromonas rubra* S4059', *Microbiol Spectr*, 9: e0117121.
- Wang, Y., L. Li, C. Hou, Y. Lai, J. Long, J. Liu, Q. Zhong, and J. Diao. 2016. 'SNARE-mediated membrane fusion in autophagy', *Semin Cell Dev Biol*, 60: 97-104.
- Wang, Y., and J. Seemann. 2011. 'Golgi biogenesis', *Cold Spring Harb Perspect Biol*, 3: a005330.
- Wang, Y., J. Seemann, M. Pypaert, J. Shorter, and G. Warren. 2003. 'A direct role for GRASP65 as a mitotically regulated Golgi stacking factor', *EMBO J*, 22: 3279-90.
- Wang, Y., J. H. Wei, B. Bisel, D. Tang, and J. Seemann. 2008. 'Golgi cisternal unstacking stimulates COPI vesicle budding and protein transport', *PLoS One*, 3: e1647.
- Wasserman, H. H., Keon Je Mc, and U. V. Santer. 1960. 'Studies related to the biosynthesis of prodigiosin in *Serratia marcescens*', *Biochem Biophys Res Commun*, 3: 146-9.

- Wasserman, H. H., R. J. Skles, P. Peverada, C. K. Shaw, R. J. Cushley, and C. R. Lipsky. 1973. 'Biosynthesis of prodigiosin. Incorporation patterns of C-labeled alanine, proline, glycine, and serine elucidated by fourier transform nuclear magnetic resonance', *J Am Chem Soc*, 95: 6874-5.
- Wen, X., and D. J. Klionsky. 2020. 'At a glance: A history of autophagy and cancer', *Semin Cancer Biol*, 66: 3-11.
- White, E. 2012. 'Deconvoluting the context-dependent role for autophagy in cancer', *Nat Rev Cancer*, 12: 401-10.
- White, E. 2015. 'The role for autophagy in cancer', *J Clin Invest*, 125: 42-6.
- Whitton, B., H. Okamoto, G. Packham, and S. J. Crabb. 2018. 'Vacuolar ATPase as a potential therapeutic target and mediator of treatment resistance in cancer', *Cancer Med*, 7: 3800-11.
- Williamson, N. R., H. T. Simonsen, R. A. Ahmed, G. Goldet, H. Slater, L. Woodley, F. J. Leeper, and G. P. Salmond. 2005. 'Biosynthesis of the red antibiotic, prodigiosin, in *Serratia*: identification of a novel 2-methyl-3-n-amy-l-pyrrole (MAP) assembly pathway, definition of the terminal condensing enzyme, and implications for undecylprodigiosin biosynthesis in *Streptomyces*', *Mol Microbiol*, 56: 971-89.
- Wrede, F., and O. Hettche. 1929. 'Über das Prodigiosin, den roten Farbstoff des *Bacillus Prodigiosus* (I. Mitteil.)', *Berichte der deutschen chemischen Gesellschaft*, 62: 2678-85.
- Wu, Y. T., H. L. Tan, G. Shui, C. Bauvy, Q. Huang, M. R. Wenk, C. N. Ong, P. Codogno, and H. M. Shen. 2010a. 'Dual role of 3-methyladenine in modulation of autophagy via different temporal patterns of inhibition on class I and III phosphoinositide 3-kinase', *J Biol Chem*, 285: 10850-61.
- Wu, You-Tong, Hui-Ling Tan, Guanghou Shui, Chantal Bauvy, Qing Huang, Markus R. Wenk, Choon-Nam Ong, Patrice Codogno, and Han-Ming Shen. 2010b. 'Dual Role of 3-Methyladenine in Modulation of Autophagy via Different Temporal Patterns of Inhibition on Class I and III Phosphoinositide 3-Kinase', *Journal of Biological Chemistry*, 285: 10850-61.
- Xiang, Y., and Y. Wang. 2010. 'GRASP55 and GRASP65 play complementary and essential roles in Golgi cisternal stacking', *J Cell Biol*, 188: 237-51.
- Xiao, L., X. Y. Shi, Y. Zhang, Y. Zhu, L. Zhu, W. Tian, B. K. Zhu, and Z. L. Wei. 2016. 'YAP induces cisplatin resistance through activation of autophagy in human ovarian carcinoma cells', *Onco Targets Ther*, 9: 1105-14.
- Xie, B. B., Y. L. Shu, Q. L. Qin, J. C. Rong, X. Y. Zhang, X. L. Chen, B. C. Zhou, and Y. Z. Zhang. 2012. 'Genome sequence of the cycloprodigiosin-producing bacterial strain *Pseudoalteromonas rubra* ATCC 29570(T)', *J Bacteriol*, 194: 1637-8.
- Xie, Z., U. Nair, and D. J. Klionsky. 2008. 'Atg8 controls phagophore expansion during autophagosome formation', *Mol Biol Cell*, 19: 3290-8.
- Yam, C., X. Xu, M. A. Davies, P. A. Gimotty, J. J. D. Morrisette, M. T. Tetzlaff, K. M. Wani, S. Liu, W. Deng, M. Buckley, J. Zhao, R. K. Amaravadi, N. B. Haas, R. R. Kudchadkar, A. C. Pavlick, J. A. Sosman, H. Tawbi, L. Walker, L. M. Schuchter, G. C. Karakousis, and T. C. Gangadhar. 2018. 'A Multicenter Phase I Study Evaluating Dual PI3K and BRAF Inhibition with PX-866 and Vemurafenib in Patients with Advanced BRAF V600-Mutant Solid Tumors', *Clin Cancer Res*, 24: 22-32.
- Yamamoto, C., H. Takemoto, K. Kuno, D. Yamamoto, A. Tsubura, K. Kamata, H. Hirata, A. Yamamoto, H. Kano, T. Seki, and K. Inoue. 1999. 'Cycloprodigiosin hydrochloride, a new H(+)/Cl(-) symporter, induces apoptosis in human and rat hepatocellular cancer cell lines in vitro and inhibits the growth of hepatocellular carcinoma xenografts in nude mice', *Hepatology*, 30: 894-902.
- Yamamoto, D., Y. Kiyozuka, Y. Uemura, C. Yamamoto, H. Takemoto, H. Hirata, K. Tanaka, K. Hioki, and A. Tsubura. 2000. 'Cycloprodigiosin hydrochloride, a H(+)/Cl(-) symporter, induces apoptosis in human breast cancer cell lines', *J Cancer Res Clin Oncol*, 126: 191-7.

- Yang, Y., G. Karsli-Uzunbas, L. Poillet-Perez, A. Sawant, Z. S. Hu, Y. Zhao, D. Moore, W. Hu, and E. White. 2020. 'Autophagy promotes mammalian survival by suppressing oxidative stress and p53', *Genes Dev*, 34: 688-700.
- Yenkeje, R. A., M. R. Sam, and M. Esmaeillou. 2017. 'Targeting survivin with prodigiosin isolated from cell wall of *Serratia marcescens* induces apoptosis in hepatocellular carcinoma cells', *Hum Exp Toxicol*, 36: 402-11.
- Yim, W. W., and N. Mizushima. 2020. 'Lysosome biology in autophagy', *Cell Discov*, 6: 6.
- Yin, Zhangyuan, Clarence Pascual, and Daniel Klionsky. 2016. 'Autophagy: machinery and regulation', *Microbial Cell*, 3: 588-96.
- Yu, L., C. Gu, D. Zhong, L. Shi, Y. Kong, Z. Zhou, and S. Liu. 2014. 'Induction of autophagy counteracts the anticancer effect of cisplatin in human esophageal cancer cells with acquired drug resistance', *Cancer Lett*, 355: 34-45.
- Yu, L., and S. Liu. 2013. 'Autophagy contributes to modulating the cytotoxicities of Bcl-2 homology domain-3 mimetics', *Semin Cancer Biol*, 23: 553-60.
- Yue, Z., S. Jin, C. Yang, A. J. Levine, and N. Heintz. 2003. 'Beclin 1, an autophagy gene essential for early embryonic development, is a haploinsufficient tumor suppressor', *Proc Natl Acad Sci U S A*, 100: 15077-82.
- Zhai, D., C. Jin, A. C. Satterthwait, and J. C. Reed. 2006. 'Comparison of chemical inhibitors of antiapoptotic Bcl-2-family proteins', *Cell Death Differ*, 13: 1419-21.
- Zhang, X., L. Wang, S. C. Ireland, E. Ahat, J. Li, M. E. Bekier, 2nd, Z. Zhang, and Y. Wang. 2019. 'GORASP2/GRASP55 collaborates with the PtdIns3K UVRAG complex to facilitate autophagosome-lysosome fusion', *Autophagy*, 15: 1787-800.
- Zhang, X., L. Wang, B. Lak, J. Li, E. Jokitalo, and Y. Wang. 2018. 'GRASP55 Senses Glucose Deprivation through O-GlcNAcylation to Promote Autophagosome-Lysosome Fusion', *Dev Cell*, 45: 245-61 e6.
- Zhao, C., S. Qiu, J. He, Y. Peng, H. Xu, Z. Feng, H. Huang, Y. Du, Y. Zhou, and Y. Nie. 2020. 'Prodigiosin impairs autophagosome-lysosome fusion that sensitizes colorectal cancer cells to 5-fluorouracil-induced cell death', *Cancer Lett*, 481: 15-23.
- Zhou, C., K. Ma, R. Gao, C. Mu, L. Chen, Q. Liu, Q. Luo, D. Feng, Y. Zhu, and Q. Chen. 2017. 'Regulation of mATG9 trafficking by Src- and ULK1-mediated phosphorylation in basal and starvation-induced autophagy', *Cell Res*, 27: 184-201.

## Licensing & Copyright

I hereby grant anyone the right to reuse any part of this dissertation, including figures 1 to 5, which I have created myself, that is not subject to explicit copyright, as credit is given (license CC BY 4.0). Please cite as follows:

Berning, Lena (2023) *Characterization of the autophagy-modulating natural compound prodigiosin for the elimination of therapy-resistant tumor cells*. Heinrich Heine University, Düsseldorf.

All non-copyrighted parts of this work are licensed under the Creative Commons Attribution 4.0 International License. To view a copy of this license, visit <https://creativecommons.org/licenses/by/4.0/> or send a letter to Creative Commons, PO Box 1866, Mountain View, CA 94042, USA.

The following parts of this dissertation are protected by copyright and have been reprinted without changes:

### **Manuscript "Prodigiosin Sensitizes Sensitive and Resistant Urothelial Carcinoma Cells to Cisplatin Treatment":**

Copyright Berning et al. 2021 (DOI: 10.3390/molecules26051294)

Reprinted under the Creative Commons CC-BY-NC-ND 4.0 license (as indicated by MDPI).

### **Manuscript "Prodiginine ligating enzymes exhibit an extended substrate acceptance for A-ring-associated alkyl-substitutions":**

Copyright Weber et al. 2023 (DOI: 10.1039/d3cy00913k)

Reprinted under the Creative Commons CC-BY-NC-ND 4.0 license (as indicated by the Royal Society of Chemistry).

### **Manuscript "The Golgi stacking protein GRASP55 is targeted by the natural compound prodigiosin":**

Copyright Berning et al. 2023 (DOI: 10.1186/s12964-023-01275-1)

Reprinted under the Creative Commons CC-BY-NC-ND 4.0 license (as indicated by BioMed Central).

# Appendix

## Publication 1

### **Prodigosin Sensitizes Sensitive and Resistant Urothelial Carcinoma Cells to Cisplatin Treatment**







Lena Berning, David Schlütermann, Annabelle Friedrich, Niklas Berleth, Yadong Sun, Wenxian Wu, María José Mendiburo, Jana Deitersen, Hannah U. C. Brass, Margaretha A. Skowron, Michèle J. Hoffmann, Günter Niegisch, Jörg Pietruszka and Björn Stork

*Molecules*, Volume 26, Issue 5, 1294, February 2021

DOI: 10.3390/molecules26051294

## Article

# Prodigosin Sensitizes Sensitive and Resistant Urothelial Carcinoma Cells to Cisplatin Treatment

Lena Berning <sup>1</sup>, David Schlütermann <sup>1</sup>, Annabelle Friedrich <sup>1</sup>, Niklas Berleth <sup>1</sup>, Yadong Sun <sup>1</sup>, Wenxian Wu <sup>1</sup> ,  
 María José Mendiburo <sup>1</sup>, Jana Deitersen <sup>1</sup>, Hannah U. C. Brass <sup>2,3</sup>, Margaretha A. Skowron <sup>4</sup> ,  
 Michèle J. Hoffmann <sup>4</sup> , Günter Niegisch <sup>4</sup> , Jörg Pietruszka <sup>2,3</sup>  and Björn Stork <sup>1,\*</sup> 

- <sup>1</sup> Institute of Molecular Medicine I, Medical Faculty, Heinrich Heine University, 40225 Düsseldorf, Germany; lena.berning@hhu.de (L.B.); david.schlütermann@hhu.de (D.S.); annabelle.friedrich@hhu.de (A.F.); niklas.berleth@hhu.de (N.B.); yadongsunsurgery@gmail.com (Y.S.); wenxian.wu@hhu.de (W.W.); mendiburo@hhu.de (M.J.M.); jana.deitersen@hhu.de (J.D.)
- <sup>2</sup> Institute of Bioorganic Chemistry, Faculty of Mathematics and Natural Sciences, Heinrich Heine University, Forschungszentrum Jülich, Stettener Forst, 52428 Jülich, Germany; h.brass@fz-juelich.de (H.U.C.B.); j.pietruszka@fz-juelich.de (J.P.)
- <sup>3</sup> Institute for Bio- and Geosciences 1: Bioorganic Chemistry (IBG-1), Forschungszentrum Jülich GmbH, 52428 Jülich, Germany
- <sup>4</sup> Department of Urology, Medical Faculty, Heinrich Heine University, 40225 Düsseldorf, Germany; margaretha.skowron@med.uni-duesseldorf.de (M.A.S.); michele.hoffmann@hhu.de (M.J.H.); guenter.niegisch@med.uni-duesseldorf.de (G.N.)
- \* Correspondence: bjoern.stork@hhu.de; Tel.: +49-(0)211-81-11954; Fax: +49-(0)211-81-11611954



**Citation:** Berning, L.; Schlütermann, D.; Friedrich, A.; Berleth, N.; Sun, Y.; Wu, W.; Mendiburo, M.J.; Deitersen, J.; Brass, H.U.C.; Skowron, M.A.; et al. Prodigosin Sensitizes Sensitive and Resistant Urothelial Carcinoma Cells to Cisplatin Treatment. *Molecules* **2021**, *26*, 1294. <https://doi.org/10.3390/molecules26051294>

Academic Editors: Vincenzo Piccialli, Wenhan Lin and Helen Osborn

Received: 22 December 2020

Accepted: 22 February 2021

Published: 27 February 2021

**Publisher's Note:** MDPI stays neutral with regard to jurisdictional claims in published maps and institutional affiliations.



**Copyright:** © 2021 by the authors. Licensee MDPI, Basel, Switzerland. This article is an open access article distributed under the terms and conditions of the Creative Commons Attribution (CC BY) license (<https://creativecommons.org/licenses/by/4.0/>).

**Abstract:** Cisplatin-based treatment is the standard of care therapy for urothelial carcinomas. However, complex cisplatin resistance mechanisms limit the success of this approach. Both apoptosis and autophagy have been shown to contribute to this resistance. Prodigosin, a secondary metabolite from various bacteria, exerts different biological activities including the modulation of these two cellular stress response pathways. We analyzed the effect of prodigosin on protein levels of different autophagy- and apoptosis-related proteins in cisplatin-sensitive and -resistant urothelial carcinoma cells (UCCs). Furthermore, we investigated the effect on cell viability of prodigosin alone or in combination with cisplatin. We made use of four different pairs of cisplatin-sensitive and -resistant UCCs. We found that prodigosin blocked autophagy in UCCs and re-sensitized cisplatin-resistant cells to apoptotic cell death. Furthermore, we found that prodigosin is a potent anticancer agent with nanomolar IC<sub>50</sub> values in all tested UCCs. In combination studies, we observed that prodigosin sensitized both cisplatin-sensitive and -resistant urothelial carcinoma cell lines to cisplatin treatment with synergistic effects in most tested cell lines. These effects of prodigosin are at least partially mediated by altering lysosomal function, since we detected reduced activities of cathepsin B and L. We propose that prodigosin is a promising candidate for the therapy of cisplatin-resistant urothelial carcinomas, either as a single agent or in combinatory therapeutic approaches.

**Keywords:** prodigosin; urothelial carcinoma; cisplatin; chemoresistance; autophagy; apoptosis

## 1. Introduction

According to the WHO, with 570,000 new cases and 210,000 deaths in 2020, bladder cancer (BC) is one of the 10 most common cancers in the world [1]. On average, one in 100 men and one in 400 women will be diagnosed with BC during their lifetime [2]. Urothelial carcinomas (UCs) can be subdivided into non-muscle-invasive (NMIBC) and muscle-invasive bladder cancers (MIBC), the latter representing one fourth of UCs and having a risk of developing metastases [3]. Patients suffering from MIBC face a poor prognosis, with a 5-year survival rate of only 50% [4] after receiving the recommended treatment consisting of a radical cystectomy in combination with perioperative chemotherapy [2,5,6]. The outcome of patients suffering from metastatic disease, in which platin-based chemotherapy

is the standard of care, have an even worse prognosis, with a long-term survival of less than 20% [7]. Even the recent introduction of immune checkpoint inhibitors in treatment algorithms did not proficiently ameliorate these results. The success of cisplatin-based therapy is limited by several factors, including the need for a sufficient renal function and the possibility of resistance development, which often necessitates second-line therapy [5].

Antitumor activity of platinum-containing anticancer agents has been mainly associated with their ability to form covalent linkages to nucleophilic residues of DNA bases. This leads to the formation of DNA adducts and DNA double strand breaks, resulting in the initiation of the intrinsic apoptotic pathway [8,9]. However, cisplatin can form multiple different adducts with nucleophilic residues and therefore affect multiple cellular pathways, and for this reason its exact mechanism of action remains unclear [9,10]. Therefore, cisplatin resistance mechanisms are complex and multifaceted, including an increased DNA repair capacity and anti-apoptotic ability, modifications in cellular transport and augmented anti-oxidative capacity [11–13]. Importantly, autophagy is another process which has been linked to the cisplatin resistance of cancer cells [14–16].

Autophagy is an intracellular catabolic process in which misfolded, damaged or aggregated proteins as well as whole cell organelles can be degraded and recycled. For the induction of autophagy, two kinase complexes are essential. The activation of the Unc-51-like autophagy activating kinase 1 (ULK1) protein kinase complex and the class III phosphatidylinositol 3-kinase (PtdIns3K) lipid kinase complex initiates the biogenesis of double-membraned vesicles named autophagosomes from specific subdomains of the endoplasmic reticulum (ER) [17]. After the engulfment of the cargo, the outer membrane of the autophagosome fuses with a lysosome, resulting in an autolysosome where the sequestered cargo and the inner autophagosomal membrane are degraded by lysosomal hydrolases [18]. Besides occurring at a basal level to maintain cell homeostasis in physiological conditions, autophagy can be stimulated by internal and external stimuli such as nutrient deprivation, stress conditions or chemotherapeutic anticancer treatment [19]. Since the cisplatin treatment-mediated upregulation of autophagy causes resistance and raises the threshold of efficacy, some autophagy inhibitors have been tested in clinical studies. The main focus hereby lies on chloroquine and hydroxychloroquine, which can inhibit autophagy by blocking the fusion of autophagosomes and lysosomes and are tested in combination studies with conventional chemotherapeutics [20,21]. Another autophagy-modulating compound that has previously been tested in clinical studies is obatoclax, a synthetic analogue of the natural compound prodigiosin [22–24].

Prodigiosin (Figure 1) is a deep red secondary metabolite with a tripyrrole structure, which was first extracted and characterized from the bacterium *Serratia marcescens* [25,26]. It can be found ubiquitously in various bacteria of the marine and terrestrial environment [25,27]. Prodigiosin has been shown to exert antimicrobial [28], antimalarial [29] and immunosuppressive [30] properties. In addition, prodigiosin and its synthetic analogue obatoclax have been tested in several pre-clinical and clinical trials alone or in combination with conventional chemotherapeutics as anticancer agents [22–24,31]. In that respect, different effects on both apoptosis and autophagy have been observed in various cancer models [31–36]. However, the molecular targets and the exact mechanisms of prodigiosin and its effects on resistant cancer cells remain unclear.

In this study, we found that prodigiosin not only decreased the viability of different cisplatin-sensitive and -resistant urothelial carcinoma cell (UCC) lines, but also sensitized them to cisplatin treatment. While autophagy was inhibited in both cisplatin-sensitive and -resistant UCCs, prodigiosin induced apoptotic cell death in cisplatin-resistant UCCs in nanomolar concentrations. Furthermore, we observed reduced activities of cathepsin B and L upon incubation with prodigiosin. Thus, we propose that treatment with prodigiosin can be a promising approach to enhance the effect of conventional chemotherapeutic drugs and potentially re-sensitize cisplatin-resistant tumors to cisplatin therapy.

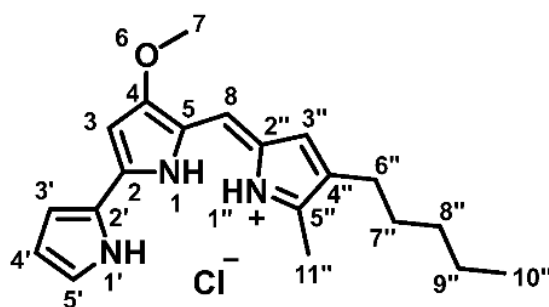


Figure 1. Chemical structure of prodigiosin.

## 2. Material and Methods

### 2.1. Antibodies and Reagents

Antibodies against  $\beta$ -actin (Sigma–Aldrich, St.Louis, MO, USA, #A5316, clone AC-74, 1:5000), LC3B (Cell Signaling Technology, Danvers, MA, USA, #2775, 1:1000), sequestosome 1 (SQSTM1) (PROGEN, Heidelberg, Germany, #GP62-C, 1:1000) and poly (ADP-ribose) polymerase (PARP)-1 (Enzo, New York, NY, USA, #BML-SA250-0050, clone C-2-10, 1:2000) were used. Isolated and purified prodigiosin was dissolved in DMSO. IRDye 680- or IRDye 800-conjugated secondary antibodies were purchased from LI-COR Biosciences (Lincoln, NE, USA, 926-68077, 926-32211 and 926-32210). Other reagents used were bafilomycin A<sub>1</sub> (Sigma–Aldrich, St.Louis, MO, USA, #B1793), cisplatin (NeoCorp, Pawtucket, RI, USA, 1 mg/mL, 39021.01.00), DMSO (PanReac AppliChem, Darmstadt, Germany, #A3672 and ROTH, Karlsruhe, Germany, #7029.1), Pepstatin A (Sigma–Aldrich, St.Louis, MO, USA, #P5318), Q-VD-OPh (MP Biomedicals, Santa Ana, CA, USA, #03OPH109), staurosporine (biomol, Hamburg, Germany, #AG-CN2-0022-M005), thiazolyl blue (MTT, ROTH, Karlsruhe, Germany, #4022.3), Torin 2 (Selleckchem, Houston, TX, USA, #S2817) and Z-Phe-Phe-FMK (abcam, Cambridge, UK, #ab141386). The cathepsin activities of RT-112 and RT-112<sup>res</sup> cells were measured using the fluorometric Cathepsin Activity Assay Kits (abcam, Cambridge, UK, #ab65300, #ab65302, #ab65306) according to the manufacturer's instructions and measured with a microplate reader (BioTek, Winooski, VT, USA, Synergy Mx).

### 2.2. Correct Identification of Natural Products

Prodigiosin (Figure 1) was produced and purified as described by Domröse et al. [37]. After column chromatography, prodigiosin was precipitated as hydrochloride as a dark red solid and a 10 mM stock in DMSO was prepared.

<sup>1</sup>H-NMR (600 MHz, CDCl<sub>3</sub>):  $\delta$  [ppm] = 0.90 (t, <sup>3</sup>J<sub>10'',9''</sub> = 7.0 Hz, 3H, 10''-H), 1.32 (m<sub>c</sub>, 4H, 8''-, 9''-H), 1.54 (m<sub>c</sub>, 2H, 7''-H), 2.39 (t, <sup>3</sup>J<sub>6'',7''</sub> = 7.6 Hz, 2H, 6''-H), 2.54 (s, 3H, 11''-H), 4.00 (s, 3H, 7-H), 6.07 (d, <sup>4</sup>J<sub>3,1</sub> = 1.9 Hz, 1H, 3-H), 6.35 (m<sub>c</sub>, 1H, 4'-H), 6.68 (d, <sup>4</sup>J<sub>3'',1''</sub> = 2.6 Hz, 1H, 3''-H), 6.91 (ddd, <sup>3</sup>J<sub>3',4'</sub> = 3.8 Hz, <sup>4</sup>J<sub>3',5'</sub> = 2.4 Hz, <sup>5</sup>J<sub>3',1'</sub> = 1.4 Hz, 1H, 3'-H), 6.95 (s, 1H, 8-H), 7.22 (m<sub>c</sub>, 1H, 5'-H), 12.56 (brs, 1H, 1'-NH), 12.71 (brs, 2H, 1-, 1''-NH); <sup>13</sup>C-NMR (151 MHz, CDCl<sub>3</sub>):  $\delta$  [ppm] = 12.6 (C-11''), 14.2 (C-10''), 22.6 (C-9''), 25.5 (C-6''), 29.9 (C-7''), 31.6 (C-8''), 58.9 (C-7), 93.0 (C-3), 111.9 (C-4'), 116.1 (C-8), 117.2 (C-3'), 120.8 (C-5), 122.4 (C-2'), 125.3 (C-2''), 127.1 (C-5'), 128.5 (C-3''), 128.6 (C-4''), 147.1 (C-5''), 147.8 (C-2), 165.9 (C-4).

The analytical data can be found in Supplementary Figure S1 and are in accordance to the literature [37].

### 2.3. Cell Lines and Cell Culture

All UCC lines were cultured in Dulbecco's Modified Eagle Medium (DMEM, Thermo Fisher Scientific, Waltham, MA, USA, #41965039) containing 10% fetal bovine serum (FBS, Sigma–Aldrich, St.Louis, MO, USA, #F0804), 4.5 g/L D-glucose, 100 units/mL penicillin and 100  $\mu$ g/mL Streptomycin (Thermo Fisher Scientific, Waltham, MA, USA, #15140122). All cells were cultivated and treated at 37 °C and 5% CO<sub>2</sub> in a humidified atmosphere. All UCC lines have been previously described [38]. Briefly, for the generation of cisplatin-

resistant cell lines, cells were treated with increasing dosages of cisplatin over several months. During cell culture, cisplatin was added to the media with every passage in concentrations of 1 µg/mL for J82, 2 µg/mL for 253J, 7 µg/mL for T24 and 12 µg/mL for RT-112 cells.

#### 2.4. Cell Viability Assay

Cell viability was measured using the MTT (3-(4,5-dimethylthiazol-2-yl)-2,5-diphenyltetrazolium bromide) assay. J82, 253J, T24 and RT-112 cisplatin-sensitive or resistant cells were seeded in 96-well plates with a density of  $5 \times 10^4$  cells/well. One day after seeding, cells were treated with cisplatin and/or prodigiosin for 24 or 72 h. After the incubation time, MTT was added to the cells and they were incubated at 37 °C and 5% CO<sub>2</sub> in a humidified atmosphere for 1 h. Upon removal of the MTT-containing medium, 100 µL DMSO per well were added for extraction of the formazan. Absorbance was measured at 570 nm and 650 nm (reference) with a microplate reader (BioTek, Winooski, VT, USA, Synergy Mx). After the subtraction of the reference value, the mean of the absorbance of the solvent control was set as 100%.

#### 2.5. Immunoblotting

For SDS PAGE and western blotting, cells were harvested by scraping, pelletized at 150 rcf and 4 °C for 5 min, washed with PBS (Thermo Fisher Scientific, Waltham, MA, USA, #14190-094) and quickly frozen in liquid nitrogen. Cells were lysed in lysis buffer (20 mM Tris-HCl, 150 mM NaCl, 500 µM EDTA, 1% (v/v) Triton X-100, 1 mM Na<sub>3</sub>VO<sub>4</sub>, 10 mM NaF, 2.5 mM Na<sub>4</sub>P<sub>2</sub>O<sub>7</sub>, 1X protease inhibitor cocktail [Roche, Basel, Switzerland, #4693132001]) for 30 min on ice and the lysates were cleared by centrifugation at 18,000 rcf and 4 °C for 15 min. The protein concentration was determined by Bradford assay and sample buffer was added (62.5 mM Tris, 8.6% [v/v] glycerol, 2% [w/v] SDS, 33.3 µg/mL bromophenol blue, 1% [v/v] β-mercaptoethanol). Samples were heated at 95 °C for 5 min and then equal amounts of protein (25 µg) were subjected to SDS-polyacrylamide gels. After separation by SDS-PAGE, proteins were transferred to PVDF membranes (Merck, Darmstadt, Germany, #IPFL00010), blocked with 5% milk powder in TBS-T (10 mM Tris-HCl, pH 7.6, 150 mM NaCl, 0.1% Tween-20 [Sigma-Aldrich, St. Louis, MO, USA, #P1379]) and analyzed using the indicated primary antibodies followed by appropriate IRDye 680- or IRDye 800-conjugated secondary antibodies (LI-COR Biosciences, Lincoln, NE, USA). Fluorescence signals were detected using an Odyssey Infrared Imaging system (LI-COR Biosciences, Lincoln, NE, USA) and signals were quantified with Image Studio (LI-COR Biosciences, Lincoln, NE, USA).

#### 2.6. Immunofluorescence

For immunofluorescence microscopy, cells were seeded in µ-Slide 8 Well (Ibidi, Gräefeling, Germany, #80826). Cells were treated with 100 nM LysoTracker™ Deep Red (Thermo Fisher Scientific, Waltham, MA, USA, #L12492). After the incubation time, the treatment medium was removed and replaced by DMEM without phenol red (Thermo Fisher Scientific, Waltham, MA, USA, #31053028). Representative images were acquired with an Axio Observer 7 fluorescence microscope (Carl Zeiss Microscopy, Jena, Germany) using a 40x/1.4 Oil DIC M27 Plan-Apochromat objective (Carl Zeiss Microscopy, Jena, Germany) and an ApoTome 2 (Carl Zeiss Microscopy, Jena, Germany).

#### 2.7. Statistical Analysis

All IC<sub>50</sub> values were calculated using GraphPad Prism 7.01. Isobologram analysis for the combined viability assays of two drugs was performed with CompuSyn [39]. The software allows for the simulation of the effects of combined drugs at any effect level and calculates the combination index (CI) of a drug combination to determine if effects are synergistic (CI < 1), additive (CI = 1) or antagonistic (CI > 1). For immunoblotting, the density of each protein band was quantified using Image Studio Lite 5.2. The density of

each protein band was then divided by the average density of all bands of this protein. These ratios of the proteins of interest were then normalized to the loading control. Each normalized density ratio was divided by the mean normalized density ratio of the solvent control lane of all replicates. For all western blot analyses, the results are shown as the mean + standard deviation and the *p* values were determined for each cell line by ordinary one-way ANOVA with Dunnett's post hoc test and are shown in the bar diagrams. For the immunofluorescence analyses, dots were quantified and analyzed using ImageJ 1.53c. The macro used for quantification is provided in the Supplementary Methods. At least 200 cells were analyzed in two biological replicates for each cell line. For comparisons between cell lines, a Student's *t*-test was performed. For cathepsin activity assays, the results are shown as the mean + standard deviation and the *p* values were determined by ordinary two-way ANOVA with Tukey's post hoc test and are shown in the bar diagrams. All *p* values were determined using GraphPad Prism 7.01.

### 3. Results

#### 3.1. Prodigiosin Is Cytotoxic in Cisplatin-Sensitive and -Resistant RT-112 Cells

To analyze the effects of prodigiosin on cisplatin-resistant UCCs, we made use of RT-112 cells and the cisplatin-resistant subline RT-112<sup>res</sup> [15,38]. Prodigiosin shows high cytotoxicity in RT-112 and RT-112<sup>res</sup> cells with IC<sub>50</sub> values of 675 nM and 157 nM after 24 h (Figure 2A) and 74 nM and 41 nM after 72 h (Figure 2B), respectively. It is noteworthy that the IC<sub>50</sub> value of prodigiosin in RT-112<sup>res</sup> cells was lower than in the sensitive RT-112 UCCs after both 24 h and 72 h, indicating an increased sensitivity of cisplatin-resistant cells against treatment with prodigiosin.

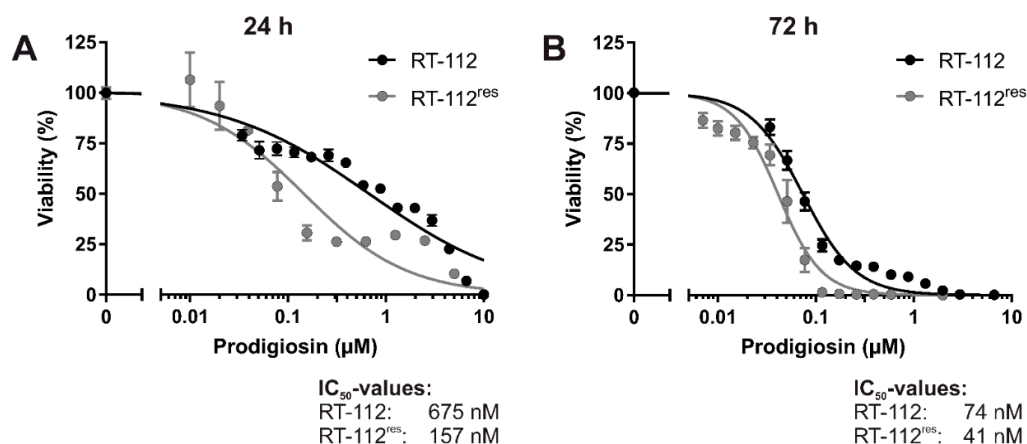


**Figure 2.** Prodigiosin is cytotoxic for cisplatin-sensitive and -resistant bladder carcinoma cells. RT-112 and RT-112<sup>res</sup> cells were treated with different concentrations of prodigiosin for 24 h (A) or 72 h (B). After treatment, cell viability was measured using an thiazolyl blue (MTT) assay. Results are shown as the mean ± SEM of three independent experiments performed in triplicates for each treatment.

#### 3.2. Prodigiosin Inhibits Autophagy in RT-112 Cells

Since increased anti-apoptotic capacity and upregulated autophagy are both associated to cisplatin resistance in UCCs, our next aim was to investigate the effect of prodigiosin in RT-112 and RT-112<sup>res</sup>. Apoptosis induction was determined by immunoblot analysis of the cleavage of the caspase-3 substrate poly (ADP-ribose) polymerase (PARP). After a 6 h incubation with prodigiosin, no significant change in PARP cleavage was observed in RT-112 and RT-112<sup>res</sup> cells (Figure 3A). In contrast, prodigiosin showed significant effects on the levels of proteins associated with autophagy starting at a concentration of 100 nM (Figure 3A,B). Increased levels of the ubiquitin-like protein microtubule-associated proteins 1A/1B light chain 3 (LC3) can be associated with induced autophagy, but also occur when

the autophagic machinery is inhibited in later steps. In this case, an autophagosome-bound form of LC3 (LC3-II) accumulates due to the absence of lysosomal degradation. This is illustrated by the effect of the vacuolar-type H<sup>+</sup>-ATPase (V-ATPase) inhibitor bafilomycin A<sub>1</sub> (BafA<sub>1</sub>), which inhibits the acidification of the lysosome and thus prevents the degradation of engulfed cargo and LC3-II by lysosomal proteases such as cathepsins [40]. To further characterize the autophagy-modulating properties of prodigiosin, sequestosome 1 (SQSTM1) levels were investigated. SQSTM1, also known as ubiquitin-binding protein p62, binds cargo proteins to selectively target them for autophagic degradation. The concentration-dependent accumulation of SQSTM1 in RT-112 in combination with the elevated LC3-II levels suggests an inhibition of the autophagic process. In contrast, there is no significant change of—the apparently elevated—SQSTM1 levels in RT-112<sup>res</sup> after treatment with up to 1 µM prodigiosin while LC3-II levels are increased (Figure 3A,B).

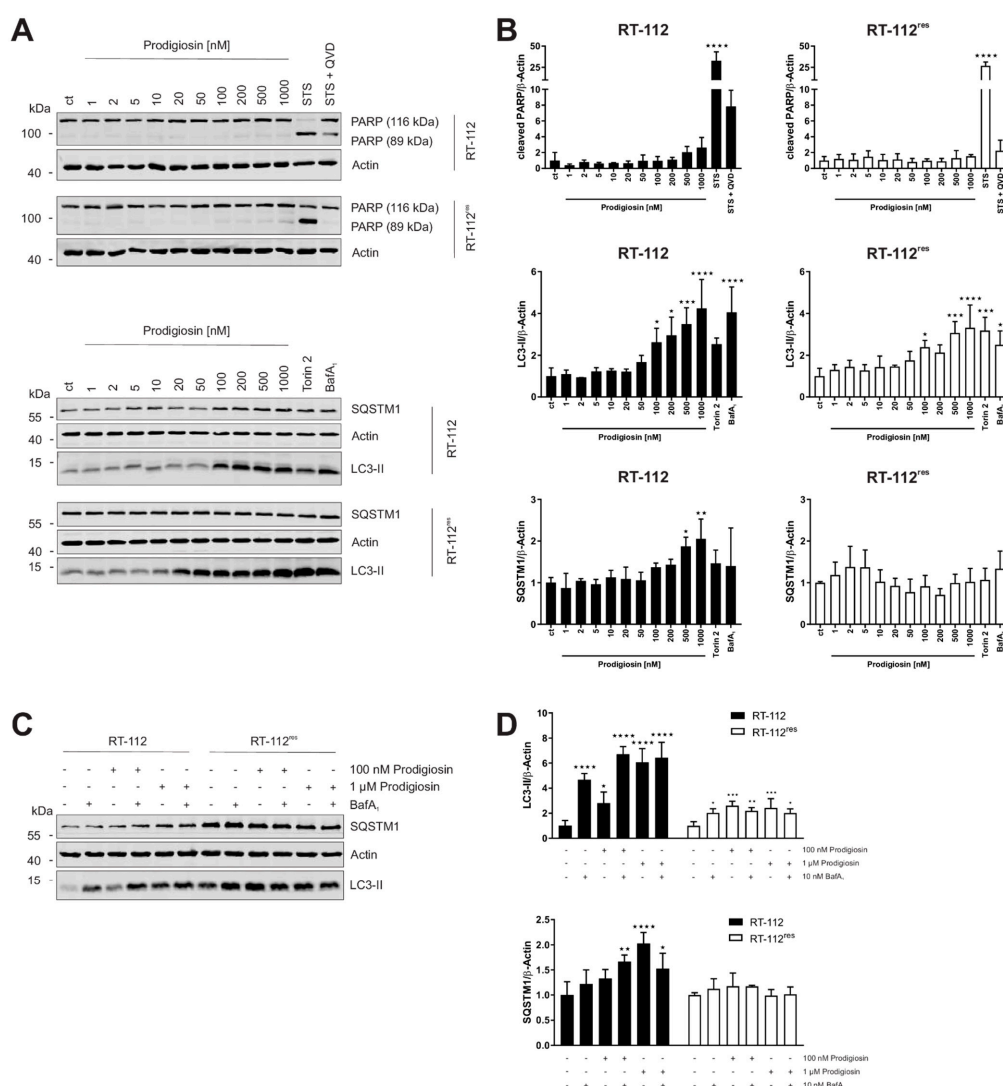


**Figure 3.** Prodigiosin modulates autophagy in RT-112 and RT-112<sup>res</sup> in a concentration-dependent manner. RT-112 and RT-112<sup>res</sup> cells were treated with the indicated concentrations of prodigiosin or 2.5 µM STS ± 10 µM QVD, 10 nM bafilomycin A<sub>1</sub> (BafA<sub>1</sub>) or 250 nM Torin 2. After 6 h, the cells were lysed and cellular lysates were immunoblotted for the indicated proteins. (A,C) One representative immunoblot is shown for each experiment. (B,D) The densities of the bands of each protein of at least three independent experiments were quantified and normalized to actin. The mean of the solvent control of RT-112 (black bars) and RT-112<sup>res</sup> (white bars) was set as 1 for each protein. Bars represent the means + SD. *p* values were determined by ordinary one-way ANOVA with Dunnett's post hoc test. \* *p* < 0.05; \*\* *p* < 0.01; \*\*\* *p* < 0.001; \*\*\*\* *p* < 0.0001. PARP: poly (ADP-ribose) polymerase; SQSTM1: sequestosome 1; LC3: light chain 3.

### 3.3. Autophagy-Related Protein Are Upregulated in RT-112<sup>res</sup> Cells

Next, we aimed at investigating whether cisplatin resistance affects the basal expression levels of LC3-II and SQSTM1 and the functional relationship of prodigiosin and BafA<sub>1</sub>. As determined by immunoblotting, the basal levels of both LC3-II and SQSTM1 are upregulated in RT-112<sup>res</sup> cells compared to RT-112 cells (Figure 3C), which matches with previous observations [15] and underlines the role of autophagy in the resistance mechanism of UCCs against cisplatin. LC3-II levels significantly increase in sensitive and resistant cells after treatment with prodigiosin and BafA<sub>1</sub>, but effects are not additive. The latter observation indicates that autophagic flux is indeed blocked. Of note, LC3-II levels in RT-112<sup>res</sup> cells increase only twofold upon prodigiosin or BafA<sub>1</sub> treatment compared to untreated cells, which might be explained by higher basal levels and lower capacity of inducible autophagy in this cell line. SQSTM1 levels increased with prodigiosin and BafA<sub>1</sub> treatment alone or in combination in RT-112, but effects are not additive, whereas SQSTM1 levels are not affected in RT-112<sup>res</sup> (Figure 3C,D). Taken together, these results suggest that RT-112<sup>res</sup> cells likely have a higher capacity for basal autophagy but that autophagy can still be modulated by prodigiosin treatment.

### 3.4. Prodigiosin Induces Apoptotic Cell Death in RT-112<sup>res</sup>

In a next step, the time-dependency of the effect of prodigiosin on apoptotic and autophagic protein markers was investigated. For these experiments, we chose a concentration of 100 nM of prodigiosin as the lowest concentration that significantly increased LC3-II levels in both RT-112 and RT-112<sup>res</sup>. In RT-112, there is no significant increase in cleaved PARP levels even after 48 h whereas in RT-112<sup>res</sup>, there is a time-dependent and significant increase in PARP cleavage after incubation with prodigiosin (Figure 4A,B), indicating apoptotic cell death in cisplatin-resistant UCCs upon this treatment. The decreased PARP and actin levels after 48 h indicate that cells are already in the late phases of apoptosis at this time point. The time-dependent accumulation of LC3-II can be seen in both cell types and is again more prominent in sensitive cells. The effects on SQSTM1 are distinct in cisplatin-sensitive and -resistant UCCs. Whereas SQSTM1 accumulates in RT-112 over time, in RT-112<sup>res</sup> there is a decrease in protein level after 24 h and 48 h treatment with prodigiosin (Figure 4A,B). Taken together, these results suggest that prodigiosin blocks autophagy in cisplatin-sensitive RT-112 cells, but does not induce apoptosis. In RT-112<sup>res</sup> cells, apoptotic cell death is induced, whereas SQSTM1 levels decrease despite the blocked autophagy.

### 3.5. Prodigiosin Synergistically Increases Cisplatin-Mediated Cytotoxicity in RT-112 and RT-112<sup>res</sup> UCCs

Since modifications in both autophagy and apoptosis seem to contribute to cisplatin resistance in UCCs, we hypothesized that targeting these processes with prodigiosin might be beneficial to increase the efficiency of cisplatin treatment in BC. To analyze whether prodigiosin can have a synergistic effect on cytotoxicity together with cisplatin, we examined the effect of prodigiosin and cisplatin alone (Figure 5A) and in combination on these cell lines and performed isobologram analyses. For this, the Chou–Talalay method is the most impactful approach to quantify synergy [41]. By applying this method, it is possible to determine the combination index (CI) values for drug combinations out of a small number of data points while still receiving the maximal amount of useful information via computer simulation. Chou and Talalay therefore propose to use multiples and dividers of the respective IC<sub>50</sub> concentrations of each drug and carry out the experiment at an equipotency ratio so that the contributions of the effects of each drug to the combination is roughly equal [42]. Here, cells were treated with concentrations in the range of 0.25, 0.5 or 1 times the IC<sub>50</sub> values of the respective cell lines and substances. For CI plots, the CI values (calculated from actual experiment points and extrapolated) are plotted against the effect level (an effect level of 0.99 represents a reduction of cell viability by 99%). CI values < 1 are considered synergistic, whereas a CI value around 1 represents additive effects and CI values > 1 indicate antagonistic effects of the applied drugs [38]. In both RT-112 and

RT-112<sup>res</sup>, the treatment with IC<sub>50</sub> concentrations of prodigiosin and cisplatin combined leads to a nearly complete decrease in cell viability (Figure 5B,C). The combination index plot shows synergistic effects in both cell types after 24 h of treatment with a combination of prodigiosin and cisplatin especially in higher administered concentrations (Figure 5D,E). After 72 h of incubation, prodigiosin synergistically sensitizes RT-112 cells to cisplatin treatment at most effect levels. In RT-112<sup>res</sup> cells, we observed synergistic effects at low- to mid-range effect levels, whereas the combination of prodigiosin and cisplatin possesses a rather additive effect at higher effect levels (Figure S2).

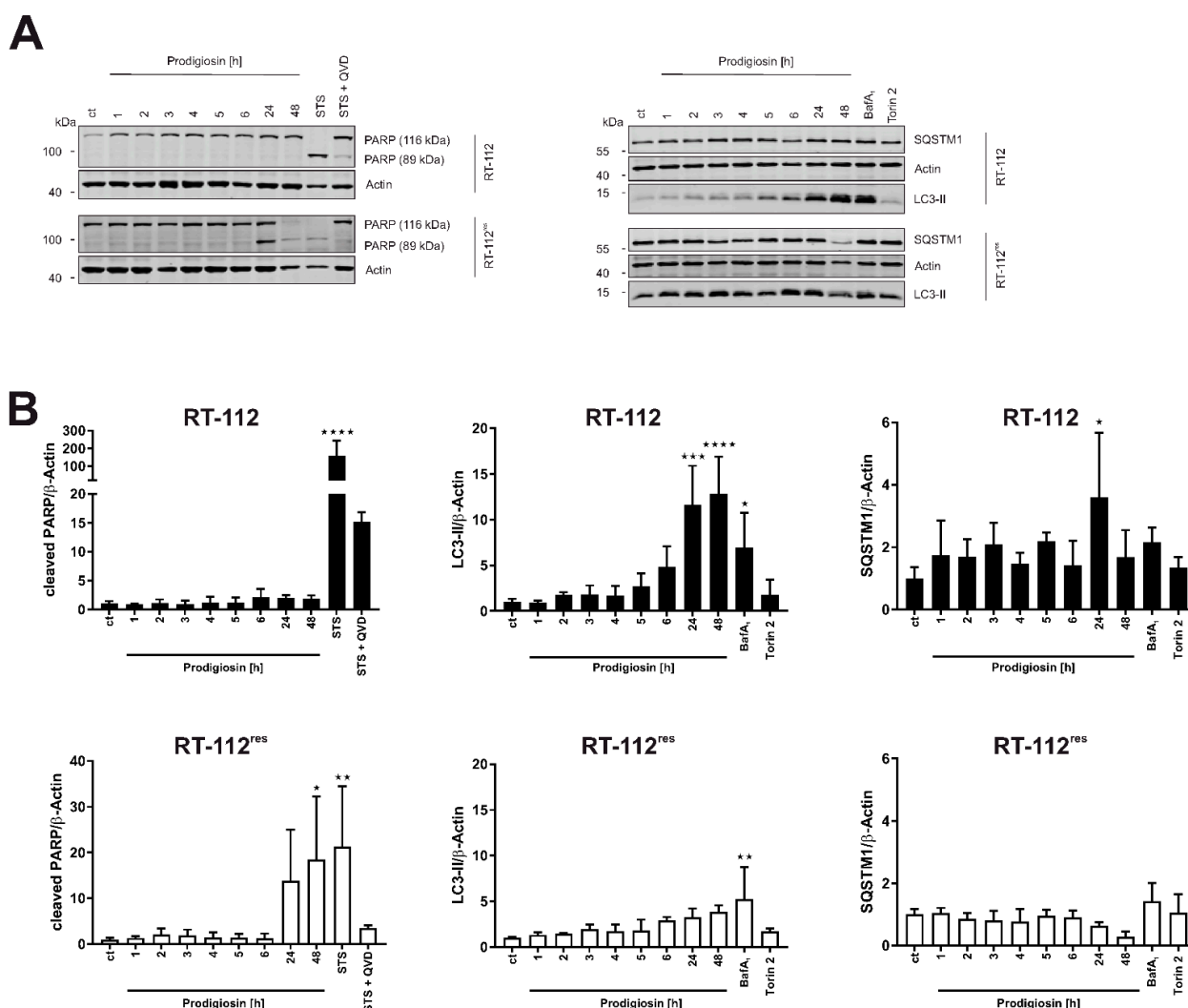


**Figure 4.** Prodigiosin blocks autophagy in RT-112 and RT-112<sup>res</sup> and induces apoptosis in RT-112<sup>res</sup> in a time-dependent manner. (A) RT-112 and RT-112<sup>res</sup> cells were treated with 100 nM prodigiosin for the indicated periods of time or with 2.5 μM STS ± 10 μM QVD, 10 nM BafA1 or 250 nM Torin 2 for 24 h. After the incubation, cells were lysed, and cellular lysates were immunoblotted for the indicated proteins. One representative immunoblot is shown for each experiment. (B) The densities of bands of each protein of at least three independent experiments were quantified and normalized to actin. The mean of the solvent control of RT-112 (black bars) and RT-112<sup>res</sup> (white bars) was set as 1 for each protein. Bars represent the means + SD. *p* values were determined by ordinary one-way ANOVA with Dunnett's post hoc test. \* *p* < 0.05; \*\* *p* < 0.01; \*\*\* *p* < 0.001; \*\*\*\* *p* < 0.0001. PARP: poly (ADP-ribose) polymerase; SQSTM1: sequestosome 1; LC3: light chain 3.

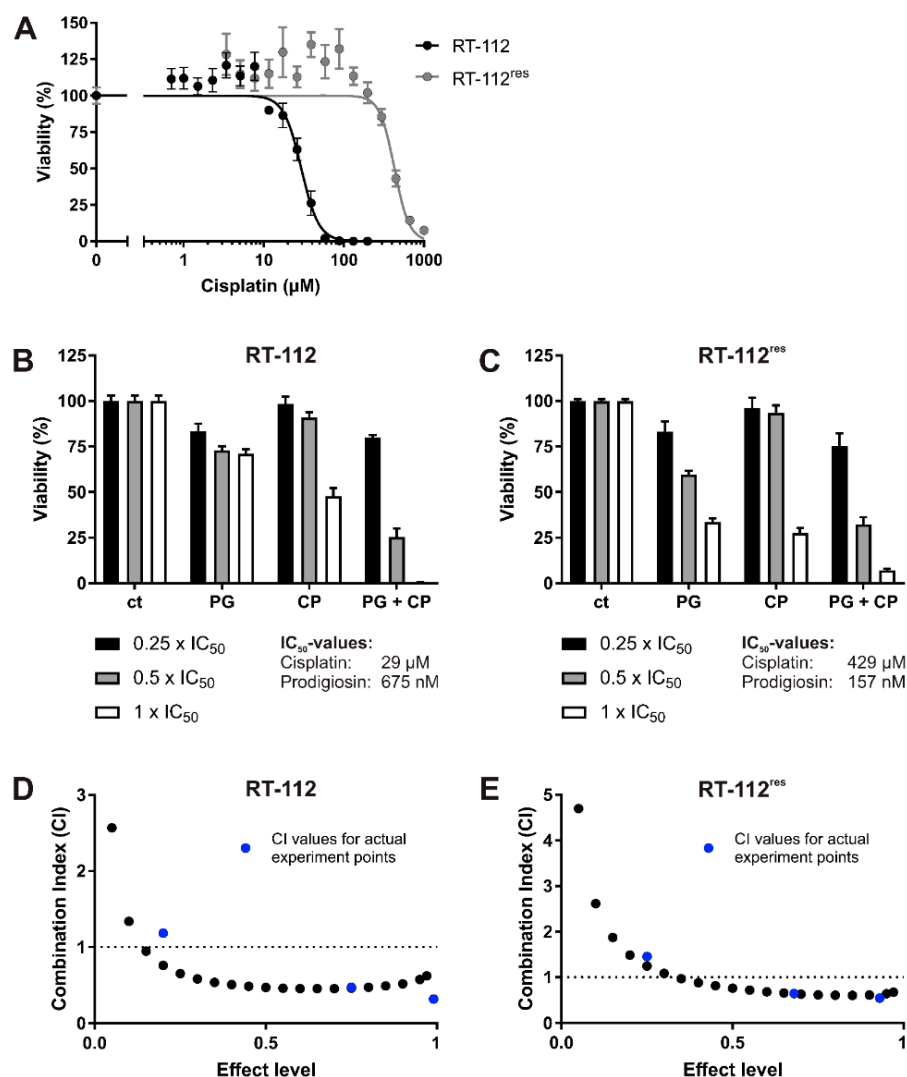


**Figure 5.** Prodigiosin increases cisplatin-mediated cytotoxicity in RT-112 and RT-112<sup>res</sup> cells after 24 h. RT-112 and RT-112<sup>res</sup> cells were treated with different concentrations of (A) cisplatin (CP) alone or (B,C) prodigiosin (PG) or CP alone or in combination for 24 h. For combinatory analysis, 0.25x, 0.5x or 1x of the  $\text{IC}_{50}$  values of the single substances in RT-112 (B) and RT-112<sup>res</sup> (C) were used. After treatment, cell viability was measured using an MTT assay. Results are shown as the mean  $\pm$  SEM of three independent experiments performed in triplicates for each treatment. The combination index (CI) for different fractions affected of RT-112 (D) and RT-112<sup>res</sup> (E) was calculated using the software CompuSyn (black dots). CompuSyn uses algorithms to extrapolate CI values for any effect level from the CI values of actual experiment points (blue dots). Synergism ( $\text{CI} < 1$ ), additivism ( $\text{CI} = 1$ ) and antagonism ( $\text{CI} > 1$ ) can thereby be determined.

### 3.6. Treatment with Prodigiosin Overcomes Apoptosis Resistance in RT-112<sup>res</sup>

Subsequently, we wanted to confirm the results of the cell viability assay by the western blot analysis of autophagic and apoptotic marker proteins.  $\text{IC}_{50}$  concentrations obtained from viability assays performed after 24 h of treatment were used for each substance and cell line, respectively. Cisplatin induced a significant increase in PARP cleavage in sensitive UCCs but not in RT-112<sup>res</sup>, confirming the described mechanism of cytotoxicity of cisplatin [8] and the resistance to these mechanisms of RT-112<sup>res</sup> cells. In contrast to RT-112 cells, in which prodigiosin has no effect on PARP cleavage, prodigiosin treatment of RT-112<sup>res</sup> cells significantly induces apoptosis, which can be rescued by the caspase inhibitor QVD (Figure 6A,B). Treatment with prodigiosin, but not with cisplatin,

led to a significant increase in LC3-II levels in both RT-112 and RT-112<sup>res</sup>. Again, the effect of prodigiosin treatment on SQSTM1 levels was contrary in resistant and sensitive UCCs. Whereas in RT-112, prodigiosin treatment alone or in combination with cisplatin and QVD led to an increase in SQSTM1, indicating that autophagy was blocked in these cells, in RT-112<sup>res</sup> cells, the SQSTM1 levels decreased significantly upon all treatment regimens (Figure 6A,C). These effects can be obtained in the cisplatin-resistant cell line RT-112<sup>res</sup> in lower concentrations than in the sensitive parental cells. Mostly, these effects are synergistic at higher effect levels, which is beneficial for cancer treatment. Collectively, it seems that the application of prodigiosin can sensitize RT-112 UCCs to cisplatin treatment.

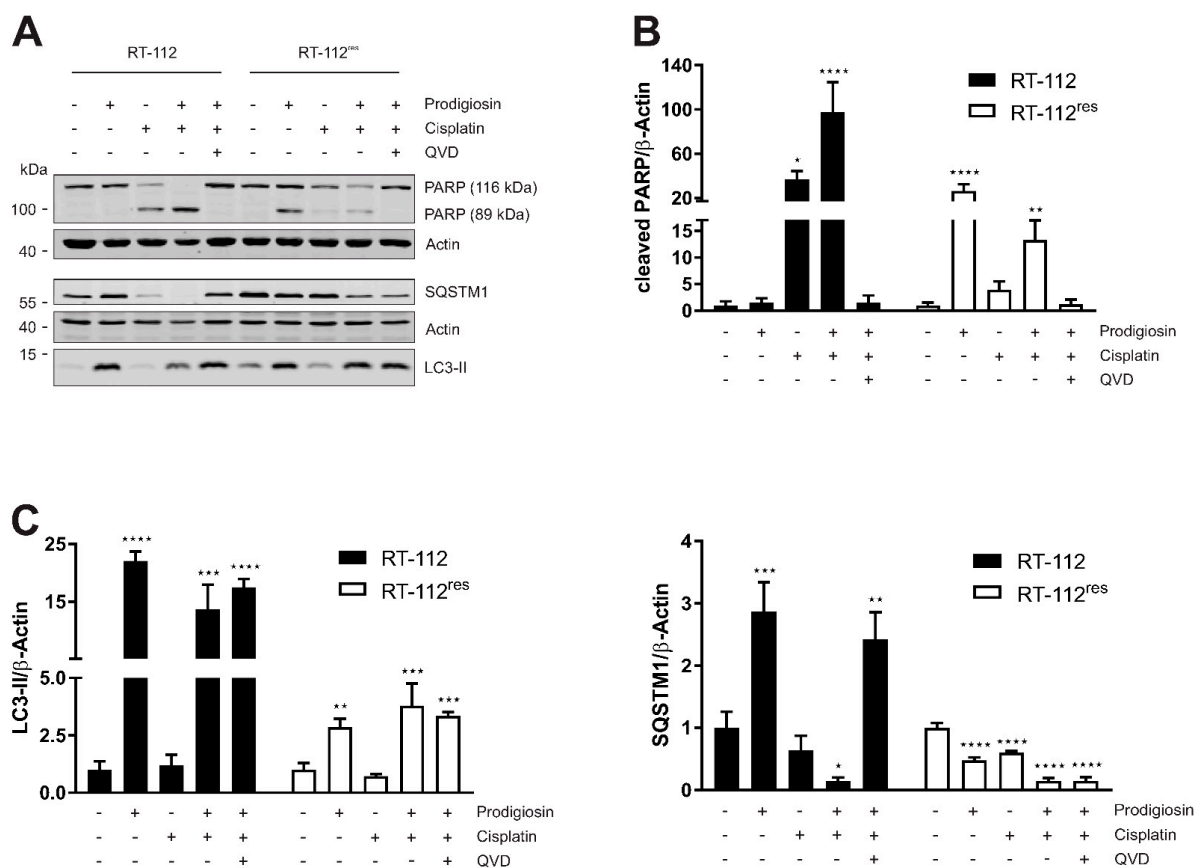


**Figure 6.** The combination of prodigiosin and cisplatin modulates apoptosis and autophagy in RT-112 and RT-112<sup>res</sup>. RT-112 and RT-112<sup>res</sup> cells were treated with IC<sub>50</sub> concentrations of prodigiosin and cisplatin alone or in combination in absence or presence of 10  $\mu$ M QVD. After 24 h, the cells were lysed and cellular lysates were immunoblotted for the indicated proteins. (A) One representative immunoblot is shown for each experiment. The densities of bands of cleaved PARP (B) or LC3-II and SQSTM1 (C) of at least three independent experiments were quantified and normalized to actin. The mean of the solvent control of each cell line was set as 1 for each protein. Bars represent the means  $\pm$  SD. *p* values were determined by ordinary one-way ANOVA with Dunnett's post hoc test. \* *p* < 0.05; \*\* *p* < 0.01; \*\*\* *p* < 0.001; \*\*\*\* *p* < 0.0001. PARP: poly (ADP-ribose) polymerase; SQSTM1: sequestosome 1; LC3: light chain 3.

### 3.7. Prodigiosin Treatment Alters Cathepsin Activity

It has previously been suggested that lysosomal functions are altered in cisplatin-resistant cell lines [43]. We next analyzed the lysosomal compartment of RT-112 and RT-112<sup>res</sup> cells by staining with LysoTracker. We observed reduced numbers but increased sizes of lysosomes in RT-112<sup>res</sup> cells (Figure 7A,B), indicating that acquired cisplatin resistance is accompanied with an altered lysosomal compartment in this cellular model. Next, we wanted to know whether prodigiosin treatment affects the activity of cathepsins, which play a key role among lysosomal proteases [44]. We employed assays for the cathepsins

B, D and L, and found that especially the activities of the cysteine cathepsins B and L are significantly reduced in both RT-112 and RT-112<sup>res</sup> cells upon prodigiosin treatment (Figure 7C). In contrast, the activity of the aspartic protease cathepsin D was apparently not affected by prodigiosin, but this might be explained by the observation that this protease shows residual activity under a neutral pH [45]. Taken together, we hypothesize that the observed effect of prodigiosin on RT-112<sup>res</sup> cells might be caused by an altered lysosomal compartment in combination with the effects on cathepsins.

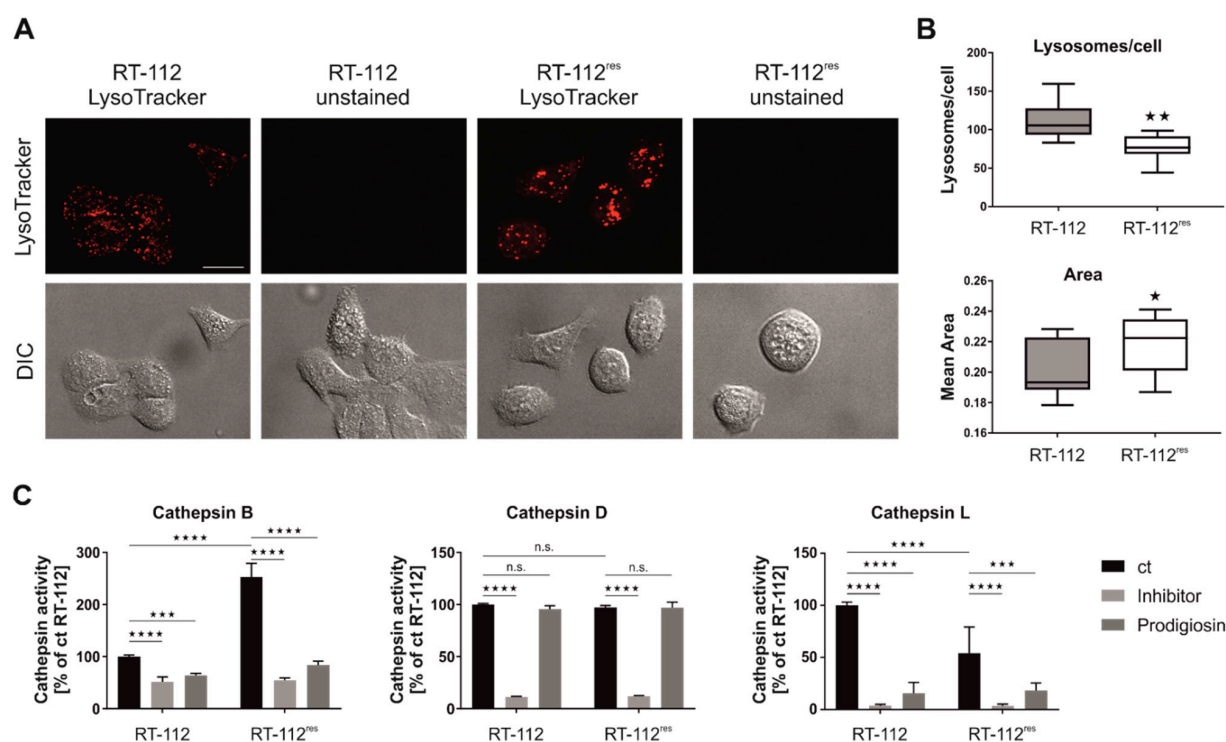


**Figure 7.** Prodigiosin treatment reduces cathepsin B and L activity in RT-112 and RT-112<sup>res</sup>. (A,B) RT-112 and RT-112<sup>res</sup> cells in chambered coverslips were treated with 100 nM LysoTracker<sup>TM</sup> Deep Red for 30 min. (A) Representative sections are depicted and (B) the number and area of lysosomes of 10 representative images from two biological replicates for each cell line were quantified using ImageJ 1.53c. *p* values were determined by Student's *t*-test. Scale bar: 20  $\mu$ m. (C) RT-112 and RT-112<sup>res</sup> cells were treated with 100 nM prodigiosin. After 24 h, the cells were lysed and cathepsin assays were performed according to the manufacturer's instructions. For cathepsin B and L assays, 20  $\mu$ M Z-Phe-Phe-FMK and for cathepsin D assays, 0.1  $\mu$ M pepstatin A were used as inhibitor control. The fluorescence of duplicates for each treatment of three independent experiments was measured and the mean of the DMSO control of RT-112 was set as 100%. Bars represent the means + SD. *p* values were determined by two-way ANOVA with Tukey's multiple comparisons post hoc test. \* *p* < 0.05; \*\* *p* < 0.01; \*\*\* *p* < 0.001; \*\*\*\* *p* < 0.0001.

### 3.8. Treatment with Prodigiosin Synergistically Sensitizes Various UCCs to Cisplatin-Mediated Cell Death

In a next step, we wanted to confirm our results in additional UCC lines to address the heterogeneity of the disease. Similar to RT-112 UCCs, we first determined the IC<sub>50</sub> values of prodigiosin and cisplatin for each cisplatin-sensitive and -resistant cell line (Figure 8A). The decreasing differences in the IC<sub>50</sub> values of cisplatin in cisplatin-sensitive and -resistant cells reflect the different permanent cisplatin concentrations in the culture media of RT-112<sup>res</sup>, T24<sup>res</sup>, 253J<sup>res</sup> and J82<sup>res</sup>, which are 12  $\mu$ g/mL (39.9  $\mu$ M), 7  $\mu$ g/mL (23.3  $\mu$ M), 2  $\mu$ g/mL (6.6  $\mu$ M) and 1  $\mu$ g/mL (3.3  $\mu$ M), respectively. Of note, IC<sub>50</sub> values of prodigiosin are lower in the resistant cell lines compared to the cisplatin-sensitive parental cells except for T24<sup>res</sup> and J82<sup>res</sup> cells after 24 h. Based on these data, we repeated the

above-described combination experiments and isobologram analyses. After 24 h treatment, CI values at different effective doses (EDs) were synergistic in all cisplatin-sensitive and -resistant cell lines, whereas after 72 h of treatment the combination effects vary between cell lines (Figure 8B). Whilst in T24 and T24<sup>res</sup>, effects were synergistic at all displayed EDs, the combination was rather additive to slightly synergistic in 253J, J82 and J82<sup>res</sup>. In RT-112<sup>res</sup> cells, CI values in the lower antagonistic range were obtained for higher effective doses, and antagonism was observed in 253J<sup>res</sup> cells for the 72 h incubation. Of note, in all tested cell lines these effects can be seen after treatment with prodigiosin in nanomolar ranges. Due to low nanomolar IC<sub>50</sub> values in cisplatin-resistant UCCs, a monotherapy with prodigiosin in a second-line treatment of cancers with acquired cisplatin resistance could also be an interesting therapeutical approach, which naturally requires further investigations. Taken together, these findings present prodigiosin as a promising candidate for the therapy of cisplatin-resistant bladder cancer.

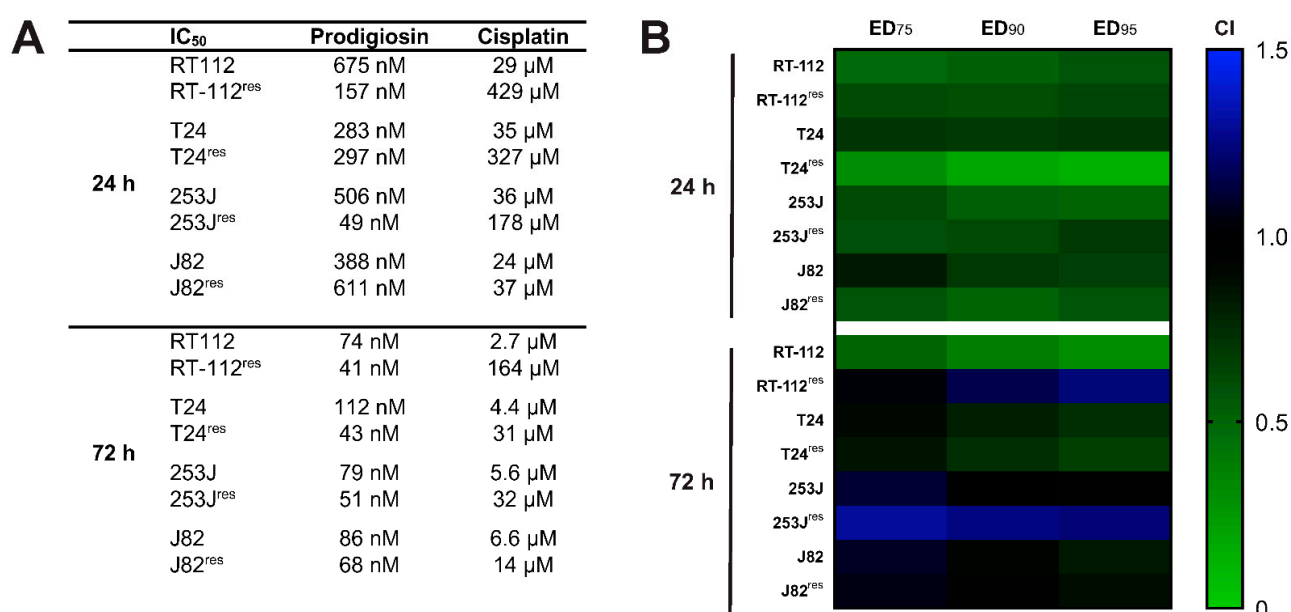


**Figure 8.** Prodigiosin increases cisplatin-mediated cytotoxicity in sensitive and -resistant bladder carcinoma cells. RT-112, RT-112<sup>res</sup>, T24, T24<sup>res</sup>, 253J, 253J<sup>res</sup>, J82 and J82<sup>res</sup> cells were treated with different concentrations of prodigiosin and cisplatin alone or in combination for 24 or 72 h. After treatment, cell viability was measured using an MTT assay. (A) IC<sub>50</sub> values were calculated using GraphPadPrism using the results of three independent experiments performed in triplicates for each treatment. (B) For combinatory analysis, cells were treated with multiples of the IC<sub>50</sub> concentrations of prodigiosin and cisplatin alone or in combination. CI values were calculated for different effective doses (ED) using the software CompuSyn. CompSyn uses algorithms to extrapolate CI values for any effect level from the CI values of actual experiment points. Synergism (CI < 1; green), additivism (CI = 1; black) and antagonism (CI > 1; blue) can thereby be determined.

#### 4. Discussion

Bladder cancer is one of the ten most common cancers and patients face a poor prognosis due to limited treatment options. Cisplatin-based combination treatment is recommended as first-line therapy, but success is often limited by harmful side effects and chemoresistance [2,5,6]. Natural compounds can be a valuable source for lead structures that increase cisplatin efficacy or overcome resistance mechanisms. In this study, we characterized the effects of the bacterial tripyrrole prodigiosin on UCC lines. We observed that prodigiosin blocks autophagy in both cisplatin-sensitive and -resistant UCCs, but preferentially induces apoptotic cell death in cisplatin-resistant UCCs. We also found that basal levels of autophagy-related proteins increased with cisplatin resistance. This stands in line with the observations by our own group [15] and by Ojha et al. [46] who demonstrated

that cell protective autophagy was upregulated in a cisplatin-treated T24 UCC line and that the inhibition of autophagy through chloroquine increased the cytotoxic effect of cisplatin.

Effects of prodigiosin on autophagy are discussed controversially in the literature. On the one hand, the inhibition of the autophagic process has been described via different mechanisms such as the extracellular signal-regulated kinase pathway or by blocking autophagosome–lysosome fusion and lysosomal cathepsin maturation [33,34,36]. On the other hand, other studies report that prodigiosin treatment led to the induction of autophagic cell death [32,47]. The discrepancies between these observations about prodigiosin suggest that effects might depend strongly on the type of cancer. In our hands, prodigiosin rather reveals an autophagy-inhibitory function in both sensitive and -resistant UCCs as determined by autophagic flux assays using bafilomycin A<sub>1</sub>. Under physiological conditions, SQSTM1 levels are relatively low due to continuous degradation by autophagy. Matching with our observations, elevated SQSTM1 levels have strongly been indicated to be involved in resistance to platinum-based cancer therapy [48]. Notably, we observe a decrease in SQSTM1 levels upon prolonged treatment with prodigiosin (i.e., 24–48 h). However, this does not necessarily indicate that SQSTM1 becomes degraded by a (macro-)autophagy-dependent pathway and might be mediated by alternative mechanisms in cells destined for death. For example, it has been described that SQSTM1 can be cleaved by caspases 6 and 8, respectively [49].

Like in cisplatin-resistant UCCs, prodigiosin has also been shown to induce apoptotic cell death in various other cell models [33,50–53]. Since apoptosis in resistant UCCs could be induced by prodigiosin, but not by cisplatin, it seems that prodigiosin is able to partially overcome cisplatin resistance by re-establishing apoptotic pathways. Generally, there is a strong relationship between autophagy and cisplatin resistance. Recently, Gasiorkiewicz et al. reviewed autophagy-modulating compounds that chemosensitize for cisplatin in cancer therapy [54]. Among these compounds are classical autophagy inhibitors, compounds with specific autophagy-related targets, and natural compounds. It appears that both the inhibition of the cyto-protective functions and the induction of death-promoting functions of autophagy can be therapeutically beneficial. We observe an altered lysosomal compartment in RT-112<sup>res</sup> cells, and prodigiosin treatment clearly affects cathepsin activity. Of note, we found that cathepsin D is less affected by prodigiosin, and this cathepsin has been reported to be partially active at neutral pH [45]. We speculate that prodigiosin influences intralysosomal cathepsin activation, and apparently the lysosomal structure in cisplatin-resistant RT-112<sup>res</sup> cells favors this effect. It has been described that prodigiosin can mediate a rise of the lysosomal pH with a concomitant non-organelle-specific increase in acidity of the cytosol [55]. However, Zhao et al. reported that prodigiosin inhibits lysosomal activity by downregulating mRNA and protein levels of cathepsins without affecting the pH [36]. Accordingly, further studies have to assess the actual target of prodigiosin mediating this effect.

The National Cancer Institute has tested prodigiosin against a suite of around 60 cancer cell lines with an average IC<sub>50</sub> of 2.1 µM [31]. In our experiments, prodigiosin had IC<sub>50</sub> values in the nanomolar range in all tested UCCs. It is noteworthy that there was a tendency to lower IC<sub>50</sub> values in cisplatin-resistant cells compared to their sensitive precursors. Furthermore, we found mostly synergistic or additive cytotoxic effects when prodigiosin was combined with cisplatin, especially at higher effect levels. As specified by Chou [42], it is important to note that synergism and antagonism can be different at different dose or effect levels. While for chronic diseases synergism at low dose or effect levels is important, for the treatment of infectious diseases or cancer therapies, synergism at high effect levels is much more therapeutically relevant.

In addition, selective synergism against the target and antagonism toward the host is also of practical importance to enlarge the therapeutic window. Several studies suggest desirable clinical properties of prodigiosin. Using the Ames and micronucleus test, Guryanov et al. could show that prodigiosin exhibited no significant genotoxic potential [56]. Furthermore, prodigiosin shows no adverse effects in a combination study with 5-fluorouracil

in colorectal cancer in mice while sensitizing cancer cells to 5-fluorouracil [36], and it has been shown to exert higher toxicity in A549 lung carcinoma cells than in primary small airway epithelial cells [57]. For therapeutic application, it has to be considered whether the concentrations for synergism are achievable in the body [42]. Prodigiosin meets Lipinski's rule of five which predicts the oral bioavailability of drugs [58,59], but certainly, further evaluations of the bioavailability of prodigiosin in the target tissue are required.

To our knowledge, this is the first study that investigates the influence of prodigiosin in combination with cisplatin in chemoresistant bladder cancer cells. Overall, we propose that treatment with prodigiosin can enhance the efficacy of cisplatin-based chemotherapy in UCCs to resensitize resistant tumors and is worthwhile further investigations.

**Supplementary Materials:** The following are available online, Figure S1:  $^1\text{H}$ - and  $^{13}\text{C}$ -NMR-spectra of Prodigiosin ( $\text{CDCl}_3$ , 600 MHz and 151 MHz, respectively), Figure S2: Prodigiosin increases cisplatin-mediated cytotoxicity in RT-112 and RT-112<sup>res</sup> cells after 72 h, Supplementary Methods: Macro for quantification of LysoTracker-stained lysosomes.

**Author Contributions:** L.B. designed the experiments and performed viability assays, immunoblot analyses, fluorescence microscopy, and cathepsin activity assays. M.A.S., M.J.H. and G.N. generated cisplatin-resistant cell lines. H.U.C.B. produced and provided prodigiosin. D.S., A.F., N.B., Y.S., W.W., M.J.M. and J.D. gave technical support. L.B. and B.S. analyzed the data and wrote the manuscript. B.S. and J.P. supervised the project. All authors discussed the results and commented on the manuscript. All authors have read and agreed to the published version of the manuscript.

**Funding:** This work was supported by the Deutsche Forschungsgemeinschaft STO 864/5-1 (to BS), STO 864/6-1 (to BS) and GRK 2158 (to B.S. and J.P.), the BMBF (031B0918A—project “AutoBiotech” to J.P.) and the Düsseldorf School of Oncology (to B.S.; funded by the Comprehensive Cancer Center Düsseldorf/Deutsche Krebshilfe and the Medical Faculty of the Heinrich-Heine-University Düsseldorf).

**Institutional Review Board Statement:** Not applicable.

**Informed Consent Statement:** Not applicable.

**Data Availability Statement:** Not applicable.

**Acknowledgments:** We would like to dedicate this article to our colleague Peter Proksch. Peter always wholeheartedly supports our interdisciplinary approaches investigating the cell biological effects of natural compounds.

**Conflicts of Interest:** The authors declare that there is no competing financial interest in relation to the work described.

**Sample Availability:** Samples of the compounds are not available from the authors.

## Abbreviations

BafA<sub>1</sub>, bafilomycin A<sub>1</sub>; Bcl-2, B-cell lymphoma 2; BC, bladder cancer; CI, combination index; ED, effective dose; ER, endoplasmic reticulum; ERK, extracellular signal-regulated kinase; (MAP1)LC3, (microtubule-associated proteins 1A/1B) light chain 3; IC<sub>50</sub>, half maximal inhibitory concentration; MIBC, muscle-invasive bladder cancer; MTT, 3-(4,5-Dimethylthiazolyl-2)-2,5-diphenyl-2H-tetrazoliumbromid; NMIBC, non-muscle-invasive bladder cancer; PARP, poly (ADP-ribose) polymerase; PtdIns3K, phosphatidylinositol 3-kinase; SQSTM1, sequestosome 1; STS, staurosporine; UC, urothelial carcinoma; UCC, urothelial carcinoma cell; ULK1, Unc-51 like autophagy activating kinase 1; V-ATPase, vacuolar-type H<sup>+</sup>-ATPase

## References

1. WHO. Available online: [https://gco.iarc.fr/today/online-analysis-table?v=2018&mode=cancer&mode\\_population=continents&population=900&populations=900&key=asr&sex=0&cancer=39&type=0&statistic=5&prevalence=0&population\\_group=0&ages\\_group%5B%5D=0&ages\\_group%5B%5D=17&group\\_cancer=1&include\\_nmssc=1&include\\_nmssc\\_other=1](https://gco.iarc.fr/today/online-analysis-table?v=2018&mode=cancer&mode_population=continents&population=900&populations=900&key=asr&sex=0&cancer=39&type=0&statistic=5&prevalence=0&population_group=0&ages_group%5B%5D=0&ages_group%5B%5D=17&group_cancer=1&include_nmssc=1&include_nmssc_other=1) (accessed on 21 December 2020).

2. Richters, A.; Aben, K.K.H.; Kiemeny, L.A.L.M. The global burden of urinary bladder cancer: An update. *World J. Urol.* **2020**, *38*, 1895–1904. [CrossRef] [PubMed]
3. Cumberbatch, M.G.K.; Party, O.B.O.T.E.Y.A.U.U.C.W.; Noon, A.P. Epidemiology, aetiology and screening of bladder cancer. *Transl. Androl. Urol.* **2019**, *8*, 5–11. [CrossRef] [PubMed]
4. Shi, M.-J.; Meng, X.-Y.; Wu, Q.-J.; Zhou, X.-H. High CD3D/CD4 ratio predicts better survival in muscle-invasive bladder cancer. *Cancer Manag. Res.* **2019**, *11*, 2987–2995. [CrossRef] [PubMed]
5. Leitlinienprogramm Onkologie (Deutsche Krebsgesellschaft, Deutsche Krebshilfe, AWMF): S3-Leitlinie Früherkennung, Diagnose, Therapie und Nachsorge des Harnblasenkarzinoms, Langversion 2.0, 2020, AWMF-Registrierungsnummer 032/038OL (In German). Available online: <https://www.leitlinienprogramm-onkologie.de/leitlinien/harnblasenkarzinom> (accessed on 21 December 2020).
6. Witjes, J.A.; Lebet, T.; Compérat, E.M.; Cowan, N.C.; De Santis, M.; Bruins, H.M.; Hernández, V.; Espinós, E.L.; Dunn, J.; Rouanne, M.; et al. Updated 2016 EAU Guidelines on Muscle-invasive and Metastatic Bladder Cancer. *Eur. Urol.* **2017**, *71*, 462–475. [CrossRef]
7. Nadal, R.; Bellmunt, J. Management of metastatic bladder cancer. *Cancer Treat. Rev.* **2019**, *76*, 10–21. [CrossRef] [PubMed]
8. Cohen, S.M.; Lippard, S.J. Cisplatin: From DNA damage to cancer chemotherapy. *Prog. Nucleic Acid Res. Mol. Biol.* **2001**, *67*, 93–130. [CrossRef] [PubMed]
9. Gatti, L.; Cassinelli, G.; Zaffaroni, N.; Lanzi, C.; Perego, P. New mechanisms for old drugs: Insights into DNA-unrelated effects of platinum compounds and drug resistance determinants. *Drug Resist. Updat.* **2015**, *20*, 1–11. [CrossRef]
10. Shen, D.-W.; Pouliot, L.M.; Hall, M.D.; Gottesman, M.M. Cisplatin Resistance: A Cellular Self-Defense Mechanism Resulting from Multiple Epigenetic and Genetic Changes. *Pharmacol. Rev.* **2012**, *64*, 706–721. [CrossRef] [PubMed]
11. Chen, S.-H.; Chang, J.-Y. New Insights into Mechanisms of Cisplatin Resistance: From Tumor Cell to Microenvironment. *Int. J. Mol. Sci.* **2019**, *20*, 4136. [CrossRef] [PubMed]
12. Drayton, R.M.; Catto, J.W.F. Molecular mechanisms of cisplatin resistance in bladder cancer. *Expert Rev. Anticancer. Ther.* **2012**, *12*, 271–281. [CrossRef]
13. Skowron, M.A.; Melnikova, M.; Van Roermund, J.G.H.; Romano, A.; Albers, P.; Thomale, J.; Schulz, W.A.; Niegisch, G.; Hoffmann, M.J. Multifaceted Mechanisms of Cisplatin Resistance in Long-Term Treated Urothelial Carcinoma Cell Lines. *Int. J. Mol. Sci.* **2018**, *19*, 590. [CrossRef]
14. Ma, K.; Li, S.; Huo, X.; Guo, M.; Du, X.; Li, C.; Liu, X.; Lv, J.; Chen, Z. Exploring the mechanism of cisplatin resistance by transcriptome sequencing and reversing the chemoresistance by autophagy inhibition in small cell lung cancer. *Biochem. Biophys. Res. Commun.* **2020**, *533*, 474–480. [CrossRef]
15. Schlütermann, D.; Skowron, M.A.; Berleth, N.; Böhrer, P.; Deitersen, J.; Stuhldreier, F.; Wallot-Hieke, N.; Wu, W.; Peter, C.; Hoffmann, M.J.; et al. Targeting urothelial carcinoma cells by combining cisplatin with a specific inhibitor of the autophagy-inducing class III PtdIns3K complex. *Urol. Oncol. Semin. Orig. Investig.* **2018**, *36*, 160.e1–160.e13. [CrossRef] [PubMed]
16. Yu, L.; Gu, C.; Zhong, D.; Shi, L.; Kong, Y.; Zhou, Z.; Liu, S. Induction of autophagy counteracts the anticancer effect of cisplatin in human esophageal cancer cells with acquired drug resistance. *Cancer Lett.* **2014**, *355*, 34–45. [CrossRef] [PubMed]
17. Wesselborg, S.; Stork, B. Autophagy signal transduction by ATG proteins: From hierarchies to networks. *Cell. Mol. Life Sci.* **2015**, *72*, 4721–4757. [CrossRef]
18. Lőrincz, P.; Juhász, G. Autophagosome-Lysosome Fusion. *J. Mol. Biol.* **2020**, *432*, 2462–2482. [CrossRef] [PubMed]
19. Li, X.; He, S.; Ma, B. Autophagy and autophagy-related proteins in cancer. *Mol. Cancer* **2020**, *19*, 1–16. [CrossRef]
20. Morel, E.; Mehrpour, M.; Botti, J.; Dupont, N.; Hamai, A.; Nascimbeni, A.C.; Codogno, P. Autophagy: A Druggable Process. *Annu. Rev. Pharmacol. Toxicol.* **2017**, *57*, 375–398. [CrossRef] [PubMed]
21. Xu, R.; Ji, Z.; Xu, C.; Zhu, J. The clinical value of using chloroquine or hydroxychloroquine as autophagy inhibitors in the treatment of cancers: A systematic review and meta-analysis. *Medicine (Baltimore)* **2018**, *97*, e12912. [CrossRef]
22. Brown, J.R.; Tesar, B.; Yu, L.; Werner, L.; Takebe, N.; Mikler, E.; Reynolds, H.M.; Thompson, C.; Fisher, D.C.; Neuberg, D.; et al. Obatoclox in combination with fludarabine and rituximab is well-tolerated and shows promising clinical activity in relapsed chronic lymphocytic leukemia. *Leuk. Lymphoma* **2015**, *56*, 3336–3342. [CrossRef]
23. Langer, C.J.; Albert, I.; Ross, H.J.; Kovacs, P.; Blakely, L.J.; Pajkos, G.; Somfay, A.; Zatloukal, P.; Kazarnowicz, A.; Moezi, M.M.; et al. Randomized phase II study of carboplatin and etoposide with or without obatoclox mesylate in extensive-stage small cell lung cancer. *Lung Cancer* **2014**, *85*, 420–428. [CrossRef]
24. Parikh, S.A.; Kantarjian, H.; Schimmer, A.; Walsh, W.; Asatiani, E.; El-Shami, K.; Winton, E.; Verstovsek, S. Phase II Study of Obatoclox Mesylate (GX15-070), a Small-Molecule BCL-2 Family Antagonist, for Patients With Myelofibrosis. *Clin. Lymphoma Myeloma Leuk.* **2010**, *10*, 285–289. [CrossRef]
25. Hu, D.X.; Withall, D.M.; Challis, G.L.; Thomson, R.J. Structure, Chemical Synthesis, and Biosynthesis of Prodigiosin Natural Products. *Chem. Rev.* **2016**, *116*, 7818–7853. [CrossRef] [PubMed]
26. Rapoport, H.; Holden, K.G. The Synthesis of Prodigiosin. *J. Am. Chem. Soc.* **1960**, *82*, 5510–5511. [CrossRef]
27. Sakai-Kawada, F.E.; Ip, C.G.; Hagiwara, K.A.; Awaya, J.D. Biosynthesis and Bioactivity of Prodigiosin Analogs in Marine Bacteria, *Pseudoalteromonas*: A Mini Review. *Front Microbiol.* **2019**, *10*, 1715. [CrossRef]
28. Danevčič, T.; Boric Vezjak, M.; Zorec, M.; Stopar, D. Prodigiosin—A Multifaceted *Escherichia coli* Antimicrobial Agent. *PLoS ONE* **2016**, *11*, e0162412. [CrossRef]

29. Castro, A.J. Antimalarial activity of prodigiosin. *Nature* **1967**, *213*, 903–904. [\[CrossRef\]](#)
30. Williamson, N.R.; Fineran, P.C.; Gristwood, T.; Chawrai, S.R.; Leeper, F.J.; Salmond, G.P. Anticancer and immunosuppressive properties of bacterial prodiginines. *Future Microbiol.* **2007**, *2*, 605–618. [\[CrossRef\]](#)
31. Perez-Tomas, R.; Vinas, M. New insights on the antitumoral properties of prodiginines. *Curr. Med. Chem.* **2010**, *17*, 2222–2231. [\[CrossRef\]](#) [\[PubMed\]](#)
32. Cheng, S.Y.; Chen, N.F.; Kuo, H.M.; Yang, S.N.; Sung, C.S.; Sung, P.J.; Wen, Z.H.; Chen, W.F. Prodigiosin stimulates endoplasmic reticulum stress and induces autophagic cell death in glioblastoma cells. *Apoptosis* **2018**, *23*, 314–328. [\[CrossRef\]](#) [\[PubMed\]](#)
33. Ji, S.; Sun, R.; Xu, K.; Man, Z.; Ji, J.; Pu, Y.; Yin, L.; Zhang, J.; Pu, Y. Prodigiosin induces apoptosis and inhibits autophagy via the extracellular signal-regulated kinase pathway in K562 cells. *Toxicol. In Vitro* **2019**, *60*, 107–115. [\[CrossRef\]](#)
34. Klein, A.S.; Domröse, A.; Bongen, P.; Brass, H.U.C.; Classen, T.; Loeschcke, A.; Drepper, T.; Laraia, L.; Sievers, S.; Jaeger, K.E.; et al. New Prodigiosin Derivatives Obtained by Mutasynthesis in *Pseudomonas putida*. *ACS Synth. Biol.* **2017**, *6*, 1757–1765. [\[CrossRef\]](#) [\[PubMed\]](#)
35. Wang, Z.; Li, B.; Zhou, L.; Yu, S.; Su, Z.; Song, J.; Sun, Q.; Sha, O.; Wang, X.; Jiang, W.; et al. Prodigiosin inhibits Wnt/beta-catenin signaling and exerts anticancer activity in breast cancer cells. *Proc. Natl. Acad. Sci. USA* **2016**, *113*, 13150–13155. [\[CrossRef\]](#) [\[PubMed\]](#)
36. Zhao, C.; Qiu, S.; He, J.; Peng, Y.; Xu, H.; Feng, Z.; Huang, H.; Du, Y.; Zhou, Y.; Nie, Y. Prodigiosin impairs autophagosome-lysosome fusion that sensitizes colorectal cancer cells to 5-fluorouracil-induced cell death. *Cancer Lett.* **2020**, *481*, 15–23. [\[CrossRef\]](#) [\[PubMed\]](#)
37. Domröse, A.; Klein, A.S.; Hage-Hülsmann, J.; Thies, S.; Svensson, V.; Classen, T.; Pietruszka, J.; Jaeger, K.E.; Drepper, T.; Loeschcke, A. Efficient recombinant production of prodigiosin in *Pseudomonas putida*. *Front Microbiol.* **2015**, *6*, 972. [\[CrossRef\]](#)
38. Skowron, M.A.; Petzsch, P.; Hardt, K.; Wagner, N.; Beier, M.; Stepanow, S.; Drechsler, M.; Rieder, H.; Köhrer, K.; Niegisch, G.; et al. Distinctive mutational spectrum and karyotype disruption in long-term cisplatin-treated urothelial carcinoma cell lines. *Sci. Rep.* **2019**, *9*, 14476. [\[CrossRef\]](#)
39. Chou, T.C. Drug combination studies and their synergy quantification using the Chou-Talalay method. *Cancer Res.* **2010**, *70*, 440–446. [\[CrossRef\]](#)
40. Vinod, V.; Padmakrishnan, C.J.; Vijayan, B.; Gopala, S. ‘How can I halt thee?’ The puzzles involved in autophagic inhibition. *Pharmacol. Res.* **2014**, *82*, 1–8. [\[CrossRef\]](#)
41. Roell, K.R.; Reif, D.M.; Motsinger-Reif, A.A. An Introduction to Terminology and Methodology of Chemical Synergy-Perspectives from Across Disciplines. *Front Pharmacol.* **2017**, *8*, 158. [\[CrossRef\]](#) [\[PubMed\]](#)
42. Chou, T.C. Theoretical basis, experimental design, and computerized simulation of synergism and antagonism in drug combination studies. *Pharmacol. Rev.* **2006**, *58*, 621–681. [\[CrossRef\]](#) [\[PubMed\]](#)
43. Chauhan, S.S.; Liang, X.J.; Su, A.W.; Pai-Panandiker, A.; Shen, D.W.; Hanover, J.A.; Gottesman, M.M. Reduced endocytosis and altered lysosome function in cisplatin-resistant cell lines. *Br. J. Cancer.* **2003**, *88*, 1327–1334. [\[CrossRef\]](#) [\[PubMed\]](#)
44. Turk, V.; Stoka, V.; Vasiljeva, O.; Renko, M.; Sun, T.; Turk, B.; Turk, D. Cysteine cathepsins: From structure, function and regulation to new frontiers. *Biochim. Biophys. Acta.* **2012**, *1824*, 68–88. [\[CrossRef\]](#)
45. Lkhider, M.; Castino, R.; Bouguyon, E.; Isidoro, C.; Ollivier-Bousquet, M. Cathepsin D released by lactating rat mammary epithelial cells is involved in prolactin cleavage under physiological conditions. *J. Cell. Sci.* **2004**, *117*, 5155–5164. [\[CrossRef\]](#)
46. Ojha, R.; Singh, S.K.; Bhattacharyya, S.; Dhanda, R.S.; Rakha, A.; Mandal, A.K.; Jha, V. Inhibition of grade dependent autophagy in urothelial carcinoma increases cell death under nutritional limiting condition and potentiates the cytotoxicity of chemotherapeutic agent. *J. Urol.* **2014**, *191*, 1889–1898. [\[CrossRef\]](#) [\[PubMed\]](#)
47. Lin, S.R.; Weng, C.F. PG-Priming Enhances Doxorubicin Influx to Trigger Necrotic and Autophagic Cell Death in Oral Squamous Cell Carcinoma. *J. Clin. Med.* **2018**, *7*, 375. [\[CrossRef\]](#) [\[PubMed\]](#)
48. Yan, X.Y.; Zhang, Y.; Zhang, J.J.; Zhang, L.C.; Liu, Y.N.; Wu, Y.; Xue, Y.N.; Lu, S.Y.; Su, J.; Sun, L.K. p62/SQSTM1 as an oncotarget mediates cisplatin resistance through activating RIP1-NF-kappaB pathway in human ovarian cancer cells. *Cancer Sci.* **2017**, *108*, 1405–1413. [\[CrossRef\]](#) [\[PubMed\]](#)
49. Norman, J.M.; Cohen, G.M.; Bampton, E.T. The in vitro cleavage of the hAtg proteins by cell death proteases. *Autophagy* **2010**, *6*, 1042–1056. [\[CrossRef\]](#) [\[PubMed\]](#)
50. Li, D.; Liu, J.; Wang, X.; Kong, D.; Du, W.; Li, H.; Hse, C.Y.; Shupe, T.; Zhou, D.; Zhao, K. Biological Potential and Mechanism of Prodigiosin from *Serratia marcescens* Subsp. *lawsoniana* in Human Choriocarcinoma and Prostate Cancer Cell Lines. *Int. J. Mol. Sci.* **2018**, *19*, 3465. [\[CrossRef\]](#) [\[PubMed\]](#)
51. Lin, P.B.; Shen, J.; Ou, P.Y.; Liu, L.Y.; Chen, Z.Y.; Chu, F.J.; Wang, J.; Jin, X.B. Prodigiosin isolated from *Serratia marcescens* in the *Periplaneta americana* gut and its apoptosis-inducing activity in HeLa cells. *Oncol. Rep.* **2019**, *41*, 3377–3385. [\[CrossRef\]](#)
52. Sam, M.R.; Ghoreishi, S. Prodigiosin produced by *Serratia marcescens* inhibits expression of MMP-9 and survivin and promotes caspase-3 activation with induction of apoptosis in acute lymphoblastic leukaemia cells. *J. Appl. Microbiol.* **2018**, *125*, 1017–1029. [\[CrossRef\]](#) [\[PubMed\]](#)
53. Yenkeje, R.A.; Sam, M.R.; Esmaeillou, M. Targeting survivin with prodigiosin isolated from cell wall of *Serratia marcescens* induces apoptosis in hepatocellular carcinoma cells. *Hum. Exp. Toxicol.* **2017**, *36*, 402–411. [\[CrossRef\]](#) [\[PubMed\]](#)
54. Gasiorkiewicz, B.M.; Koczurkiewicz-Adamczyk, P.; Piska, K.; Pekala, E. Autophagy modulating agents as chemosensitizers for cisplatin therapy in cancer. *Invest. New Drugs* **2020**. [\[CrossRef\]](#)

- 
55. Cheung, S.; Wu, D.; Daly, H.C.; Busschaert, N.; Morgunova, M.; Simpson, J.C.; Scholz, D.; Gale, P.A.; O'Shea, D.F. Real-Time Recording of the Cellular Effects of the Anion Transporter Prodigiosin. *Chem* **2018**, *4*, 879–895. [[CrossRef](#)]
  56. Guryanov, I.D.; Karamova, N.S.; Yusupova, D.V.; Gnezdilov, O.I.; Koshkarova, L.A. Bacterial pigment prodigiosin and its genotoxic effect. *Russ. J. Bioorganic Chem.* **2013**, *39*, 106–111. [[CrossRef](#)]
  57. Davient, B.; Ng, J.P.Z.; Xiao, Q.; Li, L.; Yang, L. Comparative Transcriptomics Unravels Prodigiosin's Potential Cancer-Specific Activity Between Human Small Airway Epithelial Cells and Lung Adenocarcinoma Cells. *Front. Oncol.* **2018**, *8*, 573. [[CrossRef](#)] [[PubMed](#)]
  58. Lipinski, C.A.; Lombardo, F.; Dominy, B.W.; Feeney, P.J. Experimental and computational approaches to estimate solubility and permeability in drug discovery and development settings. *Adv. Drug Deliv. Rev.* **1997**, *23*, 3–25. [[CrossRef](#)]
  59. Ravindran, A.; Anishetty, S.; Pennathur, G. Molecular dynamics of the membrane interaction and localisation of prodigiosin. *J. Mol. Graph. Model.* **2020**, *98*, 107614. [[CrossRef](#)] [[PubMed](#)]

## Publication 2





**Prodiginine ligating enzymes exhibit an extended substrate acceptance for A-ring-associated alkyl-substitutions**

Tim Moritz Weber, Alexandra Leyens, Lena Berning, Björn Stork, Jörg Pietruszka

*Catalysis Science & Technology*, Volume 13, 6165, September 2023

DOI: 10.1039/d3cy00913k

## PAPER

[View Article Online](#)  
[View Journal](#) | [View Issue](#)Cite this: *Catal. Sci. Technol.*, 2023,  
13, 6165New prodigiosin derivatives – chemoenzymatic  
synthesis and physiological evaluation against  
cisplatin-resistant cancer cells†Tim Moritz Weber, <sup>a</sup> Alexandra Leyens,<sup>b</sup> Lena Berning, <sup>c</sup>  
Björn Stork <sup>c</sup> and Jörg Pietruszka <sup>\*ab</sup>

Prodigiosin and its derivatives from the prodiginine family are a natural class of secondary metabolite alkaloids of bacterial origin. They are well known for multifarious biological activities against a broad range of bacteria, pathogenic fungi, parasites, and several cancer cell lines. Biosynthesis of natural derivatives is based on a converging route with a final ATP- and enzyme-dependent condensation reaction between the bipyrrole precursor MBC and miscellaneous substituted monopyrroles. Although these ligating enzymes have been recognised for promiscuity regarding monopyrroles, minor studies were exerted to investigate promiscuity for MBC derivatives. To overcome the current lack of structural knowledge, we synthesised six 5'-*n*-alkyl derivatives of MBC and validated their suitability for condensation with monopyrroles by the ligating enzymes PigC, TreaP, and TamQ to probe their active site experimentally. Moreover, chemically synthesised prodiginines with 5-*n*-alkylation on the A-ring were subjected to systematic cell viability screening with the urothelial cancer cell lines RT-112 (cisplatin-sensitive) and RT-112<sup>res</sup> (cisplatin-resistant) to fathom the effect of electron-donating substituents on cytotoxicity. Alongside an overall broad acceptance of short- and medium-chain alkylated MBC derivatives by the enzymes PigC, TreaP, and TamQ, we identified the A-ring substituted prodiginines with methyl substituents as superior anticancer agents against cisplatin-resistant RT-112<sup>res</sup> after 72 h (15.7–18.8 nM) compared to prodigiosin (41.1 nM) and the former phase II clinical candidate obatoclax mesylate (36.0 nM).

Received 3rd July 2023,  
Accepted 20th September 2023

DOI: 10.1039/d3cy00913k

[rsc.li/catalysis](https://rsc.li/catalysis)

## Introduction

Prodigiosin (**1**) is a deep red coloured natural pigment of bacterial origin and eponym for the generic family term of prodiginine alkaloids. During the last 70 years, the family of achiral and chiral prodiginines of natural and synthetic provenance has constantly grown and has been first under investigation for structural elucidation, but then more and more become of interest for the development of total synthesis strategies and for its manifold biological activities.<sup>1–11</sup> Common for all prodiginines is a congeneric conjugated scaffold of A-, B-, and C-ring pyrroles and

decorations on the ring systems. Prodigiosin (**1**) was once identified due to its striking colourful appearance,<sup>11</sup> but nowadays its derivatives and their cytotoxic properties have raised scientific and clinical attention.<sup>12,13</sup> The basic tripyrrolic core structure is able to bind divalent metal cations to induce oxidative stress. When binding Cu<sup>II</sup>, prodigiosin was shown to efficiently cause copper-promoted single- and double-strand breaks of DNA.<sup>14–17</sup> Moreover, protonated prodiginines are allowed to passively diffuse across biologic membranes, symporting the chloride counter ion. The co-transport implicates uncoupling and depletion of the proton gradient that is essential to acquire energy in the form of adenosine triphosphate (ATP) or, more generally, to maintain the proton motive force and associated biological processes.<sup>15,18–22</sup> Albeit prodigiosin and prodiginine alkaloids exhibit a broad range of activities against bacteria, protozoa, pathogenic fungi, plants, and nematodes,<sup>23–26</sup> prodiginines were well recognised for their activity against the malaria parasite *Plasmodium falciparum*.<sup>27–29</sup> Furthermore, prodiginines feature anti-tumour activity against several human cancer cell lines by induction of apoptosis, showing relatively low effects against non-malignant tissue.<sup>30–34</sup> The diversity of reported biophysical properties and biological

<sup>a</sup> Institute of Bioorganic Chemistry, Heinrich Heine University Düsseldorf, Wilhelm-Johnen-Straße, 52428 Jülich, Germany<sup>b</sup> Institute of Bio- and Geosciences (IBG-1): Bioorganic Chemistry, Jülich Research Centre, Wilhelm-Johnen-Straße, 52428 Jülich, Germany.E-mail: [j.pietruszka@fz-juelich.de](mailto:j.pietruszka@fz-juelich.de)<sup>c</sup> Institute of Molecular Medicine I, Medical Faculty and University Hospital Düsseldorf, Heinrich Heine University Düsseldorf, Universitätsstraße 1, 40225 Düsseldorf, Germany† Electronic supplementary information (ESI) available: Supporting spectra, chromatograms, dose response curves as well as synthesis are provided. See DOI: <https://doi.org/10.1039/d3cy00913k>

activities adumbrate the great challenge, which cells are facing after prodigiosin (**1**) treatment. Presumably, the relatively low doses being necessary to observe lethal biological activity are a consequence of blurring multidimensional modes of action.

### Biosynthesis and condensing enzymes

With an increasing number of natural prodiginines and related natural products, the quantity of known bacterial gene clusters involved in their biosynthesis has constantly risen. To date, numerous clusters among diverse bacterial species, such as *pig* (*Serratia marcescens*, prodigiosin **1**),<sup>35</sup> *red* (*Streptomyces coelicolor*, undecylprodigiosin and streptorubin B),<sup>36</sup> *trea* (*Pseudoalteromonas citrea*, tambjamine MYP1 **2**),<sup>37</sup> and *mar* (marine *Streptomyces* sp., marineosin A) have been identified by genome mining and analyses of mutant strains (Fig. 1, bottom).<sup>38–42</sup> Despite the structural diversity of prodiginine-related natural products, their biosynthesis resorts to clustered genes, encoding for non-ribosomal peptide synthetases (NRPS) of type II.<sup>36,43</sup> Using the synthesis of prodigiosin (**1**) as representative example, the assembly employs a convergent route with two key precursors, namely the bipyrrrole part (4-methoxy-2,2'-bipyrrrole-5-carbaldehyde, MBC **3a**) and the monopyrrole part (2-methyl-3-amylypyrrole, MAP **4a**), which are consolidated in an ATP-catalysed condensation reaction to give the conjugated tripyrrrole scaffold of prodigiosin (**1**) (Fig. 1, top).<sup>35,44–46</sup> For further in-depth elaboration on (bio)synthesis of MBC, MAP, the included enzymatic steps, and prodiginine-related natural products, consultation of the review from Hu *et al.* is recommended.<sup>47</sup>

The enzymes, being responsible for the C–C-bond forming condensation reaction of monopyrroles and MBC, belong to the class of ligases (EC 6.4). Here, the enzymes PigC, RedH, Treap, and MarH from afore mentioned gene clusters take on the role of ligases in the corresponding pathways. Unfortunately, crystallisation attempts of these enzymes did not lead to fruitful insights into structure-based mechanistic peculiarities. And yet, approximations of the structure were achieved by homology modelling and docking studies,<sup>48,49</sup> while mechanistic intricacies were elucidated by kinetic studies.<sup>50</sup>

### A-ring modifications of prodiginine-related natural products

The known natural prodiginine and connatural tambjamine derivatives featuring aliphatic substitutions on the A-ring are consistently belonging to the class of macrocycles, except the oddly protruding 2-(*p*-hydroxybenzyl)prodigiosin (**5**) from the marine bacterium *Pseudoalteromonas rubra* (Fig. 1, bottom).<sup>51</sup> The formation of macrocyclic prodiginines is explicitly owing to late stage oxidative carbocyclisation of long chain alkyl chains on the prodiginine C-ring, including a carbon-centred radical intermediate.<sup>52,53</sup> Because of this cyclisation, either formation of C- to A-ring (a) or C- to B-ring (b) bridging macrocycles is observed or formation of C-ring internal chiral

cycles (c) catalysed. Prominent examples for those enzymes are the RedG homologue MarG involved in marineosin biosynthesis (b) or the Rieske oxygenase RedG in the making of streptorubin B (c).<sup>53</sup>

For the C- to A-ring bridged carbomacrocycle cyclononylprodigiosin (**6**) the biosynthetic *non* gene cluster with the RedG-homologue NonG has been assigned (a).<sup>54</sup> However, the upstream condensation of bipyrrrole and monopyrrole exclusively relies on utilisation of MBC as bipyrrrole condensation partner, meaning that no naturally occurring A-ring substituted MBC derivatives have been found to date. In case of A-ring modified 2-(*p*-hydroxybenzyl)prodigiosin (**5**), no proposal on biosynthesis and related genes, based on experimental evidence, has been published.<sup>55</sup> Another well-known example of a prodigiosin-

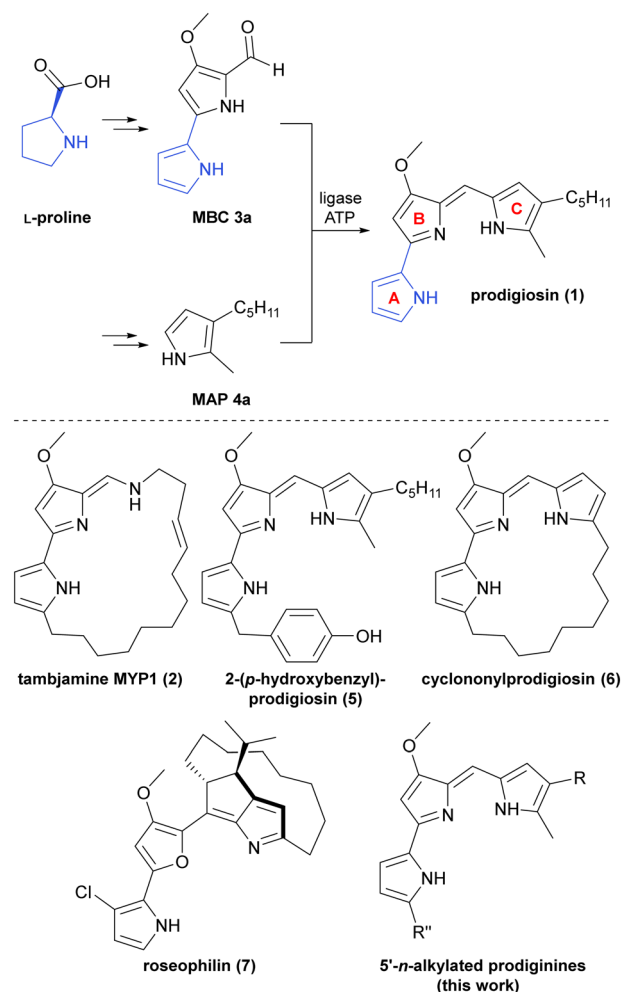


**Fig. 1** Top: Shortened biosynthesis of prodigiosin (**1**) by the related *pig* genes from *S. marcescens*. The final condensation step of MBC **3** and MAP **4a** is catalysed by a ligase (here PigC) in an ATP-consuming manner. The fate of atoms from the initial precursor L-proline in the intermediate MBC **3** and the natural product prodigiosin (**1**) is highlighted in blue. Rings (A-, B-, and C-) of the prodiginine scaffold are accentuated in red. Bottom: Examples from the class of prodiginine alkaloids and connatural natural products, illustrating the structural diversity.



related natural product is roseophilin (7) from *Streptomyces griseoviridis*, which shows 3-chlorination of the A-ring, substitution of the B-ring pyrrolyl moiety by furyl and a chiral macrocyclic C-ring.

Although the chlorination pattern implies utilisation of a chlorinated MBC analogue, comparable to the biosynthesis of pyoluteurin,<sup>56</sup> an adequate precursor and identification of the responsible halogenating enzyme is still missing. Late stage halogenation of dechlororoseophilin could be plausible, too. Indeed, the lack in discovery of substituted A-ring MBC derivatives from natural sources is not surprising, as the A-ring is built from the amino acid L-proline (cf. Fig. 1, top). Within the prodigiosin *pig* biosynthesis cluster of *S. marcescens* and undecylprodigiosin *red* gene cluster in *S. coelicolor*, the early steps of transformation include PigI/RedM-catalysed activation of proline as thioester and the subsequent oxidation of the pyrrolidine core by PigI/RedA to give acylated 1H-pyrrole.<sup>35,36,47</sup> In other words, a prerequisite for natural A-ring variation on MBC derivatives would be the acceptance of alternative canonic amino acids by PigI/RedA during the initial steps in biosynthesis or functionalisation of the A-ring pyrrole in successive steps. Nevertheless, no experimental proof has been furnished for existence of this kind of A-ring substituted MBC so far.

Shifting the focus from the bipyrrrole MBC 3a to the monopyrrole unit, promiscuity of condensing enzymes, exemplified by PigC from *S. marcescens*, is well-known for monopyrroles with cyclic and acyclic aliphatic side chains and the C-ring moiety of prodiginines.<sup>57–59</sup> Contemporaneously, little evidence was provided in the context of MBC derivatives being suitable substrates, yet. Haynes *et al.* attempted investigation of RedH-catalysed condensation of a dechlororoseophilin-inspired MBC analogue in combination with 2-undecylpyrrole, but did not observe any activity based on product formation. Since their study was conducted as feeding experiment with the mutant strain *S. coelicolor* W39, limited phase transfer across the bacterial membrane or lacking eligibility as RedH substrate were deduced as potential cause.<sup>60</sup> Chawrai *et al.* pioneered demonstration of accepted aryl substituted A-ring derivatives of MBC (e.g. thienyl-, furyl-, phenyl-) by PigC,<sup>46</sup> but since then, no studies were performed beyond that. Even though broad accessibility of A-ring substituted prodiginines by biosynthetic methods is not given from a today's perspective, those derivatives can be assessed by means of total synthesis. Melvin *et al.* attributed a negative effect on copper-promoted DNA cleavage, when the A-ring was either substituted with electron-withdrawing substituents in 5-position or replaced by aryl residues other than pyrrolyl.<sup>15</sup> Similar effects were observed by D'Alessio *et al.* with focus on cytotoxicity in extensive structure–activity-relationship studies (SAR).<sup>61</sup> At the same time, both studies denoted positive effects by adding electron-donating alkyl substitutions in 5-position of the A-ring,<sup>15,61</sup> providing substantial evidence of value to further analyse the consequences of A-ring associated alkylations. In the present study, we aim at expanding the

knowledge about acceptance of A-ring *n*-alkylated MBC derivatives by prodiginine ligases to probe the active site of investigated enzymes experimentally and systematically infer the effects on prodiginine cytotoxicity against cisplatin-sensitive and -resistant urothelial carcinoma cell lines.

## Results and discussion

### Synthesis of prodiginine precursors

Prodiginine ligases exploit the bipyrrrole MBC 3a and derivatives of 1H-monopyrroles as substrates for their ATP-catalysed reaction mechanism.<sup>62,63</sup> Thus, the chemical synthesis of monopyrroles was approached using the Trofimov procedure, which allows conversion of oximes to 2,3-dialkylated 1H-pyrroles.<sup>57,64</sup> Starting from commercially available ketones, namely octan-2-one (8a), hexan-2-one (8b), and decan-2-one (8c), the respective oximes 9a–c were synthesised in yields of ≥98% by refluxing the ketones with hydroxylamine hydrochloride and sodium acetate in EtOH/H<sub>2</sub>O (4:1) (Fig. 2). As conversions were near quantitative, no further purification was needed and the *E/Z* mixtures could be used straightaway for the subsequent Trofimov reaction. The latter allows cyclisation of alkylated oximes in the presence of 1,2-dichloroethane under superbasic reaction conditions that can be obtained by mixing DMSO, ground potassium hydroxide and a small amount of H<sub>2</sub>O.<sup>64</sup> The electron-rich pyrroles are highly sensitive towards oxygen and light. Consequently, in addition to inert reaction conditions we identified utilisation of thoroughly degassed and dried DMSO as key requirement for a reliable outcome of the reaction. Only with degassed solvent, the application of reaction temperatures of 90–100 °C over a prolonged period led to a minimal amount of polymerisation during the reaction and yielded 52–54% of pyrroles 4a–c (Fig. 2).

Apparently, the use of such synthetic schemes that enable both, use of the products as substrates for chemical synthesis of reference compounds and as potential substrates for ligating enzymes are inevitable for our approach. Based on the biomimetic two-step sequence devised by Dairi *et al.* for gaining access to the natural prodigiosin and tambjamine precursor 4-methoxy-2,2'-bipyrrrole-5-carboxaldehyde (3a, MBC),<sup>65</sup> we identified an adapted route to make 5'-*n*-alkylated

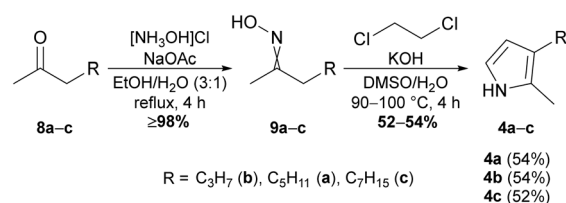


Fig. 2 Synthesis scheme of 2,3-dialkylated 1H-pyrroles 4a–c from ketones 8a–c and intermediate oximes 9a–c via Trofimov pyrrole synthesis.



derivatives of MBC accessible. Although other positions for MBC alkylation might be of interest as well, we focused on the 5'-position for this fundamental study. The devised synthetic route is predicated on the haloformylation of 4-methoxy-3-pyrrolin-2-one to give bromide **10**, followed by a palladium-catalysed Suzuki-Miyaura cross-coupling of bromide **10** with 5-*n*-alkylated pyrrole-2-boronic acids. The fundament for the desired boronic acids were 2-alkylated *N*-Boc-protected 1*H*-pyrroles, which were afforded by a consecutive Friedel-Crafts acylation of 1*H*-pyrrole with acyl chlorides **11c-g** under usage of aluminium trichloride as Lewis acid.<sup>66</sup> Reduction of the 2-acylation products **12c-g** with sodium borohydride in *i*PrOH and final *N*-protection of the 2-alkyl-pyrroles **13b-g** with Boc-anhydride yielded the target compounds **14b-g** (Fig. 3).<sup>1</sup> In this reaction sequence, we were able to reduce the purification effort due to usage of crude reaction products and exclusive purification of the Boc-protected products (**14b-g**) by ordinary flash column chromatography. By this means, the *N*-Boc-2-alkylated pyrroles were synthesised in yields of 43–59%.

Since boronic acids are more reactive than their related boronic acid pinacol or MIDA esters,<sup>68</sup> we aimed for the synthesis of free pyrrole-2-boronic acids from *N*-Boc-2-alkylated pyrroles for the cross-coupling reaction with bromide **10**. Admittedly, 2-substituted boronic acids of *N*-heterocycles, such as pyrroles or pyridines, are delicate and significantly lacking storage stability.<sup>69</sup> Thus, utilisation of crude boronic acids from pyrrole borylation reactions was considered more reliable rather than isolation of pure boronic acids. Indeed, the crude products of the borylation sequence, which comprises deprotonation of pyrroles **14b-g** with lithium tetramethylpiperidide, borylation with trimethyl borate and lastly deprotection of the methyl ester with aqueous hydrochloric acid were ideal starting materials. Catalysed by palladium acetate, SPhos-assisted Suzuki-Miyaura cross-coupling in degassed *n*-butanol/H<sub>2</sub>O (4:1) and with potassium phosphate as base allowed C-C coupling between pyrrole-2-boronic acids **15b-g** and bromide **10** under mild reaction conditions (Fig. 4). The reactions typically gave mixtures of Boc-protected and deprotected carbaldehydes. Full deprotection of crude reaction was rendered by refluxing in 2,2,2-trifluoroethanol to provide the desired products after filtration. Resulting from this sequence, the 5'-*n*-alkylated MBC derivatives **3b-g** were prepared in 52–80% yield (Fig. 4). Unsubstituted MBC **3a** was synthesised according to the published literature procedure.<sup>65</sup>

### Synthesis of prodiginines

Although the alkylated MBC derivatives were primarily synthesised for systematic characterisation of the prodigiosin ligases substrate scope, they were also eligible for chemical prodiginine synthesis. Therefore, carbaldehydes **3a-g** and pyrroles **4a-c** were subjected to a condensation reaction under acid catalysis with hydrochloric acid to yield the

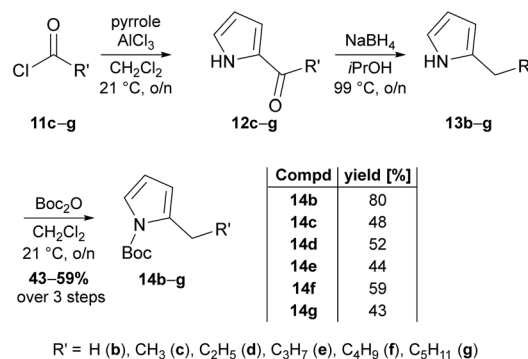


Fig. 3 Synthesis scheme of 2-*n*-alkylated *N*-Boc-pyrroles **14b-g**. 2-Methyl-1*H*-pyrrole (**13b**) was purchased from commercial suppliers. Intermediates were not purified and the yield over three steps determined after final purification of Boc-protected 2-alkylated pyrroles. For further information regarding systematic nomenclature, please see ref. 67.

corresponding prodiginines **16ba-bc** in yields of 47–82% (Fig. 4). The hydrochlorides of prodigiosin (**1**) and novel prodiginines **16ba-bc** generated thereby could be used as synthetic references for enzymatic condensation reactions, prodiginine quantification, toxicity screening, and were accessible in purities of up to 99.9%.

### Absorption spectra and molar extinction coefficients

Prodiginines are well known to display solvent-dependent absorption properties, which greatly vary with pH.<sup>70</sup> To ensure that the molecule of interest is uniformly protonated, extinction coefficients and absorption spectra are typically recorded in acidified ethanol in which the purple pigment prodigiosin exhibits an absorption maximum at 535 nm.<sup>70,71</sup> By adding a 5-*n*-alkyl substitution on the A-ring, the absorption maximum was increased to 545–547 nm, noticeable in a visible small shift from pink to purple in solution. With pentyl-substitution on the C-ring, variation in A-ring substitution greatly enhanced the molar extinction coefficient with increasing chain length, based on the inductive electron-donating effect of the attached alkyl substituents (Fig. S2A, Table S2, ESI†). For prodigiosin (**1**) a molar extinction coefficient of 139 800 M<sup>-1</sup> cm<sup>-1</sup> (535 nm) was reported in the literature.<sup>71</sup> The A-ring methyl-derivative (**16ba**), however, already presented an extinction coefficient of 163 233 M<sup>-1</sup> cm<sup>-1</sup> (546 nm), followed by the ethyl- and propyl-derivative with 177 092 M<sup>-1</sup> cm<sup>-1</sup> (**16ca**, 546 nm) and 181 692 M<sup>-1</sup> cm<sup>-1</sup> (**16da**, 546 nm), respectively. From butyl- to hexyl-substitutions **16ea-ga**, no further increase of significance was observed and the molar extinction coefficients seemed to reach a plateau around 190 000 M<sup>-1</sup> cm<sup>-1</sup> at 547 nm (Fig. S2A, ESI†). Interestingly, molar extinction coefficients at 535 nm ranged from 126 508 M<sup>-1</sup> cm<sup>-1</sup> to 138 200 M<sup>-1</sup> cm<sup>-1</sup>, showing less chain length-dependent behaviour and solely fluctuations in the magnitude of standard deviations (Fig. S2B, ESI†). With



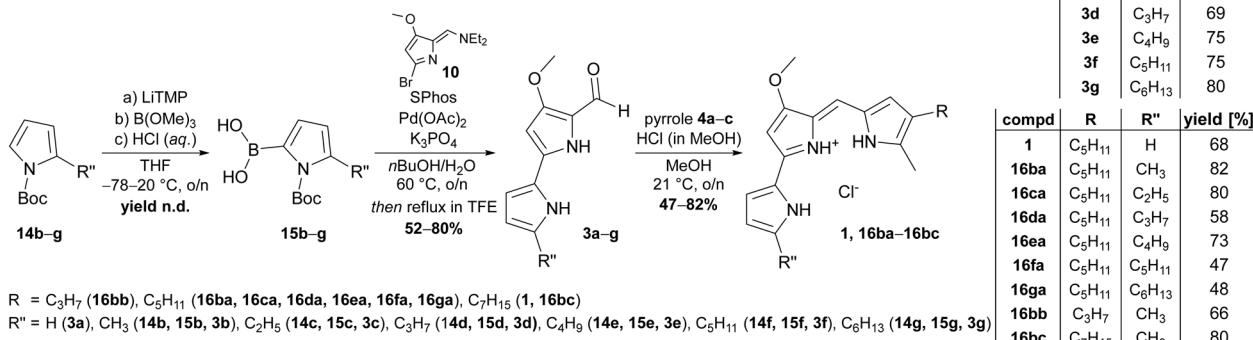


**Fig. 4** Synthesis scheme of *n*-alkylated A-ring derivatives of MBC (**3b–g**) and prodigiosin (**16ba–bc**) from *N*-Boc-pyrrole-2-boronic acid precursors (**15b–g**). Substituted prodiginines **16** were numbered in a modular fashion (**16R''R**), including the substitution pattern of the MBC derivative (**3a–g**, R'') and the monopyrrole (**4a–c**, R). For example, prodiginine **16ba** was synthesised from MBC **3b** and pyrrole **4a**, prodiginine **16bb** was synthesised from MBC **3b** and pyrrole **4b**. Abbreviations: n.d. – not determined; compd – compound; LiTMP – lithium 2,2,6,6-tetramethylpiperidide; SPhos – 2-dicyclohexylphosphino-2',6'-dimethoxybiphenyl; TFE – 2,2,2-trifluoroethanol.

constant methyl-substitution on the A-ring and variation in C-ring chain length, a linear correlation was observable at 535 nm for prodiginines **16ba**, **16bb**, and **16bc** allowing approximation of molar extinction coefficients (Table S3, ESI†) based on the experimental coefficients and the slope of linear regression (Fig. S2C, ESI†). In this way, we were able to quantify even prodiginines whose references had not been synthesised by chemical means.

### Prodigiosin ligase substrate scope for A-ring substituted MBC

Chawrai *et al.* showed that prodigiosin derivatives with alternative aromatic A-rings are accepted by the ligase PigC from *S. marcescens*. Enzymatic activity was still present when the A-ring pyrrole moiety was either substituted by 2-phenyl-, 2-thienyl-, 2-furyl-, or 2-indolyl-residues. No activity was seen for naphthyl- and biphenyl-substitution instead.<sup>46</sup> Their findings prompted us to investigate alkyl-substituted pyrrole derivatives more thoroughly, as they were not characterised as suited substrates for PigC and, moreover, with TreaP and TamQ two new ligating enzymes from *Pseudoalteromonadaceae* were found since then.<sup>59</sup>

In our experiment, we tested the three ligases PigC, TreaP, and TamQ for their substrate acceptance of A-ring substituted alkyl-derivatives **3b–g** of MBC and MBC **3a** itself and quantified the extracted prodiginines in LC-MS measurements with the corresponding extinction coefficients, which had been determined experimentally or by approximation (*vide supra*). As we used *Escherichia coli* cell lysate after expression of the corresponding genes rather than purified enzymes, *E. coli* harbouring the pET28a(+) empty vector was used as control. Unusual for this experimental setup in comparison to earlier studies on prodiginine ligases was the two-dimensional testing, varying MBC derivatives and monopyrroles at the same time (Fig. 5). We would like to emphasise that quantification was normalised to the amount

of cells and not to the amount of enzyme being used in the experiment. Thus, differences in expression efficiencies for the analysed ligases might have an impact on absolute prodiginine titres but should not affect the relative acceptance of A-ring substituted MBC derivatives for each enzyme (Fig. 6A). Firstly, we validated whether prodiginines are readily formed in a catalyst-free environment, containing pyrroles, MBC, ATP, and buffer. It was found that no background reaction takes place (control reactions 1–6, ESI† Fig. S111–S116) and that the ligating enzymes are needed for catalysis of the condensation reaction. Secondly, we performed reactions with enzyme containing cell lysates and ATP in buffer but without pyrroles and MBC to exclude formation of prodiginines from cell metabolites within the lysate. Again, no prodiginines were traced by coupled LC-MS measurements, proving that all four components (ligating enzyme, MBC, pyrrole, and ATP) are needed for their formation (negative controls, ESI† Fig. S107–S110).

During the first experiments, the most prominent enzyme PigC showed high acceptance of methyl- and unsubstituted MBC (**3b** and **3a**) in combination with the short-chain monopyrrole **4b**, whereat the natural precursor MBC **3a** turned out to be the favoured bipyrrole, yielding 25.9 mg L<sup>−1</sup> versus 16.7 mg L<sup>−1</sup> of prodiginine extracts for methyl-MBC **3b**. Other MBC derivatives were not converted to the related prodiginines in noteworthy amounts. In contrast, TamQ, which is naturally involved in tambjamine biosynthesis, apparently converted all derivatives including butyl-MBC **3e**, but not pentyl- and hexyl-MBC **3f** and **3g**. Here, the obtained product titres of prodiginines derived from short-chain MBC derivatives **3a**, **3b**, and **3c** were rather similar in a range from 10–12 mg L<sup>−1</sup>. The acceptance of MBC derivatives for TreaP was limited to C0–C3-substituted MBC **3a–d** and resulted in considerably lower titres (<3.6 mg L<sup>−1</sup>) than PigC or TamQ. However, TreaP showed highest relative product concentrations for the ethyl-substituted MBC **3c**. With



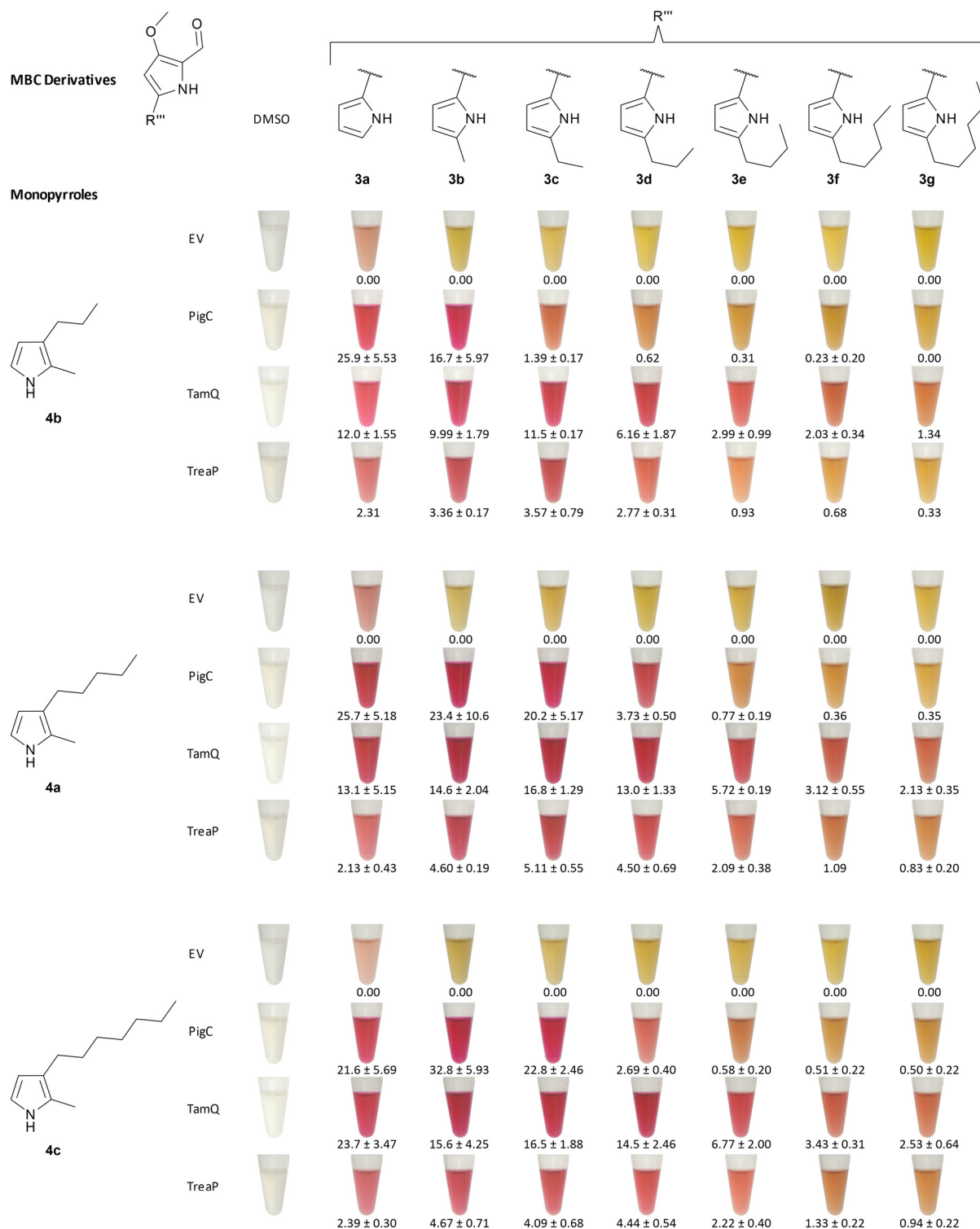


**Fig. 5** Substrate spectrum of the prodiginine ligases PigC, TamQ, and TreaP for combinations of monopyrroles **4a–c**, MBC **3a** and 5-*n*-alkylated MBC derivatives **3b–g**. Cell lysates of *E. coli* BL21 with corresponding ligases in KP<sub>i</sub> buffer were treated with pyrroles (1 mM), MBC (1 mM), and ATP (1.25 mM) and incubated at 30 °C for 4 h. Cell lysate of *E. coli* BL21 pET28a(+) was used as negative control. A red colouration of the solutions indicates the formation of products. Photographic record was employed to document the organic extracts in acidic ethanol. Product titres (mg L<sup>-1</sup>) were determined by LC-MS measurements and are given below the corresponding tubes. Abbreviations: EV – empty vector.

increasing chain length of the monopyrrole all enzymes appeared to possess greater substrate promiscuity and conversions. For both, the medium- and long-chain

monopyrroles **4a** and **4c**, the MBC substrate spectrum for PigC from *S. marcescens* was expanded to propyl-MBC **3d** but also to higher prodiginine titres. Again, unsubstituted MBC



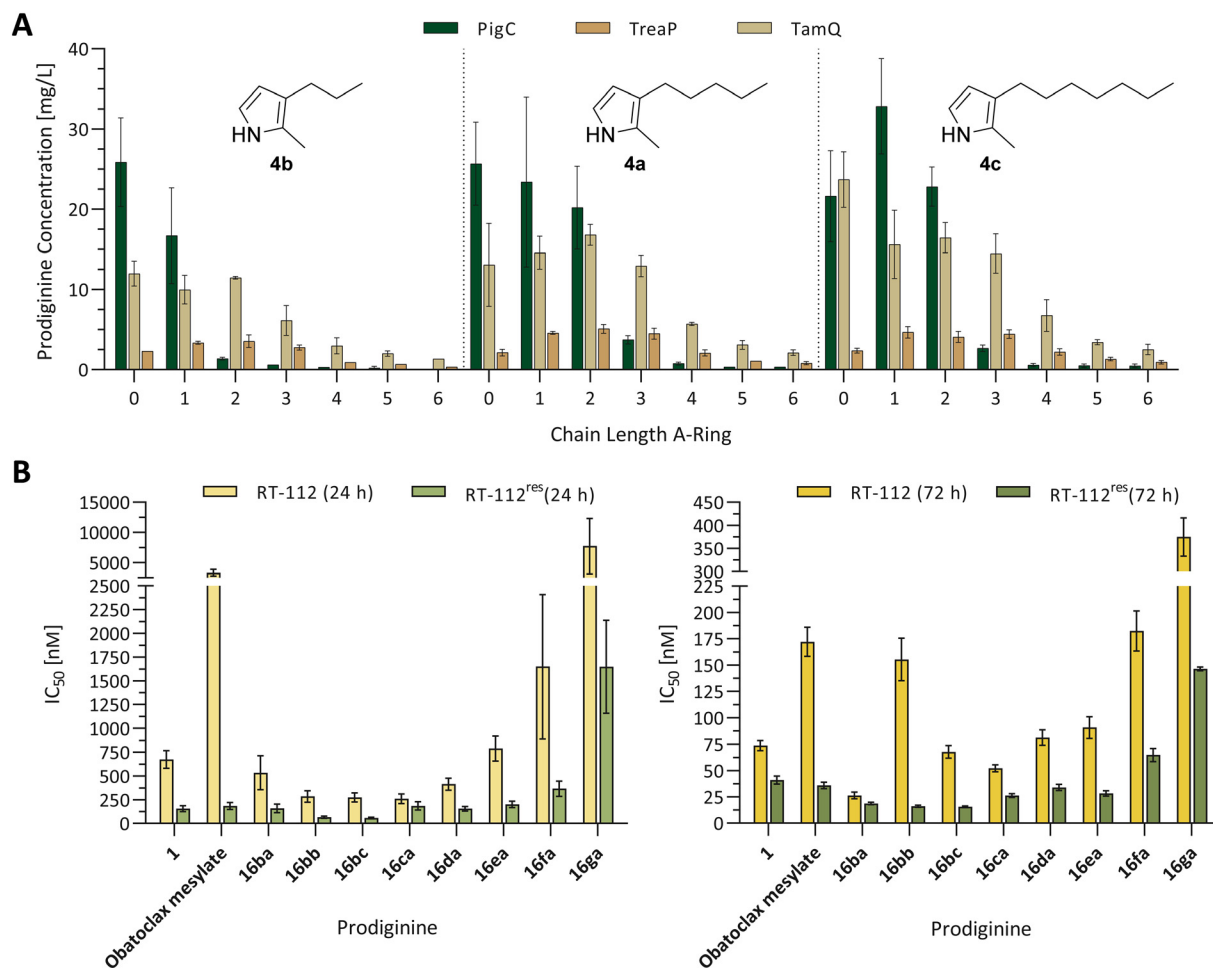


**Fig. 6** (A) Quantification of prodiginines from *in vitro* reactions with the prodiginine ligases PigC, TamQ, and TreaP with varying chain lengths on the A- and C-ring. Methanolic extracts of biocatalytic reactions between monopyrroles **4a–c** and 5-alkyl MBC derivatives **3a–g** were subjected to coupled LC-MS measurements and the amount of substance quantified from the corresponding UV absorption at 535 nm and the prodiginine extinction coefficients. The chain length of alkylated MBC is depicted on the x-axis of the bar diagram, the used monopyrrole is shown in the diagram. Since all values for the empty vector control were zero, the data is not shown, but plotted raw data can be found in the supporting information (Fig. S3†). Each experiment was performed in triplicates and the standard error is given. (B) Cell viability of urothelial cancer cell lines RT-112 (cisplatin sensitive) and RT-112<sup>res</sup> (cisplatin resistant) in the presence of prodiginosin (**1**), obatoclax mesylate, and chemically synthesised prodiginines (**16ba–ga**) after 24 h (left) and 72 h (right). For improved reading and resolution of data sets, the scales of ordinates for the 24 h and 72 h diagrams were adjusted. Experiments were performed in triplicates and cell survival was analysed using the MTT assay. Error bars are representing the 95% confidence interval. Plotted raw data and dose–response fits for determination of IC<sub>50</sub> values can be found in the supporting information (plots and fits: Fig. S117–S119, fitted IC<sub>50</sub> values: Table S4†).

**3a** was apparently converted best, but only for the medium-chain monopyrrole **4a** at 25.7 mg L<sup>−1</sup>. With the long-chain monopyrrole **4c**, the non-natural methyl-MBC derivative **3b** was identified as ideal partner for condensation, providing the related product in a titre of 32.8 mg L<sup>−1</sup>. Supported by previous findings regarding the enzymes TamQ and TreaP,<sup>59</sup> either preferentially converted long-chain monopyrroles to the corresponding prodiginines, at which TamQ in total exhibited the broadest acceptance of 5-alkyl-substituted MBC derivatives. Even though MBC **3a** is the common prodiginine and tambjamine precursor in nature for all three enzymes under investigation, TreaP and TamQ shared a similar trend of MBC derivative promiscuity for the medium-chain monopyrrole **4a**, showing highest product titres for ethyl-

MBC **3c** with 5.1 mg L<sup>−1</sup> and 16.8 mg L<sup>−1</sup>, respectively. The long-chain monopyrrole **4c** was best accepted in combination with methyl-MBC **3b** by PigC, providing the highest prodiginine product titre of 32.8 mg L<sup>−1</sup> in our experiment.

From the contingent of tested enzymes, PigC was in fact the least versatile enzyme, demonstrated by tight restraints in terms of tolerating alkyl-substitution on the MBC part. In contrast, TamQ was identified as most profitable catalyst for substitutions on the monopyrrole and the A-ring of MBC. It is hypothesised that multiple reasons contribute to the observed acceptance pattern of combinations for monopyrroles and MBC. As the monopyrrole serves as nucleophile in the proposed mechanism (devised for PigC), reviewed by Hu *et al.*,<sup>47</sup> it is believed that shorter chain



length may result in a higher degree of freedoms and flexibility of side chains, less tight binding of the pyrrole core within the enzyme pocket, potentially leading to decreased or depleted reaction rates. In addition, short chain pyrroles are lacking additional activation, which is contributed by the electron-donating effect of alkyl-chains. Significance of the latter can be seen from the drastic effect of increasing chain-length on prodiginine extinction coefficients. For the alkyl-chain variation on MBC derivatives, we assume steric reasons as principal force behind the lack of conversion with increased number of methylene groups within the alkyl chain. Electronic contributions are judged rather implausible, as the condensation chemistry between monopyrrole and MBC is taking place at the distal part of the MBC derivatives, namely the carbaldehyde.

### Evaluation of cytotoxicity for A-ring substituted prodiginines

To assess the impact of 5-*n*-alkyl substitutions on cytotoxic properties of chemically synthesised prodiginines, the urothelial carcinoma cell lines RT-112 (cisplatin sensitive) and RT-112<sup>res</sup> (cisplatin resistant) were selected for evaluation.<sup>72–74</sup> Cisplatin-based therapy is the standard of care for this kind of carcinomas, however, miscellaneous mechanisms are involved in emerging resistance against cisplatin, such as autophagy and apoptosis.<sup>72,75–78</sup> Prodigiosin (**1**) has been shown to display cytotoxic activity at nanomolar concentrations against both, cisplatin sensitive and resistant cell lines, and was thus judged as potential drug candidate for treatment of cisplatin resistant urothelial carcinomas.<sup>30</sup> Thus, prodigiosin (**1**) and the former phase II clinical candidate obatoclox mesylate were selected as benchmark compounds.<sup>12,13,79,80</sup> In order to assort the impact of A-ring associated alkyl substitutions on prodiginine derivatives, the two RT-112 cell lines were subjected to cell viability monitoring after 24 h and 72 h, using the MTT [3-(4,5-dimethylthiazol-2-yl)-2,5-diphenyltetrazolium bromide] assay (Fig. 6B, data and dose–response fits in the supporting information). For the lead compound prodigiosin (**1**), inhibitory concentrations (IC<sub>50</sub>) of 675 nM and 157 nM were traced after 24 h and were further reduced to 73.8 nM and 41.1 nM after 72 h for RT-112 and RT-112<sup>res</sup>, respectively. In contrast, obatoclox mesylate exhibited relatively low cytotoxic activity in RT-112 cells after 24 h of incubation. With 3327 nM against RT-112 and 184 nM against RT-112<sup>res</sup> after 24 h, obatoclox was acting similarly to the least cytotoxic long-chain derivatives **16ca–ga**. With increased incubation time of 72 h, improved cytotoxicity of 172 nM (RT-112) and 36.0 nM (RT-112<sup>res</sup>) were achieved, judging obatoclox significantly less effective against RT-112 than prodigiosin (**1**) and of similar value against RT-112<sup>res</sup>.

In the following, prodiginines with altered A-ring alkyl substitution, but constant C-ring substitution of prodigiosin (**1**) that originated from chemical synthesis were investigated for their cytotoxic effects. Simple addition of an electron donating methyl-group in prodiginine **16ba** resulted in a

strong increase of cytotoxicity against both cell lines. With a final IC<sub>50</sub> of 26.4 nM for RT-112 and 18.8 nM for RT-112<sup>res</sup> after 72 h, an up to 2.8-fold increase in cytotoxicity was observed. However, IC<sub>50</sub> values after 24 h initially resembled the cytotoxicity of prodigiosin (**1**) itself. Interestingly, further chain elongation on the A-ring of prodiginines **16ca–ga** led to constant loss of biological activity with each step of elongation. Especially the transition from pentyl to hexyl substitution on the A-ring displayed a turning point in cytotoxicity and was accompanied by a significant loss of biological activity, independent from the cell line and time point of analysis. Aside from the effect of A-ring substitution with invariable C-ring substitution pattern of compounds **16ba–ga**, we chose the most cytotoxic methyl-substituted prodiginine **16ba** as starting point and scrutinised which effect a substitution in 4-position of the C-ring chain toward longer or shorter alkyl residues might have. All analysed prodiginines (**16ba**, **16bb**, and **16bc**) with methyl substitution on the A-ring appeared to have unspoiled high cytotoxicity against the cisplatin resistant subtype RT-112<sup>res</sup> after 72 h when the C-ring was modulated. With IC<sub>50</sub> values ranging between 15.7 nM (**16bc**) and 18.8 nM (**16ba**), the impact was rather negligible. Nonetheless, the tested derivatives were shown to act differently after 24 h, as prodiginine **16ba** with C5-chain on the C-ring revealed slightly higher inhibitory concentrations against both cell lines than observed for derivatives **16bb** and **16bc**. Summarising the presented data from Fig. 6B, an additional methyl group in 5-position of the A-ring boosted the cytotoxicity against both, cisplatin sensitive and resistant urothelial carcinoma cell lines. In addition to this increased performance, we found prodiginine **16ba** to display the highest cytotoxicity against both cell lines after 72 h (RT-112: 26.4 nM, RT-112<sup>res</sup>: 18.8 nM). Concurrently, prodiginines **16bb** and **16bc** were outstandingly fast in unleashing their cytotoxic potential, having substantial improvements of toxicity after 24 h in comparison to derivative **16ba**, the mother compound prodigiosin (**1**) and the former phase II clinical candidate obatoclox mesylate. The tripyrrole core structure of prodigiosin (**1**) and its substituted clinical relative obatoclox is well known to inhibit the cellular process of autophagy,<sup>30,57,81,82</sup> which is essential to recycle or degrade cell organelles or anomalous proteins (misfolded, aggregated, or damaged).<sup>30</sup> At the same time, prodigiosin (**1**) was shown to induce apoptosis, an ensemble of signalling pathways of programmed cell death.<sup>33,34,83</sup> In the past, the mechanistic cause for autophagy inhibition and induction of apoptosis in prodigiosin-treated cancer cell lines was accounted to the capability of H<sup>+</sup>/Cl<sup>−</sup> symport across the membranes of lysosomes or other eukaryotic cell compartments and the cell cycle arrest.<sup>18,20,21,84</sup>

The ion pair of protonated prodigiosin and the chloride counter ion is lipophilic and tight enough to penetrate the membrane and diffuse across the permeability barrier.<sup>11</sup> A possible explanation for the increased cytotoxicity of prodiginines with short-chain electron-donating alkyl substituents on the A-ring could be a tighter bond between



the B-ring nitrogen atom and the proton from the hydrochloride complex, increasing the  $pK_a$  value and facilitating the trespass of the charged complex through the membrane. A further increase of the A-ring chain length could potentially result in a more lipophilic character for the resulting prodiginine, raising the risk of functioning as membrane anchor and attaching derivatives to the membrane rather than diffusing across, thereby reducing the cytotoxic potential. In fact, our results regarding A-ring substitution are in agreement with earlier studies on alkyl substitution on the C-ring, where short-chain propyl substitution was characterised by drastically stronger autophagy inhibition than for the long-chain octyl variant.<sup>57</sup>

## Conclusions

Prodiginine ligating enzymes are known to exhibit substrate promiscuity on C-ring monopyrroles and MBC derivatives with aromatic A-ring substitution. However, reliable structural information for these enzymes in free or substrate-bound state are still lacking. Whilst enzyme structures remain unclear, probing of the active site and testing of suitable substrate combinations is limited to means of trial and error. We were able to transfer the previously gained knowledge of enzyme promiscuity in a systematic screening on 5'-*n*-alkylated MBC derivatives, showing broad substrate acceptance for both key precursors of the convergent biosynthesis route. While PigC only accepted short-chained MBC derivatives, TamQ and TreaP displayed fewer restraints, also for longer alkyl chains. During cell viability screening of A-ring substituted prodiginines in cisplatin-sensitive and -resistant urothelial carcinoma cell lines, methyl-substituted derivatives **16ba**, **16bb**, and **16bc** were cytotoxic at low nanomolar concentrations, and thereby up to 2.6-times more potent than prodigiosin (**1**) or obatoclax mesylate against the cisplatin-resistant cell line RT-112<sup>res</sup> after 72 h. Consequently, these derivatives are suggested as potential lead compounds for future structural optimisation in terms of cytotoxicity, drug administration and drug metabolism and could be potential candidates for treatment of cisplatin resistant carcinomas.

## Experimental

### Synthetic procedures

**General considerations.** All reactions were carried out under nitrogen or argon in pre-dried glassware using Schlenk technique. Organic solvents were acquired in technical grade and distilled prior to use. Dried solvents ( $\text{CH}_2\text{Cl}_2$ , THF) were obtained from a MB-SPS 800 drying apparatus (M. Braun Inertgas-Systeme GmbH) and by storage over activated molecular sieve for >72 h (iPrOH, DMSO). If stated in the synthetic instructions, solvents were degassed using the freeze-pump-thaw procedure (3×). 2,2,6,6-Tetramethylpiperidine was refluxed for 4 h over  $\text{CaH}_2$  and then distilled under normal pressure and stored over 4 Å

molecular sieve. For flash chromatography Macherey-Nagel silica gel 60 M (40–63  $\mu\text{m}$ ) was employed. Synthesised compounds were stored at  $-20^\circ\text{C}$  under argon. Further specifications and information on instrumentation can be found in the supporting information. Obatoclax mesylate ( $\geq 98\%$ , HPLC) was purchased from Sigma Aldrich (Merck).

**General procedure for the synthesis of MBC derivatives 3b–g.** A Schlenk flask with magnetic stirring bar is sequentially charged with  $\text{Pd}(\text{OAc})_2$  (5.0 mol%), SPhos (6.0 mol%), bromide **10** (1.00 eq.), Boc-protected pyrrole boronic acid **15b–g** (3.00 eq.) and evacuated/ $\text{N}_2$ -refilled three times. Degassed *n*-butanol is added and the mixture stirred at  $20^\circ\text{C}$  until homogeneous. A 1.45 M solution of  $\text{K}_3\text{PO}_4$  (2.00 eq.) in degassed water is added to give an *n*-butanol/water ratio of 4:1. The reaction vessel is lowered into a pre-heated  $60^\circ\text{C}$  bath and the orange solution is stirred under argon overnight. The solvent is evaporated, 50 mL of water are added to the slurry and the mixture is then extracted with EtOAc (3 × 50 mL). Combined organic phases are washed with brine (2 × 25 mL), dried over  $\text{MgSO}_4$ , filtered over degassed cotton wool and the solvent is removed. The resulting solid is recovered by filtration and washed with cold distilled *n*-pentane. The green solid is refluxed for 6 h at  $90^\circ\text{C}$  in 45 eq. 2,2,2-trifluoroethanol. Evaporation of the solvent and trituration of the remaining solid in *n*-pentane provides the product as green solid that is recovered by filtration and washed with distilled *n*-pentane and  $\text{Et}_2\text{O}$ .

**4-Methoxy-5'-methyl-1*H*,1'*H*-[2,2'-bipyrrole]-5-carbaldehyde (3b).** Following the general procedure for the synthesis of MBC derivatives, bromide **10** (800 mg, 3.09 mmol, 1.00 eq.), boronic acid **15b** (2.60 g, 9.26 mmol, 3.00 eq.), SPhos (76.0 mg, 0.19 mmol, 6 mol%),  $\text{Pd}(\text{OAc})_2$  (34.7 mg, 0.15 mmol, 5 mol%), and  $\text{K}_3\text{PO}_4$  (1.31 g, 6.17 mmol, 2.00 eq.) are converted to 379 mg (1.86 mmol, 60%) of 4-methoxy-5'-methyl-1*H*,1'*H*-[2,2'-bipyrrole]-5-carbaldehyde (**3b**) after 15 h reaction time. The product is obtained as green powder.  $\delta^1\text{H}$  (600 MHz, DMSO) 2.22 (3 H, s, 6'-H), 3.82 (3 H, s, 10-H), 5.77–5.84 (1 H, m, 4'-H), 6.16–6.23 (1 H, m, 3-H), 6.58–6.66 (1 H, m, 3'-H), 9.26 (1 H, s, 7-H), 11.00 (1 H, s, 1'-NH), 11.27 (1 H, s, 1-NH).  $\delta^{13}\text{C}$  (151 MHz, DMSO) 12.7 (C-6'), 57.7 (C-10), 90.3 (C-3), 107.6 (C-4'), 108.8 (C-3'), 117.2 (C-5), 122.0 (C-2'), 130.1 (C-5'), 133.5 (C-2), 158.8 (C-4), 171.1 (C-6). FT-IR (neat,  $\text{cm}^{-1}$ ): 3254, 3205, 3127, 3071, 2954, 2837, 1585, 1546, 1514, 1426, 1357, 1333, 1296, 1280, 1254, 1203, 1177, 1164, 1033, 1018, 1000, 991, 972, 833, 790, 770, 697, 653, 624, 589, 482.  $T_m$ : 250–275  $^\circ\text{C}$  (decomposition) (*n*-pentane). HRMS-ESI ( $m/z$ ):  $[\text{M} + \text{H}]^+$  calculated for  $\text{C}_{11}\text{H}_{13}\text{N}_2\text{O}_2$  205.0973, found 205.0973.  $t_R$  (LC-MS method): 7.54 min.

**5'-Ethyl-4-methoxy-1*H*,1'*H*-[2,2'-bipyrrole]-5-carbaldehyde (3c).** Following the general procedure for the synthesis of MBC derivatives, bromide **10** (850 mg, 3.28 mmol, 1.00 eq.), boronic acid **15c** (2.35 g, 9.84 mmol, 3.00 eq.), SPhos (80.8 mg, 0.20 mmol, 6 mol%),  $\text{Pd}(\text{OAc})_2$  (36.8 mg, 0.16 mmol, 5 mol%), and  $\text{K}_3\text{PO}_4$  (1.39 g, 6.56 mmol, 2.00 eq.) are converted to 375 mg (1.72 mmol, 52%) of 5'-ethyl-4-methoxy-1*H*,1'*H*-[2,2'-bipyrrole]-5-carbaldehyde (**3c**) after 14 h reaction time. The product is obtained as green powder.



$\delta^1\text{H}$  (300 MHz, DMSO) 1.19 (3 H, q, 7'-H), 2.53–2.65 (2 H, m, 6'-H), 3.67–3.92 (3 H, m, 10-H), 5.66–5.97 (1 H, m, 4'-H), 6.08–6.35 (1 H, m, 3-H), 6.49–6.78 (1 H, m, 3'-H), 9.26 (1 H, d, 7-H), 10.95 (1 H, s, 1'-NH), 11.27 (1 H, s, 1-NH).  $\delta^{13}\text{C}$  (76 MHz, DMSO) 13.7 (C-7'), 20.4 (C-6'), 57.7 (C-10), 90.4 (C-3), 106.2 (C-4'), 108.7 (C-3'), 117.2 (C-5), 122.0 (C-2'), 133.6 (C-2), 136.6 (C-5'), 158.8 (C-4), 171.1 (C-6). FT-IR (neat,  $\text{cm}^{-1}$ ): 3250, 3197, 2972, 2833, 1593, 1553, 1513, 1445, 1422, 1357, 1302, 1284, 1248, 1199, 1175, 1161, 1147, 1039, 1014, 990, 832, 766, 740, 698, 588, 484.  $T_m$ : 243.7–245.5 °C (*n*-pentane). HRMS-ESI ( $m/z$ ):  $[\text{M} + \text{H}]^+$  calculated for  $\text{C}_{12}\text{H}_{15}\text{N}_2\text{O}_2$  219.1128, found 219.1132.  $t_R$  (LC-MS method): 7.93 min.

**4-Methoxy-5'-propyl-1*H*,1'*H*-[2,2'-bipyrrole]-5-carbaldehyde (3d).** Following the general procedure for the synthesis of MBC derivatives, bromide **10** (800 mg, 3.09 mmol, 1.00 eq.), boronic acid **15d** (2.34 g, 9.26 mmol, 3.00 eq.), SPhos (76.0 mg, 0.19 mmol, 6 mol%),  $\text{Pd}(\text{OAc})_2$  (34.7 mg, 0.15 mmol, 5 mol%), and  $\text{K}_3\text{PO}_4$  (1.31 g, 6.17 mmol, 2.00 eq.) are converted to 497 mg (2.14 mmol, 69%) of 4-methoxy-5'-propyl-1*H*,1'*H*-[2,2'-bipyrrole]-5-carbaldehyde (**3d**) after 17 h reaction time. The product is obtained as green powder.  $\delta^1\text{H}$  (600 MHz, DMSO) 0.91 (3 H, t,  $J = 7.3$  Hz, 8'-H), 1.60 (2 H, h,  $J = 7.4$  Hz, 7'-H), 2.53 (2 H, t,  $J = 7.5$  Hz, 6'-H), 3.83 (3 H, s, 10-H), 5.81–5.86 (1 H, m, 4'-H), 6.22 (1 H, s, 3-H), 6.57–6.65 (1 H, m, 3'-H), 9.26 (1 H, s, 7-H), 10.94 (1 H, s, 1'-NH), 11.27 (1 H, s, 1-NH).  $\delta^{13}\text{C}$  (151 MHz, DMSO) 13.6 (C-8'), 22.4 (C-7'), 29.2 (C-6'), 57.7 (C-10), 90.4 (C-3), 106.8 (C-4'), 108.6 (C-3'), 117.1 (C-5), 121.9 (C-2'), 133.5 (C-2), 135.0 (C-5'), 158.7 (C-4), 171.1 (C-6). FT-IR (neat,  $\text{cm}^{-1}$ ): 3253, 3201, 3135, 3071, 3008, 2956, 2929, 2870, 2381, 1593, 1553, 1516, 1462, 1447, 1421, 1356, 1343, 1302, 1248, 1224, 1199, 1176, 1161, 1041, 1016, 986, 831, 769, 692, 664, 624, 587, 484, 453.  $T_m$ : 224.7–226.8 °C (*n*-pentane). HRMS-ESI ( $m/z$ ):  $[\text{M} + \text{H}]^+$  calculated for  $\text{C}_{13}\text{H}_{17}\text{N}_2\text{O}_2$  233.1285, found 233.1286.  $t_R$  (LC-MS method): 8.23 min.

**5'-Butyl-4-methoxy-1*H*,1'*H*-[2,2'-bipyrrole]-5-carbaldehyde (3e).** Following the general procedure for the synthesis of MBC derivatives, bromide **10** (700 mg, 2.70 mmol, 1.00 eq.), boronic acid **15e** (2.17 g, 8.10 mmol, 3.00 eq.), SPhos (66.5 mg, 0.16 mmol, 6 mol%),  $\text{Pd}(\text{OAc})_2$  (30.3 mg, 0.14 mmol, 5 mol%), and  $\text{K}_3\text{PO}_4$  (1.15 g, 5.40 mmol, 2.00 eq.) are converted to 499 mg (2.03 mmol, 75%) of 5'-butyl-4-methoxy-1*H*,1'*H*-[2,2'-bipyrrole]-5-carbaldehyde (**3e**) after 17 h reaction time. The product is obtained as green powder.  $\delta^1\text{H}$  (300 MHz, DMSO) 0.90 (3 H, t,  $J = 7.3$  Hz, 9'-H), 1.25–1.40 (2 H, m, 8'-H), 1.57 (2 H, p,  $J = 7.6$  Hz, 7'-H), 2.55 (2 H, t,  $J = 8.1$  Hz, 6'-H), 3.83 (3 H, s, 10-H), 5.80–5.86 (1 H, m, 4'-H), 6.22 (1 H, t, 3-H), 6.57–6.65 (1 H, m, 3'-H), 9.26 (1 H, s, 7-H), 10.93 (1 H, s, 1'-NH), 11.26 (1 H, s, 1-NH).  $\delta^{13}\text{C}$  (76 MHz, DMSO) 13.7 (C-9'), 21.8 (C-8'), 26.9 (C-6'), 31.3 (C-7'), 57.7 (C-10), 90.4 (C-3), 106.8 (C-4'), 108.7 (C-3'), 117.1 (C-5), 121.9 (C-2'), 133.5 (C-2), 135.2 (C-5'), 158.8 (C-4), 171.1 (C-6). FT-IR (neat,  $\text{cm}^{-1}$ ): 3257, 3208, 3002, 2952, 2928, 2856, 2835, 1596, 1553, 1516, 1427, 1361, 1342, 1303, 1243, 1198, 1163, 1038, 1024, 985, 834, 782, 741, 724, 691, 667, 587, 488.  $T_m$ : 203.5–205.6 °C (*n*-pentane). HRMS-ESI ( $m/z$ ):  $[\text{M} + \text{H}]^+$  calculated for  $\text{C}_{14}\text{H}_{19}\text{N}_2\text{O}_2$  247.1441, found 247.1446.  $t_R$  (LC-MS method): 8.56 min.

**4-Methoxy-5'-pentyl-1*H*,1'*H*-[2,2'-bipyrrole]-5-carbaldehyde (3f).** Following the general procedure for the synthesis of MBC derivatives, bromide **10** (800 mg, 3.09 mmol, 1.00 eq.), boronic acid **15f** (2.60 g, 9.26 mmol, 3.00 eq.), SPhos (76.0 mg, 0.19 mmol, 6 mol%),  $\text{Pd}(\text{OAc})_2$  (34.7 mg, 0.15 mmol, 5 mol%), and  $\text{K}_3\text{PO}_4$  (1.31 g, 6.17 mmol, 2.00 eq.) are converted to 605 mg (2.33 mmol, 75%) of 4-methoxy-5'-pentyl-1*H*,1'*H*-[2,2'-bipyrrole]-5-carbaldehyde (**3f**) after 15 h reaction time. The product is obtained as green powder.  $\delta^1\text{H}$  (600 MHz, DMSO) 0.87 (3 H, t,  $J = 6.9$  Hz, 10'-H), 1.30 (4 H, tt,  $J = 7.3$  Hz, 8'-H, 9'-H), 1.58 (2 H, p,  $J = 7.5$  Hz, 7'-H), 2.54 (2 H, t,  $J = 7.7$  Hz, 6'-H), 3.82 (3 H, s, 10-H), 5.78–5.88 (1 H, m, 4'-H), 6.14–6.27 (1 H, m, 3), 6.56–6.68 (1 H, m, 3'-H), 9.25 (1 H, s, 7-H), 10.93 (1 H, s, 1'-NH), 11.26 (1 H, s, 1-NH).  $\delta^{13}\text{C}$  (151 MHz, DMSO) 14.4 (C-10'), 22.4 (C-9'), 27.6 (C-6'), 29.3 (C-7'), 31.4 (C-8'), 58.2 (C-10), 90.9 (C-3), 107.3 (C-4'), 109.2 (C-3'), 117.7 (C-5), 122.4 (C-2'), 134.0 (C-2), 135.7 (C-5'), 159.3 (C-4), 171.6 (C-6). FT-IR (neat,  $\text{cm}^{-1}$ ): 3255, 3204, 3105, 3071, 2953, 2929, 2839, 1599, 1554, 1518, 1428, 1361, 1340, 1304, 1287, 1255, 1231, 1202, 1163, 1034, 1023, 987, 833, 781, 742, 724, 692, 667, 588, 490, 454.  $T_m$ : 196.2–199.5 °C (*n*-pentane). HRMS-ESI ( $m/z$ ):  $[\text{M} + \text{H}]^+$  calculated for  $\text{C}_{15}\text{H}_{21}\text{N}_2\text{O}_2$  261.1598, found 261.1601.  $t_R$  (LC-MS method): 8.78 min.

**5'-Hexyl-4-methoxy-1*H*,1'*H*-[2,2'-bipyrrole]-5-carbaldehyde (3g).** Following the general procedure for the synthesis of MBC derivatives, bromide **10** (800 mg, 3.09 mmol, 1.00 eq.), boronic acid **15g** (2.73 g, 9.26 mmol, 3.00 eq.), SPhos (76.0 mg, 0.19 mmol, 6 mol%),  $\text{Pd}(\text{OAc})_2$  (34.7 mg, 0.15 mmol, 5 mol%), and  $\text{K}_3\text{PO}_4$  (1.31 g, 6.17 mmol, 2.00 eq.) are converted to 678 mg (2.47 mmol, 80%) of 5'-hexyl-4-methoxy-1*H*,1'*H*-[2,2'-bipyrrole]-5-carbaldehyde (**3g**) after 14 h reaction time. The product is obtained as green powder.  $\delta^1\text{H}$  (600 MHz, DMSO) 0.85 (3 H, t, 11'-H), 1.23–1.34 (6 H, m, 8'-H, 9'-H, 10'-H), 1.58 (2 H, p,  $J = 7.4$  Hz, 7'-H), 2.54 (2 H, t,  $J = 7.7$  Hz, 6'-H), 3.83 (3 H, s, 10-H), 5.78–5.87 (1 H, m, 4'-H), 6.19–6.23 (1 H, m, 3-H), 6.57–6.65 (1 H, m, 3'-H), 9.26 (1 H, s, 7-H), 10.93 (1 H, s, 1'-NH), 11.26 (1 H, s, 1-NH).  $\delta^{13}\text{C}$  (151 MHz, DMSO) 13.9 (C-11'), 22.0 (C-10'), 27.2 (C-6'), 28.3 (C-8'), 29.1 (C-7'), 31.0 (C-9'), 57.7 (C-10), 90.4 (C-3), 106.8 (C-4'), 108.7 (C-3'), 117.1 (C-5), 121.9 (C-2'), 133.5 (C-2), 135.2 (C-5'), 158.7 (C-4), 171.1 (C-6). FT-IR (neat,  $\text{cm}^{-1}$ ): 3223, 3117, 2954, 2924, 2855, 1664, 1464, 1458, 1377, 1368, 1258, 1217, 1168, 1113, 994, 956, 943, 830, 823, 724, 651, 614.  $T_m$ : 171.8–174.6 °C (*n*-pentane). HRMS-ESI ( $m/z$ ):  $[\text{M} + \text{H}]^+$  calculated for  $\text{C}_{16}\text{H}_{23}\text{N}_2\text{O}_2$  275.1754, found 275.1758.  $t_R$  (LC-MS method): 9.01 min.

**General procedure for the synthesis of 1*H*-pyrroles 4a–c.** Reactions were performed according to an earlier published procedure with modifications.<sup>57</sup> In detail, a mixture of oxime **9a–c** (1.00 eq.), pestled KOH (5.00 eq.), and water (13.7  $\mu\text{L}$   $\text{mmol}^{-1}$  oxime) is added to a three-necked flask under  $\text{N}_2$  atmosphere. Degassed and dried DMSO (1.92 mL  $\text{mmol}^{-1}$  oxime) is added under nitrogen atmosphere. The reaction is refluxed at 100 °C and a solution of 1,2-dichloroethane (3.50 eq.) in degassed DMSO (0.21 mL  $\text{mmol}^{-1}$  oxime) is added with a syringe pump over 2 h. A second batch KOH (5.00 eq.)



is added under ice cooling after the first hour of 1,2-dichloroethane addition (dichloroethane-feeding is paused during KOH addition) before the dichloroethane addition is continued for further 1 h. Once the addition of dichloroethane is completed, the reaction is refluxed for 2 h. The reaction is cooled to 0 °C and ice water is added for quenching. Extraction is performed with Et<sub>2</sub>O (3 × 100 mL). Combined organic phases are dried over MgSO<sub>4</sub>, filtered over degreased cotton wool and the solvent removed *in vacuo*. Chromatographic purification with petroleum ether/CH<sub>2</sub>Cl<sub>2</sub> + 1% (v/v) triethylamine on silica provides the product as yellow to orange oil.

**2-Methyl-3-pentyl-1H-pyrrole (4a).** Octan-2-one oxime (9a, 12.0 g, 83.8 mmol, 1.00 eq.), 1,2-dichloroethane (23.2 mL, 293 mmol, 3.50 eq.), and KOH (47.0 g, 838 mmol, 10.0 eq.) are converted to 6.89 g (45.6 mmol, 54%) 2-methyl-3-pentyl-1H-pyrrole (4a). The product is obtained as yellow volatile oil after purification with petroleum ether/CH<sub>2</sub>Cl<sub>2</sub> (90:10) + 1% triethylamine.  $\delta^1\text{H}$  (600 MHz, CDCl<sub>3</sub>) 0.90 (3 H, t, *J* = 6.7 Hz, 5"-H), 1.28–1.38 (4 H, m, 3"-H, 4"-H), 1.54 (2 H, p, *J* = 7.4 Hz, 2"-H), 2.19 (3 H, s, 1'-H), 2.39 (2 H, t, *J* = 7.7 Hz, 1"-H), 6.02 (1 H, t, *J* = 2.8 Hz, 4-H), 6.60 (1 H, t, *J* = 2.7 Hz, 5-H), 7.70 (1 H, brs, 1-NH).  $\delta^{13}\text{C}$  (151 MHz, CDCl<sub>3</sub>) 11.2 (C-1'), 14.3 (C-5"), 22.8 (C-4"), 26.0 (C-1"), 31.2 (C-2"), 31.9 (C-3"), 109.0 (C-4), 114.9 (C-5), 119.9 (C-3), 123.3 (C-2). FT-IR (neat, cm<sup>-1</sup>): 3376, 2956, 2923, 2854, 1464, 1444, 1378, 1246, 1107, 1064, 954, 901, 831, 771, 670, 551. HRMS-ESI (*m/z*): [M + H]<sup>+</sup> calculated for C<sub>10</sub>H<sub>18</sub>N 152.1434, found 152.1434. *t<sub>R</sub>* (LC-MS method): 8.52 min.

**2-Methyl-3-propyl-1H-pyrrole (4b).** Following the general procedure for the synthesis of 1H-pyrroles, hexan-2-one oxime (9b, 12.0 g, 104 mmol, 1.00 eq.), 1,2-dichloroethane (28.8 mL, 365 mmol, 3.50 eq.), and KOH (58.5 g, 1.04 mol, 10.0 eq.) are converted to 6.99 g (56.7 mmol, 54%) 2-methyl-3-propyl-1H-pyrrole (4b). The product is obtained as yellow volatile oil after purification with petroleum ether/CH<sub>2</sub>Cl<sub>2</sub> (85:15) + 1% triethylamine.  $\delta^1\text{H}$  (600 MHz, CDCl<sub>3</sub>) 0.95 (3 H, t, *J* = 7.3 Hz, 3"-H), 1.56 (2 H, h, *J* = 7.5 Hz, 2"-H), 2.19 (3 H, s, 1'-H), 2.37 (2 H, t, *J* = 7.6 Hz, 1"-H), 6.02 (1 H, t, *J* = 2.7 Hz, 4-H), 6.60 (1 H, t, *J* = 2.7 Hz, 5-H), 7.70 (1 H, brs, 1-NH).  $\delta^{13}\text{C}$  (151 MHz, CDCl<sub>3</sub>) 11.2 (C-1'), 14.2 (C-3"), 24.6 (C-2"), 28.2 (C-1"), 109.0 (C-4), 114.9 (C-5), 119.7 (C-3), 123.4 (C-2). FT-IR (neat, cm<sup>-1</sup>): 3378, 2956, 2925, 2869, 1464, 1455, 1376, 1249, 1106, 1066, 955, 904, 889, 832, 801, 712, 663, 549. HRMS-ESI (*m/z*): [M + H]<sup>+</sup> calculated for C<sub>8</sub>H<sub>14</sub>N 124.1121, found 124.1120. *t<sub>R</sub>* (LC-MS method): 7.90 min.

**3-Heptyl-2-methyl-1H-pyrrole (4c).** Decan-2-one oxime (9c, 7.50 g, 43.8 mmol, 1.00 eq.), 1,2-dichloroethane (12.1 mL, 153 mmol, 3.50 eq.), and KOH (24.6 g, 438 mmol, 10.0 eq.) are converted to 4.11 g (22.9 mmol, 52%) 3-heptyl-2-methyl-1H-pyrrole (4c). The product is obtained as yellow volatile oil after purification with petroleum ether/CH<sub>2</sub>Cl<sub>2</sub> (85:15) + 1% triethylamine.  $\delta^1\text{H}$  (600 MHz, CDCl<sub>3</sub>) 0.89 (3 H, t, 7"-H), 1.23–1.38 (8 H, m, 3"-H, 4"-H, 5"-H, 6"-H), 1.48–1.58 (2 H, m, 2"-H), 2.19 (3 H, s, 1'-H), 2.39 (2 H, t, 1"-H), 6.02 (1 H, t, *J* = 2.8 Hz, 4-H), 6.60 (1 H, t, *J* = 2.7 Hz, 5-H), 7.71 (1 H, brs, 1-NH).

$\delta^{13}\text{C}$  (151 MHz, CDCl<sub>3</sub>) 11.2 (C-1'), 14.3 (C-7"), 22.8 (C-6"), 26.1 (C-1"), 29.4 (C-3"), 29.7 (C-4"), 31.5 (C-2"), 32.1 (C-5"), 109.0 (C-4), 114.9 (C-5), 119.9 (C-3), 123.3 (C-2). FT-IR (neat, cm<sup>-1</sup>): 3485, 3377, 2955, 2923, 2871, 1583, 1463, 1445, 1377, 1272, 1247, 1144, 1108, 1064, 953, 901, 831, 711, 668, 646, 634, 548, 485, 468. HRMS-ESI (*m/z*): [M + H]<sup>+</sup> calculated for C<sub>12</sub>H<sub>22</sub>N 180.1747, found 180.1749. *t<sub>R</sub>* (LC-MS method): 9.01 min.

#### General procedure for the synthesis of (E/Z)-oximes 9a–c.

The synthesis of oximes was performed following a published procedure of Mo *et al.*<sup>85</sup> To a 500 mL round bottom flask charged with a stir bar, sodium acetate (2.00 eq.) and hydroxylamine hydrochloride (1.50 eq.) are added a solution of the ketone (1.00 eq., 0.30 M) in EtOH/water (4:1). The reaction mixture is then heated for 4 h to reflux. The mixture is cooled to room temperature and excess of EtOH is removed under reduced pressure. Water (100 mL) is added to the crude mixture and the resulting aqueous solution is extracted with EtOAc (3 × 150 mL). The combined organic layer is washed with saturated NaHCO<sub>3</sub> (2 × 100 mL) and water (2 × 100 mL), dried over MgSO<sub>4</sub>, filtered over degreased cotton wool, and concentrated *in vacuo*. The oxime products are obtained in quantitative yields as volatile oils and used without further purification.

**(E/Z)-Octan-2-one oxime (9a).** Following the general procedure for the synthesis of oximes, octan-2-one (8a, 12.0 g, 93.6 mmol, 1.00 eq.), hydroxylamine hydrochloride (9.76 g, 140 mmol, 1.50 eq.), and sodium acetate (15.36 g, 187.2 mmol, 2.00 eq.) are converted to 13.35 g (93.21 mmol, >99%) (E/Z)-octan-2-one oxime (9a) as colourless oil. *E/Z* ratio: 76:24 (NMR).  $\delta^1\text{H}$  (600 MHz, CDCl<sub>3</sub>, *E*-isomer) 0.872 (3 H, t, 8-H), 1.22–1.36 (6 H, m, 5-H, 6-H, 7-H), 1.45–1.53 (2 H, m, 4-H), 1.87 (3 H, s, 1-H), 2.12–2.24 (2 H, m, 3-H), 8.58 (1 H, brs, 10'-H).  $\delta^{13}\text{C}$  (151 MHz, CDCl<sub>3</sub>, *E*-isomer) 13.5 (C-1), 14.2 (C-8), 22.7 (C-7), 26.4 (C-4), 29.0 (C-5), 31.70 (C-6), 35.9 (C-3), 158.9 (C-2).  $\delta^1\text{H}$  (600 MHz, CDCl<sub>3</sub>, *Z*-isomer) 0.879 (3 H, t, 8'-H), 1.22–1.36 (6 H, m, 5'-H, 6'-H, 7'-H), 1.45–1.53 (2 H, m, 4'-H), 1.86 (3 H, s, 1'-H), 2.32–2.41 (2 H, m, 3'-H), 8.58 (1 H, brs, 10'-H).  $\delta^{13}\text{C}$  (151 MHz, CDCl<sub>3</sub>, *Z*-isomer) 14.2 (C-8'), 19.9 (C-1'), 22.7 (C-7), 25.6 (C-4'), 28.8 (C-3'), 29.5 (C-5'), 31.73 (C-6'), 159.3 (C-2'). FT-IR (neat, cm<sup>-1</sup>): 3224, 3120, 2955, 2926, 2858, 1664, 1466, 1458, 1376, 1369, 1261, 1247, 1179, 1111, 1031, 954, 943, 828, 796, 742, 726, 651, 613. HRMS-ESI (*m/z*): [M + H]<sup>+</sup> calculated for C<sub>8</sub>H<sub>18</sub>NO 144.1383, found 144.1383.

**(E/Z)-Hexan-2-one oxime (9b).** Following the general procedure for the synthesis of oximes, hexan-2-one (8b, 15.0 g, 150 mmol, 1.00 eq.), hydroxylamine hydrochloride (15.7 g, 226 mmol, 1.50 eq.), and sodium acetate (24.6 g, 300 mmol, 2.00 eq.) are converted to 16.9 g (147 mmol, 98%) (E/Z)-hexan-2-one oxime (9b) as pale yellow oil. *E/Z* ratio: 73:27 (NMR).  $\delta^1\text{H}$  (600 MHz, CDCl<sub>3</sub>, *E*-isomer) 0.90 (3 H, t, *J* = 7.4 Hz, 6-H), 1.32 (2 H, h, *J* = 7.3 Hz, 5-H), 1.44–1.52 (2 H, m, 4-H), 1.87 (3 H, s, 1-H), 2.15–2.23 (2 H, m, 3-H), 9.09 (1 H, brs, 8-H).  $\delta^{13}\text{C}$  (151 MHz, CDCl<sub>3</sub>, *E*-isomer) 13.5 (C-1), 13.9 (C-6), 22.4 (C-5), 28.5 (C-4), 35.6 (C-3), 158.8 (C-2).  $\delta^1\text{H}$  (600 MHz, CDCl<sub>3</sub>, *Z*-isomer) 0.92 (3 H, t, *J* = 7.30 Hz, 6'-H), 1.36 (2



H, h,  $J = 7.4$  Hz, 5'-H), 1.44–1.52 (2 H, m, 4'-H), 1.85 (3 H, s, 1'-H), 2.34–2.40 (2 H, m, 3'-H), 9.09 (1 H, brs, 8'-H).  $\delta^{13}\text{C}$  (151 MHz,  $\text{CDCl}_3$ , Z-isomer) 14.0 (C-6'), 20.0 (C-1'), 23.0 (C-5'), 27.8 (C-4'), 28.5 (C-3'), 159.2 (C-2'). FT-IR (neat,  $\text{cm}^{-1}$ ): 3222, 3118, 2957, 2928, 2873, 2862, 1664, 1467, 1433, 1368, 1331, 1262, 1207, 1105, 1010, 951, 919, 878, 823, 742, 648, 613. HRMS-ESI ( $m/z$ ):  $[\text{M} + \text{H}]^+$  calculated for  $\text{C}_6\text{H}_{14}\text{NO}$  116.1070, found 116.1071.

**(E/Z)-Decan-2-one oxime (9c).** Following the general procedure for the synthesis of oximes, decan-2-one (**8c**, 7.50 g, 48.0 mmol, 1.00 eq.), hydroxylamine hydrochloride (5.00 g, 72.0 mmol, 1.50 eq.), and sodium acetate (7.88 g, 96.1 mmol, 2.00 eq.) are converted to 8.22 g (48.0 mmol, >99%) (E/Z)-decan-2-one oxime (**9c**) as colourless oil. E/Z ratio: 76:24 (NMR).  $\delta^1\text{H}$  (600 MHz,  $\text{CDCl}_3$ , E-isomer) 0.871 (3 H, t, 10-H), 1.19–1.35 (10 H, m, 5-H, 6-H, 7-H, 8-H, 9-H), 1.49 (2 H, p, 4-H), 1.88 (3 H, s, 1-H), 2.14–2.20 (2 H, m, 3-H), 8.14 (1 H, brs, 12-H).  $\delta^{13}\text{C}$  (151 MHz,  $\text{CDCl}_3$ , E-isomer) 159.0 (C-2), 35.9 (C-3), 32.0 (C-8), 29.5 (C-6), 29.33 (C-5), 29.32 (C-7), 26.4 (C-4), 22.8 (C-9), 14.2 (C-10), 13.5 (C-1).  $\delta^1\text{H}$  (600 MHz,  $\text{CDCl}_3$ , Z-isomer) 0.874 (3 H, t, 10'-H), 1.19–1.35 (10 H, m, 5'-H, 6'-H, 7'-H, 8'-H, 9'-H), 1.49 (2 H, p, 4'-H), 1.86 (3 H, s, 1'-H), 2.33–2.38 (2 H, m, 3'-H), 8.14 (1 H, brs, 12'-H).  $\delta^{13}\text{C}$  (151 MHz,  $\text{CDCl}_3$ , Z-isomer) 159.4 (C-2'), 32.0 (C-8'), 29.9 (C-6'), 29.5 (C-5'), 29.32 (C-7'), 28.7 (C-3'), 25.6 (C-4'), 22.8 (C-9'), 19.9 (C-1'), 14.2 (C-10'). FT-IR (neat,  $\text{cm}^{-1}$ ): 3223, 3117, 2954, 2924, 2855, 1664, 1464, 1458, 1377, 1368, 1258, 1217, 1168, 1113, 994, 956, 943, 830, 823, 724, 651, 614. HRMS-ESI ( $m/z$ ):  $[\text{M} + \text{H}]^+$  calculated for  $\text{C}_{10}\text{H}_{22}\text{NO}$  172.1696, found 172.1699.

#### General procedure for the synthesis of Boc-protected pyrroles 14b–g

**Acylation of 1H-pyrrole.** The 2-acylation of 1H-pyrrole was performed according to the protocol of Ono *et al.*<sup>66</sup> In a Schlenk flask under  $\text{N}_2$  atmosphere the acid chloride **11c–g** (1.00 eq.) is dissolved in dry  $\text{CH}_2\text{Cl}_2$  (3.74 mL  $\text{mmol}^{-1}$  acid chloride) and cooled to 0 °C. Aluminium trichloride (1.20 eq.) is added slowly to give a yellow suspension and the mixture is allowed to warm to 24 °C over 30 min. The solution is cooled to 0 °C again and a solution of 1H-pyrrole (1.10 eq.) in dry  $\text{CH}_2\text{Cl}_2$  (0.42 mL  $\text{mmol}^{-1}$  acid chloride) is transferred slowly to the acid chloride solution. The reaction is stirred for further 1 h at 0 °C, then slowly thawed to 21 °C and stirred overnight. A saturated solution of  $\text{NH}_4\text{Cl}$  is used at 0 °C for reaction quenching. The phases are separated, the aqueous phase subsequently extracted with  $\text{CH}_2\text{Cl}_2$  (3  $\times$  150 mL) and the combined organic phases washed with saturated  $\text{NaHCO}_3$  (2  $\times$  150 mL) and brine (1  $\times$  150 mL). Drying over  $\text{MgSO}_4$ , filtration over degreased cotton wool and solvent removal *in vacuo* provides the crude acylation product **12c–g** as brown oil, which is used without further purification and contains mostly 2-acylated 1H-pyrrole.

**Reduction of acylated 1H-pyrrole.** The reduction of 2-acylated 1H-pyrroles to 2-alkyl-1H-pyrroles was performed according to the protocol of Fürstner *et al.*<sup>1</sup> Under  $\text{N}_2$  atmosphere sodium borohydride (2.80 eq.) is suspended in dry isopropyl alcohol (0.90 mL  $\text{mmol}^{-1}$  acylated pyrrole) and

cooled to 0 °C. The crude acylated pyrrole **12c–g** (1.00 eq.) is dissolved in dry isopropyl alcohol (3.15 mL  $\text{mmol}^{-1}$  acylated pyrrole), precooled to 0 °C and added to the sodium borohydride suspension at 0 °C. Afterwards, the solution is refluxed overnight at 99 °C. The reaction is quenched with water at 0 °C, additional water (300 mL) is added and the product extracted with MTBE (3  $\times$  200 mL). Merged organic phases are washed with brine (2  $\times$  200 mL), dried over  $\text{MgSO}_4$ , and filtered over degreased cotton wool. After solvent removal, the oily brown crude product, which contains mostly 2-alkylated 1H-pyrrole **13c–g**, is used without further purification.

**Boc-protection of alkylated 1H-pyrrole.** Boc-protection of 2-alkyl-1H-pyrroles was realised according to the protocol of Fürstner *et al.*<sup>1</sup> In a Schlenk flask under  $\text{N}_2$  atmosphere crude alkylated 1H-pyrrole **13c–g** or commercially available 2-methyl-1H-pyrrole (**13b**) (1.00 eq.) and DMAP (0.10 eq.) are dissolved in dry  $\text{CH}_2\text{Cl}_2$  (1.42 mL  $\text{mmol}^{-1}$  alkylated pyrrole). A solution of  $\text{Boc}_2\text{O}$  (1.20 eq.) in dry  $\text{CH}_2\text{Cl}_2$  (2.37 mL  $\text{mmol}^{-1}$  alkylated pyrrole) is added to the prior solution at ambient temperature and the reaction is stirred overnight. The solvent is removed under reduced pressure and the residue purified by chromatography on silica using *n*-pentane/MTBE (99:1). The Boc-protected 2-alkylated 1H-pyrroles **14b–g** are afforded as colourless to yellow liquids.

**1-tert-Butyloxycarbonyl 2-methyl-1H-pyrrole (14b).** In a Schlenk flask under  $\text{N}_2$  atmosphere are 2-methyl-1H-pyrrole (**13b**, 3.03 g, 37.4 mmol, 1.40 eq.) and DMAP (326 mg, 2.67 mmol, 0.10 eq.) dissolved in 20 mL dry  $\text{CH}_2\text{Cl}_2$ . A solution of  $\text{Boc}_2\text{O}$  (5.83 g, 26.7 mmol, 1.00 eq.) in  $\text{CH}_2\text{Cl}_2$  (100 mL) is added to the pyrrole at 20 °C, turning instantly yellow, and the reaction stirred for 18 h at 21 °C. The solvent is removed under reduced pressure and the orange residue purified by chromatography on silica using *n*-pentane/MTBE (98:2), yielding 3.88 g (21.39 mmol, 80%) of a colourless liquid.  $\delta^1\text{H}$  (600 MHz,  $\text{CDCl}_3$ ) 1.59 (9 H, s, 10-H, 11-H, 12-H), 2.43 (3 H, d,  $J = 1.1$  Hz, 1'-H), 5.92 (1 H, tt,  $J = 1.9$  Hz,  $J = 1.0$  Hz, 3-H), 6.06 (1 H, t,  $J = 3.3$  Hz, 4-H), 7.18 (1 H, dd,  $J = 3.4$  Hz,  $J = 1.8$  Hz, 5).  $\delta^{13}\text{C}$  (151 MHz,  $\text{CDCl}_3$ ) 15.6 (C-1'), 28.2 (C-10, C-11, C-12), 83.4 (C-9), 110.0 (C-4), 111.9 (C-3), 120.7 (C-5), 131.7 (C-2), 149.9 (C-6). FT-IR (neat,  $\text{cm}^{-1}$ ): 2979, 2928, 1737, 1497, 1396, 1370, 1329, 1308, 1254, 1237, 1170, 1127, 1065, 983, 883, 851, 798, 772, 715, 676, 597, 552. HRMS-ESI ( $m/z$ ):  $[\text{M} + \text{H}]^+$  calculated for  $\text{C}_{10}\text{H}_{16}\text{NO}_2$  182.1176, found 182.1176.

**1-tert-Butyloxycarbonyl 2-ethyl-1H-pyrrole (14c).** Following the general procedure for the synthesis of Boc-protected pyrroles, 11.8 g (60.3 mmol, 48% over three steps) 1-tert-butyloxycarbonyl 2-ethyl-1H-pyrrole (**14c**) was synthesised from acetyl chloride (**11c**, 9.95 g, 127 mmol, 1.00 eq.) and obtained as pale yellow liquid.  $\delta^1\text{H}$  (600 MHz,  $\text{CDCl}_3$ ) 1.23 (3 H, t,  $J = 7.4$  Hz, 2''-H), 1.59 (9 H, s, 10-H, 11-H, 12-H), 2.87 (2 H, qd,  $J = 7.4$  Hz, 1'-H), 5.96 (1 H, tt,  $J = 3.0$ , 3-H), 6.08 (1 H, t,  $J = 3.3$ , 4-H), 7.19 (1 H, dd,  $J = 3.4$  Hz, 5-H).  $\delta^{13}\text{C}$  (151 MHz,  $\text{CDCl}_3$ ) 13.4 (C-2''), 22.4 (C-1'), 28.2 (C-10, C-11, C-12), 83.4 (C-9), 110.0 (C-3), 110.0 (C-4), 120.9 (C-5), 138.2 (C-2), 149.7 (C-6). FT-IR (neat,  $\text{cm}^{-1}$ ): 2973, 2934, 2877, 1739, 1497, 1479,



1458, 1409, 1395, 1369, 1326, 1293, 1256, 1233, 1167, 1132, 1124, 1066, 1058, 1047, 1015, 977, 953, 882, 853, 840, 814, 772, 719. HRMS-ESI ( $m/z$ ):  $[M + H]^+$  calculated for  $C_{11}H_{18}NO_2$  196.1332, found 196.1331.

#### 1-*tert*-Butyloxycarbonyl 2-propyl-1*H*-pyrrole (14d).

Following the general procedure for the synthesis of Boc-protected pyrroles, 12.5 g (59.8 mmol, 52% over three steps) 1-*tert*-butyloxycarbonyl 2-propyl-1*H*-pyrrole (14d) was synthesised from propanoic acid chloride (11d, 10.7 g, 115 mmol, 1.00 eq.) and obtained as colourless liquid.  $\delta^1H$  (600 MHz,  $CDCl_3$ ) 0.98 (3 H, t,  $J = 7.4$  Hz, 3'-H), 1.59 (9 H, s, 10-H, 11-H, 12-H), 1.64 (2 H, h,  $J = 7.4$  Hz, 2'-H), 2.75–2.87 (2 H, m, 1'-H), 5.95 (1 H, ddt,  $J = 3.0$  Hz,  $J = 2.0$  Hz, 3-H), 6.08 (1 H, t,  $J = 3.3$  Hz, 4-H), 7.19 (1 H, dd,  $J = 3.4$  Hz,  $J = 1.8$  Hz, 5-H).  $\delta^{13}C$  (151 MHz,  $CDCl_3$ ) 14.1 (C-3'), 22.3 (C-2'), 28.2 (C-10, C-11, C-12), 31.1 (C-1'), 83.3 (C-9), 110.0 (C-4), 111.0 (C-3), 120.9 (C-5), 136.5 (C-2), 149.7 (C-6). FT-IR (neat,  $cm^{-1}$ ): 3006, 2961, 2933, 2873, 1739, 1495, 1479, 1457, 1436, 1407, 1394, 1369, 1327, 1318, 1254, 1169, 1127, 1060, 1010, 972, 907, 895, 884, 849, 801, 772, 716, 599, 495. HRMS-ESI ( $m/z$ ):  $[M + H]^+$  calculated for  $C_{12}H_{20}NO_2$  210.1489, found 210.1488.

**1-*tert*-Butyloxycarbonyl 2-butyl-1*H*-pyrrole (14e).** Following the general procedure for the synthesis of Boc-protected pyrroles, 9.55 g (42.8 mmol, 44% over three steps) 1-*tert*-butyloxycarbonyl 2-butyl-1*H*-pyrrole (14e) was synthesised from butanoic acid chloride (11e, 10.3 g, 96.5 mmol, 1.00 eq.) and obtained as pale yellow oil.  $\delta^1H$  (600 MHz,  $CDCl_3$ ) 0.94 (3 H, t,  $J = 7.4$  Hz, 4'-H), 1.40 (2 H, h,  $J = 7.4$  Hz, 3'-H), 1.59 (9 H, s, 10-H, 11-H, 12-H), 1.56–1.63 (2 H, m, 2'-H), 2.80–2.88 (2 H, m), 5.95 (1 H, td,  $J = 1.9$  Hz, 3-H), 6.07 (1 H, t,  $J = 3.3$  Hz, 4-H), 7.19 (1 H, dd,  $J = 3.4$  Hz,  $J = 1.8$  Hz, 5-H).  $\delta^{13}C$  (151 MHz,  $CDCl_3$ ) 14.2 (C-4'), 22.7 (C-3'), 28.2 (C-10, C-11, C-12), 28.8 (C-1'), 31.2 (C-2'), 83.3 (C-9), 110.0 (C-4), 110.8 (C-3), 120.9 (C-5), 136.7 (C-2), 149.7 (C-6). FT-IR (neat,  $cm^{-1}$ ): 2958, 2932, 2872, 2863, 1737, 1495, 1478, 1458, 1407, 1394, 1369, 1325, 1315, 1254, 1235, 1221, 1166, 1123, 1059, 1013, 999, 883, 852, 804, 772, 714, 599. HRMS-ESI ( $m/z$ ):  $[M + H]^+$  calculated for  $C_{13}H_{22}NO_2$  224.1645, found 224.1641.

**1-*tert*-Butyloxycarbonyl 2-pentyl-1*H*-pyrrole (14f).** Following the general procedure for the synthesis of Boc-protected pyrroles, 16.9 g (71.1 mmol, 59% over three steps) 1-*tert*-butyloxycarbonyl 2-pentyl-1*H*-pyrrole (14f) was synthesised from pentanoic acid chloride (11f, 14.5 g, 120 mmol, 1.00 eq.) and obtained as colourless oil.  $\delta^1H$  (600 MHz,  $CDCl_3$ ) 0.84–0.97 (3 H, m, 5'-H), 1.36 (4 H, ddd,  $J = 7.1$  Hz, 3'-H, 4'-H), 1.59 (9 H, s), 1.62 (2 H, q,  $J = 7.7$  Hz, 2'-H), 2.76–2.88 (2 H, m, 1'-H), 5.95 (1 H, ddt,  $J = 3.0$  Hz,  $J = 2.0$  Hz, 3-H), 6.07 (1 H, t,  $J = 3.3$  Hz, 4-H), 7.19 (1 H, dd,  $J = 3.4$  Hz,  $J = 1.8$  Hz, 5-H).  $\delta^{13}C$  (151 MHz,  $CDCl_3$ ) 14.2 (C-5'), 22.7 (C-4'), 28.2 (C-10, C-11, C-12), 28.8 (C-2'), 29.0 (C-1'), 31.8 (C-3'), 83.3 (C-9), 110.0 (C-4), 110.8 (C-3), 120.9 (C-5), 136.7 (C-2), 149.7 (C-6). FT-IR (neat,  $cm^{-1}$ ): 2957, 2931, 2871, 2861, 1738, 1495, 1478, 1458, 1408, 1394, 1369, 1326, 1317, 1254, 1235, 1166, 1125, 1059, 1010, 963, 883, 851, 844, 800, 772, 715, 599, 560, 497, 461. HRMS-ESI ( $m/z$ ):  $[M + H]^+$  calculated for  $C_{14}H_{24}NO_2$  238.1802, found 238.1801.

**1-*tert*-Butyloxycarbonyl 2-hexyl-1*H*-pyrrole (14g).** Following the general procedure for the synthesis of Boc-protected pyrroles, 12.1 g (48.2 mmol, 43% over three steps) 1-*tert*-butyloxycarbonyl 2-hexyl-1*H*-pyrrole (14g) was synthesised from hexanoic acid chloride (11g, 15.0 g, 111 mmol, 1.00 eq.) and obtained as colourless oil.  $\delta^1H$  (600 MHz,  $CDCl_3$ ) 0.83–0.94 (3 H, m, 6'-H), 1.24–1.35 (4 H, m, 4'-H, 5'-H), 1.34–1.42 (2 H, m, 3'-H), 1.57–1.64 (2 H, m, 2'-H), 1.59 (9 H, s, 10-H, 11-H, 12-H), 2.77–2.86 (2 H, m, 1'-H), 5.95 (1 H, td,  $J = 1.9$  Hz, 3-H), 6.07 (1 H, t,  $J = 3.3$  Hz, 4-H), 7.19 (1 H, dd,  $J = 3.4$  Hz,  $J = 1.8$  Hz, 5-H).  $\delta^{13}C$  (151 MHz,  $CDCl_3$ ) 14.2 (C-6'), 22.8 (C-5'), 28.2 (C-10, C-11, C-12), 29.1 (C-3'), 29.3 (C-2'), 31.9 (C-4'), 83.3 (C-9), 110.0 (C-4), 110.8 (C-3), 120.9 (C-5), 136.7 (C-2), 149.7 (C-6). FT-IR (neat,  $cm^{-1}$ ): 2956, 2927, 2858, 1740, 1495, 1478, 1458, 1407, 1394, 1369, 1327, 1319, 1253, 1234, 1165, 1127, 1061, 1008, 887, 851, 803, 772, 715. HRMS-ESI ( $m/z$ ):  $[M + H]^+$  calculated for  $C_{15}H_{26}NO_2$  252.1958, found 252.1959.

**General procedure for the synthesis of pyrrole-2-boronic acids 15b–g.** Following the procedure of Cai and Snider, Boc-protected pyrrole-2-boronic acids were accessed.<sup>86</sup> In a Schlenk flask under  $N_2$  atmosphere *n*-butyl lithium (2.10 eq., 2.5 M in hexane) is added dropwise to a solution of distilled 2,2,6,6-tetramethylpiperidine (2.00 eq.) in dry THF (2.36 mL  $mmol^{-1}$  pyrrole) at  $-78$  °C. After stirring for 15 min the mixture is allowed to warm to  $0$  °C over 30 min and then cooled again to  $-78$  °C. In a three necked flask is Boc-2-alkyl-1*H*-pyrrole 14b–g (1.00 eq.) dissolved in dry THF (4.00 mL  $mmol^{-1}$  pyrrole) and cooled to  $-78$  °C. The LiTMP is then transferred dropwise to the pyrrolic solution in THF with a transfer cannula. The internal temperature is constantly kept below  $-70$  °C and the rate adjusted if needed. The reaction mixture is stirred for 2 h at  $-78$  °C, before trimethyl borate (3.00 eq.) in THF (1.07 mL  $mmol^{-1}$  pyrrole) is added slowly. The solution is stirred for 15 min at  $-78$  °C, then 30 min at  $0$  °C, and finally at  $21$  °C overnight. The reaction is quenched at  $0$  °C by dropwise addition of 0.20 M HCl (aq.) (2.10 eq.). The aqueous phase is extracted with  $Et_2O$  ( $3 \times 50$  mL). Merged organic phases are washed with water (100 mL), brine (100 mL), and dried over  $MgSO_4$ . The solvent is almost completely removed by evaporation at room temperature (water bath at  $20$  °C). The residue in  $Et_2O$ /THF is transferred to a Schlenk flask and residual solvent is removed *in vacuo* while stirring to prevent bumping and the crude product is recovered as viscous orange solid or oil. The delicate crude product is used without further purification for the next synthetic step on the same day.

#### NMR data of crude boronic acids

**(1-(*tert*-Butoxycarbonyl)-5-methyl-1*H*-pyrrol-2-yl)boronic acid (15b).**  $\delta^1H$  (300 MHz,  $CDCl_3$ ) 7.09 (2 H, brs, 7-H, 8-H), 7.00 (1 H, d,  $J = 3.3$  Hz, 3-H), 6.01 (1 H, dd,  $J = 3.2$  Hz, 4-H), 2.42 (3 H, s, 1'-H), 1.62 (9 H, s, 13-H, 14-H, 15-H).  $\delta^{13}C$  (76 MHz,  $CDCl_3$ ) 153.4 (C-9), 137.8 (C-5), 127.6 (C-3), 113.8 (C-4), 85.9 (C-12), 28.2 (C-13, C-14, C-15), 17.8 (C-1').  $\delta^{11}B$  (96 MHz,  $CDCl_3$ ) 26.5.



**(1-(*tert*-Butoxycarbonyl)-5-ethyl-1*H*-pyrrol-2-yl)boronic acid (15c).**  $\delta^1\text{H}$  (300 MHz,  $\text{CDCl}_3$ ) 7.01 (1 H, d,  $J = 3.4$  Hz, 1-H), 6.66 (2 H, brs, H-14, H-15), 6.06 (1 H, dt,  $J = 3.4$  Hz, 2-H), 2.83 (2 H, q,  $J = 7.5$  Hz, 16-H), 1.63 (9 H, s, 10-H, 11-H, 12-H), 1.27–1.19 (3 H, m, 18-H).  $\delta^{13}\text{C}$  (76 MHz,  $\text{CDCl}_3$ ) 153.4 (C-6), 144.1 (C-3), 127.5 (C-1), 111.8 (C-2), 85.9 (C-9), 28.1 (C-10, C-11, C-12), 24.1 (C-16), 13.9 (C-18).  $\delta^{11}\text{B}$  (96 MHz,  $\text{CDCl}_3$ ) 25.8.

**(1-(*tert*-Butoxycarbonyl)-5-propyl-1*H*-pyrrol-2-yl)boronic acid (15d).**  $\delta^1\text{H}$  (300 MHz,  $\text{CDCl}_3$ ) 7.00 (1 H, d,  $J = 3.3$  Hz, 1-H), 6.04 (1 H, d,  $J = 3.3$  Hz, 2-H), 2.77 (2 H, t,  $J = 7.8$  Hz, 16-H), 1.67–1.58 (11 H, m, H-13, H-14, H-15, H-18), 0.97 (3 H, t,  $J = 7.5$  Hz, 19-H).  $\delta^{13}\text{C}$  (76 MHz,  $\text{CDCl}_3$ ) 153.3 (C-6), 142.2 (C-3), 127.2 (C-1), 112.8 (C-2), 85.8 (C-12), 32.8 (C-16), 28.0 (C-13, C-14, C-15), 22.7 (C-18), 13.9 (C-19).  $\delta^{11}\text{B}$  (96 MHz,  $\text{CDCl}_3$ ) 25.0.

**(1-(*tert*-Butoxycarbonyl)-5-butyl-1*H*-pyrrol-2-yl)boronic acid (15e).**  $\delta^1\text{H}$  (300 MHz,  $\text{CDCl}_3$ ) 7.00 (1 H, d,  $J = 3.3$  Hz, 1-H), 6.71 (2 H, brs, 14-H, 15-H), 6.04 (1 H, d,  $J = 3.3$  Hz, 2-H), 2.80 (2 H, t,  $J = 7.6$  Hz, 16-H), 1.63 (9 H, s, 10-H, 11-H, 12-H), 1.62–1.52 (2 H, m, 18-H), 1.47–1.33 (2 H, m, 19-H), 0.94 (3 H, t,  $J = 7.3$  Hz, 20-H).  $\delta^{13}\text{C}$  (76 MHz,  $\text{CDCl}_3$ ) 153.4 (C-6), 142.6 (C-3), 127.4 (C-1), 112.6 (C-2), 85.9 (C-9), 31.6 (C-18), 30.6 (C-16), 28.1 (C-10, C-11, C-12), 22.7 (C-19), 14.1 (C-20).  $\delta^{11}\text{B}$  (96 MHz,  $\text{CDCl}_3$ ) 25.5.

**(1-(*tert*-Butoxycarbonyl)-5-pentyl-1*H*-pyrrol-2-yl)boronic acid (15f).**  $\delta^1\text{H}$  (300 MHz,  $\text{CDCl}_3$ ) 7.35 (2 H, brs, 7-H, 8-H), 7.02 (1 H, d,  $J = 3.4$  Hz, 3-H), 6.04 (1 H, d,  $J = 3.4$  Hz, 4-H), 2.79 (2 H, t,  $J = 7.7$  Hz, 1'-H), 1.68–1.51 (11 H, m, 2'-H, 13-H, 14-H, 15-H), 1.40–1.28 (4 H, m, 3'-H, 4'-H), 0.96–0.85 (3 H, m, 5'-H).  $\delta^{13}\text{C}$  (76 MHz,  $\text{CDCl}_3$ ) 153.4 (C-9), 142.6 (C-5), 127.5 (C-3), 112.7 (C-4), 85.9 (C-12), 31.8 (C-3'), 30.9 (C-1'), 29.2 (C-2'), 28.1 (C-13, C-14, C-15), 22.7 (C-4'), 14.2 (C-5').  $\delta^{11}\text{B}$  (96 MHz,  $\text{CDCl}_3$ ) 23.8.

**(1-(*tert*-Butoxycarbonyl)-5-hexyl-1*H*-pyrrol-2-yl)boronic acid (15g).**  $\delta^1\text{H}$  (300 MHz,  $\text{CDCl}_3$ ) 7.00 (1 H, d,  $J = 3.3$  Hz, 1-H), 6.04 (1 H, d,  $J = 3.4$  Hz, 2-H), 2.79 (2 H, t,  $J = 7.6$  Hz, 16-H), 1.63 (9 H, s, 13-H, 14-H, 15-H), 1.62–1.53 (2 H, m, 18-H), 1.43–1.22 (6 H, m, 19-H, 20-H, 21-H), 0.94–0.83 (3 H, m, 22-H).  $\delta^{13}\text{C}$  (76 MHz,  $\text{CDCl}_3$ ) 153.4 (C-6), 142.6 (C-3), 127.4 (C-1), 112.6 (C-2), 85.8 (C-12), 31.9 (C-20), 30.9 (C-16), 29.5 (C-18), 29.3 (C-19), 28.1 (C-13, C-14, C-15), 22.7 (C-21), 14.2 (C-22).  $\delta^{11}\text{B}$  (96 MHz,  $\text{CDCl}_3$ ) 25.5.

**General procedure for the synthesis of prodiginines 16ba–bc.** MBC and pyrrole derivatives were transformed to prodiginines under acid catalysis as performed by Boger and Patel.<sup>87</sup> An MBC derivative **3a–g** (1.00 eq.) is dissolved in MeOH (10 mM solution). After addition of 1*H*-pyrrole **4a–c** (2.00 eq.), the solution is cooled to 0 °C. After 15 min of stirring, 1.25 M HCl in MeOH (1.80 eq.) is added dropwise. With completed HCl addition, the reaction is thawed and then stirred at 21 °C overnight. Water is added and the mixture then quenched with 25%  $\text{NH}_3$  (aq.). The product is extracted with  $\text{CH}_2\text{Cl}_2$  (3  $\times$  50 mL). Merged organic phases are dried over  $\text{MgSO}_4$  and filtered over degreased cotton wool. After removal of the solvent, the residue is chromatographed on silica with  $\text{CH}_2\text{Cl}_2$  and 0.7% 7 N  $\text{NH}_3$  in MeOH. Product containing fractions are merged and

chromatographed on silica with *n*-pentane/ $\text{CH}_2\text{Cl}_2$  (60:40) and 4% 7 N  $\text{NH}_3$  in MeOH to remove unconverted MBC precursor. Evaporation of the solvent and acidification with 1 M HCl in  $\text{Et}_2\text{O}$  yields a purple film that is precipitated by repeated addition of petroleum ether. A deep purple amorphous solid is obtained.

**(*Z*)-4'-Methoxy-5-methyl-5'-((5-methyl-4-propyl-1*H*-pyrrol-2-yl)methylene)-1*H*,5'*H*-[2,2'-bipyrrol]-1'-ium chloride (16bb).** Following the general procedure for the synthesis of prodiginines, carbaldehyde **3b** (54.0 mg, 0.26 mmol, 1.00 eq.), pyrrole **4b** (65.2 mg, 0.53 mmol, 2.00 eq.) and HCl in MeOH (381  $\mu\text{L}$ , 0.48 mmol, 1.80 eq.) were converted to 60.1 mg (0.17 mmol, 66%, 95.7%  $\pm$  0.85% purity by qNMR) of a deep purple amorphous solid.  $\delta^1\text{H}$  (300 MHz,  $\text{CDCl}_3$ ) 0.92 (3 H, t,  $J = 7.3$  Hz, 9''-H), 1.54 (2 H, h,  $J = 7.4$ , 8''-H), 2.34 (2 H, t,  $J = 7.5$  Hz, 7''-H), 2.43 (3 H, s, 6-H), 2.50 (3 H, s, 6''-H), 3.94 (3 H, s, 7'-H), 5.97 (1 H, d, 3'-H), 6.03 (1 H, t, 4-H), 6.59 (1 H, d, 3''-H), 6.82 (2 H, d, 3-H, 6'-H), 12.38 (1 H, brs, 1'-NH), 12.44–12.63 (2 H, brs, 1-NH, 1''-NH).  $\delta^{13}\text{C}$  (76 MHz,  $\text{CDCl}_3$ ) 12.3 (C-6''), 13.6 (C-6), 13.9 (C-9''), 23.5 (C-8''), 27.5 (C-7''), 58.7 (C-7'), 92.6 (C-3'), 111.4 (C-4), 114.6 (C-6'), 118.9 (C-3), 121.0 (C-2), 121.3 (C-5'), 124.9 (C-2''), 127.2 (C-3''), 127.5 (C-4''), 139.6 (C-5), 145.1 (C-5''), 147.7 (C-2'), 165.7 (C-4'). FT-IR (neat,  $\text{cm}^{-1}$ ): 3221, 3164, 3143, 3115, 3115, 3105, 3066, 3010, 2958, 2914, 2873, 2859, 2854, 2818, 1635, 1608, 1552, 1537, 1517, 1493, 1441, 1415, 1403, 1370, 1338, 1252, 1208, 1184, 1159, 1128, 1083, 1045, 995, 980, 967, 909, 891, 884, 867, 844, 823, 792, 769, 752, 743, 732, 668, 647, 638, 621, 548, 478.  $T_m$ : 158.6–160.5 °C (petroleum ether). HRMS-ESI ( $m/z$ ):  $[\text{M}-\text{Cl}]^+$  calculated for  $\text{C}_{19}\text{H}_{24}\text{N}_3\text{O}$  310.1914, found 310.1911.  $t_R$  (LC-MS method): 7.56 min.

**(*Z*)-4'-Methoxy-5-methyl-5'-((5-methyl-4-pentyl-1*H*-pyrrol-2-yl)methylene)-1*H*,5'*H*-[2,2'-bipyrrol]-1'-ium chloride (16ba).** Following the general procedure for the synthesis of prodiginines, carbaldehyde **3b** (100 mg, 0.49 mmol, 1.00 eq.), pyrrole **4a** (148 mg, 0.98 mmol, 2.00 eq.) and HCl in MeOH (705  $\mu\text{L}$ , 0.88 mmol, 1.80 eq.) were converted to 150 mg (0.40 mmol, 82%, 89.5%  $\pm$  0.94% purity by qNMR) of a deep purple amorphous solid.  $\delta^1\text{H}$  (300 MHz,  $\text{CDCl}_3$ ) 0.80–0.94 (4 H, m, 11''-H), 1.30 (4 H, qq, 9''-H, 10''-H), 1.53 (2 H, p,  $J = 7.4$  Hz, 8''-H), 2.38 (2 H, t,  $J = 7.6$  Hz, 7''-H), 2.45 (3 H, s, 6-H), 2.52 (3 H, s, 6''-H), 3.97 (3 H, s, 7'-H), 6.00 (1 H, d,  $J = 1.9$ , 3'-H), 6.03–6.11 (1 H, m, 4-H), 6.61 (1 H, d, 3''-H), 6.81–6.87 (2 H, m, 3-H, 6'-H), 12.44 (1 H, brs, 1'-NH), 12.54 (2 H, brs, 1-NH, 1''-NH).  $\delta^{13}\text{C}$  (76 MHz,  $\text{CDCl}_3$ ) 12.4 (C-6''), 13.7 (C-6), 14.2 (C-11''), 22.6 (C-10''), 25.5 (C-7''), 30.1 (C-8''), 31.6 (C-9''), 58.8 (C-7'), 92.6 (C-3'), 111.4 (C-4), 114.7 (C-6'), 118.9 (C-3), 121.1 (C-2), 121.3 (C-5'), 125.0 (C-2''), 127.3 (C-3''), 127.8 (C-4''), 139.7 (C-5), 145.3 (C-5''), 147.7 (C-2'), 165.8 (C-4'). FT-IR (neat,  $\text{cm}^{-1}$ ): 3171, 3141, 3101, 3067, 2954, 2922, 2855, 1630, 1605, 1579, 1538, 1493, 1447, 1414, 1402, 1348, 1286, 1253, 1207, 1151, 1130, 1099, 1078, 1037, 994, 965, 899, 882, 841, 805, 785, 768, 732, 698, 666, 643, 623, 550, 502.  $T_m$ : 77.6–80.1 °C (petroleum ether). HRMS-ESI ( $m/z$ ):  $[\text{M}-\text{Cl}]^+$  calculated for  $\text{C}_{21}\text{H}_{28}\text{N}_3\text{O}$  338.2227, found 338.2228.  $t_R$  (LC-MS method): 7.83 min.



**(Z)-4'-Methoxy-5-methyl-5'-((5-methyl-4-heptyl-1H-pyrrol-2-yl)methylene)-1H,5'H-[2,2'-bipyrryl]-1'-ium chloride (16bc).** Following the general procedure for the synthesis of prodiginines, carbaldehyde **3b** (50.0 mg, 0.24 mmol, 1.00 eq.), pyrrole **4c** (87.8 mg, 0.49 mmol, 2.00 eq.) and HCl in MeOH (353  $\mu$ L, 0.44 mmol, 1.80 eq.) were converted to 79.0 mg (0.20 mmol, 80%, 97.3%  $\pm$  0.87% purity by qNMR) of a deep purple amorphous solid.  $\delta^1\text{H}$  (300 MHz,  $\text{CDCl}_3$ ) 0.79–0.92 (3 H, m, 13"-H), 1.17–1.36 (8 H, m, 9"-H, 10"-H, 11"-H, 12"-H), 1.51 (2 H, p,  $J$  = 7.3 Hz, 8"-H), 2.36 (2 H, t,  $J$  = 7.5 Hz, 7"-H), 2.43 (3 H, s, 6"-H), 2.50 (3 H, s, 6"-H), 3.94 (3 H, s, 7"-H), 5.97 (1 H, d, 3'-H), 6.03 (1 H, dd, 4-H), 6.59 (1 H, d, 3"-H), 6.78–6.84 (2 H, m, 3-H, 6'-H), 12.38 (1 H, brs, 1'-NH), 12.50 (2 H, brs, 1-NH, 1'-NH).  $\delta^{13}\text{C}$  (76 MHz,  $\text{CDCl}_3$ ) 12.3 (C-6"), 13.6 (C-6), 14.2 (C-13"), 22.8 (C-12"), 25.5 (C-7"), 29.2 (C-9"), 29.3 (C-10"), 30.3 (C-8"), 31.9 (C-11"), 58.7 (C-7'), 92.6 (C-3'), 111.4 (C-4), 114.6 (C-6'), 118.9 (C-3), 121.0 (C-2), 121.2 (C-5'), 125.0 (C-2"), 127.2 (C-3"), 127.7 (C-4"), 139.6 (C-5), 145.1 (C-5"), 147.6 (C-2'), 165.7 (C-4'). FT-IR (neat,  $\text{cm}^{-1}$ ): 3223, 3171, 3144, 3116, 3073, 3062, 2953, 2921, 2851, 1629, 1605, 1581, 1540, 1516, 1494, 1447, 1403, 1369, 1347, 1289, 1257, 1205, 1174, 1089, 1042, 976, 887, 841, 829, 818, 810, 792, 779, 765, 741, 726, 705, 683, 661, 642, 605, 543, 517, 505, 476.  $T_m$ : 120.5–122.6  $^\circ\text{C}$  (petroleum ether). HRMS-ESI ( $m/z$ ):  $[\text{M}-\text{Cl}]^+$  calculated for  $\text{C}_{23}\text{H}_{32}\text{N}_3\text{O}$  366.2540, found 366.2546.  $t_R$  (LC-MS method): 7.95 min.

**(Z)-5-Ethyl-4'-methoxy-5'-((5-methyl-4-pentyl-1H-pyrrol-2-yl)methylene)-1H,5'H-[2,2'-bipyrryl]-1'-ium chloride (16ca).** Following the general procedure for the synthesis of prodiginines, carbaldehyde **3c** (50.0 mg, 0.24 mmol, 1.00 eq.), pyrrole **4a** (87.8 mg, 0.49 mmol, 2.00 eq.) and HCl in MeOH (353  $\mu$ L, 0.44 mmol, 1.80 eq.) were converted to 79.0 mg (0.20 mmol, 80%, 94.6%  $\pm$  0.59% purity by qNMR) of a deep purple amorphous solid.  $\delta^1\text{H}$  (300 MHz,  $\text{CDCl}_3$ ) 0.83–0.92 (3 H, m, 11"-H), 1.21–1.36 (4 H, m, 9"-H, 10"-H), 1.38 (3 H, t,  $J$  = 7.6 Hz, 7-H), 1.46–1.59 (2 H, m, 8"-H), 2.37 (2 H, t, 7"-H), 2.51 (3 H, s, 6"-H), 2.80 (2 H, q,  $J$  = 7.6 Hz, 6-H), 3.96 (3 H, s, 7"-H), 6.00 (1 H, d,  $J$  1.9, 3'-H), 6.09 (1 H, dd, 4-H), 6.61 (1 H, d, 3"-H), 6.79–6.89 (2 H, m, 3-H, 6'-H), 12.49 (2 H, brs, 1-NH, 1'-NH), 12.58 (1 H, brs, 1"-NH).  $\delta^{13}\text{C}$  (76 MHz,  $\text{CDCl}_3$ ) 12.3 (C-6"), 13.4 (C-7), 14.2 (C-11"), 21.6 (C-6), 22.6 (C-10"), 25.5 (C-7"), 30.0 (C-8"), 31.6 (C-9"), 58.7 (C-7'), 92.6 (C-3'), 110.0 (C-4), 114.6 (C-6'), 118.7 (C-3), 121.1 (C-2), 121.3 (C-5'), 125.0 (C-2"), 127.3 (C-3"), 127.8 (C-4"), 145.2 (C-5"), 146.0 (C-5), 147.8 (C-2'), 165.7 (C-4'). FT-IR (neat,  $\text{cm}^{-1}$ ): 3221, 3171, 3145, 3118, 3063, 2950, 2923, 2853, 1632, 1606, 1580, 1547, 1540, 1493, 1447, 1402, 1375, 1360, 1308, 1290, 1257, 1202, 1174, 1146, 1077, 1058, 1043, 1004, 985, 969, 887, 841, 820, 807, 785, 764, 737, 648, 626, 610.  $T_m$ : 111.9–117.3  $^\circ\text{C}$  (petroleum ether). HRMS-ESI ( $m/z$ ):  $[\text{M}-\text{Cl}]^+$  calculated for  $\text{C}_{22}\text{H}_{30}\text{N}_3\text{O}$  352.2383, found 352.2387.  $t_R$  (LC-MS method): 7.92 min.

**(Z)-4'-Methoxy-5-propyl-5'-((5-methyl-4-pentyl-1H-pyrrol-2-yl)methylene)-1H,5'H-[2,2'-bipyrryl]-1'-ium chloride (16da).** Following the general procedure for the synthesis of prodiginines, carbaldehyde **3d** (116 mg, 0.50 mmol, 1.00 eq.), pyrrole **4a** (151 mg, 1.00 mmol, 2.00 eq.) and HCl in MeOH

(719  $\mu$ L, 0.90 mmol, 1.80 eq.) were converted to 116 mg (0.29 mmol, 58%, 99.5%  $\pm$  0.94% purity by qNMR) of a deep purple amorphous solid.  $\delta^1\text{H}$  (300 MHz,  $\text{CDCl}_3$ ) 0.84–0.93 (3 H, m, 11"-H), 0.99 (3 H, t,  $J$  = 7.3 Hz, 8-H), 1.22–1.38 (4 H, m, 9"-H, 10"-H), 1.52 (2 H, p,  $J$  = 7.4 Hz, 8"-H), 1.82 (2 H, h,  $J$  = 7.4 Hz, 7-H), 2.38 (2 H, t,  $J$  = 7.6 Hz, 7"-H), 2.52 (3 H, s, 6"-H), 2.75 (2 H, t,  $J$  = 7.6 Hz, 6-H), 3.98 (3 H, s, 7'-H), 6.01 (1 H, d, 3'-H), 6.10 (1 H, dd, 4-H), 6.62 (1 H, d, 3"-H), 6.83–6.88 (2 H, m, 3-H, 6'-H), 12.51 (2 H, brs, 1-NH, 1'-NH), 12.59 (1 H, brs, 1"-NH).  $\delta^{13}\text{C}$  (76 MHz,  $\text{CDCl}_3$ ) 12.4 (C-6"), 14.0 (C-8), 14.2 (C-11"), 22.6 (C-7), 22.7 (C-10"), 25.5 (C-7"), 30.1 (C-8"), 30.4 (C-6), 31.6 (C-9"), 58.8 (C-7'), 92.6 (C-3'), 110.7 (C-4), 114.7 (C-6'), 118.7 (C-3), 121.1 (C-2), 121.3 (C-5'), 125.0 (C-2"), 127.3 (C-3"), 127.8 (C-4"), 144.7 (C-5), 145.3 (C-5"), 147.8 (C-2'), 165.7 (C-4'). FT-IR (neat,  $\text{cm}^{-1}$ ): 3170, 3144, 3111, 3010, 2961, 2927, 2869, 2857, 1632, 1605, 1577, 1537, 1519, 1495, 1463, 1447, 1407, 1384, 1346, 1284, 1251, 1207, 1187, 1151, 1131, 1065, 1044, 998, 972, 955, 891, 883, 836, 816, 806, 786, 728, 695, 677, 655, 623, 545, 505, 477.  $T_m$ : 105.7–107.5  $^\circ\text{C}$  (petroleum ether). HRMS-ESI ( $m/z$ ):  $[\text{M}-\text{Cl}]^+$  calculated for  $\text{C}_{23}\text{H}_{32}\text{N}_3\text{O}$  366.2540, found 366.2542.  $t_R$  (LC-MS method): 8.02 min.

**(Z)-5-Butyl-4'-methoxy-5'-((5-methyl-4-pentyl-1H-pyrrol-2-yl)methylene)-1H,5'H-[2,2'-bipyrryl]-1'-ium chloride (16ea).** Following the general procedure for the synthesis of prodiginines, carbaldehyde **3e** (120 mg, 0.49 mmol, 1.00 eq.), pyrrole **4a** (147 mg, 0.97 mmol, 2.00 eq.) and HCl in MeOH (702  $\mu$ L, 0.88 mmol, 1.80 eq.) were converted to 148 mg (0.36 mmol, 73%, 99.9%  $\pm$  0.40% purity by qNMR) of a deep purple amorphous solid.  $\delta^1\text{H}$  (300 MHz,  $\text{CDCl}_3$ ) 0.84–0.92 (3 H, m, 11"-H), 0.95 (3 H, t, 9-H), 1.23–1.35 (4 H, m, 9"-H, 10"-H), 1.35–1.45 (2 H, m, 8-H), 1.46–1.60 (3 H, m, 8"-H), 1.69–1.83 (2 H, m, 7-H), 2.38 (2 H, t, 7"-H), 2.52 (3 H, s, 6"-H), 2.77 (2 H, t, 6-H), 3.98 (3 H, s, 7'-H), 6.01 (1 H, d, 3'-H), 6.10 (1 H, dd, 4-H), 6.62 (1 H, d, 3"-H), 6.85 (2 H, d, 3-H, 6'-H), 12.51 (2 H, brs, 1-NH, 1'-NH), 12.59 (1 H, brs, 1"-NH).  $\delta^{13}\text{C}$  (76 MHz,  $\text{CDCl}_3$ ) 12.4 (C-6"), 13.9 (C-9), 14.2 (C-11"), 22.5 (C-8), 22.7 (C-10"), 25.5 (C-7"), 28.0 (C-6), 30.1 (C-8"), 31.3 (C-7), 31.6 (C-9"), 58.8 (C-7'), 92.6 (C-3'), 110.6 (C-4), 114.6 (C-6'), 118.7 (C-3), 121.0 (C-2), 121.3 (C-5'), 125.0 (C-2"), 127.3 (C-3"), 127.8 (C-4"), 145.0 (C-5), 145.3 (C-5"), 147.8 (C-2'), 165.7 (C-4'). FT-IR (neat,  $\text{cm}^{-1}$ ): 3170, 3142, 3109, 3008, 2960, 2926, 2856, 1632, 1605, 1577, 1536, 1495, 1464, 1452, 1406, 1350, 1299, 1257, 1240, 1208, 1186, 1151, 1131, 1066, 1043, 1000, 972, 956, 891, 882, 837, 816, 806, 785, 732, 695, 675, 655, 545, 505, 475.  $T_m$ : 96.7–100.7  $^\circ\text{C}$  (petroleum ether). HRMS-ESI ( $m/z$ ):  $[\text{M}-\text{Cl}]^+$  calculated for  $\text{C}_{24}\text{H}_{34}\text{N}_3\text{O}$  380.2696, found 380.2704.  $t_R$  (LC-MS method): 8.11 min.

**(Z)-4'-Methoxy-5-pentyl-5'-((5-methyl-4-pentyl-1H-pyrrol-2-yl)methylene)-1H,5'H-[2,2'-bipyrryl]-1'-ium chloride (16fa).** Following the general procedure for the synthesis of prodiginines, carbaldehyde **3f** (130 mg, 0.50 mmol, 1.00 eq.), pyrrole **4a** (151 mg, 1.00 mmol, 2.00 eq.) and HCl in MeOH (719  $\mu$ L, 0.90 mmol, 1.80 eq.) were converted to 100 mg (0.23 mmol, 47%, 99.9%  $\pm$  0.78% purity by qNMR) of a deep purple amorphous solid.  $\delta^1\text{H}$  (300 MHz,  $\text{CDCl}_3$ ) 0.82–0.95 (6 H, m, 10-H, 11"-H), 1.21–1.43 (8 H, m, 8-H, 9-H, 9"-H, 10"-H), 1.45–



1.61 (2 H, p,  $J = 7.3$  Hz, 8''-H), 1.70–1.85 (2 H, m, 7-H), 2.38 (2 H, t,  $J = 7.6$  Hz, 7''-H), 2.52 (3 H, s, 6''-H), 2.77 (2 H, t, 6-H), 3.98 (3 H, s, 7'-H), 6.01 (1 H, d, 3'-H), 6.10 (1 H, dd, 4-H), 6.62 (1 H, d, 3''-H), 6.83–6.88 (2 H, m, 3-H, 6'-H), 12.51 (2 H, brs, 1-NH, 1'-NH), 12.60 (1 H, brs, 1''-NH).  $\delta^{13}\text{C}$  (76 MHz,  $\text{CDCl}_3$ ) 12.4 (C-6''), 14.2 (C-10, C-11''), 22.5 (C-9), 22.7 (C-10''), 25.5 (C-7''), 28.3 (C-6), 28.9 (C-7), 30.1 (C-8''), 31.6 (C-8, C-9''), 58.8 (C-7'), 92.6 (C-3'), 110.6 (C-4), 114.6 (C-6'), 118.7 (C-3), 121.0 (C-2), 121.3 (C-5'), 125.0 (C-2''), 127.3 (C-3''), 127.8 (C-4''), 145.0 (C-5), 145.3 (C-5''), 147.8 (C-2'), 165.7 (C-4'). FT-IR (neat,  $\text{cm}^{-1}$ ): 3171, 3144, 3111, 3058, 3015, 2952, 2925, 2870, 2854, 1632, 1606, 1578, 1537, 1495, 1464, 1451, 1406, 1383, 1349, 1322, 1285, 1254, 1208, 1186, 1045, 971, 955, 891, 882, 836, 816, 805, 789, 731, 708, 696, 685, 675, 656, 622, 546, 505, 471.  $T_m$ : 98.0–99.7 °C (petroleum ether). HRMS-ESI ( $m/z$ ):  $[\text{M}-\text{Cl}]^+$  calculated for  $\text{C}_{25}\text{H}_{36}\text{N}_3\text{O}$  394.2853, found 394.2855.  $t_R$  (LC-MS method): 8.09 min.

**(Z)-5-Hexyl-4'-methoxy-5'-((5-methyl-4-pentyl-1H-pyrrol-2-yl)methylene)-1H,5'H-[2,2'-bipyrrol]-1'-ium chloride (16ga).** Following the general procedure for the synthesis of prodiginines, carbaldehyde **3g** (140 mg, 0.51 mmol, 1.00 eq.), pyrrole **4a** (154 mg, 1.02 mmol, 2.00 eq.) and HCl in MeOH (735  $\mu\text{L}$ , 0.92 mmol, 1.80 eq.) were converted to 109 mg (0.25 mmol, 48%, 99.3%  $\pm$  3.73% purity by qNMR) of a deep purple amorphous solid.  $\delta^1\text{H}$  (300 MHz,  $\text{CDCl}_3$ ) 0.81–0.93 (6 H, m, 11-H, 11''-H), 1.20–1.42 (10 H, m, 8-H, 9-H, 9''-H, 10-H, 10''-H), 1.52 (2 H, p,  $J = 7.4$  Hz, 8''-H), 1.77 (2 H, p,  $J = 7.5$  Hz, 7-H), 2.37 (2 H, t,  $J = 7.6$  Hz, 7''-H), 2.51 (3 H, s, 6''-H), 2.75 (2 H, t,  $J = 7.7$  Hz, 6-H), 3.96 (3 H, s, 7'-H), 5.99 (1 H, d, 3'-H), 6.08 (1 H, dd, 4-H), 6.60 (1 H, d, 3''-H), 6.84 (2 H, d, 3-H, 6'-H), 12.47 (2 H, brs, 1-NH, 1'-NH), 12.57 (1 H, brs, 1''-NH).  $\delta^{13}\text{C}$  (76 MHz,  $\text{CDCl}_3$ ) 12.3 (C-6''), 14.2 (C-11, C-11''), 22.7 (C-10, C-10''), 25.4 (C-7''), 28.3 (C-6), 29.1 (C-7, C-8), 30.0 (C-8''), 31.6 (C-9, C-9''), 58.7 (C-7'), 92.6 (C-3'), 110.6 (C-4), 114.5 (C-6'), 118.7 (C-3), 121.0 (C-2), 121.3 (C-5'), 125.0 (C-2''), 127.2 (C-3''), 127.7 (C-4''), 144.9 (C-5), 145.1 (C-5''), 147.7 (C-2'), 165.7 (C-4'). FT-IR (neat,  $\text{cm}^{-1}$ ): 3171, 3144, 3115, 3072, 3015, 2953, 2919, 2868, 2855, 1636, 1613, 1580, 1549, 1539, 1497, 1466, 1450, 1421, 1407, 1386, 1362, 1333, 1293, 1263, 1253, 1215, 1204, 1185, 1157, 1129, 1101, 1092, 1044, 991, 978, 969, 891, 843, 817, 808, 782, 767, 735, 709, 694, 653, 625, 614, 553, 497, 456.  $T_m$ : 96.6–98.7 °C (petroleum ether). HRMS-ESI ( $m/z$ ):  $[\text{M}-\text{Cl}]^+$  calculated for  $\text{C}_{26}\text{H}_{38}\text{N}_3\text{O}$  408.3009, found 408.3017.  $t_R$  (LC-MS method): 8.30 min.

### Determination of molar extinction coefficients

Prodiginines were weighed in and dissolved in acidic EtOH (+ 4% 1 M HCl) to give a 10 mM solution. By means of serial 1:10 dilutions, the stock was diluted to 10  $\mu\text{M}$  in acidic EtOH. Firstly, the absorption spectra of 10  $\mu\text{M}$  solutions was collected on a Shimadzu UV-1800 UV Spectrophotometer, using the following instrument settings: 20 °C, 200–800 nm, 1.0 nm increment, Hellma Analytics quartz glass cuvette SUPRASIL QS ( $d = 10$  mm light path length).

Secondly, from the diluted 10  $\mu\text{M}$  stock, three concentrations were prepared in acidic EtOH, namely 1  $\mu\text{M}$ , 3  $\mu\text{M}$  and 5  $\mu\text{M}$ . The extinction was measured at 20 °C for each concentration at 535 nm, 545 nm and at the wavelength of maximum absorption, if the wavelength varied from the two aforementioned and the solvent background was subtracted on the instrument. The procedure was repeated three times for each compound. Resulting from the Beer-Lambert law ( $E = \epsilon \cdot c \cdot d$ ), the molar extinction  $E$  was plotted against the molar concentration  $c$  and the molar extinction coefficient  $\epsilon$  determined from the slope of a linear regression curve using Origin 2019 (ESI†).

### Biologic procedures

Chemically competent cells of *E. coli* BL21 (DE3) were transformed with of pET28a(+)-derived plasmids using the heat-shock protocol. In detail, 50  $\mu\text{L}$  of cells were thawed on ice for 10 min and 1  $\mu\text{L}$  of plasmid DNA was added. Incubation on ice for 30 min was followed by a heat shock at 42 °C for 30 s. The cells were again incubated on ice for 10 min and 700  $\mu\text{L}$  lysogeny broth (LB) medium was added to allow cell proliferation at 37 °C for 1.5 h. Finally, the cells were plated on LB agar, containing 50  $\mu\text{g mL}^{-1}$  kanamycin, and grown overnight at 37 °C.

### Protein production of prodiginine ligating enzymes

Single colonies of transformed *E. coli* BL21 (DE3) with pET28a(+) (empty vector, EV), pPigC<sub>3</sub>, pET28a(+):*tamQ* or pET28a(+):*treaP* were used to inoculate 50 mL of LB media (50  $\mu\text{g mL}^{-1}$  kanamycin) in a 250 mL Erlenmeyer flask and incubated overnight at 37 °C and 130 RPM. The precultures were used to inoculate 2  $\times$  1 L of terrific broth (TB) media (50  $\mu\text{g mL}^{-1}$  kanamycin) in 3 L baffled flasks to an optical density at 600 nm ( $\text{OD}_{600}$ ) of 0.05 and then cultivated at 37 °C and 130 RPM. At an  $\text{OD}_{600}$  of 0.6–0.9, the cultures were cooled at room temperature for 15 min and then induced by addition of 100  $\mu\text{M}$  isopropyl  $\beta$ -D-1-thiogalactopyranoside (IPTG). The cultures were then transferred to 25 °C and incubated overnight at 130 RPM. Cells were harvested by centrifugation (15 min, 4500 RPM, 4 °C), the supernatant discarded and dry pellets stored at –20 °C until further use.

### Cell lines and cell culture

RT-112 and RT-112<sup>res</sup> cells (kindly provided by Margaretha A. Skowron, Michèle J. Hoffmann, and Günter Niegisch; Department of Urology, Medical Faculty and University Hospital Düsseldorf, Heinrich Heine University Düsseldorf) were cultured in Dulbecco's modified Eagle medium (DMEM, Thermo Fisher Scientific) containing 10% fetal bovine serum (FBS, Sigma-Aldrich), 4.5 g  $\text{L}^{-1}$  D-glucose, 100 units  $\text{mL}^{-1}$  penicillin and 100  $\mu\text{g mL}^{-1}$  streptomycin (Thermo Fisher Scientific). The cells were cultivated and treated at 37 °C and 5%  $\text{CO}_2$  in a humidified atmosphere. RT-112<sup>res</sup> cells have been previously described.<sup>73</sup> Briefly, for the generation of this cisplatin-resistant cell line, RT-112 cells were treated with



increasing dosages of cisplatin over several months. During cell cultivation  $12 \mu\text{g mL}^{-1}$  cisplatin (NeoCorp, Pawtucket, RI, USA) was added to the media of RT-112<sup>res</sup> cells with every passage.

### Cell viability assay

Viability of RT-112 and RT-112<sup>res</sup> cells was measured using the MTT [3-(4,5-dimethylthiazol-2-yl)-2,5-diphenyltetrazolium bromide] assay. RT-112 and RT-112<sup>res</sup> cells were seeded in 96-well plates with a density of  $2.5 \times 10^3$  or  $5.0 \times 10^3$  cells per well, respectively. One day after seeding, cells were treated with prodigiosin (**1**) or derivatives **16ba–bc** for 24 or 72 h.  $5 \mu\text{M}$  staurosporine was used as a positive control and 0.1% DMSO (PanReac AppliChem, Darmstadt, Germany) was used as a solvent control. After the incubation time, thiazolyl blue was added to the cells and they were incubated at  $37^\circ\text{C}$  and 5%  $\text{CO}_2$  in a humidified atmosphere for 45 min. After removal of the MTT-containing medium,  $100 \mu\text{L}$  DMSO were added per well for extraction of the formazan. Absorbance was measured at 570 nm and 650 nm (reference) with a microplate reader (BioTek, Synergy Mx). After subtraction of the reference signal and the mean value of the positive control from each value, the mean of the absorbance of the solvent control was set as 100% and relative viability was calculated for each sample. All  $\text{IC}_{50}$  values were calculated using GraphPad Prism 7.01.

### *In vitro* assay with prodiginine ligating enzymes

Cells of *E. coli* BL21 (DE3) with the desired pET expression vector were resuspended after expression of the corresponding ligating enzyme in 50 mM potassium phosphate buffer, pH 7.0 ( $\text{KPi}$ ) to a final mass concentration of  $0.2 \text{ g mL}^{-1}$  and cooled on ice. To disrupt the cells, sonication on ice was performed (40% amplitude,  $3 \times 5$  min with 5 min rest on ice between each cycle, 0.5 s pulse and 0.5 s rest per pulse cycle).

The 1*H*-pyrroles **4a–c**, as well as the MBC derivatives **3a–g** were freshly dissolved in DMSO to a final concentration of 20 mM. For ATP, a 62.5 mM stock solution in water was prepared from the disodium salt  $\text{Na}_2\text{-ATP} \times 3 \text{ H}_2\text{O}$ .

In a 1.5 mL reaction tube,  $10 \mu\text{L}$  of 62.5 mM ATP,  $25 \mu\text{L}$  of 20 mM MBC, and  $25 \mu\text{L}$  of 20 mM pyrrole were mixed. Subsequently, the reaction was initiated by supplementation with  $440 \mu\text{L}$  of homogenous sonicated cells in  $\text{KPi}$  buffer with a concentration of  $0.20 \text{ g mL}^{-1}$  (cell debris was not removed, as the enzymes are attached to the inner membrane). After carefully inverting the tubes, the reactions were incubated at  $30^\circ\text{C}$  and 300 RPM for a total reaction time of 4 h. Afterwards, the analytical reactions were centrifuged (20 300 rcf, 20 min,  $4^\circ\text{C}$ ) and the supernatant was disposed. Depending on the further utilisation of samples, two workup procedures were used as follows.

### *In vitro* assay – workup for LC-MS measurements

The cell debris was resuspended in  $400 \mu\text{L}$  of MeOH, however, the resuspension process was assisted by an ultrasound bath. Centrifugation (20 300 rcf, 20 min,  $4^\circ\text{C}$ ) was used to remove cell debris and the supernatant transferred into a new reaction tube. MeOH was evaporated in a vacuum centrifuge at  $45^\circ\text{C}$  and the residue was taken up in  $200 \mu\text{L}$  water. Extraction with  $\text{CH}_2\text{Cl}_2$  ( $2 \times 200 \mu\text{L}$ ) and successive evaporation of the solvent provided a residue, which was dissolved in  $200 \mu\text{L}$  MeOH, filtered through a  $0.45 \mu\text{m}$  syringe filter and subjected to LC-MS chromatography.

### *In vitro* assay – workup for photographic documentation

The cell debris was resuspended in  $300 \mu\text{L}$  acidic EtOH (+ 4% 1 M HCl) and the resuspension process assisted by an ultrasound bath. Centrifugation (20 300 rcf, 20 min,  $4^\circ\text{C}$ ) was used to remove cell debris and the supernatant was then transferred into a new 1.5 mL reaction tube for documentation (ESI<sup>+</sup>).

### LC-MS parameters

Coupled LC-MS measurements were performed on a Thermo Scientific UltiMate 3000 UHPLC instrument with an Atlantis T3  $3 \mu\text{m}$ ,  $3 \times 100$  mm column (Waters) and an ISQ-ES mass spectrometer. Sample volumes of  $5 \mu\text{L}$  were injected at a temperature of  $30^\circ\text{C}$  and a flow rate of  $0.60 \text{ mL min}^{-1}$ . UV detection was realised at 535 nm via photo diode array detector. Gradient elution with MeOH + 0.1% formic acid (solvent A) and Millipore water + 0.1% formic acid (solvent B) allowed separation of prodiginines from MBC and pyrrole precursors. Elution profile:  $-5$ – $0$  min with 10% solvent A,  $0$ – $4$  min with 10–60% solvent A,  $4$ – $6$  min with 60–100% solvent A,  $6$ – $13$  min with 100% solvent A. The following parameters were used for the ISQ-MS detection – mode: positive, vaporiser temperature:  $282^\circ\text{C}$ , ITT temperature:  $300^\circ\text{C}$ , source voltage positive ions: 3000 V, source voltage negative ions:  $-2000$  V, sheath gas pressure: 49.9 psig, aux gas pressure: 5.7 psig, sweep gas pressure: 0.5 psig, mass area 10–1000, CID 20.

### Quantification of prodiginines from LC chromatograms

Based on the measured and approximated molar extinction coefficients for chemically synthesised prodiginine references, quantification of prodiginines in methanolic extracts from *in vitro* assays was performed. Therefore, eqn (1.2), devised by Torsi *et al.*, was deployed.<sup>88</sup>

$$c[\mu\text{mol mL}^{-1}] = \frac{n[\mu\text{mol}]}{V_{\text{inj}}[\mu\text{L}]} \quad (1.1)$$

with

$$n[\text{mol}] = E[\text{AU min}] \cdot F[\text{L min}^{-1}] \cdot \frac{1}{\varepsilon[\text{M}^{-1} \text{cm}^{-1}] \cdot d[\text{cm}]} \quad (1.2)$$



$c$ : prodiginine concentration in the methanolic extract  
 $n$ : amount of substance applied to chromatography  
 $V_{inj}$ : injected volume applied to chromatography  
 $E$ : integrated extinction at 535 nm  
 $F$ : chromatographic flow rate  
 $\epsilon$ : molar extinction coefficient at 535 nm  
 $d$ : flow cell path length

The UV traces at 535 nm and the extracted ion chromatograms (EIC) of the appropriate  $m/z$  ratio for the proposed products were generated from the total ion chromatograms (TIC). EIC spectra were used to validate the estimated product masses and UV absorbance at 535 nm was utilised to calculate the corresponding peak areas by integration. For quantification of prodiginines from the methanolic extracts, the mean value of absorbance from triplicates was used to determine the amount of substance that had been injected to the chromatographic system (eqn (1.2)), based on the extinction coefficients, which had been determined experimentally or by approximation. From the results of eqn (1.2), the concentrations in methanolic extracts were calculated by eqn (1.1).

## Abbreviations

Compd	Compound
LiTMP	Lithium 2,2,6,6-tetramethylpiperidide
SPhos	2-Dicyclohexylphosphino-2',6'-dimethoxybiphenyl
TFE	2,2,2-Trifluoroethanol
$t_R$	Retention time
LB	Lysogeny broth
TB	Terrific broth
KP <sub>i</sub>	Potassium phosphate
IC <sub>50</sub>	Half maximal inhibitory concentration
MTT	3-(4,5-Dimethylthiazol-2-yl)-2,5-diphenyltetrazolium bromide
o/n	Overnight

## Author contributions

Tim Moritz Weber: conceptualisation, methodology, investigation, writing – original draft, writing – review & editing, visualisation, supervision, project administration, funding acquisition; Alexandra Leyens: investigation; Lena Berning: investigation, visualisation, writing – original draft; Björn Stork: writing – review & editing, supervision, funding acquisition; Jörg Pietruszka: conceptualisation, writing – review & editing, supervision, funding acquisition, project administration.

## Conflicts of interest

There are no conflicts to declare.

## Acknowledgements

We gratefully acknowledge the Jürgen Manchot Stiftung (scholarship to T. M. W.), the Deutsche

Forschungsgemeinschaft DFG (GRK2158, project #270650915; to J. P. and B. S.) for funding as well as the Heinrich Heine University Düsseldorf and the Forschungszentrum Jülich GmbH for their ongoing support. We kindly acknowledge Birgit Henßen, Vera Ophoven, and Irene Küberl for their support in LC-MS data acquisition, chemical synthesis, and photo documentation, respectively. We thank Margaretha A. Skowron, Michèle J. Hoffmann, and Günter Niegisch (Department of Urology, Medical Faculty and University Hospital Düsseldorf, Heinrich Heine University Düsseldorf) for providing RT-112 and RT-112<sup>res</sup> cell lines.

## Notes and references

- 1 A. Fürstner, J. Grabowski and C. W. Lehmann, *J. Org. Chem.*, 1999, **64**(22), 8275–8280.
- 2 H. Rapoport and C. D. Willson, *J. Am. Chem. Soc.*, 1962, **84**(4), 630–635.
- 3 D. L. Boger and M. Patel, *J. Org. Chem.*, 1988, **53**(7), 1405–1415.
- 4 H. H. Wasserman and L. J. Lombardo, *Tetrahedron Lett.*, 1989, **30**(13), 1725–1728.
- 5 R. E. Johnson, T. de Rond, V. N. Lindsay, J. D. Keasling and R. Sarpong, *Org. Lett.*, 2015, **17**(14), 3474–3477.
- 6 H. H. Wasserman, G. C. Rodgers and D. D. Keith, *J. Am. Chem. Soc.*, 1969, **91**(5), 1263–1264.
- 7 M. D. Clift and R. J. Thomson, *J. Am. Chem. Soc.*, 2009, **131**(40), 14579–14583.
- 8 A. Fürstner, K. Radkowski and H. Peters, *Angew. Chem., Int. Ed.*, 2005, **44**(18), 2777–2781.
- 9 A. Fürstner and H. Weintritt, *J. Am. Chem. Soc.*, 1998, **120**(12), 2817–2825.
- 10 J. H. Frederich and P. G. Harran, *J. Am. Chem. Soc.*, 2013, **135**(10), 3788–3791.
- 11 A. Fürstner, *Angew. Chem., Int. Ed.*, 2003, **42**(31), 3582–3603.
- 12 S. A. Parikh, H. Kantarjian, A. Schimmer, W. Walsh, E. Asatiani, K. El-Shami, E. Winton and S. Verstovsek, *Clin. Lymphoma, Myeloma Leuk.*, 2010, **10**(4), 285–289.
- 13 A. D. Schimmer, S. O'Brien, H. Kantarjian, J. Brandwein, B. D. Cheson, M. D. Minden, K. Yee, F. Ravandi, F. Giles and A. Schuh, *Clin. Cancer Res.*, 2008, **14**(24), 8295–8301.
- 14 A. Fürstner and E. J. Grabowski, *ChemBioChem*, 2001, **2**(9), 706–709.
- 15 M. S. Melvin, M. W. Calcutt, R. E. Nofle and R. A. Manderville, *Chem. Res. Toxicol.*, 2002, **15**(5), 742–748.
- 16 M. S. Melvin, J. T. Tomlinson, G. R. Saluta, G. L. Kucera, N. Lindquist and R. A. Manderville, *J. Am. Chem. Soc.*, 2000, **122**(26), 6333–6334.
- 17 M. S. Melvin, K. E. Wooton, C. C. Rich, G. R. Saluta, G. L. Kucera, N. Lindquist and R. A. Manderville, *J. Inorg. Biochem.*, 2001, **87**(3), 129–135.
- 18 H. Konno, H. Matsuya, M. Okamoto, T. Sato, Y. Tanaka, K. Yokoyama, T. Kataoka, K. Nagai, H. H. Wasserman and S. Ohkuma, *J. Biochem.*, 1998, **124**(3), 547–556.
- 19 H. Matsuya, M. Okamoto, T. Ochi, A. Nishikawa, S. Shimizu, T. Kataoka, K. Nagai, H. H. Wasserman and S. Ohkuma, *Biochem. Pharmacol.*, 2000, **60**(12), 1855–1863.



- 20 S. Ohkuma, T. Sato, M. Okamoto, H. Matsuya, K. Arai, T. Kataoka, K. Nagai and H. H. Wasserman, *Biochem. J.*, 1998, **334**(3), 731–741.
- 21 T. Sato, H. Konno, Y. Tanaka, T. Kataoka, K. Nagai, H. H. Wasserman and S. Ohkuma, *J. Biol. Chem.*, 1998, **273**(34), 21455–21462.
- 22 T. Kataoka, M. Muroi, S. Ohkuma, T. Waritani, J. Magae, A. Takatsuki, S. Kondo, M. Yamasaki and K. Nagai, *FEBS Lett.*, 1995, **359**(1), 53–59.
- 23 S. S. Habash, H. U. Brass, A. S. Klein, D. P. Klebl, T. M. Weber, T. Classen, J. Pietruszka, F. M. Grundler and A. S. S. Schleker, *Front. Plant Sci.*, 2020, **11**, 579807.
- 24 J. Lapenda, P. Silva, M. Vicalvi, K. Sena and S. Nascimento, *World J. Microbiol. Biotechnol.*, 2015, **31**, 399–406.
- 25 D. C. Woodhams, B. C. LaBumbard, K. L. Barnhart, M. H. Becker, M. C. Bletz, L. A. Escobar, S. V. Flechas, M. E. Forman, A. A. Iannetta and M. D. Joyce, *Microb. Ecol.*, 2018, **75**, 1049–1062.
- 26 W. McRary, E. Beaver and E. Noble, *Exp. Parasitol.*, 1953, **2**(2), 125–128.
- 27 H.-S. Kim, M. Hayashi, Y. Shibata, Y. Wataya, T. Mitamura, T. Horii, K. Kawauchi, H. Hirata, S. Tsuboi and Y. Moriyama, *Biol. Pharm. Bull.*, 1999, **22**(5), 532–534.
- 28 J. Lazaro, J. Nitchau, R. Z. Predicala, G. C. Mangalindan, F. Nesslany, D. Marzin, G. P. Concepcion and B. Diquet, *Nat. Toxins*, 2002, **11**(4), 367–377.
- 29 M. Isaka, A. Jaturapat, J. Kramyu, M. Tanticharoen and Y. Thebtaranonth, *Antimicrob. Agents Chemother.*, 2002, **46**(4), 1112–1113.
- 30 L. Berning, D. Schlütermann, A. Friedrich, N. Berleth, Y. Sun, W. Wu, M. J. Mendiburo, J. Deitersen, H. U. Brass, M. A. Skowron, M. J. Hoffmann, G. Niegisch, J. Pietruszka and B. Stork, *Molecules*, 2021, **26**(5), 1294.
- 31 C. Yamamoto, H. Takemoto, K. Kuno, D. Yamamoto, A. Tsubura, K. Kamata, H. Hirata, A. Yamamoto, H. Kano and T. Seki, *Hepatology*, 1999, **30**(4), 894–902.
- 32 D. Yamamoto, Y. Kiyozuka, Y. Uemura, C. Yamamoto, H. Takemoto, H. Hirata, K. Tanaka, K. Hioki and A. Tsubura, *J. Cancer Res. Clin. Oncol.*, 2000, **126**, 191–197.
- 33 B. Montaner, S. Navarro, M. Piqué, M. Vilaseca, M. Martinell, E. Giral, J. Gil and R. Pérez-Tomás, *Br. J. Pharmacol.*, 2000, **131**(3), 585–593.
- 34 B. Montaner and R. Pérez-Tomás, *Life Sci.*, 2001, **68**(17), 2025–2036.
- 35 A. K. Harris, N. R. Williamson, H. Slater, A. Cox, S. Abbasi, I. Foulds, H. T. Simonsen, F. J. Leeper and G. P. Salmond, *Microbiology*, 2004, **150**(11), 3547–3560.
- 36 A. M. Cerdeño, M. J. Bibb and G. L. Challis, *Chem. Biol.*, 2001, **8**(8), 817–829.
- 37 K. J. Picott, J. A. Deichert, E. M. deKemp, G. Schatte, F. Sauriol and A. C. Ross, *MedChemComm*, 2019, **10**(3), 478–483.
- 38 S. M. Salem, P. Kancharla, G. Florova, S. Gupta, W. Lu and K. A. Reynolds, *J. Am. Chem. Soc.*, 2014, **136**(12), 4565–4574.
- 39 X. Wang, T. Isbrandt, E. Ø. Christensen, J. Melchiorson, T. O. Larsen, S.-D. Zhang and L. Gram, *Microbiol. Spectrum*, 2021, **9**(2), e01171-21.
- 40 N. L. Grenade, D. S. Chiriac, A. O. Pasternak, J. L. Babulic, B. E. Rowland, G. W. Howe and A. C. Ross, *ACS Chem. Biol.*, 2023, **18**(2), 223–229.
- 41 N. R. Williamson, H. T. Simonsen, R. A. Ahmed, G. Goldet, H. Slater, L. Woodley, F. J. Leeper and G. P. Salmond, *Mol. Microbiol.*, 2005, **56**(4), 971–989.
- 42 E. Coco, K. Narva and J. Feitelson, *Mol. Genet. Genomics*, 1991, **227**, 28–32.
- 43 M. J. Jaremko, T. D. Davis, J. C. Corpuz and M. D. Burkart, *Nat. Prod. Rep.*, 2020, **37**(3), 355–379.
- 44 H. Wasserman, C. Shaw, R. Sykes and R. Cushley, *Tetrahedron Lett.*, 1974, **15**(33), 2787–2790.
- 45 H. Wasserman, R. Sykes, P. Peverada, C. Shaw, R. Cushley and S. Lipsky, *J. Am. Chem. Soc.*, 1973, **95**(20), 6874–6875.
- 46 S. R. Chawrai, N. R. Williamson, G. P. Salmond and F. J. Leeper, *Chem. Commun.*, 2008, 1862–1864.
- 47 D. X. Hu, D. M. Withall, G. L. Challis and R. J. Thomson, *Chem. Rev.*, 2016, **116**(14), 7818–7853.
- 48 Z. You, X. Liu, S. Zhang and Y. Wang, *Biochem. Eng. J.*, 2018, **134**, 1–11.
- 49 S. Brands, H. U. Brass, A. S. Klein, J. G. Sikkens, M. D. Davari, J. Pietruszka, A. J. Ruff and U. Schwaneberg, *Catal. Sci. Technol.*, 2021, **11**(8), 2805–2815.
- 50 K. J. Picott, J. A. Deichert, E. M. DeKemp, V. Snieckus and A. C. Ross, *ChemBioChem*, 2020, **21**(7), 1036–1042.
- 51 D. Fehér, R. S. Barlow, P. S. Lorenzo and T. K. Hemscheidt, *J. Nat. Prod.*, 2008, **71**(11), 1970–1972.
- 52 D. M. Withall, S. W. Haynes and G. L. Challis, *J. Am. Chem. Soc.*, 2015, **137**(24), 7889–7897.
- 53 C. Perry, E. L. De los Santos, L. M. Alkhalaf and G. L. Challis, *Nat. Prod. Rep.*, 2018, **35**(7), 622–632.
- 54 A. E. Silva, L. A. Guimarães, E. G. Ferreira, M. d. C. M. Torres, A. B. d. Silva, P. C. Branco, F. A. S. Oliveira, G. G. Silva, D. V. Wilke and E. R. Silveira, *J. Braz. Chem. Soc.*, 2017, **28**, 465–474.
- 55 F. E. Sakai-Kawada, C. G. Ip, K. A. Hagiwara and J. D. Awaya, *Front. Microbiol.*, 2019, **10**, 1715.
- 56 P. C. Dorrestein, E. Yeh, S. Garneau-Tsodikova, N. L. Kelleher and C. T. Walsh, *Proc. Natl. Acad. Sci. U. S. A.*, 2005, **102**(39), 13843–13848.
- 57 A. S. Klein, A. Domröse, P. Bongen, H. U. Brass, T. Classen, A. Loeschcke, T. Drepper, L. Laraia, S. Sievers and K.-E. Jaeger, *ACS Synth. Biol.*, 2017, **6**(9), 1757–1765.
- 58 A. S. Klein, H. U. C. Brass, D. P. Klebl, T. Classen, A. Loeschcke, T. Drepper, S. Sievers, K. E. Jaeger and J. Pietruszka, *ChemBioChem*, 2018, **19**(14), 1545–1552.
- 59 H. U. Brass, A. S. Klein, S. Nyholt, T. Classen and J. Pietruszka, *Adv. Synth. Catal.*, 2019, **361**(11), 2659–2667.
- 60 S. W. Haynes, P. K. Sydor, A. E. Stanley, L. Song and G. L. Challis, *Chem. Commun.*, 2008, 1865–1867.
- 61 R. D'Alessio, A. Bargiotti, O. Carlini, F. Colotta, M. Ferrari, P. Gnocchi, A. Isetta, N. Mongelli, P. Motta and A. Rossi, *J. Med. Chem.*, 2000, **43**(13), 2557–2565.
- 62 U. V. Santer and H. J. Vogel, *Biochim. Biophys. Acta*, 1956, **19**(3), 578–579.



- 63 H. H. Wasserman, J. E. McKeon and U. V. Santer, *Biochem. Biophys. Res. Commun.*, 1960, **3**(2), 146–149.
- 64 B. Trofimov, A. Mikhaleva, A. Vasil'ev, S. Korostova and S. Shevchenko, *Chem. Heterocycl. Compd.*, 1985, **21**, 46–49.
- 65 K. Dairi, S. Tripathy, G. Attardo and J.-F. Lavallée, *Tetrahedron Lett.*, 2006, **47**(15), 2605–2606.
- 66 T. Ono, D. Koga and Y. Hisaeda, *Chem. Lett.*, 2017, **46**(2), 260–262.
- 67 For the early steps in the synthesis of MBC derivatives (Fig. 3 and 4), the letter **a** was left out for acid chlorides, acyl pyrroles, alkyl pyrroles, Boc-protected alkyl pyrroles and Boc-protected pyrrole-2-boronic acids. As unsubstituted MBC **3a** was synthesised by a different route (supporting information), omission allows systematic description and significantly enhances readability of the manuscript.
- 68 A. J. Lennox and G. C. Lloyd-Jones, *Chem. Soc. Rev.*, 2014, **43**(1), 412–443.
- 69 D. M. Knapp, E. P. Gillis and M. D. Burke, *J. Am. Chem. Soc.*, 2009, **131**(20), 6961–6963.
- 70 R. Hubbard and C. Rimington, *Biochem. J.*, 1950, **46**(2), 220.
- 71 A. Domröse, A. S. Klein, J. Hage-Hülsmann, S. Thies, V. Svensson, T. Classen, J. Pietruszka, K.-E. Jaeger, T. Drepper and A. Loeschcke, *Front. Microbiol.*, 2015, **6**, 972.
- 72 D. Schlütermann, M. A. Skowron, N. Berleth, P. Böhler, J. Deitersen, F. Stuhldreier, N. Wallot-Hieke, W. Wu, C. Peter and M. J. Hoffmann, *Urol. Oncol.: Semin. Orig. Invest.*, 2018, **36**(4), 160.
- 73 M. A. Skowron, P. Petzsch, K. Hardt, N. Wagner, M. Beier, S. Stepanow, M. Drechsler, H. Rieder, K. Köhrer and G. Niegisch, *Sci. Rep.*, 2019, **9**(1), 14476.
- 74 M. A. Skowron, G. Niegisch, G. Fritz, T. Arent, J. G. van Roermund, A. Romano, P. Albers, W. A. Schulz and M. J. Hoffmann, *J. Exp. Clin. Cancer Res.*, 2015, **34**(1), 1–15.
- 75 K. Ma, S. Li, X. Huo, M. Guo, X. Du, C. Li, X. Liu, J. Lv and Z. Chen, *Biochem. Biophys. Res. Commun.*, 2020, **533**(3), 474–480.
- 76 M. A. Skowron, M. Melnikova, J. G. Van Roermund, A. Romano, P. Albers, J. Thomale, W. A. Schulz, G. Niegisch and M. J. Hoffmann, *Int. J. Mol. Sci.*, 2018, **19**(2), 590.
- 77 S.-H. Chen and J.-Y. Chang, *Int. J. Mol. Sci.*, 2019, **20**(17), 4136–4156.
- 78 R. M. Drayton and J. W. Catto, *Expert Rev. Anticancer Ther.*, 2012, **12**(2), 271–281.
- 79 S. M. O'Brien, D. F. Claxton, M. Crump, S. Faderl, T. Kipps, M. J. Keating, J. Viallet and B. D. Cheson, *Blood*, 2009, **113**(2), 299–305.
- 80 A. D. Schimmer, A. Raza, T. H. Carter, D. Claxton, H. Erba, D. J. DeAngelo, M. S. Tallman, C. Goard and G. Borthakur, *PLoS One*, 2014, **9**(10), e108694.
- 81 F. McCoy, J. Hurwitz, N. McTavish, I. Paul, C. Barnes, B. O'Hagan, K. Odrzywol, J. Murray, D. Longley and G. McKerr, *Cell Death Dis.*, 2010, **1**(12), e108–e108.
- 82 B. C. Koehler, A. Jassowicz, A.-L. Scherr, S. Lorenz, P. Radhakrishnan, N. Kautz, C. Elssner, J. Weiss, D. Jaeger and M. Schneider, *BMC Cancer*, 2015, **15**, 1–11.
- 83 S. Ji, R. Sun, K. Xu, Z. Man, J. Ji, Y. Pu, L. Yin, J. Zhang and Y. Pu, *Toxicol. In Vitro*, 2019, **60**, 107–115.
- 84 W. Castillo-Ávila, M. Abal, S. Robine and R. Pérez-Tomás, *Life Sci.*, 2005, **78**(2), 121–127.
- 85 X. Mo, T. D. Morgan, H. T. Ang and D. G. Hall, *J. Am. Chem. Soc.*, 2018, **140**(15), 5264–5271.
- 86 X.-C. Cai and B. B. Snider, *J. Org. Chem.*, 2013, **78**(23), 12161–12175.
- 87 D. L. Boger and M. Patel, *Tetrahedron Lett.*, 1987, **28**(22), 2499–2502.
- 88 G. Torsi, G. Chiavari, C. Laghi, A. Asmundsdottir, F. Fagioli and R. Vecchietti, *J. Chromatogr. A*, 1989, **482**(1), 207–214.



## Publication 3

### **The Golgi stacking protein GRASP55 is targeted by the natural compound prodigiosin**

Lena Berning, Thomas Lenz, Ann Kathrin Bergmann, Gereon Poschmann, Hannah U. C. Brass, David Schlütermann, Annabelle Friedrich, María José Mendiburo, Céline David, Seda Akgün, Jörg Pietruszka, Kai Stühler, Björn Stork

*Cell Communication and Signaling, Volume 21, Issue 1, 275, October 2023*

*DOI: 10.1186/s12964-023-01275-1*

RESEARCH

Open Access



# The Golgi stacking protein GRASP55 is targeted by the natural compound prodigiosin

Lena Berning<sup>1</sup>, Thomas Lenz<sup>2</sup>, Ann Kathrin Bergmann<sup>3</sup>, Gereon Poschmann<sup>4</sup>, Hannah U. C. Brass<sup>5</sup>, David Schlöter<sup>1</sup>, Annabelle Friedrich<sup>1</sup>, Marla JosÉ Mendiburo<sup>1</sup>, Céline David<sup>1</sup>, Seda Akgün<sup>1</sup>, Jörg Pietruszka<sup>5,6</sup>, Kai Stähler<sup>2,4</sup> and Björn Stork<sup>1\*</sup>

## Abstract

**Background** The bacterial secondary metabolite prodigiosin has been shown to exert anticancer, antimalarial, antibacterial and immunomodulatory properties. With regard to cancer, it has been reported to affect cancer cells but not non-malignant cells, rendering prodigiosin a promising lead compound for anticancer drug discovery. However, a direct protein target has not yet been experimentally identified.

**Methods** We used mass spectrometry-based thermal proteome profiling in order to identify target proteins of prodigiosin. For target validation, we employed a genetic knockout approach and electron microscopy.

**Results** We identified the Golgi stacking protein GRASP55 as target protein of prodigiosin. We show that prodigiosin treatment severely affects Golgi morphology and functionality, and that prodigiosin-dependent cytotoxicity is partially reduced in GRASP55 knockout cells. We also found that prodigiosin treatment results in decreased cathepsin activity and overall blocks autophagic flux, whereas co-localization of the autophagosomal marker LC3 and the lysosomal marker LAMP1 is clearly promoted. Finally, we observed that autophagosomes accumulate at GRASP55-positive structures, pointing towards an involvement of an altered Golgi function in the autophagy-inhibitory effect of this natural compound.

**Conclusion** Taken together, we propose that prodigiosin affects autophagy and Golgi apparatus integrity in an inter-linked mode of action involving the regulation of organelle alkalization and the Golgi stacking protein GRASP55.

**Keywords** Prodigiosin, Golgi apparatus, Natural compound, Autophagy, Target identification

\*Correspondence:

Björn Stork  
bjoern.stork@hhu.de

<sup>1</sup> Institute of Molecular Medicine I, Medical Faculty and University Hospital D, sseldorf, Heinrich Heine University, D, sseldorf 40225, Germany

<sup>2</sup> Molecular Proteomics Laboratory, Biological Medical Research Centre, Heinrich Heine University, 40225 D, sseldorf, Germany

<sup>3</sup> Core Facility for Electron Microscopy, Medical Faculty and University Hospital D, sseldorf, Heinrich Heine University, D, sseldorf 40225, Germany

<sup>4</sup> Institute of Molecular Medicine I, Proteome Research, Medical Faculty and University Hospital D, sseldorf, Heinrich Heine University, D, sseldorf 40225, Germany

<sup>5</sup> Institute of Bioorganic Chemistry, Heinrich Heine University D, sseldorf at Forschungszentrum J, lich and Bioeconomy Science Center (BioSC), 52426 J, lich, Germany

<sup>6</sup> Institute of Bio- and Geosciences: Biotechnology (IBG-1), Forschungszentrum J, lich, 52428 J, lich, Germany



© The Author(s) 2023. **Open Access** This article is licensed under a Creative Commons Attribution 4.0 International License, which permits use, sharing, adaptation, distribution and reproduction in any medium or format, as long as you give appropriate credit to the original author(s) and the source, provide a link to the Creative Commons licence, and indicate if changes were made. The images or other third party material in this article are included in the article's Creative Commons licence, unless indicated otherwise in a credit line to the material. If material is not included in the article's Creative Commons licence and your intended use is not permitted by statutory regulation or exceeds the permitted use, you will need to obtain permission directly from the copyright holder. To view a copy of this licence, visit <http://creativecommons.org/licenses/by/4.0/>. The Creative Commons Public Domain Dedication waiver (<http://creativecommons.org/publicdomain/zero/1.0/>) applies to the data made available in this article, unless otherwise stated in a credit line to the data.

## Background

Historically, natural products have played a key role in drug discovery. Especially for cancer and infectious diseases, nature-derived compounds make up a considerable proportion of medication [52]. Stimulated by evolutionary pressure, plants, fungi and microorganisms can produce an almost inexhaustible diversity of bioactive compounds. These compounds often display a complex structure and stereochemistry, which— in some cases— can hardly be mimicked by synthetic approaches [12]. However, natural compounds have their pitfalls when it comes to disposability, purity, and bioavailability. To overcome these drawbacks, semi-synthetic approaches allowed by advances in genomics, bioinformatics and replicating synthesis have been deployed. Natural products can target miscellaneous molecular pathways in eukaryotic cells and though various methods for target identification have been developed in the previous decades, it remains challenging to identify the molecular targets of these often highly bioactive metabolites due to widely varied mechanisms of action and diverse and often multiple targets [9]. Knowing the mechanisms of action of natural products can pave the way to the discovery of new targets and cellular pathways with high specificity towards cancerous cells in order to fulfil the enormous need for new therapeutic options caused by therapeutic failure as a result of drug resistance or relapse.

In recent years, the natural compound prodigiosin has been shown to exert promising biomedical activities. It is a deeply red secondary metabolite with a tripyrrole structure (reviewed in [22, 27]). Although 'optically' known for centuries, prodigiosin was first extracted from *Serratia marcescens* by Wrede and Hettche in 1929 [75], followed by partial and total syntheses in the 1960s [60, 73]. In addition to the extraction from various bacterial strains, prodigiosin and its analogues can be produced via semi-synthetic and synthetic approaches [20, 35, 36, 45, 79]. Prodigiosin has been shown to possess various beneficial effects like anticancer [74], antimalarial [8] and antimicrobial [13] properties. The anticancer properties of this natural compound have so far been linked to the modulation of autophagy [10, 35, 36], lysosomal activity [82] or apoptosis [30]. Mechanistically, prodigiosin has been described as an  $H^+/Cl^-$  symporter, which can lead to an alkalization of acidic organelles such as endosomes, lysosomes or the Golgi apparatus by uncoupling the vacuolar-type  $H^+$ -ATPase (V-ATPase) [61, 63].

The Golgi apparatus is an essential organelle located in the perinuclear region of mammalian cells [39]. As a receiver of the majority of the endoplasmic reticulum (ER) output, the Golgi apparatus acts as the central hub for post-translational modifications and sorting of

proteins and lipids for the secretory pathway [5]. For its proper functioning, the Golgi is organized in stacks of flattened cisternae that are often laterally linked into a ribbon-like structure. The only proteins that have been shown to be responsible for establishing the stacked structure of the Golgi so far are the Golgi reassembly stacking proteins of 55 kDa (GRASP55, primary gene name: GORASP2) and of 65 kDa (GRASP65, primary gene name: GORASP1), which are localized to the *trans* and *cis* cisternae, respectively [4, 64]. These GRASP proteins are peripheral membrane proteins which form trans-oligomers from adjacent cisternae to link the Golgi stacks into a ribbon [58, 71, 76]. In addition to its role in Golgi stacking, GRASP55 has been previously described to be involved in unconventional secretion [1, 53] and autophagy [43, 80, 81].

Autophagy is an intracellular catabolic process in which misfolded, damaged or aggregated proteins as well as whole cell organelles can be degraded and recycled (reviewed in [18, 78]). Late stage autophagy is dependent on autophagosome-lysosome fusion and the hydrolase activity of lysosomal enzymes for the breakdown of the autophagic cargo. The above described alkalization of lysosomes and the resulting inhibition of pH-dependent lysosomal hydrolases likely represent one mechanism of prodigiosin-mediated autophagy inhibition. In addition to the alkalization of lysosomes, prodigiosin has previously been described to block the fusion of autophagosome and lysosome [82]. The potent autophagy-inhibitory property of prodigiosin has also been reported in a previous work from our groups, in which we observed that prodigiosin re-sensitized cisplatin-resistant cells to apoptotic cell death [6]. Furthermore, prodigiosin derivatives have been identified that displayed more potent autophagy inhibitory activity than the parent compound or the synthetic derivative obato-clax [35, 36]. However, no molecular target of prodigiosin has been identified so far.

A commonly used technique for target engagement is the cellular thermal shift assay (CETSA) which is based on the principle of thermal stabilization of an intracellular protein when it is bound to a small molecule [29, 46]. The temperature at which denaturation and irreversible precipitation of a protein occurs within thermally treated cells can be shifted by complexation with a ligand and the non-denatured, soluble protein fraction can then be investigated by immunoblotting. A huge advantage of this method is the possibility to assess drug-protein interactions under physiological conditions in living cells without labelling or immobilization of the compound or the protein of interest. To analyze several thousands of proteins in an unbiased approach, CETSA can be combined with multiplexed quantitative MS analysis. This approach

for identifying novel protein targets of small molecules in living cells has been termed thermal proteome profiling (TPP) [21, 62]. Recently, the TPP technique has been extended so that, in addition to protein thermal stability alteration, differences in protein abundance can also be detected in the same experiment, termed ratio-based thermal shift assay analysis (RTSA) [33].

In this study, we used the TPP/RTSA approach to identify protein targets and other affected proteins of the natural compound prodigiosin. We found that prodigiosin thermally stabilizes the Golgi protein GRASP55, affects lysosomal proteins as well as proteins involved in autophagy, and that prodigiosin treatment severely alters the structure of the Golgi apparatus while the knockout of GRASP55 partly reverses prodigiosin cytotoxicity. We also observed that autophagosomes accumulate at the

Golgi apparatus while overall autophagic flux is inhibited in cells treated with prodigiosin. Thus, we propose GRASP55 as a target protein of prodigiosin.

## Results

### Prodigiosin exhibits cytotoxic properties in HeLa cells and alters Golgi apparatus morphology

Prodigiosin (Fig. 1A) has been shown to exert cytotoxic effects in various cancer cell lines [6, 30, 42]. In HeLa cells, prodigiosin was confirmed to be highly cytotoxic with  $IC_{50}$  values in the nanomolar range both after 24 h and 72 h (Fig. 1B). Aiming to identify the molecular mechanism of prodigiosin cytotoxicity, we examined if we could observe structural changes in cell morphology after prodigiosin treatment through transmission electron microscopy (TEM). We chose 10 and 100 nM

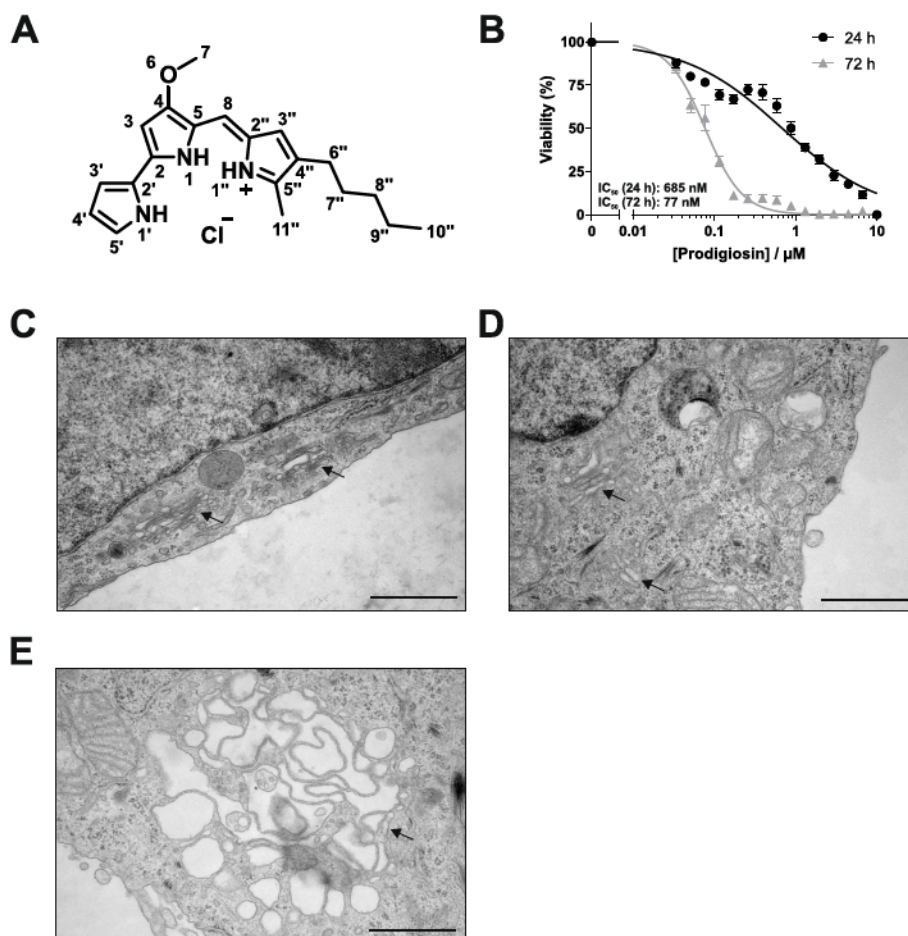


**Fig. 1** Prodigiosin exhibits cytotoxic properties in HeLa wt cells and alters Golgi apparatus morphology. **A** Chemical structure of prodigiosin. **B** HeLa wt cells were treated with different concentrations of prodigiosin for 24 h or 72 h. After treatment, cell viability was measured using a thiazolyl blue (MTT) assay. Results are shown as the mean  $\pm$  SEM of three independent experiments performed in triplicates for each treatment. HeLa wt cells were treated with **C** DMSO, **D** 10 nM or **E** 100 nM prodigiosin for 24 h and effects on cell morphology were investigated by transmission electron microscopy. Arrows indicate changes in Golgi apparatus morphology after prodigiosin treatment. Representative electron micrographs are shown. Scale bar: 1  $\mu$ m

prodigiosin and a treatment duration of 24 h, since cells remained mostly viable under these conditions. While we observed distinct Golgi stacks with multiple long and thin cisternae in vehicle (DMSO) treated cells (Fig. 1C), cisternae number and length decreased and cisternae were more voluminous upon treatment with 10 nM prodigiosin (Fig. 1D). After treatment with 100 nM prodigiosin, we observed a distinct swelling of the Golgi apparatus (Fig. 1E).

To further examine potential prodigiosin effects on Golgi apparatus structure and function, we utilized the brefeldin A (BFA) washout assay. The fungal metabolite BFA inhibits ER to Golgi transport and causes Golgi disassembly and a reversible redistribution of Golgi cisternae into the ER [34]. The effects of BFA treatment can be

reversed by removing the drug and allowing the Golgi apparatus to reassemble its structure. For the BFA washout experiment, HeLa cells were pre-treated with DMSO as a control or with 10 or 100 nM prodigiosin. Then, Golgi apparatus structure was disassembled by 2 h treatment with BFA. To monitor Golgi reassembly during BFA washout, we immunostained for the Golgi membrane protein *trans*-Golgi network glycoprotein 46 (TGN46) and the Golgi enzyme  $\beta$ -1,4-galactosyltransferase 1 (B4GALT1) (Fig. 2A) and quantified average size and number of stained structures (Fig. 2B-E). After incubation with BFA, normal Golgi structures (as determined by TGN46 or B4GALT1 staining) completely disappeared, and small structures with weak fluorescence signal were observed homogeneously distributed over the cell. In cells

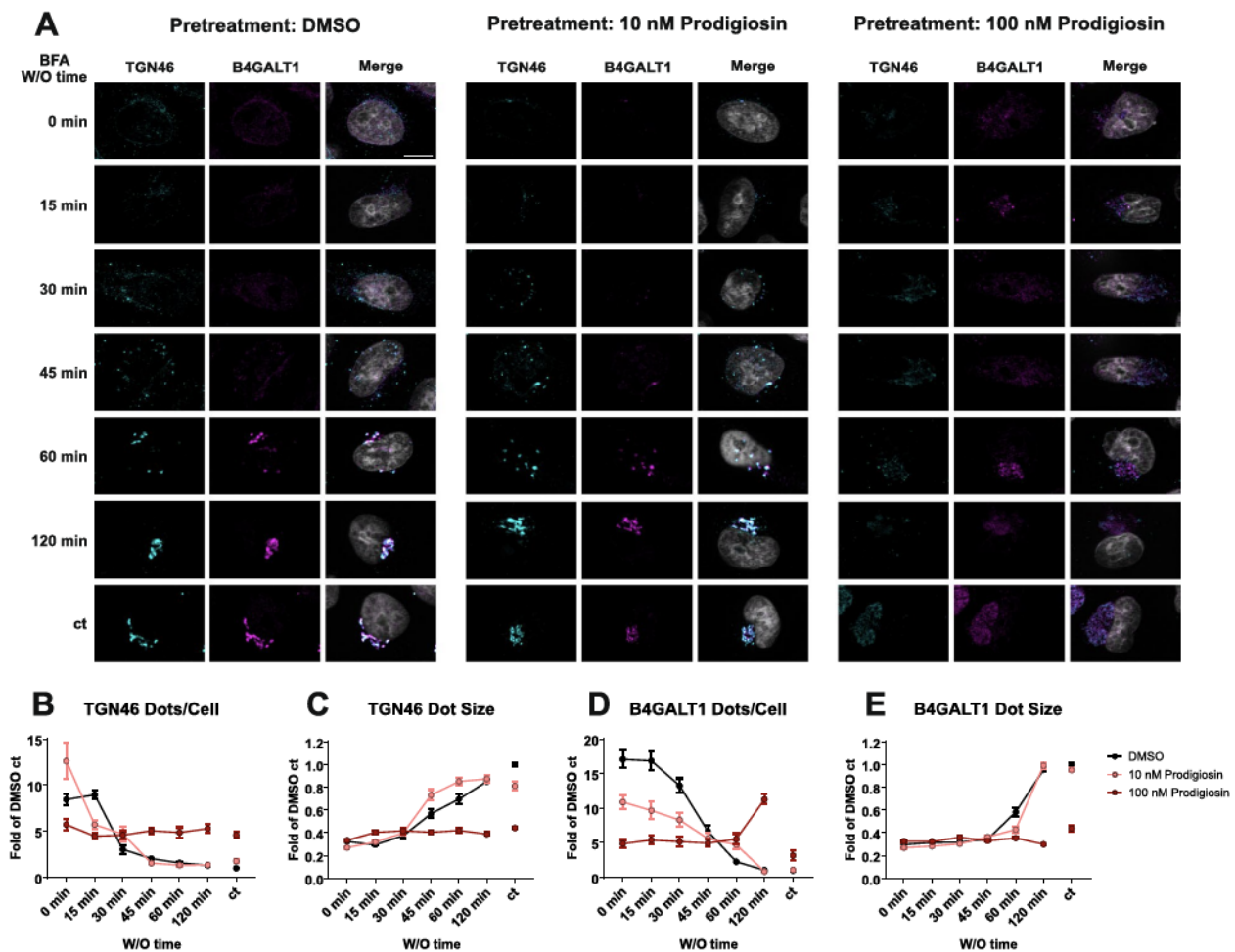


**Fig. 2** Pre-treatment with prodigiosin impairs Golgi apparatus reassembly after BFA treatment. HeLa wt cells were seeded on cover slips. On the next day, cells were treated with DMSO, 10 nM prodigiosin or 100 nM prodigiosin for 24 h. Cells were washed once and treated with 5  $\mu$ g/mL brefeldin A (BFA) or DMSO (ct) for 2 h. BFA was washed out with DPBS 4 times and cells were incubated in fresh growth medium to wash out (W/O) BFA for 0/15/30/45/60/120 min. After treatment, cover slips were prepared for microscopy. **A** Representative sections are depicted. Scale bar: 10  $\mu$ m. **B-E** The relative number per cell and mean area of TGN46 and B4GALT1 positive structures of 15 representative images from three biological replicates for each treatment were quantified using ImageJ 1.53c

pre-treated with DMSO or 10 nM prodigiosin, TGN46 structures started to reform 30 min after onset of Golgi regeneration. During ongoing BFA washout, less (Fig. 2B) but bigger (Fig. 2C) TGN46-positive structures rebuilt under these two conditions, representing the reassembly of the Golgi apparatus. After 120 min washout, TGN46 dot size, number and localization were similar to cells that had not been treated with BFA (cf. Fig. 2B and C). In contrast, no changes in dot size or number for TGN46 were observed during BFA washout in cells pre-treated with 100 nM prodigiosin (Fig. 2B and C). Directly after Golgi disassembly, cells pre-treated with 100 nM prodigiosin had less dots than cells pre-treated with DMSO, and the overall dot number remained constant over the 120 min period. Furthermore, no reassembly of larger structures was observed in cells pre-treated with 100 nM prodigiosin even after 120 min washout time, suggesting a severely disturbed Golgi reassembly. Similarly, in cells that were not exposed to BFA the typical dense perinuclear staining was not found, but instead a diffuse and more dispersed staining in the perinuclear region. Essentially, similar observations were made for the second marker protein, B4GALT1 (Fig. 2D and E): a decrease of dot number and an increase in dot size over time for cells pre-treated with DMSO or 10 nM prodigiosin indicating a fully reformed Golgi complex, but a rather constant number and size of dots in cells pre-treated with 100 nM prodigiosin (please note that the dot number even increased after 120 min of BFA washout). Taken together, we observed clear effects on Golgi structure and reassembly upon prodigiosin treatment.

### Thermal proteome profiling identifies GRASP55 as a target protein of prodigiosin

Taking these immense effects on the Golgi apparatus into account, we next aimed to identify the molecular target of

prodigiosin to elucidate the mechanism of action of this potent natural compound. We chose the TPP approach [62] due to its ability for target protein identification and engagement in an unperturbed live cell system using non-derivatized prodigiosin (Fig. S1). TPP is based on the principle of thermal stabilization (or less frequently destabilization) of a protein when bound to a small molecule (or other ligands), resulting in altered protein melting characteristics, and exploits the differential protein denaturation and irreversible precipitation in the bound and unbound state upon thermal treatment. In complement to identify prodigiosin-induced thermal stability alternation of proteins, as is done with the classical TPP setup, we chose an experimental setup similar to that described [33], which allowed us to detect prodigiosin-affected differential protein abundance (e.g., by differential protein expression, degradation or secretion) as well.

For prodigiosin-treated (100 nM, 6 h) HeLa cells, prodigiosin-affected differential melting (recorded at ten distinct temperature points in the range between  $36.5 \pm 67^\circ\text{C}$ ) and abundance data were obtained for 2480 proteins selected according to the data quality criteria of the RTSA software [33] (Supplementary Table S1). Among the prodigiosin-affected proteins (38 with positive and 55 with negative RTSA distance score) determined by the RTSA analysis (Fig. 3A; combined thermal stability and abundance effect), GRASP55 was the statistically most significant thermally stabilized protein (Fig. 3B), suggesting a direct (or indirect) prodigiosin interaction. No effect of prodigiosin on GRASP55 abundance was observed (Fig. 3C), indicating that prodigiosin does not affect GRASP55 expression levels (at 100 nM within 6 h). Melting curves for GRASP55 showing these prodigiosin effects (thermal stabilization without abundance alternation) are given in Fig. 3D. As described for the CETSA assay [29], we also quantified the non-denatured fraction

(See figure on next page.)

**Fig. 3** Thermal proteome profiling (TPP) for the identification of prodigiosin targets and prodigiosin-affected proteins: GRASP55 is thermally stabilized by treatment with prodigiosin. **A** RTSA analysis plot of the statistical significance vs. the extent of the effect of prodigiosin on protein intensity collated over the different temperatures. Differential protein intensities may result from prodigiosin-mediated thermal protein stability alternation and/or a change in protein abundance (caused by, e.g., differential protein expression, degradation or secretion), where these two effects cannot be distinguished in the current plot. Significant proteins given by the RTSA software are colored in green or red for positive or negative RTSA distance score, respectively. **B** Volcano-like plot of the statistical significance vs. the extent of prodigiosin-mediated thermal protein stabilization (mean  $\Delta T_m > 0$ ) or destabilization (mean  $\Delta T_m < 0$ ). The color code refers to significant proteins by RTSA (see panel A). GRASP55 is the RTSA significant protein with the highest statistical significance among the stabilized proteins and, thus, a highly promising prodigiosin target protein candidate. **C** Volcano-like plot of the statistical significance vs. the extent of prodigiosin-mediated change in protein abundance (higher or lower for mean  $\log_2$  ratio  $> 0$  or  $< 0$ , respectively) calculated from protein intensities at  $36.5^\circ\text{C}$ . The color code refers to significant proteins by RTSA (see panel A). **D** Melting curves (solid lines) of GRASP55 from prodigiosin or DMSO treated cells (RTSA software output of TPP-TR analysis). Datapoints and whiskers represent the arithmetic mean  $\pm$  SD of three replicates. Datapoints for temperatures showing significant intensity differences are dash-boxed, next to which the collation ratio and (uncorrected) p-value are given. The thermal stabilization of GRASP55 by prodigiosin (with a mean melting point difference of  $2.1^\circ\text{C}$ ) is indicated by dashed lines and a measure for statistical significance is provided ( $-\lg(p)$ , same as y-axis of panel B). **E** Immunoblotting for GRASP55 protein quantification from the non-denatured protein fractions of prodigiosin or DMSO treated HeLa cells (CETSA). **F** Melting curves of GRASP55 from quantitative immunoblotting (CETSA, see panel E) using the same RTSA analysis and representation as for TPP-TR (see panel D). The thermal stabilization of GRASP55 by prodigiosin was confirmed

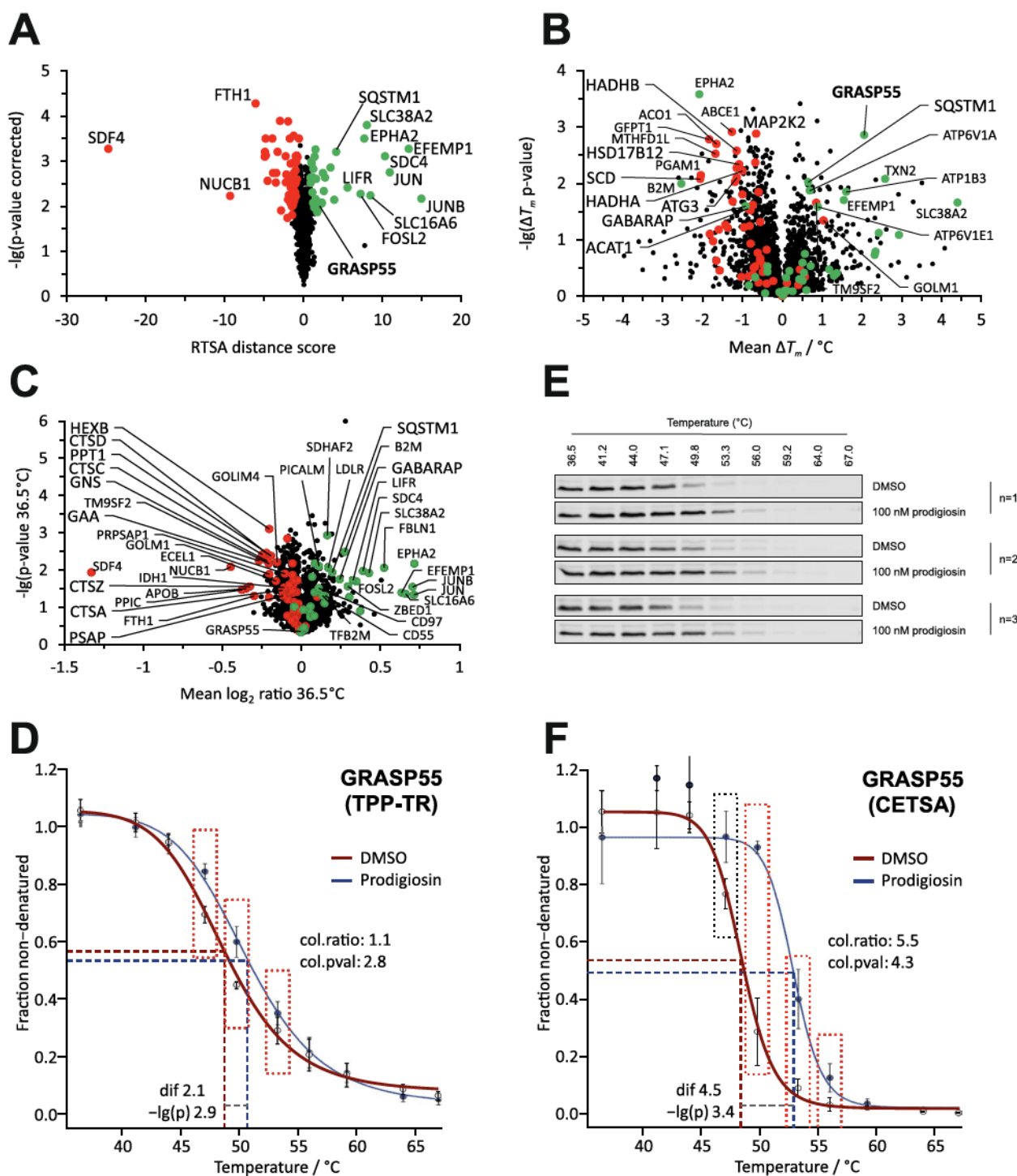


**Fig. 3** (See legend on previous page.)

of GRASP55 by immunoblotting (Fig. 3E and F) and, thus, validated and verified the prodigiosin-induced stabilization of GRASP55 as detected by MS-based TPP-TR.

A STRING protein-protein association network analysis [66] of the 93 prodigiosin-affected proteins revealed

several clusters including fatty acid metabolism, lysosome, and autophagy associated proteins (Fig. S2). Moreover, 22 of these 93 proteins are associated with the Golgi apparatus (GO:0005794), thereof twelve with the Golgi membrane (GO:0000139), and thereof six with

Golgi-associated vesicles (GO:0005798). Considering these secondary prodigiosin-mediated effects, the Golgi protein GRASP55, although not a central node in the protein network, represents a highly interesting potential direct (or indirect) molecular target candidate of prodigiosin, as it has been previously described to be involved in unconventional secretion [1, 53] and in physically linking autophagosomes with lysosomes [80].

#### GRASP55 is stabilized at low nanomolar prodigiosin concentrations

To investigate the affinity of prodigiosin to potential protein targets, we estimated the prodigiosin concentration at which 50% of the stabilizing effect can be observed ( $EC_{50}$ : half-maximal effective concentration,  $pEC_{50}$ : negative decadic logarithm of  $EC_{50}$  on the molar scale) by TPP compound concentration range (TPP-CCR) [62]. In contrast to TPP-TR performed at different denaturation temperatures and fixed prodigiosin concentrations, for TPP-CCR, HeLa cells were treated with different concentrations of prodigiosin for 6 h and subsequently heated for 3 min at a fixed temperature of 50 °C, around which most proteins exhibit partial melting and, if present, small molecule induced effects on melting characteristics [62]. In line with the TPP-TR results, the vast majority of proteins (3741 of 4139 proteins with at least two replicates of full dose response data excluding contaminants, reverse hits and only by site identifications; Supplementary Table S2) remained unaffected by prodigiosin treatment in these TPP-CCR experiments, rated by a pseudo-coefficient of determination ( $\text{pseudo-}R^2$ ; the term “pseudo” refers to employing a non-linear model) below 0.8 of the sigmoidal dose response curve. With  $\text{pseudo-}R^2 \geq 0.8$ , 162 proteins exhibited increasing (Fig. 4A) and 236 proteins decreasing (Fig. 4B) dose response characteristics. To distinguish thermal (de) stabilization from abundance effects, a control data set at 37 °C was generated. In case of pure thermal stability alteration, the absence of dose response effects is expected at 37 °C, whereas an abundance effect would lead to similar dose response characteristics at 37 °C as for 50 °C and, thus, to similar  $\text{pseudo-}R^2$  values at both temperatures, i.e., a low  $\text{pseudo-}R^2$  (50 °C  $\pm$  37 °C) difference (encoded by the point size in Fig. 4A and B). Of the 162 proteins with increasing dose response characteristics at 50 °C (Fig. 4A), GRASP55 was affected at the lowest prodigiosin concentration ( $pEC_{50} = 8.58 \pm 0.06$ ,  $EC_{50} = 2.6$  nM, Fig. 4C) with a very high  $\text{pseudo-}R^2$  (0.97), whereas, for samples treated at 37 °C, no dose response effects were observed for GRASP55 (Fig. 4D). We conclude that GRASP55 is stabilized at low nanomolar prodigiosin concentrations at a steady abundance level, suggesting, together with the effects on Golgi apparatus structure, GRASP55 as a highly probable direct (or indirect) target of prodigiosin.

Of the proteins exhibiting dose response characteristics at 50 °C with negative slope, i.e., decreasing intensity (Fig. 4B), the nine proteins with the highest  $pEC_{50}$  (underlined in Fig. 4B) are all associated with the lysosome (UniProt annotated keyword KW-0458) and exhibit similar  $\text{pseudo-}R^2$  values for 50 °C and 37 °C (low  $\text{pseudo-}R^2$  (50 °C  $\pm$  37 °C) difference expressed by small datapoints in Fig. 4B), indicating a decrease in abundance, e.g., by downregulation, degradation or secretion. This result is in line with the abundance decrease of the similar lysosomal protein cluster observed for the TPP-TR experiments (Fig. 3C and S2). The other two proteins with  $pEC_{50} > 8$  (HADHA/B) were mainly thermally destabilized (relatively high  $\text{pseudo-}R^2$  (50 °C  $\pm$  37 °C) difference) in accordance with the TPP-TR results, where they grouped in the fatty acid metabolism protein cluster (Fig. S2).

#### Knockout of GRASP55 inhibits prodigiosin cytotoxicity and alters prodigiosin effects on the Golgi apparatus

The TPP results and the results of the ultrastructural analysis of the Golgi apparatus encouraged us to investigate prodigiosin cytotoxicity in cells deficient for GRASP55. For that purpose, we generated a GRASP55 KO HeLa cell line as described by Bekier et al. (Fig. 5A) [5]. In GRASP55 KO cells, prodigiosin still displayed a high cytotoxicity (Fig. 5B), but  $IC_{50}$  values were significantly increased in comparison to HeLa wild-type (wt) cells after both 24 and 72 h (Fig. 5C). After 24 h treatment with prodigiosin, the  $IC_{50}$  value of KO cells is approximately threefold higher than in wt cells. These results suggest that cytotoxic effects of prodigiosin partially depend on GRASP55 and/or its cellular function.

Utilizing TEM, severe changes in Golgi apparatus morphology after treatment with prodigiosin became apparent in HeLa wt cells (see Fig. 1B–D). Since GRASP55 is a major protein for the stacking of the *trans* Golgi cisternae, we decided to investigate the influence of prodigiosin treatment on Golgi apparatus structure in GRASP55 KO cells (Fig. 5D). It has been shown previously that deletion of GRASP55 leads to an impairment of the Golgi stacking, as displayed in partly swollen and shorter Golgi cisternae and a higher frequency of disorganized Golgi membranes [5]. Both prodigiosin treatment and GRASP55 KO resulted in a reduced cisternae length (Fig. 5E) and cisternae number per Golgi stack (Fig. 5F), but effects of GRASP55 KO and prodigiosin treatment were not additive. Quantification of the TEM images revealed that the ratio between disorganized membranes and distinguishable Golgi stacks was clearly increased after treatment with 10 nM prodigiosin compared to the DMSO control in HeLa wt cells (Fig. 5G).

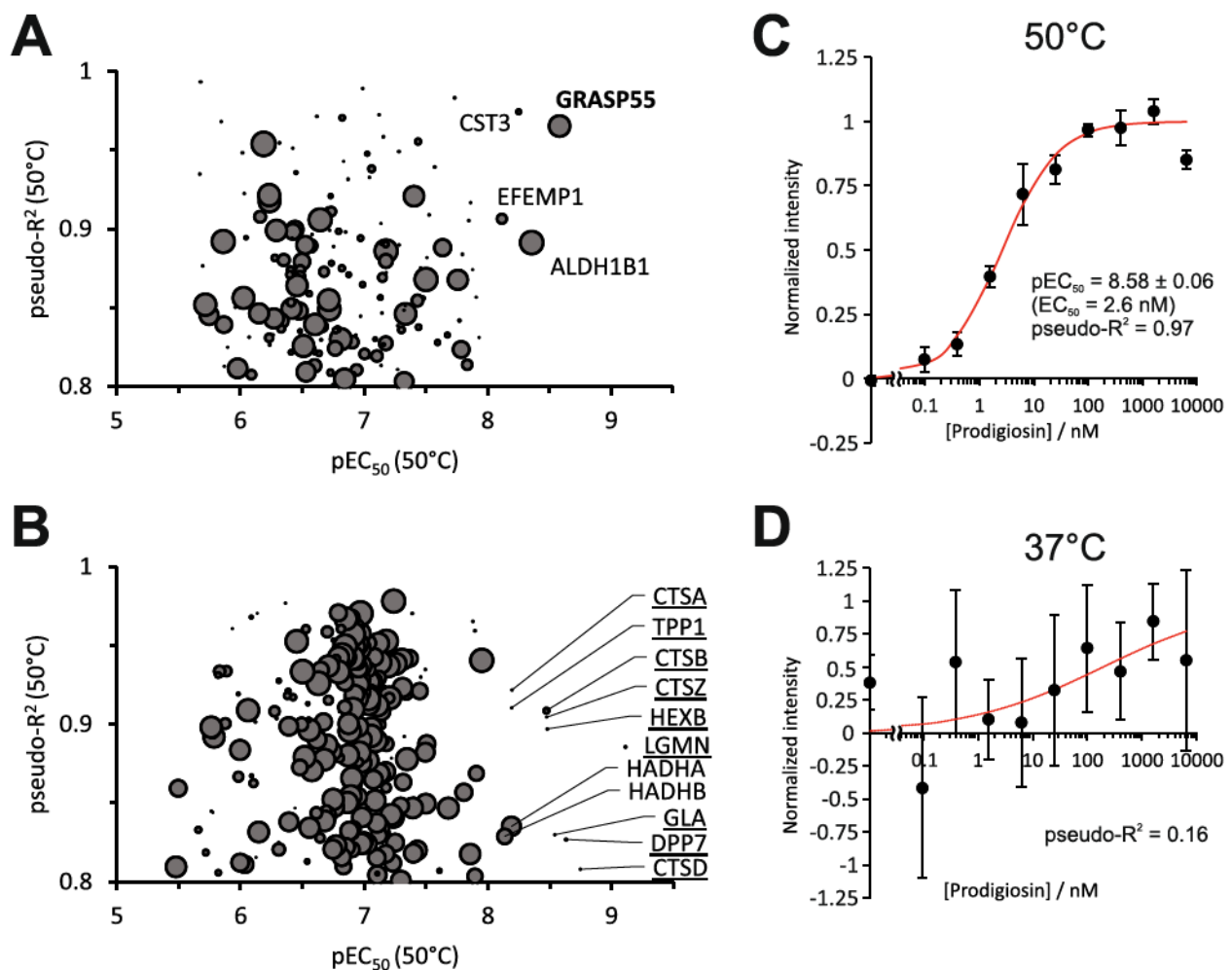


**Fig. 4** GRASP55 is stabilized at low nanomolar prodigiosin concentrations. For thermal proteome profiling compound concentration range (TPP-CCR) experiments, HeLa wt cells were treated with ten different concentrations of prodigiosin for 6 h, harvested, and cell suspensions were exposed to a short (3 min) constant temperature treatment at 50 °C (or 37 °C to test for abundance effects). Cells were lysed and the non-denatured protein fraction was recovered after centrifugation followed by quantitative MS analysis as described for TPP-TR, resulting in dose response characteristics for prodigiosin-affected proteins. **A** Plot of the dose response curve fitting parameters pseudo- $R^2$  (proteins with a pseudo- $R^2$  value of >0.8 were considered to have prodigiosin dose response characteristics) vs. pEC<sub>50</sub> (the negative decadic logarithm of the half-maximal effective concentration) for proteins exhibiting increasing intensities at increasing prodigiosin concentrations (positive dose response). The data point diameter encodes the pseudo- $R^2$  (50 °C ± 37 °C) difference (high for solely (de)stabilized proteins, low for solely abundance affected proteins). Proteins with pEC<sub>50</sub> > 8 (EC<sub>50</sub> < 10 nM) are labeled. GRASP55 is the protein affected (stabilized) at the lowest prodigiosin concentrations among the proteins with positive dose response. **B** Same representation as for panel **A** but for proteins with negative dose response. Lysosome associated proteins (UniProt annotated keyword KW-0458) are underlined. **C** Dose response characteristics and fitting results for GRASP55 at 50 °C. Data points and whiskers represent the arithmetic mean ± SD of three replicates and the fitted dose response curve is shown in red. **D** Same representation as in panel **C** but for 37 °C, with the absence of a dose response effect (irrelevant pseudo- $R^2$  < 0.8) represented by a thin dotted fitting curve (in red)

In contrast, no change in the ratio between disorganized membranes and distinguishable Golgi stacks was observed in HeLa GRASP55 KO cells after treatment with 10 nM prodigiosin. Severe structural changes of the Golgi apparatus could be observed in both wt and KO cells after 24 h treatment with 100 nM prodigiosin. No well-organized Golgi could be observed in the perinuclear region, instead we found groups of vacuoles and

irregularly dilated non-stacked cisternae. In addition, we classified Golgi structures into containing predominantly flat or bulky/swollen cisternae (Fig. 5H). Treatment with 10 nM prodigiosin reduced the amount of mainly flat cisternae in wt cells, but not in GRASP55 KO, whereas treatment with 100 nM prodigiosin resulted cell line-independently in heavily dilated Golgi structures.

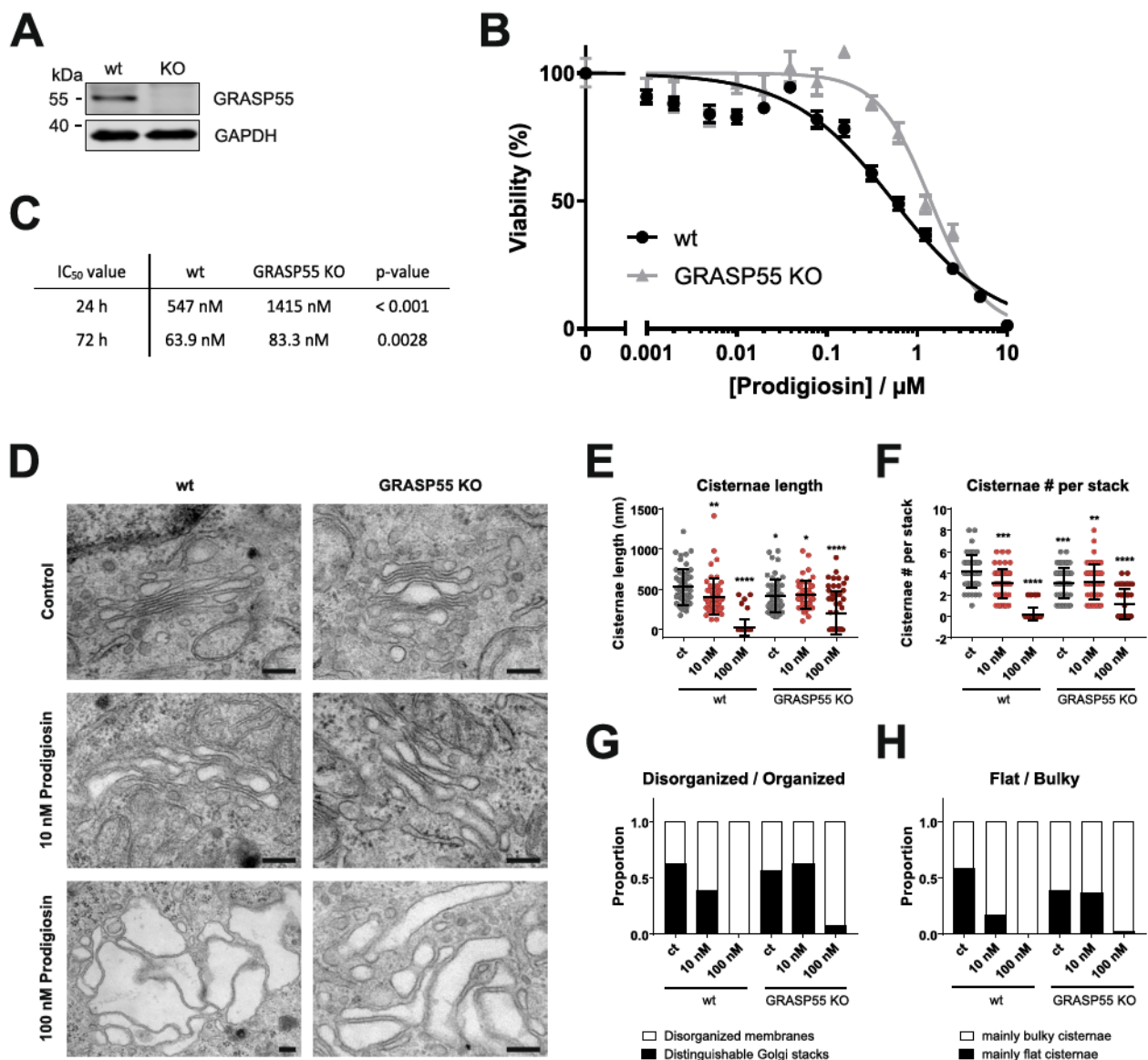


**Fig. 5** Knockout of GRASP55 impairs prodigiosin cytotoxicity and alters prodigiosin effects on the Golgi apparatus. **A** GRASP55 was knocked out in HeLa wt cells and KO was verified by western blot. **B** HeLa wt and HeLa GRASP55 KO cells were treated with different concentrations of prodigiosin for 24 h. After treatment, cell viability was measured using a thiazolylblue (MTT) assay. Results are shown as the mean  $\pm$  SEM of three independent experiments performed in triplicates for each treatment. **C** IC<sub>50</sub> values and statistical analysis for MTT assays in HeLa wt and HeLa GRASP55 KO cells after 24 and 72 h treatment with prodigiosin. Please note that the MTT assay for HeLa wt cells was independent from the one shown in Fig. 1B; accordingly, IC<sub>50</sub> values slightly differ. **(D–H)** HeLa wt and HeLa GRASP55 KO cells were treated with DMSO, 10 nM or 100 nM prodigiosin for 24 h and effects on Golgi apparatus structure were investigated by transmission electron microscopy. **D** Representative electron micrographs are shown. Scale bar: 200 nm. **E** Cisternae length and **F** cisternae number per stack were quantified. **G** Golgi stacks were categorized into organized (stacked structures with three or more cisternae) and disorganized (multiple unstacked cisternae and vesicles). **H** Stacks were classified as containing mainly flat or mainly bulky/swollen cisternae. At least 50 Golgis per treatment were quantified after blinding and randomization. Bars represent the means  $\pm$  SD. p values were determined by ordinary one-way ANOVA with Dunnett's post hoc test. \*  $p < 0.05$ ; \*\*  $p < 0.01$ ; \*\*\*  $p < 0.001$ ; \*\*\*\*  $p < 0.0001$

Since alterations in Golgi apparatus morphology have been associated with altered protein secretion [77], we investigated cellular secretion in HeLa wt and HeLa GRASP55 KO cells after treatment with

100 nM prodigiosin for 24 h (Fig. S3). Beside profound changes in the pattern of secreted proteins induced by GRASP55 knockout, we found also prodigiosin-mediated abundance changes of certain protein groups

differing between wt and KO cells. Notably, proteins containing signal peptides (SP)— which might represent classically secreted proteins— showed higher abundances in the secretome of GRASP55 KO cells upon prodigiosin treatment which was not apparent in wt cells. Furthermore, proteins associated with the extracellular matrix (ECM) and the lysosome were higher abundant after prodigiosin treatment exclusively in KO cells. Taken together, these results support the hypothesis that the Golgi stacking protein GRASP55 represents a protein target of prodigiosin.

#### Prodigiosin treatment leads to the accumulation of autophagosomes at the Golgi apparatus and blocks autophagic flux

It has been previously reported that GRASP55 participates in the autophagic process by promoting autophagosome-lysosome fusion through binding to the autophagosome-bound ubiquitin-like protein microtubule-associated proteins 1A/1B light chain 3 ([MAP1] LC3; LC3 hereafter) [81]. Since modulation of autophagy

has been reported as one mechanism of action of prodigiosin and its derivatives by others and us [6, 10, 35, 36, 82], our next aim was to investigate if prodigiosin modulates the interplay between GRASP55 and autophagy by analyzing the subcellular localization of GRASP55 and LC3 upon treatment with different concentrations of prodigiosin or the late-stage autophagy inhibitor bafilomycin A<sub>1</sub> (BafA<sub>1</sub>) as a control (Fig. 6A). After all applied treatments, GRASP55 was observed in the perinuclear region, which is consistent with the localization of the Golgi apparatus in literature [77]. The number of GRASP55 dots/cell remained unaltered upon different treatments (Fig. 6B). Interestingly, after treatment with all concentrations of prodigiosin, but not BafA<sub>1</sub>, the mean area of GRASP55 dots was significantly increased compared to the DMSO control (Fig. 6C). These results are in line with the observation of an enlarged Golgi in TEM and BFA washout assays. LC3-positive structures can be observed as dots, which represent autophagosomes. As expected, LC3 dots were enriched after treatment with the autophagy inhibitor BafA<sub>1</sub> (Fig. 6D). In prodigiosin

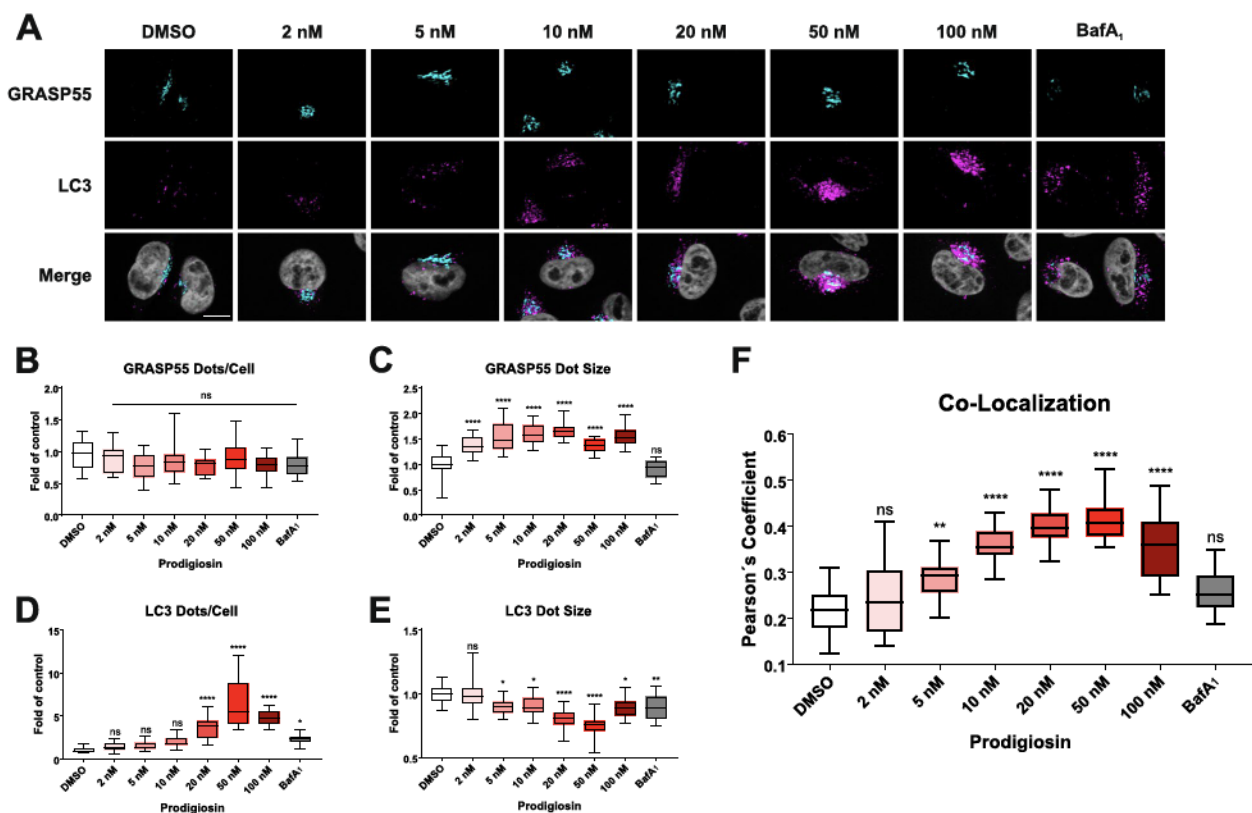


**Fig. 6** GRASP55 and LC3 co-localize upon treatment with prodigiosin. HeLa wt cells were seeded on cover slips. On the next day, cells were treated with different concentrations of prodigiosin, 10 nM bafilomycin A<sub>1</sub> (BafA<sub>1</sub>) or DMSO for 6 h. After treatment, cover slips were prepared for microscopy. **A** Representative sections are depicted. Scale bar: 10  $\mu$ m. **B–E** The relative number per cell and mean area of GRASP55 and LC3 positive structures and **F** the co-localization (Pearson's coefficient) after Costes thresholding of GRASP55 and LC3 of 15 representative images from three biological replicates for each treatment were quantified using ImageJ 1.53c. p values were determined by ordinary one-way ANOVA with Dunnett's post hoc test. \*  $p < 0.05$ ; \*\*  $p < 0.01$ ; \*\*\*  $p < 0.001$ ; \*\*\*\*  $p < 0.0001$ ; ns, non-significant

treated cells, the number of LC3 dots increased dose-dependently and the number of LC3 dots was higher than after treatment with BafA<sub>1</sub> (Fig. 6D). Furthermore, after both treatments, LC3-positive structures are significantly smaller than in DMSO treated cells (Fig. 6E). We also analyzed the co-localization of LC3 and GRASP55 and observed a highly significant, dose-dependent increase in co-localization of these two proteins after treatment with prodigiosin, whereas after treatment with BafA<sub>1</sub> there is no significant increase in co-localization (Fig. 6F). This observation suggests an accumulation of autophagosomes or their precursor membranes at the Golgi apparatus or in its close vicinity.

To investigate effects on the autophagic flux directly, immunoblot analysis of LC3 and of the ubiquitin-binding protein p62 (also known as sequestosome 1 [SQSTM1]) often represent the method of choice. Increased levels of the autophagosome-bound, lipidated form of LC3 (termed LC3-II) occur when autophagy is induced but also when the autophagic process is blocked in later steps. Investigation of the autophagy receptor SQSTM1, which accumulates upon autophagy blocking, can help distinguish between autophagy induction and inhibition. After 6 h of treatment with prodigiosin, LC3-II accumulated and the starvation-induced degradation of SQSTM1 was blocked in HeLa wt cells (Fig. 7A). These effects on the protein levels of LC3-II and SQSTM1 were similar to the effects of the V-ATPase inhibitor BafA<sub>1</sub>. BafA<sub>1</sub> inhibits the acidification of lysosomes and thereby impairs the function of lysosomal proteases such as cathepsins and thus prevents the degradation of engulfed cargo and LC3-II [69]. We have previously described that the activity of pH-dependent cathepsins is severely reduced after treatment with prodigiosin in urothelial bladder carcinoma cells [6]. Likewise, in HeLa wt cells treatment with prodigiosin led to a significantly reduced cathepsin B activity in a concentration-dependent manner (Fig. 7B). To further investigate the effects of prodigiosin, we performed immunofluorescence analysis and stained for LC3 (autophagosomes) and lysosomal-associated membrane protein 1 (LAMP1) (Fig. 7C). In line with the immunoblot analysis, an increase of LC3-positive structures after treatment with prodigiosin was observed in immunofluorescence analysis (Fig. 7D). In contrast, unlike in immunoblot analysis, the increase of LC3-positive structures upon BafA<sub>1</sub> treatment was only minor, which might be attributable to the shorter treatment duration. LAMP1-positive structures remained unaltered upon different treatments (Fig. 7E). Interestingly, both autophagosomes and lysosomes significantly shrank after treatment with prodigiosin, whereas the size difference to DMSO treated cells was not as prominent for BafA<sub>1</sub> treated cells (Fig. 7F and G). Moreover,

there was a highly significant increase in co-localization of LC3- and LAMP1-positive structures after treatment with prodigiosin, whilst changes after BafA<sub>1</sub> treatment were comparatively low (Fig. 7H). The spatial proximity of autophagosomes and lysosomes after prodigiosin treatment would suggest a facilitated fusion of autophagosomes and lysosomes and therefore an increased autophagic flux. On the contrary, the inhibition of starvation-induced SQSTM1 degradation clearly indicates a blockage of autophagic flux. Collectively, these results suggest a different mechanism of autophagy inhibition by prodigiosin compared to BafA<sub>1</sub>. Prodigiosin treatment results in reduced cathepsin activity and blocks overall autophagic flux, whereas LC3-LAMP1 co-localization is clearly promoted. At the same time, the prodigiosin-induced accumulation of autophagosomes at GRASP55-positive structures points towards an involvement of an altered Golgi function in the autophagy-inhibitory effect of this natural compound.

## Discussion

Despite frequent advances in research, cancer remains a leading cause of death, accounting for nearly ten million deaths every year (<https://www.who.int/news-room/factsheets/detail/cancer>). To address this unmet therapeutic need, natural compounds display a valuable source for an almost inexhaustible diversity of bioactive compounds with a complexity in structure that is often superior to compounds derived from synthetic approaches. To elucidate the mechanism of action of these often highly bioactive compounds, TPP displays a valuable tool for unbiased target identification. In this study, we used TPP to identify the Golgi protein GRASP55 as target protein of the natural compound prodigiosin. We observed that prodigiosin treatment leads to severe structural changes in Golgi apparatus morphology and function. We also found that autophagosomes accumulate at the Golgi apparatus while autophagy is impaired in cells treated with prodigiosin.

Utilizing TPP, we identified several proteins as target candidates of the natural compound prodigiosin. By offering an unimpaired approach that is not dependent on pre-functionalization of the small molecule or of proteins, TPP represents a highly versatile target identification strategy [31]. Prioritizing candidates for target validation can be challenging due to multiple possible candidates. However, with severe structural changes in Golgi morphology, a high statistical significance of the thermal shift, validation through immunoblotting and being a target candidate in both independent TPP approaches (TPP-TR and TPP-CCR), GRASP55 was selected for further investigations. Distinguishing between thermal stability changes and abundance

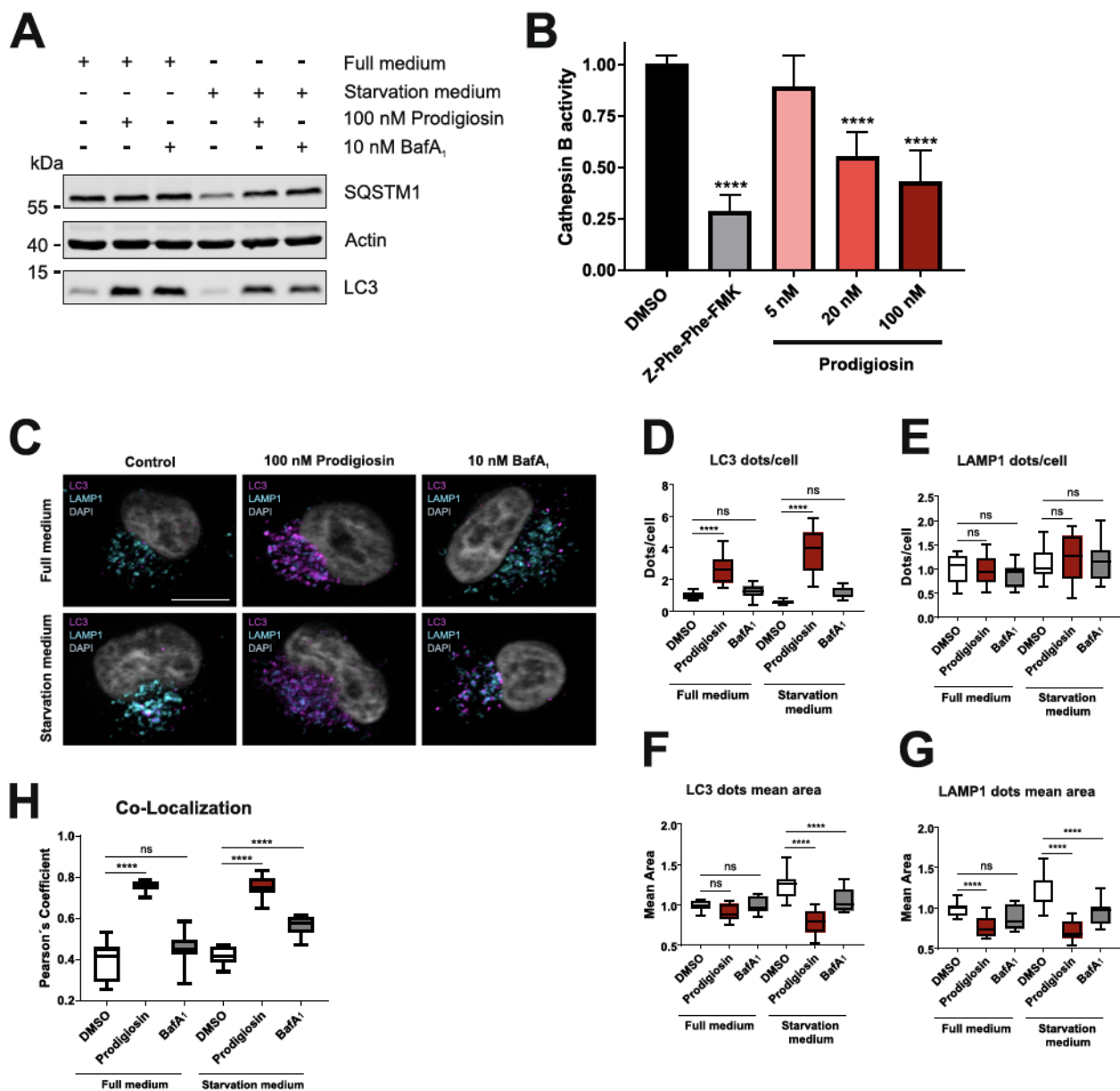


**Fig. 7** Prodigiosin blocks autophagy and inhibits cathepsin activity. **A** HeLa wt cells were treated with DMSO, 100 nM prodigiosin or 10 nM bafilomycin A<sub>1</sub> (BafA<sub>1</sub>) in DMEM or EBSS. After 6 h, the cells were lysed and cellular lysates were immunoblotted for the indicated proteins. One representative immunoblot of three independent experiments is shown. LC3: light chain 3; SQSTM1: sequestosome 1. **B** HeLa wt cells were treated with different concentrations of prodigiosin or DMSO. After 24 h, the cells were lysed and a cathepsin B assay was performed according to the manufacturer's instructions. 20  $\mu$ M Z-Phe-Phe-FMK was used as inhibitor control. The absence of duplicates for each treatment of three independent experiments was measured and the mean of the DMSO control was set as 100%. Bars represent the means  $\pm$  SD. **C** HeLa wt cells were seeded on cover slips. On the next day, cells were treated with DMSO, 100 nM prodigiosin or 10 nM BafA<sub>1</sub> in DMEM or EBSS for 2 h. After treatment, cover slips were prepared for microscopy. Representative sections are depicted. Scale bar: 10  $\mu$ m. **D-G** The relative number per cell and mean area of LC3- and LAMP1-positive structures and **H** the co-localization (Pearson's coefficient) after Costes thresholding of LC3 and LAMP1 of 15 representative images from three biological replicates for each treatment were quantified using ImageJ 1.53c. p values were determined by ordinary one-way ANOVA with Dunnett's post hoc test. \*\*\*\*  $p < 0.0001$ ; ns, non-significant

changes can be challenging [33], but neither in the TPP-TR/RTSA nor in the TPP-CCR analysis, GRASP55 showed differential intensities at 36.5/37 kDa, excluding

an abundance effect and establishing GRASP55 as a highly probable molecular target of prodigiosin with low nanomolar affinity.

To avoid focussing on false positive targets, Johnson et al. proposed orthogonal target identification methods like computational target prediction [31]. To our knowledge, only the N-terminal GRASP domain of GRASP55 (residues 1–207) has been successfully crystallized so far [41, 67], hindering reliable computational modelling of a direct prodigiosin-GRASP55 interaction. Future disclosure of the whole protein structure is desirable to find and characterize a potential specific binding site of prodigiosin. This knowledge would allow structure optimization of this highly active natural compound with regard to its binding affinity, pharmacokinetic properties and adverse effects. Of note, we found that KO of GRASP55 significantly reduces prodigiosin cytotoxicity in HeLa cells, indirectly confirming GRASP55 as a target. Xiang et al. reported that depletion of GRASP55 does not cause apoptosis in HeLa cells [77]. We do not think that prodigiosin-mediated effects on GRASP55 mimic its genetic depletion, but, next to apoptosis, additional cell death subroutines might be involved, e.g. lysosome-dependent cell death [23]. Prodigiosin is still clearly cytotoxic in GRASP55 KO cells, demonstrating that other target candidates and/or mechanisms contribute to the observed reduction in cell viability upon prodigiosin treatment. Along these lines, small molecules can be bioactive through mechanisms that do not involve direct binding of proteins and, thus, those target processes may not be revealed by TPP.

In our hands, prodigiosin treatment leads to a severely dilated and disorganized Golgi apparatus in a concentration-dependent manner. In mammalian cells, Golgi membranes are organized as stacks of multiple flat cisternae, which are further linked into a ribbon-like structure by the two peripheral membrane proteins GRASP55 and GRASP65 [37]. The conserved GRASP domain at the N-terminus of GRASP proteins contains a membrane anchor and forms dimers and trans-oligomers to glue the adjacent cisternae into stacks [2]. We speculate that low nanomolar concentrations of prodigiosin interfere with the oligomerization of GRASP55 leading to a Golgi phenotype with less and shorter Golgi cisternae that is similar to GRASP55 KO cells [5]. Notably, these effects become visible after treatment with 10 nM prodigiosin in EM analysis and GRASP55 immunofluorescence, but not after TGN46 and B4GALT1 immunostaining for BFA washout assays. Upon GRASP55 deletion, Bekier et al. observed minor but significant Golgi fragmentation by immunofluorescence [5]. Interestingly, after treatment with 100 nM prodigiosin, we observed heavily dilated and disorganized structures in both TEM and BFA washout assays. These morphological changes in

Golgi morphology are similar to phenotypes observed in cells after treatment with the bacterial metabolite monensin [19, 49, 68]. As an ionophore, monensin is able to dissipate proton gradients by exchanging  $\text{Na}^+/\text{H}^+$  across membranes leading to a disruption of the Golgi pH. Golgi apparatus function is dependent on a pH gradient that is maintained along the secretory pathway by proton pumps [15] with an acidic pH in the *trans*-cisternae and newly formed vesicles [3, 51, 54]. Several studies suggest that prodigiosin can alter organelle pHs by acting as an  $\text{H}^+/\text{Cl}^-$  symporter [61, 63]. Therefore, we hypothesize that the alteration of Golgi apparatus morphology after treatment with prodigiosin is mediated by both direct effects on GRASP55 oligomerization and alkalization-induced cisternae swelling.

The Golgi apparatus is the central hub for post-translational modifications of proteins and their sorting and transport to their real destinations, such as secretory vesicles, endosomes, lysosomes, or the plasma membrane [7]. It has been hypothesized that accelerated protein trafficking and impaired protein glycosylation after unstacking of the Golgi cisternae due to GRASP55 depletion or impairment can be explained by an enlarged membrane area that is accessible for faster vesicle budding and cargo transport through the Golgi [70, 72]. Therefore, it is not surprising that in our hands the severe impairment of the Golgi apparatus structure led to alterations in the pattern of classically secreted proteins as well as proteins associated with extracellular matrix and lysosomes. This stands in line with the observations of Xiang et al. that Golgi unstacking after GRASP depletion led to a missorting of lysosomal enzymes such as cathepsin D [77]. Since GRASP55 is not only involved in conventional secretion due to its Golgi stacking activity, but also plays a role in unconventional protein secretion [24, 25, 53], it is comprehensible that we also found a prodigiosin mediated upregulation in the secretion of different protein groups. Taken together, we show that prodigiosin treatment leads to severe changes in Golgi morphology and function, which has—to our knowledge—not been described in the literature so far.

In addition to its functions in Golgi stacking and unconventional secretion, GRASP55 has been described as a specific energy and nutrient sensor [2] acting as a bridging protein that facilitates autophagosome-lysosome fusion through an LC3-interaction region (LIR) motif and interaction with LAMP2 [80, 81]. Prodigiosin and its autophagy-modulating properties have been discussed controversially in recent literature. While some groups describe an induction of autophagic cell death [10, 42], Zhao et al. report an inhibition of autophagy via blocking lysosomal cathepsin maturation and

autophagosome-lysosome fusion [82]. In this study, we observed an increased spatial proximity of autophagosomes and lysosomes, as visualized by the co-immunostaining of LC3 and LAMP1 after treatment with prodigiosin. However, we also observed that prodigiosin ultimately blocks autophagic cargo degradation, as shown by the accumulation of LC3-II, the inhibition of SQSTM1 degradation, and a reduced cathepsin activity. The Golgi has previously been designated as “assembly line” to the autophagosome [14], and key regulators of the autophagic pathway traffic from the Golgi to the forming autophagosome, including the lipid scramblase ATG9A and the phosphatidylinositol 4-kinase PI4KIII $\beta$ , which mediates PI4P production at the initiation membrane site [32]. Furthermore, the signalling of mTORC1—a major autophagy-regulating kinase—is closely linked to the morphology of the Golgi [44], and mTORC1 directly phosphorylates GRASP55 and thus regulates its localization [53]. Accordingly, a prodigiosin-mediated control of the autophagy pathway via its effects on Golgi structure in general and/or on GRASP55 in particular appears likely. Overall, we propose an at least dual mode of action how prodigiosin inhibits late stage autophagy. First, prodigiosin treatment leads to an alkalization of lysosomes by acting as an H<sup>+</sup>/Cl<sup>−</sup> symporter [61, 63] and simultaneously impairs proper functionalization and trafficking of lysosomal proteins via unstacking of Golgi cisternae and/or alkalization of this compartment. Second, prodigiosin might directly interfere with the role of GRASP55 as a tethering factor for autophagosome-lysosome fusion. Further studies will be required to determine the individual contribution of these two possible modes of action. Notably, Zhang et al. reported that knockout of GRASP55 reduces LC3 and LAMP2 co-localization [80]. Since we observed a clear co-accumulation of LC3- and LAMP1-positive structures upon prodigiosin treatment, it appears that not necessarily the GRASP55-mediated tethering of autophagosomes and lysosomes itself is negatively affected by this compound. Alternatively, it might be that the prodigiosin-mediated Golgi unstacking or pH alterations influence biogenesis and trafficking of LC3- and/or LAMP1-positive compartments. Along these lines, we also observed reduced sizes of these puncta, potentially pointing towards an altered transfer of proteins and/or lipids into these structures. The general importance of the Golgi apparatus for autophagosome biogenesis during starvation has been described above. Due to the severe damage of the Golgi induced by prodigiosin, selective autophagy processes (i.e., Golgiphagy) might add another layer of complexity in this case. The massive co-localization of GRASP55 and LC3 induced by prodigiosin might reflect the de novo

synthesis of autophagosomal membranes at the damaged organelle. The induction of Golgiphagy together with the block of late stage autophagy might explain the extreme accumulation of autophagosomal membranes in the perinuclear area upon prodigiosin treatment.

In 2013, Krishna et al. published an *in silico* molecular docking analysis of prodigiosin and cycloprodigiosin as COX-2 inhibitors [38]. Additionally, the identification of protein targets of prodigiosin using inverse virtual screening methods has been described in a recent manuscript, and reported potential prodigiosin-interacting proteins include HER-2, MEK, and S6K [55]. However, the interaction of prodigiosin with these candidate proteins has not been experimentally proven so far. Here, we identify GRASP55 as downstream effector protein of prodigiosin and characterize the immense effects of this bacterial metabolite on Golgi apparatus structure and function. Increased knowledge about the protein target enables the structural modification of this very potent natural compound in order to obtain a more selective mode of action and optimize the binding affinity and pharmacokinetic properties. The sensitivity of cancer cells towards prodigiosin treatment and the concomitant absence of effects on normal or non-malignant cells has previously been proposed [26, 50], making this natural product a promising lead compound for anti-cancer drug discovery. We hope that our results contribute to deciphering the molecular mode of action of this compound.

## Material and methods

### Antibodies and reagents

Antibodies against  $\beta$ -actin (Sigma-Aldrich, St. Louis, MO, USA, #A5316, clone AC-74, 1:5000), B4GALT1 (Sigma-Aldrich, St. Louis, MO, USA, #HPA010807, 1:200), GAPDH (abcam, Cambridge, UK, #ab8245, 1:5000), GRASP55 (Proteintech, Chicago, IL, USA, #10,598 $\pm$ 1-AP, 1:200 for IF and 1:2000 for WB), LAMP1 (Sigma-Aldrich, St. Louis, MO, USA, #L1418, 1:200), LC3B (MBL, Woburn, MA, USA, #M-152 $\pm$ 3, 1:200 for IF and Cell Signalling Technology, Danvers, MA, USA, #2775, 1:1000 for WB), SQSTM1 (PROGEN, Heidelberg, Germany, #GP62-C, 1:1000) and TGN46 (Bio-Rad, Hercules, CA, USA, #AHP500GT, 1:200) were used. For WB, IRDye 800- or IRDye 680-conjugated secondary antibodies were purchased from LI-COR Biosciences (Lincoln, NE, USA, #926 $\pm$ 68,077, #926 $\pm$ 32,211 and #926 $\pm$ 32,210). Secondary antibodies for immunofluorescence analyses were purchased from Jackson ImmunoResearch (Alexa Fluor 488-AffiniPure Goat Anti-Mouse IgG, 1:500, #115 $\pm$ 545-003; Alexa Fluor

488-AffiniPure Goat Anti-Rabbit IgG, 1:500, #111±545-003; Alexa Fluor 647-AffiniPure Goat Anti-Mouse IgG, 1:500, #115±605-003 and Alexa Fluor 647-AffiniPure Goat Anti-Rabbit IgG, 1:500, #111±605-144) and abcam (Alexa Fluor 488 Donkey Anti-Sheep IgG, 1:500, #ab150177). Isolated and purified prodigiosin was provided in DMSO as reported previously [20]. Other reagents used were bacitracin A<sub>1</sub> (Sigma-Aldrich, St. Louis, MO, USA, #B1793), brefeldin A (BFA, Sigma-Aldrich, St. Louis, MO, USA, #B6542), DMSO (PanReac AppliChem, Darmstadt, Germany, #A3672 and ROTH, Karlsruhe, Germany, #7029.1), staurosporine (biomol, Hamburg, Germany, #AG-CN2-0022-M005), Thiazolyl blue (MTT, ROTH, Karlsruhe, Germany, #4022.3) and Z-Phe-Phe-FMK (abcam, Cambridge, UK, #ab65306). The cathepsin activity of treated HeLa cells was quantified using the fluorimetric Cathepsin B Activity Assay Kit (abcam, Cambridge, UK, #ab65300) according to the manufacturer's instructions and measured with a microplate reader (SynergyMx, BioTek, Winooski, VT, USA).

#### Correct Identification of natural products

Prodigiosin was produced and purified as described by Domröse et al. [20]. After column chromatography prodigiosin was precipitated as hydrochloride as a dark red solid and a 10 mM stock in DMSO was prepared.

<sup>1</sup>H-NMR (600 MHz, CDCl<sub>3</sub>): δ [ppm]=0.90 (t, <sup>3</sup>J<sub>10'',9''</sub>=7.0 Hz, 3H, 10''-H), 1.32 (m, 4H, 8''-, 9''-H), 1.54 (m, 2H, 7''-H), 2.39 (t, <sup>3</sup>J<sub>6'',7''</sub>=7.6 Hz, 2H, 6''-H), 2.54 (s, 3H, 11''-H), 4.00 (s, 3H, 7-H), 6.07 (d, <sup>4</sup>J<sub>3,1</sub>=1.9 Hz, 1H, 3-H), 6.35 (m, 1H, 4'-H), 6.68 (d, <sup>4</sup>J<sub>3'',1''</sub>=2.6 Hz, 1H, 3''-H), 6.91 (ddd, <sup>3</sup>J<sub>3',4'</sub>=3.8 Hz, <sup>4</sup>J<sub>3',5'</sub>=2.4 Hz, <sup>5</sup>J<sub>3',1'</sub>=1.4 Hz, 1H, 3'-H), 6.95 (s, 1H, 8-H), 7.22 (m, 1H, 5'-H), 12.56 (brs, 1H, 1'-NH), 12.71 (brs, 2H, 1-, 1''-NH); <sup>13</sup>C-NMR (151 MHz, CDCl<sub>3</sub>): δ [ppm]=12.6 (C-11''), 14.2 (C-10''), 22.6 (C-9''), 25.5 (C-6''), 29.9 (C-7''), 31.6 (C-8''), 58.9 (C-7), 93.0 (C-3), 111.9 (C-4'), 116.1 (C-8), 117.2 (C-3'), 120.8 (C-5), 122.4 (C-2'), 125.3 (C-2''), 127.1 (C-5'), 128.5 (C-3''), 128.6 (C-4''), 147.1 (C-5''), 147.8 (C-2), 165.9 (C-4).

The analytical data are in accordance to literature [20].

#### Cell lines and cell culture

All HeLa cell lines were cultured in Dulbecco's Modified Eagle Medium (DMEM, Thermo Fisher Scientific, Waltham, MA, USA, #41,965,039) containing 10% Fetal Bovine Serum (FBS, Sigma-Aldrich, St. Louis, MO, USA, #F0804), 4.5 g/l D-glucose, 100 units/mL penicillin and 100 µg/mL streptomycin (Thermo Fisher Scientific, Waltham, MA, USA, #15,140,122). All cells were

cultivated and treated at 37 °C and 5% CO<sub>2</sub> in a humidified atmosphere.

#### Cell viability assay

Cell viability was measured using the MTT (3-(4,5-dimethylthiazol-2-yl)-2,5-diphenyltetrazolium bromide) assay. HeLa cells were seeded in 96-well plates with a density of 5×10<sup>3</sup> cells/well. One day after seeding, cells were treated with different concentrations of prodigiosin, 0.1% DMSO as a solvent control or 5 µM staurosporine as a positive control for 24 or 72 h. After the incubation time, 20 µL of a 5 mg/mL MTT stock solution (ROTH, Karlsruhe, Germany, #4022.3) were added to the cells and they were incubated at 37 °C and 5% CO<sub>2</sub> in a humidified atmosphere for 30 min. Upon removal of the MTT-containing medium 100 µL DMSO per well were added for extraction of the formazan. Absorbance was measured at 570 nm and 650 nm (reference) with a microplate reader (SynergyMx, BioTek, Winooski, VT, USA). After subtraction of the reference value, the mean of the absorbance of the solvent control was set as 100% and the relative viability was calculated for each sample.

#### Transmission electron microscopy (TEM)

HeLa wt and HeLa GRASP55 KO cells were seeded into 10 cm dishes. On the next day, cells were treated with 0.1% DMSO, 10 nM prodigiosin or 100 nM prodigiosin for 24 h. After treatment, cells were washed with Dulbecco's phosphate-buffered saline (DPBS, Thermo Fisher Scientific, Waltham, MA, USA, #14,190,250) and then fixed using 2.5% glutaraldehyde and 4% paraformaldehyde in 0.1 M sodium cacodylate, pH 7.4 overnight at 4 °C. Then, cells were harvested with a cell scraper and centrifuged at 4,000×g for 5 min. Cell pellets were washed twice with 0.1 M sodium cacodylate buffer, pH 7.2, then heated to 40 °C and embedded into 3% low melting agarose. The agarose was dissolved at 40 °C in a water bath and after aspiration of the supernatant a volume of approximately 10 µL was left, which was resuspended in agarose. After centrifugation at approximately 4,000 × g for 2 min, the samples were covered with 1% OsO<sub>4</sub> in 0.1 M sodium cacodylate buffer for 60 min at RT. After washing two times with sodium cacodylate buffer for 10 min and twice with 70% EtOH for 15 min at RT, block contrast was applied using 1% uranyl acetate/1% phosphotungstic acid in 70% EtOH (freshly prepared and filtered) for 1 h at RT. The samples were dehydrated in a graded ethanol series (90% EtOH, 96% EtOH, 100% EtOH) and embedded in SPURR epoxy resin (Serva, Heidelberg, Germany, #21,050). After polymerization at 70 °C for 24 h, 70 nm ultrathin sections were cut using an Ultracut EM UC7 (Leica, Wetzlar, Germany). TEM images were

captured using an H7100 TEM (Hitachi, Tokyo, Japan) at 100 V equipped with a Morada camera (EMSIS GmbH, Münster, Germany).

**BFA washout assay**

For BFA washout assays, HeLa wt cells were seeded on glass coverslips in 24-well plates. On the next day, cells were treated with 0.1% DMSO, 10 nM prodigiosin or 100 nM prodigiosin. After 24 h, the treatment medium was removed, cells were washed once with DPBS and then treated with 5 µg/mL BFA or 0.1% DMSO as a control for 2 h. Cells were then washed with DPBS four times and incubated with fresh culture medium for 0/15/30/45/60/120 min. After the respective BFA wash-out time, cells were fixed in ice-cold methanol for 15 min on ice, washed three times with DPBS and blocked in 3% BSA (Roth, Karlsruhe, Germany, #8076) overnight. Samples were incubated with primary antibodies diluted in 3% BSA for 2 h and then washed three times with DPBS, incubated with the appropriate secondary antibodies diluted in 3% BSA for 30 min and washed three times with DPBS. Afterwards, cells were embedded in Pro-Long Glass Antifade Mountant (Thermo Fisher Scientific, Waltham, MA, USA, #P36980) containing 1 µg/mL DAPI (Roth, Karlsruhe, Germany, #6335.1). Images were recorded with an Axio Observer 7 Fluorescence microscope (Carl Zeiss Microscopy, Oberkochen, Germany) using a 40x/1.4 Oil DIC M27 Plan-Apochromat objective (Carl Zeiss Microscopy, Oberkochen, Germany) and an ApoTome 2 (Carl Zeiss Microscopy, Oberkochen, Germany).

**Thermal proteome profiling**

TPP was performed essentially as described [40, 65], but with major modifications to the TMT labeling sets and statistical data analysis for TPP-TR.

**Compound and temperature treatment**

For thermal proteome profiling temperature range (TPP-TR) experiments, 6\*10<sup>6</sup> HeLa wt cells were seeded per

15 cm dish and, on the next day, incubated with 100 nM prodigiosin (final concentration in final 0.1% v/v DMSO in cell culture medium) or 0.1% v/v DMSO in cell culture medium as vehicle control for 6 h. For thermal proteome profiling compound concentration range (TPP-CCR) experiments, 2.35\*10<sup>6</sup> HeLa wt cells were seeded per 10 cm dish and, on the next day, incubated with the indicated final concentrations (Table 1) of prodigiosin (in final 0.1% v/v DMSO in cell culture medium) for 6 h.

Adherent cells were washed in the dish once with DPBS and harvested by Trypsin+EDTA (0.25%, Thermo Fisher Scientific, Waltham, MA, USA, #25,200,056) treatment. After addition of 35 mL DPBS, the cells were pelleted by centrifugation (300 rcf, 5 min, 4 °C), and washed twice by re-suspending and pelleting using 45 mL and 1 mL DPBS, respectively, to remove excess trypsin and for transfer into pre-weighed 2 mL Eppendorf tubes to determine the cell pellet wet weights as quality check after centrifugation (300 rcf, 5 min, 4 °C) and complete removal of the supernatant. Cells for TPP-TR were resuspended using 1 mL, and cells for TPP-CCR were resuspended using 0.4 mL ice-cold DPBS, respectively, supplemented with protease inhibitor cocktail (Roche, Basel, Switzerland, #5,892,791,001). TPP-TR samples were aliquoted into 10x100 µL, and 2x100 µL aliquots were generated from TPP-CCR samples, respectively, into PCR tube strips such that samples with different prodigiosin concentrations and the same treatment temperature (described below) were contained in the same strip. Cell suspensions were shortly centrifuged (1 s or less) using a benchtop centrifuge to release trapped air and to achieve an even liquid level without pelleting the cells. The samples were then temperature treated by a 7 min pre-incubation at RT, 3 min temperature treatment in the PCR cycler (DNA Engine Tetrad 2, lid temperature 70 °C) at different temperatures (37 °C or 50 °C for TPP-CCR or the temperatures given in Table 2 for TPP-TR) and a 3 min post-incubation at RT in a metal heating block for uniform heat dissipation.

**Table 1** TPP-CCR treatment concentrations

Sample	1	2	3	4	5	6	7	8	9	10
[Prodigiosin] / nM	0	0.098	0.39	1.56	6.25	25	100	400	1600	6400

**Table 2** TPP-TR treatment temperatures

PCR strip	1	2	3	4	5	6	7	8	9	10
Treatment temperature / °C	36.5	41.2	44.0	47.1	49.8	53.3	56.0	59.2	64.0	67.0

After temperature treatment, samples were supplemented with lysis buffer (final concentrations: 0.36 U/ $\mu$ L benzonase, 1.5 mM  $MgCl_2$ , 1 mM  $Na_3VO_4$ , 10 mM NaF, 2.5 mM  $Na_4P_2O_7$ , 0.8% w/v NP-40) for 1 h on ice. The lysates were cleared from cell debris as well as denatured and precipitated proteins by centrifugation at 20,000 rcf and 4 °C for 30 min. The total protein concentration of the resulting cell extracts containing the fraction of soluble, non-denatured proteins was determined (Pierce 660 nm Protein Assay, BSA as standard). Cell extracts were shock frozen in liquid nitrogen and stored at -80 °C. The three replicates for TPP-TR and TPP-CCR were prepared on consecutive days, respectively. The two (37 °C or 50 °C) x ten (concentrations) x three (replicates)=60 TPP-CCR samples and two (treatment and control) x ten (temperatures) x three (replicates)=60 TPP-TR samples were analyzed by LC-MS/MS. GRASP55 was additionally quantified from the TPP-TR samples by immunoblotting as described in the respective section.

#### Single-pot, solid-phase-enhanced sample preparation (SP3) for MS

For TPP-CCR, SP3 was performed as described [40] with slight modifications to the original protocol [28] using on average 5  $\mu$ g total protein per sample and resulting in theoretically 5  $\mu$ g peptides in 22  $\mu$ L 50 mM triethylammonium bicarbonate per sample. For each of the two (treatment and control) x three (replicates)=six TPP-TR temperature treatment sample sets, the same volume for each of the ten temperature samples was used for SP3 processing, thus, maintaining the information about the temperature dependent non-denatured protein content. This volume was calculated such that the lowest two temperature samples (36.5 °C and 41.2 °C) contained 10  $\mu$ g total protein on average. The samples were diluted using SDS containing buffer (20  $\mu$ L final, final concentrations: 7.5% glycerol, 3% SDS, 37.5 mM Tris/HCl pH 7.0) and the proteins were reduced, alkylated, and precipitated on the solid phase as described [40] using adjusted volumes (2x due to processing 10  $\mu$ g instead of 5  $\mu$ g). Volumes for washing of the aggregated proteins on the solid phase and for tryptic digestion were kept unchanged, however, to maintain the maximal total protein to trypsin/Lys-C ratio at 50:1 in the two rounds of digestion (13 h and 4 h), respectively, 2x0.2  $\mu$ g trypsin/Lys-C was used per sample, theoretically resulting in at most about 10  $\mu$ g peptides in 22  $\mu$ L 50 mM triethylammonium bicarbonate.

#### TMT labeling and high pH fractionation

Peptides (10  $\mu$ L of the peptide solutions, respectively, containing about 2.3  $\mu$ g peptides for TPP-CCR or at most

about 4.5  $\mu$ g peptides for TPP-TR, respectively) were TMT labeled (1  $\mu$ L for TPP-CCR or 2  $\mu$ L for TPP-TR of the respective TMT 10plex label from 0.8 mg TMT label in 41  $\mu$ L dry acetonitrile, 1 h, RT; quenched by 0.8  $\mu$ L for TPP-CCR or 1.6  $\mu$ L for TPP-TR of 2.5% w/v hydroxylamine, 15 min, RT), the samples of a labeling set were combined and offline high pH fractionated as described [40]. For TPP-CCR, a TMT 10plex labeling set contained the ten concentration samples according to the following scheme:

[Prodigiosin] / nM	0	0.098	0.39	1.56	6.25	25	100	400	1600	6400
TMT label	126	127N	127C	128N	128C	129N	129C	130N	130C	131

For TPP-TR, however, in order to determine compound induced melting curve shifts and, at the same time, allow for precise relative protein quantification for differential protein expression analysis, corresponding temperature samples of treatment and control were kept within the same TMT 10plex labeling set and the ten different temperature treatments were split up into two TMT 10plex labeling sets according to the following scheme:

#### TMT 10plex labeling set 1

Temperature / °C	64.0	64.0	56.0	56.0	49.8	49.8	44.0	44.0	36.5	36.5
Compound treatment	-	+	-	+	-	+	-	+	-	+
TMT label	126	127N	127C	128N	128C	129N	129C	130N	130C	131

#### TMT 10plex labeling set 2

Temperature / °C	67.0	67.0	59.2	59.2	53.3	53.3	47.1	47.1	41.2	41.2
Compound treatment	-	+	-	+	-	+	-	+	-	+
TMT label	126	127N	127C	128N	128C	129N	129C	130N	130C	131

This approach is similar to the previously described RTSA approach [33], however, allowing for ten instead of nine temperature treatments by omitting common reference temperature samples in the two TMT sets and, instead, using a global melting curve fitting procedure described below.

#### LC-MS/MS analysis

In total, eight (high pH fractions per TMT set) x two (TMT sets per temperature; 37 °C and 50 °C) x three (replicates)=48 TPP-CCR and eight (high pH fractions per TMT set) x two (TMT sets per replicate) times three (replicates)=48 TPP-TR MS samples were analyzed using a Rapid Separation Liquid Chromatography System

(Ultimate 3000, Thermo Fisher) and a nano-source ESI interface equipped Orbitrap Fusion Lumos Tribrid mass spectrometer (Thermo Fisher Scientific, Dreieich, Germany) operated in synchronous precursor selection (SPS) [47] mode as described [40].

#### MS data analysis, protein identification, and quantification

MS data was processed as described [40] using the MaxQuant software (Max Planck Institute for Biochemistry, Planegg, Germany) version 1.6.17.0 based on 75,777 Homo sapiens protein entries, downloaded from the UniProtKB on 27 January 2021, yielding protein quantifications by TMT reporter ions at the MS3 level for a total of 5992 and 4590 identified protein groups for TPP-CCR and TPP-TR, respectively (including potential contaminants, reverse hits and only by site identifications). In the following, for simplicity and readability, a MaxQuant "protein group" is referred to as "identified protein", "protein ID", or just "protein," and a representative protein for the protein group is selected.

#### Statistical analysis of melting curves

Statistical data analysis was performed using the R programming language (R version 4.1.2 (2021+11-01) on a x86\_64-w64-mingw32/x64 (64-bit) platform). For TPP-CCR, data normalization, dose response curve fitting, and pseudo- $R^2$  calculation was performed as described [40] with the different starting values for pEC50 (9.5, 8.2, 6.8, 5.5) and H (-3, -0.33, 0.33, 3) for the series of fits.

The `nls()` or `nlsLM()` functions of the R packages `stats` or `minpack.lm`, respectively, were used for non-linear melting curve fitting as detailed below. The procedure consists of two main steps: 1) Preparation of TPP-TR data, 2) RTSA analysis.

**Preparation of TPP-TR data by a three-step normalization procedure** **Normalization for each temperature** For each treatment temperature, the reporter ion intensities of the two (treatment and control) x three (replicates)=six samples were normalized such that when each sample was compared to a (selected) reference sample, the median of the logarithmized ( $\log_2$ ) fold changes (FCs, i.e., the ratios) of all protein reporter ion intensities (median  $\log_2$ FCs) was zero. The sample to which the other samples had the highest number of positive median  $\log_2$ FCs was selected as the reference sample within each temperature sample set. The intensities of the other samples were adjusted by multiplying by the calculated constant  $c = 2^{(\text{median } \log_2 \text{FCs})}$ . This initial normalization step accounts for pipetting errors and

unnoticed differences in the number of cells used and makes the reasonable assumption that the vast majority of proteins are unaffected by treatment with the compound. Note that henceforth all protein reporter ion intensity ratios between the corresponding treatment and control samples (same temperature and replicate) remain unaffected, allowing for differential protein abundance analysis.

**Normalization to a global melting curve** For each of the ten temperatures, the mean of a set of 36 median  $\log_2$ FCs was determined by pairwise comparison of all six samples of the given temperature with all six samples of the lowest temperature ( $T_{\text{low}} = 36.5^\circ\text{C}$ ), which served as a reference. These obtained intensity means for each of the ten temperatures,  $I(T)$ , were plotted on the linear scale ( $I(T) = 2^{\text{mean}(\text{median } \log_2 \text{FCs}(T \text{ vs. } T_{\text{low}}))}$ ) against their corresponding temperatures,  $T$ , and a melting curve (Eq. 1) [40] was fitted to the data points using the parameters  $I_{\text{min}}$  and  $I_{\text{max}}$  for the asymptotic intensity minimum and maximum (plateaus), respectively, as well as  $T_m$  and  $s$  as parameters for melting point and slope, respectively. Equation 1 was derived from Eq. 2 with  $T_m = a/b$  and  $s = -b^2/a$  and Eq. 2 originates from the original three parameter ( $I_{\text{max}} = 1$ , using normalized data) description [62] considering that four parameters ( $I_{\text{max}}$  as fitting parameter) have been shown to be more appropriate [48].

$$I(T) = I_{\text{min}} + (I_{\text{max}} - I_{\text{min}}) / (1 + \exp[(T_m/T - 1)sT_m]) \quad (1)$$

$$I(T) = I_{\text{min}} + (I_{\text{max}} - I_{\text{min}}) / (1 + \exp[-(a/T - b)]) \quad (2)$$

Each set of six samples per temperature point was then shifted in the direction of the global melting curve by multiplying it by a constant  $c(T)$ , which was the ratio between the fitted value,  $I_{\text{fit}}(T)$ , and the value of the data point  $I(T)$  ( $c(T) = I_{\text{fit}}(T)/I(T)$ ) at that temperature. Analogous to the previous step (normalization of samples **within** each temperature treatment), the present step normalizes samples **between** temperature treatments to account for pipetting errors and differences in cell number. It is important to note that the present normalization step does not affect the ratios of the six samples **within** a temperature treatment (normalized in the previous step), because these six samples are all multiplied by the same constant. Also note that all single protein reporter ion intensity ratios within each TMT 10plex labeling set stay unaffected from here on, resulting in six pairs (three replicates of TMT 10plex labeling set 1 and three replicates of TMT 10plex labeling set 2, each comprising treatment and control) of melting curve data per protein.

**Normalization of protein-wise melting curves from each TMT 10plex labeling set** First, a rough leveling of the six pairs of melting curve data (six labeling sets) was performed for each protein individually by multiplying all protein intensities in a labeling set by the ratio between the maximum intensity of that protein across all sets and the maximum intensity of that protein in that set. Melting curves (Eq. 1) for each protein were then fitted to the combined data from all six labeling sets using four parameters ( $I_{\min}$ ,  $I_{\max}$ ,  $T_m$ , and  $s$ ) or, as failure alternative, three parameters ( $I_{\max}$ ,  $T_m$ , and  $s$ ;  $I_{\min}=0$ ). The fitted parameters ( $I_{\min}$ ,  $I_{\max}$ ,  $T_m$ , and  $s$ ) were retained as constants in the next fits to determine the scaling factors,  $sf_i$ , for each of the six TMT-10plex labeling sets according to (Eq. 3), where  $i$  denotes labeling sets 1 through 6.

$$I_i(T) = sf_i I_{\min} + (I_{\max} - I_{\min}) / (1 + \exp[(T_m/T - 1)sT_m]) \quad (3)$$

After applying the scaling to the six individual label sets per protein, the process of melting curve fitting over the combined labeling sets and scaling the individual labeling sets by scaling factors derived from the second fitting with only the scaling factor as a free parameter was repeated two more times to approach self-consistency. It is emphasized that the intensity ratios within the labeling sets were unaffected, so that the information about the protein intensity ratios between treatment and control (fold changes,  $FC$ s) was preserved.

**RTSA analysis** For determining the effects of prodigiosin treatment on both protein thermal stability and protein abundance, the normalized reporter intensity data were used as input for the RTSA software (R package v1.0, [33]), which was run without another normalization of the data and was slightly modified to accept the present input data (no common reference data in the two present TMT labeling sets and 36.5 °C instead of 37 °C as lowest temperature).

### Immunoblotting

For SDS PAGE and western blotting, cells were harvested by scraping, pelletized at 150 rcf and 4 °C for 5 min, washed with DPBS and quickly frozen in liquid nitrogen. Cells were lysed in lysis buffer (20 mM Tris±HCl, 150 mM NaCl, 500 µM EDTA, 1% [v/v] Triton X-100, 1 mM  $\text{Na}_3\text{VO}_4$ , 10 mM NaF, 2.5 mM  $\text{Na}_4\text{P}_2\text{O}_7$ , 1X protease inhibitor cocktail [Roche, Basel, Switzerland, #4693132001]) for 30 min on ice and the lysates were cleared by centrifugation at 18,000 rcf and 4 °C for 15 min. Protein concentration was determined by Bradford assay and sample buffer was added (62.5 mM Tris, 8.6% [v/v] glycerol, 2% [w/v] SDS, 33.3 µg/mL

bromophenol blue, 1% [v/v] β-mercaptoethanol). Samples were heated at 95 °C for 5 min and then equal amounts of protein (25 µg) were subjected to SDS±polyacrylamide gels. For CETSA analysis of TPP-TR samples, the protein concentration was determined by Pierce 660 nm Protein Assay and the protein concentration of the 36.5 °C treated sample of each treatment and replicate was used for the other nine samples of the respective sample set to display temperature-dependent total protein aggregation and precipitation. 20 µg of protein were supplemented with sample buffer (62.5 mM Tris, 8.6% [v/v] glycerol, 2% [w/v] SDS, 33.3 µg/mL bromophenol blue, 1% [v/v] β-mercaptoethanol) and heated at 95 °C for 5 min before loading on SDS±polyacrylamide gels. After separation by SDS-PAGE, proteins were transferred to PVDF membranes (Merck, Darmstadt, Germany, #IPFL00010), blocked with 5% milk powder in TBST and analyzed using the indicated primary antibodies followed by appropriate IRDye 800- or IRDye 680-conjugated secondary antibodies (LI-COR Biosciences, Lincoln, NE, USA). Fluorescence signals were detected using an Odyssey Infrared Imaging system (LI-COR Biosciences, Lincoln, NE, USA) and signals were quantified with Image Studio (LI-COR Biosciences, Lincoln, NE, USA). For GRASP55 CETSA analysis, differential melting curve analysis was performed using the RTSA software as described for TPP-TR using normalized quantitative immunoblot data as input. Normalization was performed by dividing each of the two (treatment and control) × three (replicates) = six data sets (ten temperatures each) by the respective fitted  $I_{\max}$  of three parameter ( $I_{\max}$ ,  $T_m$ , and  $s$ ;  $I_{\min}=0$ ) melting curve fits (Eq. 1).

### Generation of knock-out cell lines

GRASP55 KO cells were generated using the CRISPR/Cas9 system developed by the Zhang lab [59]. Double-stranded DNA oligos (5'-CACCGTCGCAAAGCGTCGAGATCCC-3', 3'-AAACGGGATCTCGACGCTTTGCGAC-5'), encoding guide RNAs (gRNAs) against the target gene were cloned into the BbsI restriction site of pSpCas9(BB)-2A-GFP (PX458) vector gifted from Feng Zhang (Addgene plasmid #48,138; <http://n2t.net/addgene:48138>; RRID:Addgene\_48138). Cells were transfected with the resulting vector by electroporation using the Amaxa® Cell Line Nucleofector® Kit R (Lonza, Basel, Switzerland, #VCA-1001) according to the manufacturer's instructions. Four days after transfection, individual clones were generated by cell sorting for GFP positive cells. GRASP55 knockout was validated by immunoblotting, immunofluorescence and DNA sequencing. For GRASP55 sequencing, genomic DNA was isolated using the GeneJET Genomic DNA

Purification Kit (Thermo Fisher Scientific, Waltham, MA, USA, #K0721) according to the manufacturer's instructions. Genomic loci were amplified by PCR using the following primers: 5'-GGGAACGCGTCTGCATAAATC-3', 3'-TCCAGCCCGTCCTCCTACAG-5'. After poly(A) tailing using a TAQ DNA Polymerase (New England Biolabs, Ipswich, MA, USA, #M0267), PCR products were cloned into the pCR™ 2.1-TOPO™ TA-vector using a TOPO™ TA Cloning™ Kit (Thermo Fisher Scientific, Waltham, MA, USA, #450,641). The DNA sequence of 20 clones was determined by Sanger Sequencing using the M13for standard sequencing primer (5'-TGTAACACGACGGCCAG-3') and the sequencing results were aligned with NCBI Reference Sequences of GRASP55 ([https://www.ncbi.nlm.nih.gov/nuccore/NM\\_015530.4](https://www.ncbi.nlm.nih.gov/nuccore/NM_015530.4)).

### Secretome analysis

For the preparation of secretomes,  $2 \times 10^5$  HeLa wt or HeLa GRASP55 KO cells per well were seeded in a 6-well plate ( $n=5$  replicates for 4 different groups). On the next day, the cells were washed three times with DPBS and three times with serum-free culture medium and afterwards incubated in serum-free culture medium containing 0.1% DMSO or 100 nM prodigiosin for 24 h. After incubation, the medium was collected, centrifuged at  $1,000 \times g$  and 4 °C for 10 min and filtered through a 0.2 µm Acrodisc syringe filter (VWR, Radnor, PA, USA, #514±4131). After adding protease inhibitor cocktail (Roche, Basel, Switzerland, #5,892,791,001), the samples were snap frozen in liquid nitrogen and stored at -80 °C. Proteins were prepared for mass spectrometric analysis by a modified single-pot, solid-phase-enhance sample preparation (SP3) method. Here, 450 µl of conditioned medium was mixed with 50 µl of an 1 M aqueous 2-[4-(2-hydroxyethyl)piperazin-1-yl]ethanesulfonic acid solution, 250 µg of an 1:1 mixture of Sera-Mag Speed-Beads GE45152105050250 and GE65152105050250 (Merck, Darmstadt, Germany) and 1.25 ml acetonitrile and incubated for 10 min under constant shaking. Beads were washed with 70% ethanol and acetonitrile, proteins reduced with 10 mM dithiothreitol for 45 min at 56 °C and alkylated by adding 50 mM iodoacetamide. Subsequently, acetonitrile was added up to a concentration of 70% and after a 10 min incubation, beads were washed once with 70% ethanol, two times with 80% ethanol and finally with acetonitrile once. Proteins were digested with 0.05 µg trypsin in 50 mM triethylammonium bicarbonate in water overnight and for additional 4 h with newly added 0.05 µg trypsin. Tryptic peptides were collected, vacuum-dried and desalted using solid phase extraction (Oasis HLB µElution, Waters) using the manufacturers protocol. Finally, the sample was reconstituted in 0.1%

trifluoroacetic acid and half of the sample analyzed by mass spectrometry.

First, peptides were separated over 1 h on C18 material using an Ultimate 3000 Rapid Separation Liquid Chromatography system (RSLC, Thermo Fisher Scientific, Waltham, MA, USA) essentially as described [57] and second injected into a Fusion Lumos mass spectrometer (Thermo Fisher Scientific, Waltham, MA, USA) via a nano-source electrospray interface. The mass spectrometer was operated in data-independent positive mode. First, a survey scan was recorded in profile mode (resolution 60,000, scan range  $380 \pm 985$  m/z, maximum injection time 100 ms, AGC target 400,000) followed by fragment spectra collected in the orbitrap analyser from mass windows of 10 Dalton size from a precursor range of  $380 \pm 980$  m/z (resolution 15,000, scan range  $145 \pm 1450$  m/z, maximum injection time 40 ms, AGC target 100,000, higher energy collisional dissociation, 30% collision energy).

Data analysis was carried out with DIA-NN version 1.8.1 [16] using standard parameters if not stated otherwise. A spectral library for the search was generated from protein sequences including potential contaminants (from MaxQuant 2.1.0.0, Max Planck Institute for Biochemistry, Planegg, Germany) and 81,837 homo sapiens entries from the UniProt KB proteome section (UP000005640, downloaded on 12<sup>th</sup> January 2023). Beside carbamidomethylation at cysteines as fixed modification, N-terminal methionine excision as well as methionine oxidation were considered as variable modifications.

Only proteins identified with at least two different peptides and 4 valid intensity values (MaxLFQ) in at least one experimental group were considered for further analysis. Missing values of  $\log_2$  transformed normalized intensities were filled in with values drawn from a down-shifted normal distribution (0.3 standard deviations width, 1.8 standard deviations down-shift) and differences of group means calculated for following pairs: wt prodigiosin treated ± wt DMSO treated, KO prodigiosin treated ± KO DMSO treated. Data was further annotated by ontology information provided by Perseus version 1.6.6.0 (Max Planck Institute for Biochemistry, Planegg, Germany) and OutCytte [83]. Annotation dependent significant abundance changes of protein groups were analysed using 1D and 2D annotation enrichment [11] and respective differences visualized with split-violin plots with OriginPro 2020b.

### Immunofluorescence

For immunofluorescence microscopy, HeLa cells were seeded on glass coverslips in 24-well plates. After treatment, cells were fixed in 4% paraformaldehyde for 15 min

on ice, quenched with 50 mM NH<sub>4</sub>Cl for 15 min and permeabilized with 50 µg/mL digitonin (Sigma-Aldrich, St. Louis, MO, USA, #D141) for 5 min. Fixed samples were blocked with 3% BSA (Roth, Karlsruhe, Germany, #8076) for 30 min or overnight and incubated with primary antibodies diluted in 3% BSA for 2 h. Samples were then washed three times with DPBS, incubated with the appropriate secondary antibodies diluted in 3% BSA for 30 min and washed three times with DPBS. Afterwards, cells were embedded in ProLong Glass Antifade Mountant (Thermo Fisher Scientific, Waltham, MA, USA, #P36980) containing 1 µg/mL DAPI (Roth, Karlsruhe, Germany, #6335.1). Images were recorded with an Axio Observer 7 Fluorescence microscope (Carl Zeiss Microscopy, Oberkochen, Germany) using a 40x/1.4 Oil DIC M27 Plan-Apochromat objective (Carl Zeiss Microscopy, Oberkochen, Germany) and an ApoTome 2 (Carl Zeiss Microscopy, Oberkochen, Germany).

### Statistical analysis

All IC<sub>50</sub> values were calculated using GraphPad Prism 7.01. For transmission electron microscopy quantification, at least 50 Golgis per treatment and cell line were quantified after blinding and randomization. Results for cisternae number and length are shown in boxplot diagrams and P values were determined by ordinary one-way ANOVA with Dunnett's post hoc test and are shown in the diagrams. For immunofluorescence analyses, dots, nuclei and co-localization were quantified and analyzed using ImageJ 1.53c. A dot to nuclei ratio was calculated for each image to determine the average number of dots per cell, and dots per cell and dot size were normalized by dividing through the mean dot number/size of the solvent control. All macros used for quantifications are provided in Supplementary Table S3. At least 15 representative images from three biological replicates per experiment were analyzed. For all immunofluorescence analyses, results are shown in boxplot diagrams and P values were determined by ordinary one-way ANOVA with Dunnett's post hoc test and are shown in the diagrams.

### Abbreviations

B4GALT1	β-1,4-galactosyltransferase 1
BafA <sub>1</sub>	Bafilomycin A <sub>1</sub>
BFA	Brefeldin A
CETSA	Cellular thermal shift assay
EC <sub>50</sub>	Half maximal effective concentration
ECM	Extracellular matrix
ER	Endoplasmic reticulum
GRASP55	Golgi reassembly stacking protein of 55 kDa
GRASP65	Golgi reassembly stacking protein of 65 kDa
IC <sub>50</sub>	Half maximal inhibitory concentration
LAMP1	Lysosomal-associated membrane protein 1
LIR	LC3-interacting region
(MAP1)LC3	(Microtubule-associated proteins 1A/1B) light chain 3,

MS	Mass spectrometry
MTT	3-(4,5-Dimethylthiazolyl)-2,5-diphenyl-2H-tetrazoliumbromide
pEC <sub>50</sub>	Negative decadic logarithm of the half maximal effective concentration
SP	Signal peptide
SQSTM1	Sequestosome 1
TEM	Transmission electron microscopy
TGN46	trans-Golgi network glycoprotein 46
T <sub>m</sub>	Melting temperature
TMT	Tandem mass tag
TPP-CCR	Thermal proteome profiling compound concentration range
TPP-TR	Thermal proteome profiling temperature range
V-ATPase	Vacuolar-type H <sup>+</sup> -ATPase

## Supplementary Information

The online version contains supplementary material available at <https://doi.org/10.1186/s12964-023-01275-1>.

**Additional file 1: Figure S1.** Schematic representation of the thermal proteome profiling temperature range (TPP-TR) workflow. HeLa wt cells were treated with 100 nM prodigiosin or DMSO for 6 h. After the incubation, cells were harvested, washed and aliquots of the cell suspensions were exposed to short (3 min) treatments at different temperatures in the range between 36.5 °C and 67 °C. Cells were lysed and the non-denatured protein fraction was recovered after centrifugation. Quantitative protein analysis was performed by immunoblotting (CETSA) or MS (TPP). For MS, proteins underwent tryptic digest and the resulting peptides were labeled using TMT 10plex. The samples were combined such that prodigiosin treated and corresponding control samples belonging to the same temperature were analyzed within the same TMT set (similarly as described before for RTSA), allowing for studying not only thermal stability but also abundance effects upon prodigiosin treatment.

**Additional file 2: Figure S2.** STRING protein-protein association network analysis of the 93 significant prodigiosin-affected proteins given by the RTSA analysis (see Figure 3A; significant proteins given by the RTSA software are colored in green or red for positive or negative RTSA distance score, respectively). Protein stabilization or destabilization (with p-value < 0.05 cutoff) is indicated by green or red squares, respectively, to the upper left of the circles representing the proteins. Likewise, an in- or decrease in abundance (with p-value < 0.05 and abs(mean log<sub>2</sub> ratio 36.5 °C) > 0.1 cutoffs) is indicated by green or red squares to the lower left. Prominent clusters are outlined in blue (KEGG:hsa01212, fatty acid metabolism, destabilized proteins), purple (KEGG:hsa04142, lysosome, protein abundance decrease), and orange (KEGG:hsa04140, autophagy - animal). Proteins related to the Golgi apparatus (GO:0005794), Golgi membrane (GO:0000139), or Golgi-associated vesicles (GO:0005798) are labelled by **GO** **TR** or **TR** respectively.

**Additional file 3: Figure S3.** Secretome analysis upon prodigiosin treatment. HeLa wt and GRASP55 knockout cells were incubated for 24 h in serum free medium with and without 100 nM prodigiosin (n=5 per group). The conditioned medium was harvested and proteins analyzed by quantitative data-independent mass spectrometry. Differences of mean values of log<sub>2</sub> normalized intensities between prodigiosin and DMSO treated samples were analyzed for distribution changes associated with protein categories including gene ontology cellular component (GOCC) and OutCyte using an 1D annotation enrichment analysis. OutCyte predicts signal peptides (SP, potential classical secretion pathway), transmembrane regions and leaderless secretion candidate proteins. Positive scores indicate a shift to higher abundances of proteins of a certain protein category, q-values represent for multiple comparisons corrected p-values (Benjamini-Hochberg method).

**Additional file 4. Supplementary Table S1.**

**Additional file 5. Supplementary Table S2.**

**Additional file 6. Supplementary Table S3.** (Macros used for quantifications).

**Additional file 7.** Original, uncropped immunoblots of Fig. 3E, 5A, and 7A.

## Acknowledgements

We thank Jianchao Zhang and Yanzhuang Wang for providing a protocol for the BFA washout assay.

## Resource availability

Further information and requests for resources and reagents should be directed to and will be fulfilled by the Lead Contact, Björn Stork (bjorn.stork@hhu.de). Plasmids and cell lines generated in this study are available from the Lead Contact without restriction upon request. The mass spectrometry proteomics data have been deposited to the ProteomeXchange Consortium [17] via the PRIDE [56] partner repository with the dataset identifiers PXD043247 and PXD042909, respectively.

## Authors' contributions

L.B. designed the experiments, performed viability assays, immunoblot analyses, cathepsin activity assays, fluorescence microscopy, generation of a GRASP55 KO cell line and preparation of samples for TPP, TEM and secretome analysis. H.U.C.B. produced and provided prodigiosin. T.L. performed TPP sample preparation, measurement and analysis. A.K.B. performed sample preparation and imaging for TEM. G.P. performed sample preparation, measurement and data evaluation for secretome analysis. D.S., A.F., M.J.M., C.D., and S.A. gave technical support. L.B. and B.S. analyzed the data and wrote the manuscript. J.P., K.S. and B.S. supervised the project. All authors discussed the results and commented on the manuscript.

## Funding

Open Access funding enabled and organized by Projekt DEAL. This work was supported by the Deutsche Forschungsgemeinschaft (DFG) STO 864/4+3 (to B.S.; project #267192581), GRK 2158 (to B.S. and J.P.; project #270650915), GRK 2578 (to B.S.; project #417677437), and by the BMBF (to J.P.; AutoBiotech: 031B0918A).

## Declarations

### Competing interests

The authors declare no competing interests.

Received: 12 July 2023 Accepted: 13 August 2023

Published online: 05 October 2023

## References

- Ahat E, Bui S, Zhang J, da Veiga Leprevost F, Sharkey L, Reid W, Nesvizhskii AI, Paulson HL, Wang Y. GRASP55 regulates the unconventional secretion and aggregation of mutant huntingtin. *J Biol Chem*. 2022;298: 102219.
- Ahat E, Li J, Wang Y. New Insights Into the Golgi Stacking Proteins. *Front Cell Dev Biol*. 2019;7:131.
- Anderson RG, Pathak RK. Vesicles and cisternae in the trans Golgi apparatus of human fibroblasts are acidic compartments. *Cell*. 1985;40:635±43.
- Barr FA, Puype M, Vandekerckhove J, Warren G. GRASP65, a protein involved in the stacking of Golgi cisternae. *Cell*. 1997;91:253±62.
- Bekier ME 2nd, Wang L, Li J, Huang H, Tang D, Zhang X, Wang Y. Knockout of the Golgi stacking proteins GRASP55 and GRASP65 impairs Golgi structure and function. *Mol Biol Cell*. 2017;28:2833±42.
- Berning L, Schlattermann D, Friedrich A, Berleth N, Sun Y, Wu W, Mendiburo MJ, Deitersen J, Brass HUC, Skowron MA, Hoffmann MJ, Niegisch G, Pietruszka J, Stork B. Prodigiosin sensitizes sensitive and resistant urothelial carcinoma cells to cisplatin treatment. *Molecules*. 2012;26(5):1294.
- Bravo DA, Gleason JB, Sanchez RI, Roth RA, Fuller RS. Accurate and efficient cleavage of the human insulin proreceptor by the human proprotein-processing protease furin. Characterization and kinetic parameters using the purified, secreted soluble protease expressed by a recombinant baculovirus. *J Biol Chem*. 1994;269:25830±7.
- Castro AJ. Antimalarial activity of prodigiosin. *Nature*. 1967;213:903±4.
- Chen X, Wang Y, Ma N, Tian J, Shao Y, Zhu B, Wong YK, Liang Z, Zou C, Wang J. Target identification of natural medicine with chemical proteomics approach: probe synthesis, target fishing and protein identification. *Signal Transduct Target Ther*. 2020;5:72.
- Cheng SY, Chen NF, Kuo HM, Yang SN, Sung CS, Sung PJ, Wen ZH, Chen WF. Prodigiosin stimulates endoplasmic reticulum stress and induces autophagic cell death in glioblastoma cells. *Apoptosis*. 2018;23:314±28.
- Cox J, Mann M. 1D and 2D annotation enrichment: a statistical method integrating quantitative proteomics with complementary high-throughput data. *BMC Bioinformatics*. 2012;13(Suppl 16):S12.
- Cragg GM, Newman DJ. Natural products: a continuing source of novel drug leads. *Biochim Biophys Acta*. 2013;1830:3670±95.
- Danevic T, Boric Vežjak M, Zorec M, Stopar D. Prodigiosin - a multifaceted *Escherichia coli* antimicrobial agent. *PLoS ONE*. 2016;11: e0162412.
- De Tito S, Hervas JH, van Vliet AR, Tooze SA. The Golgi as an assembly line to the autophagosome. *Trends Biochem Sci*. 2020;45:484±96.
- Demaurex N. pH Homeostasis of cellular organelles. *News Physiol Sci*. 2002;17:1±5.
- Demichiev V, Messner CB, Vernardis SI, Lilley KS, Ralser M. DIA-NN: neural networks and interference correction enable deep proteome coverage in high throughput. *Nat Methods*. 2020;17:41±4.
- Deutsch EW, Bandeira N, Perez-Riverol Y, Sharma V, Carver JJ, Mendoza L, Kundu DJ, Wang S, Bandla C, Kamatchinathan S, Hewapathirana S, Pullman BS, Wertz J, Sun Z, Kawano S, Okuda S, Watanabe Y, MacLean B, MacCoss MJ, Zhu Y, Ishihama Y, Vizcaino JA. The ProteomeXchange consortium at 10 years: 2023 update. *Nucleic Acids Res*. 2023;51:D1539±48.
- Dikic I, Elazar Z. Mechanism and medical implications of mammalian autophagy. *Nat Rev Mol Cell Biol*. 2018;19:349±64.
- Dinter A, Berger EG. Golgi-disturbing agents. *Histochem Cell Biol*. 1998;109:571±90.
- Domröse A, Klein AS, Hage-Hulsman J, Thies S, Svensson V, Classen T, Pietruszka J, Jaeger KE, Drepper T, Loeschcke A. Efficient recombinant production of prodigiosin in *Pseudomonas putida*. *Front Microbiol*. 2015;6:972.
- Franken H, Mathieson T, Childs D, Sweetman GM, Werner T, Togel I, Doce C, Gade S, Bantscheff M, Drewes G, Reinhard FB, Huber W, Savitski MM. Thermal proteome profiling for unbiased identification of direct and indirect drug targets using multiplexed quantitative mass spectrometry. *Nat Protoc*. 2015;10:1567±93.
- Frutiger A. Chemie und Biologie des Roseophilins und der Prodigiosin-Alkaloide: 2500 Jahre im Überblick. *Angew Chem*. 2003;115:3706±28.
- Galluzzi L, Vitale I, Aaronson SA, Abrams JM, Adam D, Agostinis P, Alnemri ES, Altucci L, Amelio I, Andrews DW, Annicchiarico-Petruzzelli M, Antonov AV, Arama E, Baehrecke EH, Barlev NA, Bazan NG, Bernassola F, Bertrand MJM, Bianchi K, Blagosklonny MV, Blomgren K, Borner C, Boya P, Brenner C, Campanella M, Candi E, Carmona-Gutierrez D, Cecconi F, Chan FK, Chandel NS, Cheng EH, Chipuk JE, Cidlowski JA, Ciechanover A, Cohen GM, Conrad M, Cubillos-Ruiz JR, Czabotar PE, D'Angioliella V, Dawson TM, Dawson VL, De Laurenzi V, De Maria R, Debatin KM, DeBerardinis RJ, Deshmukh M, Di Daniele N, Di Virgilio F, Dixit VM, Dixon SJ, Duckett CS, Dynlacht BD, El-Deiry WS, Elrod JW, Fimia GM, Fulda S, Garcia-Saez AJ, Garg AD, Garrido C, Gavathiotis E, Golstein P, Gottlieb E, Green DR, Greene LA, Gronemeyer H, Gross A, Hajnóczky G, Hardwick JM, Harris IS, Hengartner MO, Hetz C, Ichijo H, Jaattela M, Joseph B, Jost PJ, Juin PP, Kaiser WJ, Karin M, Kaufmann T, Kepp O, Kimchi A, Kitsis RN, Klionsky DJ, Knight RA, Kumar S, Lee SW, Lemasters JJ, Levine B, Linkermann A, Lipton SA, Lockshin RA, Lopez-Otin C, Lowe SW, Luedde T, Lugli E, MacFarlane M, Madeo F, Malewicz M, Malorni W, Manic G, Marine JC, Martin SJ, Martinou JC, Medema JP, Mehlen P, Meier P, Melino S, Miao EA, Molkenkin JD, Moll UM, Munoz-Pinedo C, Nagata S, Nunez G, Oberst A, Oren M, Overholtzer M, Pagano M, Panaretakis T, Pasparakis M, Penninger JM, Pereira DM, Pervaiz S, Peter ME, Piacentini M, Pinton P, Prehn JHM, Puthalakath H, Rabinovich GA, Rehm M, Rizzuto R, Rodrigues CMP, Rubinsztein DC, Rudel T, Ryan KM, Sayan E, Scorrano L, Shao F, Shi Y, Silke J, Simon HU, Sistigu A, Stockwell BR, Strasser A, Szabadkai G, Tait SWG, Tang D, Tavernarakis N, Thorburn A, Tsujimoto Y, Turk B, Vanden Berghe T, Vandenabeele P, Vander Heiden MG, Villunger A, Virgin HW, Vousden KH, Vucic D, Wagner EF, Walczak H, Wallach D, Wang Y, Wells JA, Wood W, Yuan J, Zakeri Z, Zhivotovskiy B, Zitvogel L, Melino G, Kroemer G. Molecular mechanisms of cell death: recommendations of the nomenclature committee on cell death 2018. *Cell Death Differ*. 2018;25:486±541.

24. Gee HY, Noh SH, Tang BL, Kim KH, Lee MG. Rescue of DeltaF508-CFTR trafficking via a GRASP-dependent unconventional secretion pathway. *Cell*. 2011;146:746±60.
25. Giuliani F, Grieve A, Rabouille C. Unconventional secretion: a stress on GRASP. *Curr Opin Cell Biol*. 2011;23:498±504.
26. Hong B, Prabhu VV, Zhang S, van den Heuvel AP, Dicker DT, Kopelovich L, El-Deiry WS. Prodigiosin rescues deficient p53 signaling and antitumor effects via upregulating p73 and disrupting its interaction with mutant p53. *Cancer Res*. 2014;74:1153±65.
27. Hu DX, Withall DM, Challis GL, Thomson RJ. Structure, chemical synthesis, and biosynthesis of prodiginine natural products. *Chem Rev*. 2016;116:7818±53.
28. Hughes CS, Moggridge S, Muller T, Sorensen PH, Morin GB, Krijgsvelde J. Single-pot, solid-phase-enhanced sample preparation for proteomics experiments. *Nat Protoc*. 2019;14:68±85.
29. Jafari R, Almqvist H, Axelsson H, Ignatushchenko M, Lundback T, Nordlund P, Martinez Molina D. The cellular thermal shift assay for evaluating drug target interactions in cells. *Nat Protoc*. 2014;9:2100±22.
30. Ji S, Sun R, Xu K, Man Z, Ji J, Pu Y, Yin L, Zhang J, Pu Y. Prodigiosin induces apoptosis and inhibits autophagy via the extracellular signal-regulated kinase pathway in K562 cells. *Toxicol In Vitro*. 2019;60:107±15.
31. Johnson FD, Hughes CS, Liu A, Lockwood WW, Morin GB. Tandem mass tag-based thermal proteome profiling for the discovery of drug-protein interactions in cancer cells. *STAR Protoc*. 2023;4: 102012.
32. Judith D, Jefferies HBJ, Boeing S, Frith D, Snijders AP, Tooze SA. ATG9A shapes the forming autophagosome through Arfaptin 2 and phosphatidylinositol 4-kinase IIIbeta. *J Cell Biol*. 2019;218:1634±52.
33. Kaldorf M, Gunthner I, Becher I, Kurzawa N, Knecht S, Savitski MM, Eberl HC, Bantscheff M. Cell surface thermal proteome profiling tracks perturbations and drug targets on the plasma membrane. *Nat Methods*. 2021;18:84±91.
34. Klausner RD, Donaldson JG, Lippincott-Schwartz J, Brefeldin A: insights into the control of membrane traffic and organelle structure. *J Cell Biol*. 1992;116:1071±80.
35. Klein AS, Brass HUC, Klebl DP, Classen T, Loeschcke A, Drepper T, Sievers S, Jaeger KE, Pietruszka J. Preparation of Cyclic Prodiginines by Mutagenesis in *Pseudomonas putida* KT2440. *ChemBioChem*. 2018;19:1545±52.
36. Klein AS, Domrose A, Bongen P, Brass HUC, Classen T, Loeschcke A, Drepper T, Larai L, Sievers S, Jaeger KE, Pietruszka J. New prodiginosin derivatives obtained by mutagenesis in *pseudomonas putida*. *ACS Synth Biol*. 2017;6:1757±65.
37. Klumperman J. Architecture of the mammalian Golgi. *Cold Spring Harb Perspect Biol*. 2011;3(7):a005181.
38. Krishna PS, Vani K, Prasad MR, Samatha B, Bindu NS, Charya MA, Reddy Shetty P. In-silico molecular docking analysis of prodiginosin and cycloprodiginosin as COX-2 inhibitors. *Springerplus*. 2013;2:172.
39. Ladinsky MS, Mastrorade DN, McIntosh JR, Howell KE, Staehelin LA. Golgi structure in three dimensions: functional insights from the normal rat kidney cell. *J Cell Biol*. 1999;144:1135±49.
40. Lenz T, Stihler K. Small molecule arranged thermal proximity coaggregation (smarTPCA)-a novel approach to characterize protein-protein interactions in living cells by similar isothermal dose-responses. *Int J Mol Sci*. 2022;23(10):5605.
41. Li X, Feng Y, Liu X. Crystallization and preliminary crystallographic studies of GRASP65 GRASP domain from *Rattus norvegicus*. *Acta Crystallogr Sect F Struct Biol Cryst Commun*. 2013;69:792±5.
42. Lin SR, Weng CF. PG-priming enhances doxorubicin influx to trigger necrotic and autophagic cell death in oral squamous cell carcinoma. *J Clin Med*. 2018;7(10):375.
43. Lorincz P, Juhasz G. Autophagosome-lysosome fusion. *J Mol Biol*. 2020;432:2462±82.
44. Makhoul C, Gleeson PA. Regulation of mTORC1 activity by the Golgi apparatus. *Fac Rev*. 2021;10:50.
45. Manderville RA. Synthesis, proton-affinity and anti-cancer properties of the prodiginosin-group natural products. *Curr Med Chem Anticancer Agents*. 2001;1:195±218.
46. Martinez Molina D, Jafari R, Ignatushchenko M, Seki T, Larsson EA, Dan C, Sreekumar L, Cao Y, Nordlund P. Monitoring drug target engagement in cells and tissues using the cellular thermal shift assay. *Science*. 2013;341:84±7.
47. McAlister GC, Nusinow DP, Jedrychowski MP, Wuhr M, Huttlin EL, Erickson BK, Rad R, Haas W, Gygi SP. MultiNotch MS3 enables accurate, sensitive, and multiplexed detection of differential expression across cancer cell line proteomes. *Anal Chem*. 2014;86:7150±8.
48. McCracken NA, Peck Justice SA, Wijeratne AB, Mosley AL. InSect: optimizing computational workflows for thermal proteome profiling data analysis. *J Proteome Res*. 2021;20:1874±88.
49. Mollenhauer HH, Morre DJ, Rowe LD. Alteration of intracellular traffic by monensin; mechanism, specificity and relationship to toxicity. *Biochim Biophys Acta*. 1990;1031:225±46.
50. Montaner B, Navarro S, Pique M, Vilaseca M, Martinell M, Giralt E, Gil J, Perez-Tomas R. Prodigiosin from the supernatant of *Serratia marcescens* induces apoptosis in hematopoietic cancer cell lines. *Br J Pharmacol*. 2000;131:585±93.
51. Nakamura N, Tanaka S, Teko Y, Mitsui K, Kanazawa H. Four Na<sup>+</sup>/H<sup>+</sup> exchanger isoforms are distributed to Golgi and post-Golgi compartments and are involved in organelle pH regulation. *J Biol Chem*. 2005;280:1561±72.
52. Newman DJ, Cragg GM. Natural products as sources of new drugs over the 30 years from 1981 to 2010. *J Nat Prod*. 2012;75:311±35.
53. Nchell J, Tauber M, Nolte JL, Morgelin M, Turk C, Eckes B, Demetriades C, Plomann M. An mTORC1-GRASP55 signaling axis controls unconventional secretion to reshape the extracellular proteome upon stress. *Mol Cell*. 2021;81(3275±93): e12.
54. Ohgaki R, van Uzendoom SC, Matsushita M, Hoekstra D, Kanazawa H. Organellar Na<sup>+</sup>/H<sup>+</sup> exchangers: novel players in organelle pH regulation and their emerging functions. *Biochemistry*. 2011;50(4):443±50.
55. Paul T, Bhardwaj P, Mondal A, Bandyopadhyay TK, Mahata N, and Bhunia B. Identification of novel protein targets of prodiginosin for breast cancer using inverse virtual screening methods. *Appl Biochem Biotechnol*. 2023. <https://doi.org/10.1007/s12010-023-04426-9>.
56. Perez-Riverol Y, Bai J, Bandla C, Garcia-Seisdedos D, Hewapathirana S, Kamatchinathan S, Kundu DJ, Prakash A, Frericks-Zipper A, Eisenacher M, Walzer M, Wang S, Brazma A, Vizcaino JA. The PRIDE database resources in 2022: a hub for mass spectrometry-based proteomics evidences. *Nucleic Acids Res*. 2022;50:D543±52.
57. Prescher N, Hansch S, Knobbe-Thomsen CB, Stuhler K, Poschmann G. The migration behavior of human glioblastoma cells is influenced by the redox-sensitive human macrophage capping protein CAPG. *Free Radic Biol Med*. 2021;167:81±93.
58. Puthenveedu MA, Bachert C, Puri S, Lanni F, Linstedt AD. GM130 and GRASP65-dependent lateral cisternal fusion allows uniform Golgi-enzyme distribution. *Nat Cell Biol*. 2006;8:238±48.
59. Ran FA, Hsu PD, Wright J, Agarwala V, Scott DA, Zhang F. Genome engineering using the CRISPR-Cas9 system. *Nat Protoc*. 2013;8:2281±308.
60. Rapoport H, Holden KG. Synthesis of Prodigiosin. *J Am Chem Soc*. 1962;84:635±0.
61. Sato T, Konno H, Tanaka Y, Kataoka T, Nagai K, Wasserman HH, Ohkuma S. Prodigiosins as a new group of H<sup>+</sup>/Cl<sup>-</sup> symporters that uncouple proton translocators. *J Biol Chem*. 1998;273:21455±62.
62. Savitski MM, Reinhard FB, Franken H, Werner T, Savitski MF, Eberhard D, Martinez Molina D, Jafari R, Dovega RB, Klaeger S, Kuster B, Nordlund P, Bantscheff M, Drewes G. Tracking cancer drugs in living cells by thermal profiling of the proteome. *Science*. 2014;346:1255784.
63. Seganish L, and Davis JT. Prodigiosin is a chloride carrier that can function as an anion exchanger. *Chem Commun (Camb)*. 2005;5781±3.
64. Shorter J, Watson R, Giannakou ME, Clarke M, Warren G, Barr FA. GRASP55, a second mammalian GRASP protein involved in the stacking of Golgi cisternae in a cell-free system. *EMBO J*. 1999;18:4949±60.
65. Stuhldreier F, Schmitt L, Lenz T, Hinxlage I, Zimmermann M, Wollnitzke P, Schliehe-Diecks J, Liu Y, Jager P, Geyh S, Teusch N, Peter C, Bhatia S, Haas R, Levkau B, Reichert AS, Stuhler K, Proksch P, Stork B, Wesselborg S. The mycotoxin viriditoxin induces leukemia- and lymphoma-specific apoptosis by targeting mitochondrial metabolism. *Cell Death Dis*. 2022;13:938.
66. Szklarczyk D, Kirsch R, Koutrouli M, Nastou K, Mehryary F, Hachilif R, Gable AL, Fang T, Doncheva NT, Pyysalo S, Bork P, Jensen LJ, von Mering C. The STRING database in 2023: protein-protein association networks and functional enrichment analyses for any sequenced genome of interest. *Nucleic Acids Res*. 2023;51:D638±46.
67. Truschel ST, Sengupta D, Foote A, Heroux A, Macbeth MR, Linstedt AD. Structure of the membrane-tethering GRASP domain reveals a unique

- PDZ ligand interaction that mediates Golgi biogenesis. *J Biol Chem*. 2011;286:20125±9.
68. Vanneste M, Huang Q, Li M, Moose D, Zhao L, Stamnes MA, Schultz M, Wu M, Henry MD. High content screening identifies monensin as an EMT-selective cytotoxic compound. *Sci Rep*. 2019;9:1200.
  69. Vinod V, Padmakrishnan CJ, Vijayan B, Gopala S. 'How can I halt thee?' The puzzles involved in autophagic inhibition. *Pharmacol Res*. 2014;82:1±8.
  70. Wang Y, Seemann J. Golgi biogenesis. *Cold Spring Harb Perspect Biol*. 2011;3: a005330.
  71. Wang Y, Seemann J, Pypaert M, Shorter J, Warren G. A direct role for GRASP65 as a mitotically regulated Golgi stacking factor. *EMBO J*. 2003;22:3279±90.
  72. Wang Y, Wei JH, Bisel B, Tang D, Seemann J. Golgi cisternal unstacking stimulates COPI vesicle budding and protein transport. *PLoS ONE*. 2008;3: e1647.
  73. Wasserman HH, Mckee JE, Smith L, Forgione P. Prodigiosin - structure and partial synthesis. *J Am Chem Soc*. 1960;82:506±7.
  74. Williamson NR, Fineran PC, Gristwood T, Chawrai SR, Leeper FJ, Salmond GP. Anticancer and immunosuppressive properties of bacterial prodiginines. *Future Microbiol*. 2007;2:605±18.
  75. Wrede F, Hettche O. «ber das Prodigiosin, den roten Farbstoff des *Bacillus Prodigiosus* (I. Mitteil.). *Ber Dtsch Chem Ges*. 1929;62:2678±85.
  76. Xiang Y, Wang Y. GRASP55 and GRASP65 play complementary and essential roles in Golgi cisternal stacking. *J Cell Biol*. 2010;188:237±51.
  77. Xiang Y, Zhang X, Nix DB, Katoh T, Aoki K, Tiemeyer M, Wang Y. Regulation of protein glycosylation and sorting by the Golgi matrix proteins GRASP55/65. *Nat Commun*. 2013;4:1659.
  78. Yamamoto H, Zhang S, Mizushima N. Autophagy genes in biology and disease. *Nat Rev Genet*. 2023;24:382±400.
  79. Yip CH, Yarkoni O, Ajioka J, Wan KL, Nathan S. Recent advancements in high-level synthesis of the promising clinical drug, prodiginosin. *Appl Microbiol Biotechnol*. 2019;103:1667±80.
  80. Zhang X, Wang L, Ireland SC, Ahat E, Li J, Bekier ME 2nd, Zhang Z, Wang Y. GORASP2/GRASP55 collaborates with the PtdIns3K UVRAG complex to facilitate autophagosome-lysosome fusion. *Autophagy*. 2019;15:1787±800.
  81. Zhang X, Wang L, Lak B, Li J, Jokitalo E, Wang Y. GRASP55 senses glucose deprivation through O-GlcNAcylation to promote autophagosome-lysosome fusion. *Dev Cell*. 2018;45(245±61): e6.
  82. Zhao C, Qiu S, He J, Peng Y, Xu H, Feng Z, Huang H, Du Y, Zhou Y, Nie Y. Prodigiosin impairs autophagosome-lysosome fusion that sensitizes colorectal cancer cells to 5-fluorouracil-induced cell death. *Cancer Lett*. 2020;481:15±23.
  83. Zhao L, Poschmann G, Waldera-Lupa D, Raftoyiannis N, Kollmann M, Stuhler K. OutCyte: a novel tool for predicting unconventional protein secretion. *Sci Rep*. 2019;9:19448.

## Publisher's Note

Springer Nature remains neutral with regard to jurisdictional claims in published maps and institutional affiliations.

**Ready to submit your research? Choose BMC and benefit from:**

- fast, convenient online submission
- thorough peer review by experienced researchers in your field
- rapid publication on acceptance
- support for research data, including large and complex data types
- gold Open Access which fosters wider collaboration and increased citations
- maximum visibility for your research: over 100M website views per year

**At BMC, research is always in progress.**

Learn more [biomedcentral.com/submissions](https://biomedcentral.com/submissions)

